



CARDIFF UNIVERSITY

# **Creating 3D City Models from Satellite Imagery for Integrated Assessment and Forecasting of Solar Energy**

by

Nada M. S. M. Kadhim

A thesis submitted in partial fulfillment of the requirements for  
the degree of Doctor of Philosophy (PhD)

Cardiff School of Engineering  
Cardiff, Wales, United Kingdom

9th January 2018

*Dedicated to*

*My Parents, **Amirah** and **Mohammed Salih***

*With all my heart and soul!*

## **Declaration of Authorship**

I, Nada Mohammed Salih Mohammed Kadhim, declare that this thesis titled, 'Creating 3D City Models from Satellite Imagery for Integrated Assessment and Forecasting of Solar Energy' and the work presented in it are my own. I confirm that:

- This work was done wholly or mainly while in candidature for a research degree at this University.
- Where any part of this thesis has previously been submitted for a degree or any other qualification at this University or any other institution, this has been clearly stated.
- Where I have consulted the published work of others, this is always clearly attributed.
- Where I have quoted from the work of others, the source is always given. With the exception of such quotations, this thesis is entirely my own work.
- I have acknowledged all main sources of help.
- Where the thesis is based on work done by myself jointly with others, I have made clear exactly what was done by others and what I have contributed myself.

Signed:

---

Date:

---

*"I hated every minute of training, but I said, 'Don't quit. Suffer now and live the rest of your life as a champion.' "*

Muhammad Ali Clay.

# Acknowledgements

“In the name of Allah, the Entirely Merciful, the Especially Merciful. [All] praise is [due] to Allah, Lord of the worlds”(1:2), Al-Fatiyah, Quran. I am grateful to **ALLAH** for the good health and wellbeing that were necessary to complete this thesis.

I would like to express my deep gratitude to my supervisory team: **Prof. Monjur Mourshed** and **Dr. Michaela Bray**, for their patient guidance, enthusiastic encouragement and useful critiques of this research work. In particular, **Prof. Monjur Mourshed** spared no effort in providing vital feedback, assistance in keeping my progress on schedule, the continuous support of my Ph.D study and related research; I thank him also, for his patience, motivation, and immense knowledge.

I would also like to thank the following university staff: **Dr. Peter Cleall** and **Mrs. Aderyn Reid**, as well as School of Engineering and Cardiff student support (Financial Assistance Programme Awards) for their unfailing support and assistance for funding a part of the PhD research.

This research has been funded by a grant from the **Higher Committee of Education Development (HCED)** in Iraq. I gratefully acknowledge the grant support by **HCED** in achieving this work. I also thank the staff of Diyala School of Engineering and University of Diyala for their cooperation during the research project. I would like to express my sincere gratitude to my beloved country **Iraq** for providing me with such a great opportunity to pursue my dream and achieve my ambition.

I would also like to acknowledge **Dr. Ali Ozgun Ok**, **Dr. Massimo DL**, **Dr. Muhammad Ahmad**, **Dr. Ahmed M. A. Al-Sabaawi**, **Dr. Saad M. S. Al-Azawi**, and **Mrs. Sharon Pointer** for useful discussion and significant scientific information as well as for their aspiring guidance, invaluable constructive criticism, and friendly advice during the project work.

Finally, I must express my very profound gratitude to my parents **Mrs. Amira Ali Al-Ansari** and **Mr. Mohammed Salih Mohammed Kadhim Al-Ansari**, my brothers **Dr. Hani M. S. Al-Ansari**, **Mr. Ali M. S. Al-Ansari** and **Mr. Nabil M. S. Al-Ansari**, as well as my sisters **Prof. Maha M. S. Al-Ansari** and **Ms. Huda M. S. Al-Ansari** for providing me with unfailing support and continuous encouragement throughout my years of study and through the process of researching and writing this thesis. This accomplishment would not have been possible without them. Thank you from the bottom of my heart.

# Abstract

Buildings are the most prominent component in the urban environment. The geometric identification of urban buildings plays an important role in a range of urban applications, including 3D representations of buildings, energy consumption analysis, sustainable development, urban planning, risk assessment, and change detection. In particular, 3D building models can provide a comprehensive assessment of surfaces exposed to solar radiation. However, the identification of the available surfaces on urban structures and the actual locations which receive a sufficient amount of sunlight to increase installed power capacity (e.g. Photovoltaic systems) are crucial considerations for solar energy supply efficiency. Although considerable research has been devoted to detecting the rooftops of buildings, less attention has been paid to creating and completing 3D models of urban buildings. Therefore, there is a need to increase our understanding of the solar energy potential of the surfaces of building envelopes so we can formulate future adaptive energy policies for improving the sustainability of cities.

The goal of this thesis was to develop a new approach to automatically model existing buildings for the exploitation of solar energy potential within an urban environment. By investigating building footprints and heights based on shadow information derived from satellite images, 3D city models were generated. Footprints were detected using a two level segmentation process: (1) the iterative graph cuts approach for determining building regions and (2) the active contour method and the adjusted-geometry parameters method for modifying the edges and shapes of the extracted building footprints. Building heights were estimated based on the simulation of artificial shadow regions using identified building footprints and solar information in the image metadata at pre-defined height increments. The difference between the actual and simulated shadow regions at every height increment was computed using the Jaccard similarity coefficient. The 3D models at the first level of detail were then obtained by extruding the building footprints based on their heights by creating image voxels and using the marching cube approach.

In conclusion, 3D models of buildings can be generated solely from 2D data of the buildings' attributes in any selected urban area. The approach outperforms the past attempts, and mean error is reduced by at least 21%. Qualitative evaluations of the study illustrate that it is possible to achieve 3D building models based on satellite images with a mean error of less than 5 m. This comprehensive study allows for 3D city models to be generated in the absence of elevation attributes and additional data. Experiments revealed that this novel, automated method can be useful in a number of spatial analyses and urban sustainability applications.

# Contents

<b>Declaration of Authorship</b>	<b>ii</b>
<b>Acknowledgements</b>	<b>iv</b>
<b>List of Figures</b>	<b>ix</b>
<b>List of Tables</b>	<b>xi</b>
<b>Abbreviations</b>	<b>xii</b>
<b>1 Introduction</b>	<b>1</b>
1.1 Background of the study . . . . .	2
1.1.1 Research rationale . . . . .	6
1.1.2 Research motivation . . . . .	7
1.2 Aim and scope of the research . . . . .	8
1.3 Research questions . . . . .	10
1.4 Contribution of the present work . . . . .	11
1.5 Outline of the Thesis . . . . .	14
1.6 Summary . . . . .	15
<b>2 Advances in remote sensing applications for urban sustainability</b>	<b>17</b>
2.1 Remote sensing technology in urban studies . . . . .	18
2.2 Urban Remote Sensing (URS) . . . . .	19
2.2.1 remote sensing technology and systems . . . . .	19
2.2.2 remote sensing applications in urban environments . . . . .	22
2.3 Sustainable urban environments . . . . .	29
2.3.1 Sustainable development . . . . .	30
2.3.2 Urban sustainability using remote sensing technology . . . . .	31
2.3.3 Renewable energy . . . . .	32
2.4 Remote sensing challenges and opportunities and key trends in the existing literature . . . . .	33
2.5 Summary . . . . .	40
<b>3 Current state of 3D object creation</b>	<b>41</b>
3.1 Optical satellite images characteristics . . . . .	42
3.1.1 The importance of using satellite images . . . . .	43
3.1.2 Image enhancement . . . . .	44

3.2 The extraction of information from satellite imagery . . . . .	45
3.2.1 The importance of shadow detection in urban environments . . . . .	46
3.2.2 Shadow detection and extraction . . . . .	49
3.3 The creation of 3D models of urban buildings . . . . .	52
3.3.1 Geometry identification: Building detection and footprint extraction . . . . .	53
3.3.2 Geometry identification: Building height estimation . . . . .	55
3.3.3 The reconstruction of 3D building models . . . . .	58
3.4 The effect of building geometry on energy efficiency . . . . .	61
3.5 Summary . . . . .	65
<b>4 Methodology</b> . . . . .	<b>67</b>
4.1 Research design . . . . .	68
4.1.1 Rationale for the selected present methodology . . . . .	69
4.1.2 Data selection . . . . .	69
4.1.3 Shadow information and the theoretical concept . . . . .	72
4.2 Shadow detection and extraction . . . . .	74
4.2.1 The detection of shadow regions using Near-Infrared information . . . . .	74
4.2.2 Shadow region extraction . . . . .	78
4.3 Building detection and extraction . . . . .	78
4.3.1 Shadow post-processing . . . . .	78
4.3.2 Building footprint detection . . . . .	81
4.3.3 Geometry adjustment of the extracted building footprints . . . . .	83
4.4 Estimation of building heights . . . . .	87
4.5 Automated creation of 3D models of urban buildings . . . . .	90
4.6 Assessment of solar energy potential . . . . .	94
4.7 Validation techniques . . . . .	96
4.8 Summary . . . . .	99
<b>5 Results</b> . . . . .	<b>100</b>
5.1 Results and study objectives . . . . .	101
5.2 Utilised satellite imagery and its preparation . . . . .	101
5.3 Study area . . . . .	103
5.4 The new approach's outputs . . . . .	104
5.4.1 Shadows . . . . .	105
5.4.2 Building footprints . . . . .	107
5.4.3 Edge adjustment of the building footprints . . . . .	109
5.4.4 Heights . . . . .	110
5.4.5 3D models . . . . .	111
5.5 3D models' assessment and the validation of results . . . . .	111
5.6 The findings of the selected image patches . . . . .	114
5.6.1 Experimental results . . . . .	114
5.6.2 Solar rooftops analysis . . . . .	121
5.6.3 Computational time . . . . .	124
5.7 Summary . . . . .	125
<b>6 Discussion</b> . . . . .	<b>126</b>
6.1 Interpretation and discussion of the findings . . . . .	127
6.1.1 A reminder of the purpose of the study . . . . .	127

6.1.2 The study's major findings . . . . .	128
6.1.3 An indication of the importance of the findings . . . . .	128
6.2 Discussion and explanation of the results . . . . .	130
6.3 Implications and practical applications of the study . . . . .	136
6.4 Limitations of the study . . . . .	139
6.5 A summary of the results . . . . .	141
<b>7 Conclusions and future work</b>	<b>142</b>
7.1 Significance of the study . . . . .	143
7.1.1 Restatement of aims . . . . .	144
7.1.2 Summarising research findings . . . . .	144
7.2 The conclusion of the study . . . . .	146
7.3 Implications for the field of urban modelling . . . . .	149
7.4 Recommendations for future research . . . . .	150

# List of Figures

1.1	The utility of 3D city models in a multitude of application domains for urban sustainability and decision support . . . . .	3
1.2	The steadily rising demand for electricity in Iraq . . . . .	9
1.3	The structure of the thesis . . . . .	16
2.1	A comparison of satellite generations in terms of detail, feature recognition, and planning requirements . . . . .	20
2.2	Classification of remote sensing sensors based on their characteristics . . . . .	21
2.3	An overview of the spectral, spatial, temporal, and radiometric resolution of different optical satellite systems . . . . .	22
2.4	A comparison of environmental considerations and critical requirements between optical and non-optical sensors for urban change detection and the monitoring of city expansion . . . . .	23
2.5	The texture-based identification of urban slums from remote sensing data . . . . .	26
2.6	Increasing temperature due to increased city size and the number of city dwellers . . . . .	27
2.7	Key urban sustainability applications of remote sensing . . . . .	31
2.8	Previous work on urban growth and sprawl, and land-cover and land-use changes . . . . .	34
2.9	Previous work on slums, air and water quality, temperature assessment, and renewable energy . . . . .	35
2.10	The hypothetical deterioration of environmental systems and the potential for the use of remote sensing in their restoration . . . . .	37
3.1	Raster data concept . . . . .	43
3.2	Image contrast stretch as applied to the image band . . . . .	45
3.3	The direction of illumination and the geometry of the shadow pattern . . . . .	48
3.4	The fundamental concept of a building's geometry . . . . .	54
3.5	The effect of building geometry on energy efficiency . . . . .	65
4.1	The employed data: pan-sharpened multispectral satellite imagery . . . . .	72
4.2	Shadow conditions from the VHR pan-sharpened multispectral satellite imagery . . . . .	73
4.3	Shadow progressions: the shadows of a point (top left), a line (top right), a plane (bottom left) and a solid (bottom right) . . . . .	74
4.4	The developed shadow detection framework . . . . .	77
4.5	The concept of image pixel connectivity and region growth . . . . .	79
4.6	Curve propagating in a normal direction . . . . .	84
4.7	Building edges enhancement . . . . .	86
4.8	Framework of the shadow-overlapping algorithm <i>A<sub>SO</sub></i> for building height estimation . . . . .	91
4.9	The five LODs of CityGML 2.0 . . . . .	92

4.10 The conception of the voxel and pixel . . . . .	92
4.11 3D model with triangles placed along the sides of voxel cubes . . . . .	94
4.12 The conception of the marching cubes $A_{MC}$ . . . . .	94
4.13 The measurement of the given object . . . . .	96
5.1 The pan-sharpened ortho-rectified multispectral images, its metadata file, and sensor bands . . . . .	102
5.2 WorldView-3 pan-sharpened image, before and after the contrast adjustment . .	103
5.3 Reference data (ground truth) . . . . .	104
5.4 Shadow detection . . . . .	106
5.5 The extraction of the final shadow regions . . . . .	107
5.6 The extraction of the building footprints . . . . .	109
5.7 The modification of the building footprints by active contour without edges approach . . . . .	110
5.8 The modification of the building footprints by the building shape fitting: a new approach . . . . .	110
5.9 Estimation of the building heights . . . . .	111
5.10 The creation of the 3D building with the meshgrid surface . . . . .	112
5.11 3D models of the buildings at different viewing angles . . . . .	112
5.12 The estimated values of building heights . . . . .	115
5.13 Sensitivity analysis for building heights estimation . . . . .	116
5.14 Automated creation of 3D building models . . . . .	119
5.15 The validation of the perimeters of the 3D city models . . . . .	122
5.16 Solar building roof analysis . . . . .	123
5.17 Solar building roof analysis for two different urban areas . . . . .	124
7.1 Proposed future work —a solar assessment tool . . . . .	152

# List of Tables

2.1	Consequences of expansion of cities against observation variables, impacts, potential and limitations of urban remote sensing applications . . . . .	28
2.1	Consequences of expansion ... (cont. from previous page) . . . . .	29
2.2	State-of-the-art studies in taxonomy, detection, extraction and pattern recognition in urban applications . . . . .	36
2.3	Directions for future research . . . . .	39
4.1	The methodology flowchart for a 3D building creation algorithm. The flowchart provides the summary of the key processes, formulae and parameters . . . . .	71
5.1	The main parameter settings of the present study . . . . .	108
5.2	Effects of different threshold values on the performance results of the present study . . . . .	113
5.3	Estimated building heights using the proposed algorithm . . . . .	117
5.4	Algorithm performance against previous works . . . . .	118
5.5	Numerical results of the creation of 3D building models. The values between ground truth data and the results of the present study are compared to assess the algorithm performance . . . . .	120

# Abbreviations

<b>AOT</b>	aerosol optical thickness
<b>CRF</b>	conditional random field
<b>DEM</b>	digital elevation model
<b>DSM</b>	digital surface model
<b>DTM</b>	digital terrain model
<b>EMR</b>	electromagnetic radiation
<b>ETM+</b>	enhanced thematic mapper plus
<b>GIS</b>	geographic information system
<b>GMM</b>	gaussian mixture models
<b>GRR</b>	generalised rewriting rule
<b>GSD</b>	ground sample distance
<b>GUI</b>	graphical user interface
<b>HSI</b>	hue saturation intensity
<b>LiDAR</b>	light detection and ranging
<b>LOD</b>	level of detail
<b>LST</b>	land surface temperature
<b>MAE</b>	mean absolute error
<b>MEED</b>	Middle East Economic Digest
<b>MIR</b>	mid infra-red
<b>MODIS</b>	moderate-resolution imaging spectroradiometer
<b>MRF</b>	markov random field
<b>MSS</b>	multispectral scanner system
<b>NDVI</b>	normalised difference vegetation index
<b>NIR</b>	near infra-red
<b>NSVDI</b>	normalising saturation value difference index
<b>DEM</b>	digital elevation models
<b>OBIA</b>	object-based image analysis

<b>OLI</b>	operational land image
<b>OS</b>	Ordnance Survey
<b>OSM</b>	open street map
<b>NIR</b>	near infra-red
<b>PAN</b>	panchromatic
<b>PV</b>	photovoltaic
<b>RET</b>	renewable energy technologies
<b>RMSE</b>	root mean square error
<b>ROI</b>	region of interest
<b>SWIR</b>	short-wave infra-red
<b>SVM</b>	support vector machine
<b>TIR</b>	thermal infra-red
<b>TM</b>	thermatic mapper
<b>UHI</b>	urban heat island
<b>ULQ</b>	urban landscape quality
<b>UNCED</b>	United Nations Conference on Environment and Development
<b>URS</b>	urban remote sensing
<b>VHR</b>	very high resolution
<b>VIS</b>	Vegetation impervious soil
<b>VLS</b>	visible light spectrum
<b>VSA</b>	volumetric shadow analysis
<b>WV3</b>	worldview-3

# **Chapter 1**

## **Introduction**

This chapter introduces the purpose of the study, the need for geometry identification and the creation of 3D models of urban buildings for different urban applications, particularly solar energy potential assessments. Furthermore, the motivation for reviewing the formulated demand for spatially enhanced spatial data in support of sustainable energy supply is explained. This chapter also introduces the usability of geospatial data, such as satellite imagery, in 3D geometry reconstruction. Finally, the chapter concludes with the main aim, objectives, research rationale, research questions, and the contribution in scientific research, along with the thesis structure and summary.

## 1.1 Background of the study

Rapid urbanisation and population growth are the main cause of the depletion of natural resources (e.g. minerals, vegetation, water, and soil) and the use of non-renewable energy (e.g. coal, petroleum, and natural gas) [1, 2]. City expansion which does not take into account sustainable development may contribute to unplanned or poorly planned urbanisation, leading in turn to unsustainable urban environments. As unplanned urban growth can have a long-term negative impact on urban sustainability on a range of scales (local, regional, and national), urban sustainability must therefore be considered for the expansion of cities in order to minimise our reliance on natural resources and conventional energy sources. Sustainable cities can mitigate the impacts of climate change by minimising ecological footprints, reducing pollution, increasing land-use efficiency, recycling waste, and increasing the use of sustainable materials; moreover, climate change impacts can be mitigated by maximising renewable energy use [3–8].

A promising energy source for sustainable urban development is renewable energy. Such resources are eco-friendly and clean, and they have less environmental impact than other energy sources (e.g. fossil fuels). Solar energy is the most rapidly growing form of clean, renewable energy and is widely used globally for energy production (e.g. electricity and thermal energy). However, due to the complexity of the urban environment, it is difficult to determine how much of the available area of a building can be successfully used for the deployment of photovoltaic (PV) solar modules. This is particularly true for other solar energy applications, generally in modern urban landscapes.

To conduct an assessment of solar radiation potential at a building level, one of the key requirements is to identify the geometry of urban structures within urban areas. Geometric information, location, and orientation of existing buildings make up the essential data required to evaluate actual shadow regions and building surface brightness (including building roofs and facades). This, in turn, requires the creation of 3D models of urban buildings to maximise the exploitation of solar energy potential in a city. Generating such 3D building models can play a significant role in increasing our understanding of the coverage of shaded zones in daylight hours with high solar radiation. The 3D models, which are derived from genuine geospatial data, can depict a building's surrounding environment and the nearby urban fabric through advanced technology such as remote sensing platforms [9]. As such, this research focuses on

the exploitation of advanced remote sensing techniques (e.g. optical satellite sensors) in creating 3D models of urban buildings, not only for solar energy systems but also for a wide range of urban applications.

The geometry of a building, including the dimensions of the footprint and the elevation measurements, provides the key elements for the creation of a 3D city model; such information is indispensable in acquiring a comprehensive understanding of urban structures. A 3D city model is defined as a three-dimensional depiction of the urban environment, concentrating on the geometry of urban structures and objects where buildings are dominant [10, 11]. Because 3D building models provide significant supplemental information and navigation databases, they offer an important contribution to our knowledge and brings us closer to a better understanding of the complex phenomenon of the urban environment, as well as the needs of a city. Therefore, 3D building models can be used not only for visualising an environment, but also for various urban applications in a wide range of research domains, as shown in Figure 1.1. Despite the crucial role of 3D building models for urban applications, the reliability of the techniques used and the availability of data for reconstructing and deriving 3D building models are hurdles that are yet to be overcome. The reliability of the processing techniques used to generate 3D building models can be achieved by taking into account the cost, time, and effort of the implementation process. In addition, there is the problem of obtaining genuine and up-to-date data on the geospatial information of buildings within an urban environment.

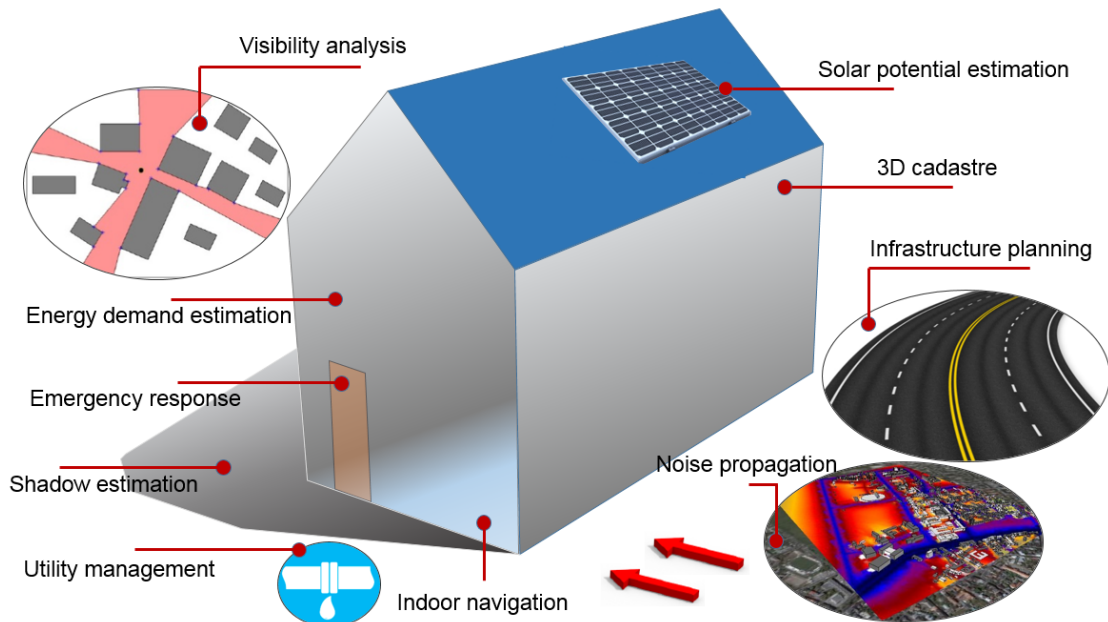


**Figure 1.1:** The utility of 3D city models in a multitude of application domains for urban sustainability and decision support

Over the past few decades, diverse techniques have been employed in the identification of building geometry. These techniques for generating 3D building models are based on ongoing developments in data capture in urban areas. The most common acquisition techniques are: photogrammetry and laser scanning, Light Detection and Ranging (LiDAR), radar, multispectral satellite images (stereo-pair images), extrusion from 2D footprints, architectural models and drawings, handheld devices, procedural modelling, and volunteered geoinformation. However, in the context of the current work, the focus is on the extraction of the 3D geometry of observed buildings within an urban area from which 3D building models can be derived with minimal data usage. The key challenge is to detect, extract, and generate dependable 3D models of urban structures with minimal data, low user effort (without human intervention), and sufficient processing performance. Many developing countries (e.g. Iraq) do not have the basic requirements to facilitate the creation of 3D models. They do not have an effective survey system to monitor the urban environment and they may even lack an inventory of existing buildings. There is also often a lack of geospatial and statistical data, poor internet access (e.g. using online 3D modelling software), and/or advanced field devices (e.g. portable measuring devices and drones). In particular, the reconstruction process of 3D models becomes more complicated if several buildings, a district, or even an entire city is to be reconstructed as a 3D model.

In this regard, the unprecedented technological developments in satellites and their sensors offer magnificent opportunities to cost-effectively monitor urban areas with a variety of collected data. Continuous spatial and temporal data which cover large urban areas, such as remote sensing satellite data, can provide the actual locations of urban buildings. Most significantly, some remote sensing satellite sensors can capture surface heights and provide the elevation data of urban objects, such as tree canopies and buildings. Three advanced remote sensing technologies can be used in reconstructing 3D models of buildings: stereo imaging [12], LiDAR [13], and imaging radar [14]. However, although the 3D models of urban buildings derived from such remote sensing technologies are highly accurate, the reconstruction process of the 3D models is still primarily achieved manually. In other words, a common property of the data generated by remote sensing technologies is that they employ high-level data calibration and processing using sophisticated parameters to obtain a reliable Digital Terrain Models (DTM) and/or Digital Surface Models (DSM) [15]. In addition, it should be noted that the complicated extraction process of elevation data, as used in numerous studies on 3D models (especially 3D urban buildings), requires the use of extra complementary data and sufficient knowledge [16]. Studies using such data to generate 3D building models are often logically constrained by

factors such as: the availability of data from technologies; costs associated with LiDAR, aerial images, and terrestrial laser scanning; the lengthy time for data pre- and post-processing (e.g. point cloud processing); making desirable adjustments/editing (e.g. hypothesis for training and testing data); and the cognitive skills of the researcher. Moreover, many images are needed to build a satisfactory and complete view of a building's size and shape.

In recent years, there has been renewed interest in creating 3D building models by employing a single data source (e.g. a monocular satellite image) in order to reduce the limitations of using costly remote sensing data [17], and monocular Very High Resolution (VHR) multispectral satellite images for 3D modelling [18]. There is a need for 3D building model creation using minimal cost, time, and effort, to meet the needs of urban applications, such as urban planning and identifying the availability of building surfaces for solar dissemination policies. However, the creation of the 3D building models from a single satellite image (2D) is a very challenging task. Although satellite images provide very useful solar information [19] and actual geospatial information of building locations, inferring 3D information from 2D scenes is a process with embedded geometric and radiometric difficulties. Due to the insufficient information about the 3D structure of an urban object associated with using a single image, the identification of a building's envelope<sup>1</sup> becomes a geometric problem. The radiometric and spectral characteristics in which satellite images are captured can increase the complexity of object recognition and detection processes. This is especially true for dense urban areas as a result of the spectral similarity of some surfaces.

On the other hand, due to the unprecedented technological development of the satellite sensors and the characteristics of the captured image, there is an increasing need to address the performance problems of the algorithms used for object detection, extraction, and 3D model reconstruction, using VHR satellite images within complex urban landscapes [19–21]. This is especially true when there is no extra data available to support the performance of the algorithms in extracting meaningful information for the generation of 3D models of urban buildings from single satellite images. The performance of the algorithms in many current and proposed semi-automatic approaches for identifying and segmenting the boundaries of building footprints from other urban objects in satellite scenes is still not efficient enough to produce realistic 3D building models with precise geometry. Although the identification process of building edges and

---

<sup>1</sup>The building envelope is the physical separator between the interior and exterior of a building. Components of the envelope are typically: walls, floors, roofs, fenestrations and doors. Fenestrations are any opening in the structure: windows, skylights, and clerestories. <https://sustainabilityworkshop.autodesk.com/buildings/building-envelope>

shapes with user/operator aid may provide building geometry extraction results precise enough to generate a 3D building model from the images, the general issue with semi-automatic methods is that they are time consuming, they have a low update rate, and they are tedious and extremely difficult for modelling many buildings. The move towards process automation of image-processing algorithms is therefore an increasingly important area in object detection and extraction from images. Hence, this study to date has focused on the detection, extraction, and creation processes for modelling urban buildings from single VHR images in an automatic manner, rather than the implementation of semi-automatic methods. Nevertheless, fully automated approaches must be characterised by their propensity to overcome a number of aspects including: (1) the influence of atmospheric and solar illumination, including shadow, shade, and haze; (2) perspective viewing problems, such as occlusions and relief distortions; and (3) the similarity between the building region characteristics and their background, including spectral, textural, and geometric properties, such as shape.

### 1.1.1 Research rationale

Developing realistic 3D models of urban environments may be crucial for generating the energy required to power a city. Energy is an indispensable element in every sector of life and is the foundation of the evolution of economy. The ongoing worldwide impetus to employ renewable energy to generate electricity for heating, cooling and lighting buildings, for heating water, and for a variety of industrial processes, is driven by the negative environmental impacts of fossil fuel production and use, such as global warming. One source of renewable energy is solar power. The process of converting direct sunlight into electricity using solar photovoltaic (PV) technology is one of the best options for the sustainable future energy demands of cities [22]. The assessment of suitable local areas for PV systems plays a critical role in the exploitation of solar energy for successfully integrated solar installations in urban areas. Since buildings are an integral part of the urban scene, roofs should be assessed for solar potential as well as the areas available on the facades of buildings in modern urban landscapes. In addition to the evaluation of the roofs and surfaces, the computation of real shadowing and its effective value should be calculated using the envelope of the shaded zones in daylight hours with the highest solar radiation. To this end, a complete 3D city model is required [23].

In recent decades, the efficient and highly precise detection of complex urban details has been achieved due to the advent of high resolution space-borne images. Existing research recognises the critical role played by optical VHR satellite images, which are considered one of the most important data input sources for a wide range of urban applications [18, 19]. Although extensive research has been carried out using VHR images for detecting and extracting urban features like building roofs, very few studies have investigated the significant area of other surfaces in addition to rooftops available for PV technology based on the identification of the building's envelope geometry through the creation of a 3D city model. Accordingly, this study has identified a gap in the knowledge required to create 3D models of urban buildings from 2D scenes of urban landscapes, captured by the space platforms of remote sensing technology. The creation of 3D models from monocular VHR satellite images to produce reliable geometrical building envelopes with no extra information and in an automated manner is still a difficult task to achieve. The specific problems for this study are based on the urgent need for: (1) a robust, novel, automated approach to derive the heights of buildings using only 2D scenes; (2) an accurate detection method of building footprints (or rooftops) in sophisticated environments, such as urban areas; (3) a way to mitigate the deficiencies of cutting-edge algorithms used for image-processing and computer vision techniques. The latter is complicated by the need to deal with the precise extraction of the geometry of objects (e.g. building edges), the separation of objects from their background, image contrast enhancement, and fully automated implementation.

### 1.1.2 Research motivation

The key motivation of this study can be broken down into three aspects. First, the Middle East Economic Digest MEED's Iraq Power research report [24], using statistics from the Iraqi Ministry of Electricity, noted that improvements in the electricity sector are urgently required. The country's electricity supply was ranked the worst-rated service offered to its citizens following the Gulf War in 1991 and the American invasion in 2003. The report indicates that the average Iraqi household receives electricity for just 7.6 hours a day. As a result of this shortfall, families receive about half of their power needs from household and neighbourhood generators.

Second, with the steadily rising consumption of electricity, as shown in Figure 1.2a<sup>2</sup>, and the inability to meet current demands, the Ministry of Electricity put in place a master plan which

---

<sup>2</sup>[data.worldbank.org/indicator/EG.USE.ELEC.KH.PC?locations=IQ](http://data.worldbank.org/indicator/EG.USE.ELEC.KH.PC?locations=IQ)

operated from 2012 to 2017, as shown in Figure 1.2b<sup>3</sup>. Although the priority of the Iraqi government is to use renewable energy including solar energy, the percentage of power supplied by this sector of energy is much less than that of other energy sectors. Fossil fuel is still the main source of energy. The continuous use of fossil fuel increases  $CO_2$  emissions, leading eventually to negative impacts on the environment (e.g. global warming and pollution). It is thus essential to encourage the government and the population to reduce the potential risk of using the available fossil fuel energy supply by seeking alternative energy sources, thereby mitigating environmental degradation.

Third, the availability of necessary data to achieve any urban project is most likely to be the first requirement and/or task of a project, and this may form a problem for researchers, planners and decision-makers. The collected data from LiDAR, radar, laser scanning and aerial photography is not easily available for a required project in the specific area, as it stands in a developing country. This is due to the cost of employing such technologies, the limited area coverage, and the amount of time and effort, in addition to safety and security issues in conflict areas, compared to Earth observation technology using remote sensing satellites. According to Weng [25], remote sensing is an essential geospatial tool which can be effectively used in sustainable cities, such as Baghdad in Iraq. Therefore, one purpose of this study was to assess the extent to which satellite imageries are capable of narrowing the gap created by the lack of elevation data for creating 3D building models. Further, there is an urgent need to promote the relationship between the two disciplines of remote sensing and sustainability science, in terms of exploiting the great advantages of satellite images in one major field of sustainability, such as energy.

Due to the electricity shortage, Iraq's dependence on fossil fuel and the lack of current studies in third world contexts, it is imperative that research be conducted to find a solution that is both cost effective and environmentally friendly.

## 1.2 Aim and scope of the research

The primary aim of an extensive number of recently published research papers has been to process satellite images to be adequately represented and extracted in a compact form amenable to subsequent recognition and representation. Typically, these representations can be one

<sup>3</sup>[www.meed.com/countries/iraq/power-generation-a-top-priority-in-iraq/3129589.article](http://www.meed.com/countries/iraq/power-generation-a-top-priority-in-iraq/3129589.article)

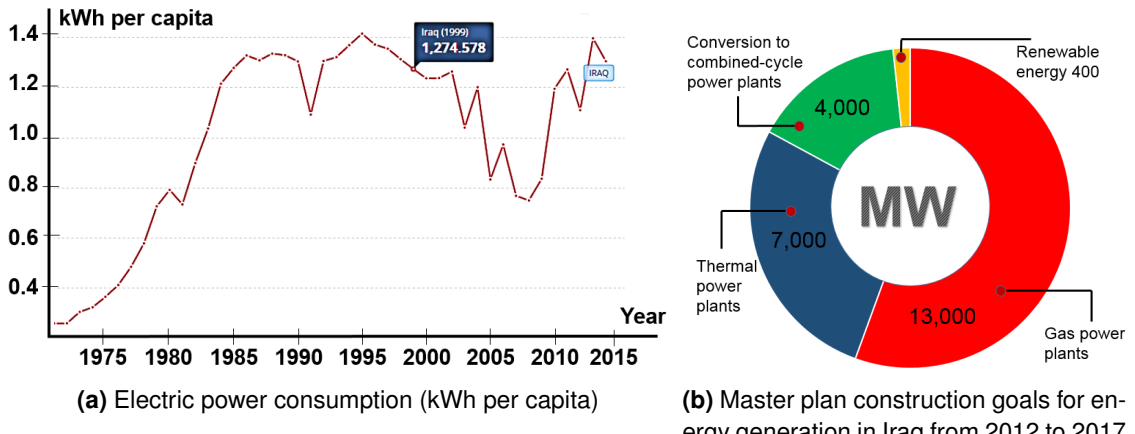


**Figure 1.2:** The steadily rising demand for electricity in Iraq shown by (a) electrical power consumption of time and (b) construction goals for energy generation from 2012 to 21017.

of two basic types: internal, which comprises a region within the pixels, and external, which comprises a region within the boundary. However, the manual process of labelling satellite images is subject to a certain degree of uncontrollable error and requires continuous human labour and attention. Accordingly, one of the great challenges of current image processing/computer vision research is to automate of landmark finding. Hence, this study aims to develop a new approach to model the available surfaces for assessing and exploiting the solar energy potential within an urban environment in an integrated analytical framework.

The main aim of the study can be broken down into the following six objectives:

1. Undertake a detailed review and critique of current methods of feature extraction from remote sensing imageries, and recognise the key challenges of the current image processing and computer vision algorithms and techniques for identifying the geometry of the existing buildings.
2. Develop a method for the automated extraction of significant information in a generic manner with good precision from satellite images, such as shadow regions. Also, improve the precision of shadow region detection by applying efficient morphological processing procedures.
3. Develop an algorithm for the automated detection of buildings and accurately extract their edges to derive actual building geometry within a complex urban landscape using improved shadow regions. Also, use the derived building footprints for computing building orientation and available roof area for solar energy potential assessments.

4. Develop an automated technique for estimating building heights based on the derived shadow regions of buildings. Also, validate the outcomes of the estimation process.
5. Automatically create 3D models of urban buildings by developing an algorithm that reconstructs 3D city models using the outputs of identified building geometry, including the extracted footprints and the estimated building heights.
6. Evaluate and validate the developed approach's results in terms of accuracy and precision in addition to the performance of the developed algorithm using a novel verification approach.

To achieve the aim of the study and its objectives precisely, a strong set of research questions was composed to determine the requirements of data, techniques, and execution environment and to allow the scope of the study to be satisfactory and robust in terms of findings, performance and applicability.

### 1.3 Research questions

The objectives of this study were used to shape the following research questions. These research questions are divided into two categories, as follows:

1. **Can remote sensing data (in particular, optical satellite sensors) be effectively used to extract significant information to support the identification of building geometry?**

This question relates to Objectives Two, Three and Four, and the answer will determine the kind of satellite remote sensing data which will be employed. Therefore, to develop an approach to detecting buildings automatically, the following questions are necessary:

- I. What kind of optical satellite data source can be used to increase the discrimination and/or separation of urban objects and man-made structures?
- II. What types of information need to be extracted and inferred from optical satellite data to help characterise and detect the building regions in urban areas?
- III. Can shadow detection algorithms be used effectively to characterise the buildings, and can shadow regions that belong to building regions be identified effectively after applying the shadow post-processing technique?

IV. Can the heights of buildings be derived from the shadow regions, and can the Jaccard similarity coefficient technique be applied effectively to increase the accuracy of the derived building heights to obtain accurately estimated height values?

**2. How can the derived information from optical satellite images in 2D format be employed to reconstruct building envelopes for implementing 3D models of buildings automatically?**

In order to develop a new automated algorithm for implementing 3D models of buildings from 2D scenes, an integrated framework will be generated. The framework includes the validation and evaluation of the 3D models of buildings that will also be created. This question relates to objectives five and six, and the following questions are necessary:

- I. Can graph-based approaches, such as the GrabCut algorithm, be successfully used for the automated extraction of building footprints based on their shadow regions?
- II. How can the extracted building footprints be modified in case their edges are not straight edges and the final shape of the extracted footprints is not regular?
- III. How can the 3D models of the buildings be produced using the extracted footprints and the estimated heights?
- IV. What level of detail in the created 3D models of urban buildings will be sufficient to illustrate a building's envelope and its available surfaces?
- V. How can the surface availability, orientation and area of the derived building roof be calculated and specified for a primary solar energy potential assessment and analysis?
- VI. How can the developed algorithm and the results from processing the data of the whole developed approach be validated?

## 1.4 Contribution of the present work

With continuous advances in data collection by Earth Observation satellites, remote sensing has become an essential tool for understanding our planet through monitoring natural resources and environments, pre-disclosure, and then managing the risks and disasters caused by nature and humans. Remote sensing data can also help the sustainability and productivity

of natural and human ecosystems [25]. Accordingly, this thesis opens the door to new horizons for emerging collaboration and cooperation between both remote sensing and sustainability science through producing accurate and actionable knowledge using satellite images.

This study contributes to the current body of knowledge in three key ways. The first contribution is developing an approach for extracting building shadow regions from 2D satellite scenes. The detection of shadow regions is remarkably improved through extracting only those shadows (the dark regions) that relate to building regions, in terms of overcoming the complexity and spectral heterogeneity that often exist in urban landscape scenes. This valuable information extracted from VHR images is effectively used to derive urban building structures and determine their geometry.

The second contribution of this study is the performance of the building detection approach, which is based on the graph partitioning theory. The approach is refined to cope with very challenging data in terms of illumination conditions, and image characteristics. Recently released data from modern satellite sensors were used for the first time in this study, and thus, the results from these processed data can help to guide and widen knowledge as researchers in different urban contexts use these data. This is a great advantage because previous studies using Earth Observation data have not dealt with such new data collected by such an advanced optical satellite sensor.

The third contribution of this study is the creation of 3D models of urban buildings from 2D scenes by developing an approach based on shadow information derived from 2D scenes without requiring extra data. The developed approach will enable users to provide 3D building models within urban areas even in places where there is a lack of sufficient data or other methods prove too costly. The geometric representation consists of a polygonal ground plan and the wall and roof surfaces per building, which can be used to make 3D visualisations of buildings and can assist in a range of analytical applications across both public and commercial sectors. In addition, the creation of 3D building models using remote sensing data provides the real locations of buildings and a significant geospatial database with the ability to be updated; it can deal simultaneously and automatically with large areas and many buildings with different geometries and various characteristics. Most importantly, the algorithm developed for deriving the heights of buildings from monocular satellite images reduces much of the processing required for aerial photography or stereo-pair satellite images. The developed approach for estimating building heights can be effectively used in a wide range of urban applications, urban change

detection, risk assessments and urban planning. Particularly, the findings of the present study were encouraging and outperform past approaches, with a 21% reduction in mean error and an overall accuracy of 80%.

Moreover, the automatic process of the shadow detection is a vital pre-processing step for many urban remote sensing applications, especially for images acquired with high spatial resolution. This is because the process can be applied afterwards on different types of optical satellite images for applications that might benefit from the information derived from shadow detection. For example, the detected shadow regions can be used as an element in the process of the automated detection, or these regions can be removed and replaced with actual information of existing ground features to improve the performance of the image classification process, or the shadow regions can be exploited to extract the geometric footprints of urban structures. In this context, the algorithm developed to detect building footprints and extract the 3D models of urban buildings will assist researchers, users, and specialists to overcome the hurdles associated with the manual production of building footprints. Generally, Geographic Information Systems GIS-based approaches for creating building footprints and other traditional methods of producing mastermaps are employed to identify and define the ground boundary of each building, which can take a lot of time. Moreover, the developed approach is fully independent of a user at every stage of data processing and model creation because of data-dependent thresholding.

Regarding renewable energy for urban sustainability, the fourth contribution is the computation of real shadowing from genuine data that can facilitate the assessment of the available building surfaces for integrated solar installations. The information about shadow regions is advantageous for conducting roof and facade brightness analyses for buildings. According to Ko et al. [26], the assessment of solar PV energy potential of rooftops indicates that the shadow cast by building structures substantially influences the amount of installed energy capacity. Therefore, an algorithm is developed in this presented study which is capable of evaluating the overlap of the derived shadow regions and other shadow regions of buildings or man-made, non-building objects.

Lastly, the identification of building geometry by creating 3D building models in complex urban landscapes can increase our understanding of the envelope of the shaded zones in daylight hours that have the highest solar radiation and exploit the solar energy potential in a city. In this respect, the developed study is designed to aid Iraqis in addressing the need to employ solar

PV technology at the local level, which should help mitigate the severe shortage of electric energy in the whole country. Nevertheless, the present study can be applied to any city in the world, especially cities that do not have effective field surveys and advanced techniques to obtain valuable information which can be used in various urban applications. It is also important to reduce greenhouse gas emissions in our atmosphere, caused by human activities such as burning fossil fuels for energy [27]. Therefore, this new methodology presented here can be used to satisfy the requirements of the automated extraction of 3D models of urban buildings for the optimal location of solar energy applications on the rooftops and facades of buildings. The 3D building models can also be used for the preliminary analysis of solar potential at the municipal or neighbourhood level, in addition to larger efforts toward sustainable development and urban planning that the government intends to implement. It is anticipated that this study will be the first of its kind in Iraq in terms of both remote sensing and urban sustainability sciences.

## 1.5 Outline of the Thesis

The thesis has seven chapters, including the present one. The content of each of the chapter is described below. A schematic of the thesis structure is shown in Figure 1.3.

***Chapter 2 - Advances in remote sensing applications for urban sustainability:*** This chapter provides the background of remote sensing systems as an advanced science, technology and indispensable tool for Earth observations. Remote sensing data can play a key role in depicting complex urban landscapes. This chapter also illustrates the applications of remote sensing in urban sustainability development, especially in the realm of renewable energy.

***Chapter 3 - Current state of 3D object creation:*** : This chapter reviews the relevant pioneering image processing algorithms within the scope of this work. It starts with the use of optical VHR satellite images, the available processing techniques, and the ability to infer necessary information and extract objects. The aim of the building shadow region's extraction and the theory behind shadow information are also investigated intensively. Thereafter, the chapter provides a critical and comprehensive review of the existing methods for building detection, geometry identification, and 3D model reconstruction. The chapter concludes by discussing the relationship between building geometry and its impacts on energy efficiency.

**Chapter 4 - Methodology:** This chapter explains the philosophical approach of the research methods that have been adopted and refined to develop a new approach for generating 3D building models. The chapter presents the research design and theoretical methodological framework and also justifies various aspects of the entire employed methodology.

**Chapter 5 - The experiments and results:** This chapter presents the findings of the study. It summarises the collected data, the parameters for conducting data processing, the statistical and computational implementation, and the strategy for accuracy assessment. The outputs of the novel approach taken in this thesis were analysed at every phase of the developed algorithm, starting from image enhancement, then the extraction of shadow regions, building detection, building height estimation, and finally the creation of 3D building models.

**Chapter 6 - Discussion and interpretation of the results:** This chapter discusses the research findings, presenting the implications of the results, particularly the generalisability of the results and their practical applications. This chapter also provides the limitations, justifications, and a critical evaluation of the study in terms of how well the findings address the original research questions.

**Chapter 7 - Conclusion and future work:** This chapter presents the key points of the entire thesis by summarising what was achieved, highlighting the key findings, and reviewing its contributions to the growing body of knowledge on this subject. All conclusions drawn from the study findings are provided in this chapter, with indications of how these findings might be useful for both researchers and practitioners. Future work and recommendations for research are also discussed.

After the body of the thesis, there are appendices for reference, which include the characteristics of the remote sensing systems, the data used in this study, the Matlab code structure, a list of publications generated by this thesis, and skills and achievements certificates.

## 1.6 Summary

This first chapter of the thesis consists of four main sections. Section one includes the research rationale and motivation for this research. Section two presents the main aim of the research and the study objectives. Section three presents the research questions, and section four provides the scientific contribution of the present. In summation, there is an increasing

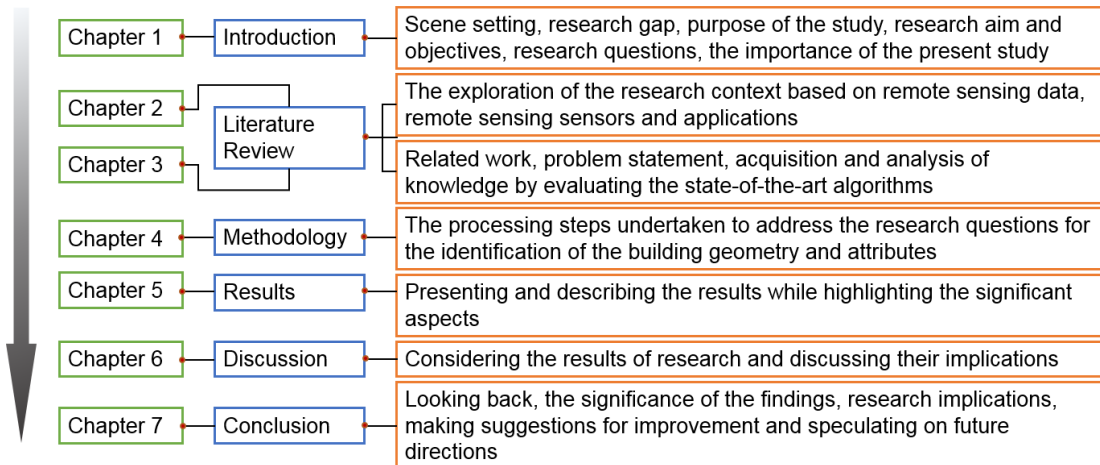


**Figure 1.3:** The structure of the thesis

interest in 3D city models for many different applications and users worldwide. In particular, the use of 3D models of urban buildings is a key part of ongoing research projects geared towards applying renewable energy for sustainable development. A growing interest in renewable energy has resulted in the increased use of remote sensing for the planning, operation, and maintenance of energy infrastructures, particularly ones with spatial variability, such as solar, wind, and geothermal energy.

It is essential to improve our understanding of 3D solar buildings, which enables solar planners, installers, property owners, decision-makers, and authorities to more efficiently measure and assess the availability of building surfaces for PV applications. This will support sustainable urban development in cities. Therefore, this study presents a new approach for the automated modelling of 3D urban buildings from single VHR multispectral images.

## **Chapter 2**

# **Advances in remote sensing applications for urban sustainability**

The current chapter presents a review of the key applications of remote sensing in urban sustainability, and highlights their potential to address problems associated with the expansion of cities. The content of this chapter is divided into four main sections. First, why remote sensing technology is useful in urban studies. Second, existing remote sensing systems and available satellite data resources are reviewed and categorised to provide the context for subsequent discussions. The information will also act as an indispensable resource for urban professionals in identifying appropriate remote sensing data for specific applications. Third, a state-of-the-art review is presented on the applications of remote sensing in urban sustainability. Fourth, the limitations of the reviewed applications are highlighted with a discussion on future directions for research and development.

## 2.1 Remote sensing technology in urban studies

Although cities are engines of economic prosperity and social development that arise from the concentration of people and economic activities, they often manifest in unsustainable urban environments [28]. Economic opportunities in cities act as a catalyst for rapid urbanisation across the globe, but urbanisation rates are uneven and much faster in developing countries [29]. By 2030, the annual average rate of urban growth is expected to be 0.04% in Europe, 1.5% in the USA, 2.2% in East Asia and the Pacific, 2.7% in South Asia, 2.3% in the Middle East and North Africa, and 3.6% in Sub-Saharan Africa [30]. Increasing urban migration has contributed to the unplanned, or poorly planned and implemented, growth and expansion of cities. The latter is a critical factor for urban stakeholders, as unplanned urban growth can have a long-term negative impact on urban sustainability at the local, regional, national and, potentially, inter-governmental scales [22]. Impacts include detrimental economic consequences such as: a reduction in the productivity of key economic sectors [31]; environmental degradation, for example poor air quality and increased urban temperatures and surface run-off [32–34]; and, negative societal impacts, such as increased morbidity and mortality, poorer quality of life, and the fragmentation of neighbourhoods and related communities [35].

Such undesirable changes can be mitigated using evidence-based approaches for the effective risk management of the reformation of urban landscapes and related environmental systems. Gathering evidence of urban change is typically a time and resource intensive process that needs the application of appropriate technologies to identify such risks. Recent advances in satellite remote sensing offer opportunities to cost-effectively monitor urban change and its impact on the complex urban socio-technical systems, enabling stakeholders to make informed decisions which can reduce negative impacts on the environment. Remotely sensed data are an important and powerful source of information on urban morphology and changes over time [36]. In contrast, conventional observation techniques are often logistically constrained in that they require a great deal of effort, cost, and time to obtain information over a large spatial expanse in a consistent manner [37]. The lower cost and availability of data have facilitated the way researchers accomplish research objectives, and have fostered public engagement with remote sensing science.

There is a growing body of literature on the application of urban remote sensing, from the investigation of land-cover and land-use changes, to the monitoring of micro-climatic parameters

and the assessment of renewable energy potential. Increased vulnerability to the impact of climate change and disaster risks, and urban growth resulting from rapid urbanisation, have influenced recent developments on integrated risk modelling that combine remote sensing analysis with social and economic data for urban sustainability assessment [28]. Collaboration between expert stakeholders is essential to realise the full potential offered by remote sensing for urban sustainability [36]. However, there is a lack of understanding among urban professionals of the technical characteristics of remotely sensed data and their suitability for analysis, their limitations, and their application potential. Therefore, the aim is to fill these gaps and increase our understanding of the potential of remote sensing data in sustaining cities by critically reviewing the technical characteristics of available remote sensing sources and their applications for urban sustainability. This chapter of the present thesis can act not only as supportive evidence of research literature to this work but also as a comprehensive resource for the state-of-the-art approaches and solutions, with the ability to provide directions for future research.

## 2.2 Urban Remote Sensing (URS)

Cities are unique because of the existence of dense artificial structures. However, the increasing urbanisation rate will eventually lead to the expedited consumption of non-renewable land resources such as water (at and under ground level) and food Longley [38], and energy resources such as oil, coal and gas with environmental, social and economic impacts on developing and developed countries alike [39]. Thus, the growth of urban areas can result in substantial land-cover and land-use changes, and these make an ideal sustainability case for the use of remote sensing. The next sections are devoted to a review of remote sensing systems and applications within urban environments, focusing on urban growth, sprawl and change, the environmental impacts of urban growth, and sustainable energy applications.

### 2.2.1 remote sensing technology and systems

Remote sensing is able to know what an object is without physical contact, as in [40], which was inspired by [41]. The three distinct stages of the development of remote sensing instruments are illustrated in Figure 2.1. First generation remote sensing instruments were of low spatial resolution, 1 km–100 m, increasing to 30 m–10 m in the second generation. The third generation instruments are more capable of observing the Earth's surface with a very high

spatial resolution, 5 m–0.5 m and less, enabling the acquisition of further spatial details, resulting in more accurate feature recognition. To enable the reader to gain a high-level overview of remote sensing characteristics, satellites are categorised based on their orbit, their sensor mode and instrument, resolution, and the wavelength of the electromagnetic radiation (EMR), as shown in Figure 2.2.

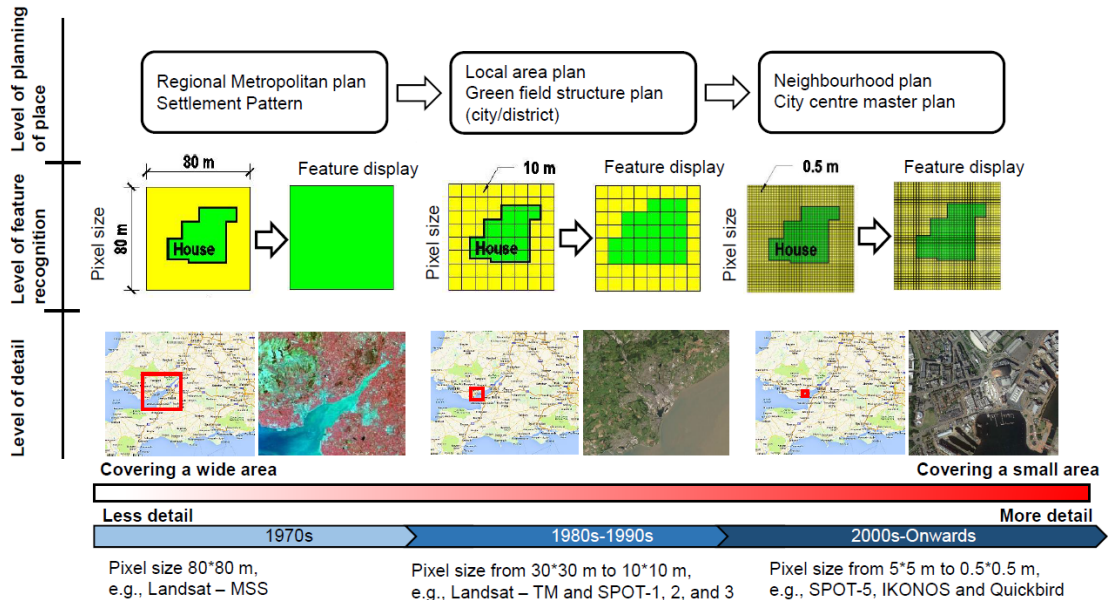


**Figure 2.1:** A comparison of satellite generations in terms of detail, feature recognition, and planning requirements. The red square represents the spatial resolution of the adjacent remote sensing image. An image with a pixel size of 80 m (Landsat-MSS) cannot recognise an object such as a house, but its features can be effectively recognised with a pixel size of 0.6 m (QuickBird)

**Orbit.** Remote sensing satellites roam in two kinds of orbit, sun-synchronous and geostationary. Most remote sensing platforms such as Landsat, SPOT, and IKONOS operate in a near-polar (i.e. sun-synchronous) orbit at low altitudes, passing over each area before noon, at 10.30 am local time [19]. This allows the acquisition of clearer images of the Earth's surface over a particular area on a series of days in similar illumination conditions, i.e. when the sun position is optimal, between 9.30 am and 11.30 am local time [42]. In contrast, geostationary satellites are ideal for some communication and meteorological applications because of their very high altitudes, allowing continuous coverage of a large area of the Earth's surface, although with the trade-off of low spatial resolution.

**Sensor mode and instrument.** Spatial resolution is based on pixel size and is said to be low when it is greater than 100 m, medium when between 10 m -100 m, and high when less than

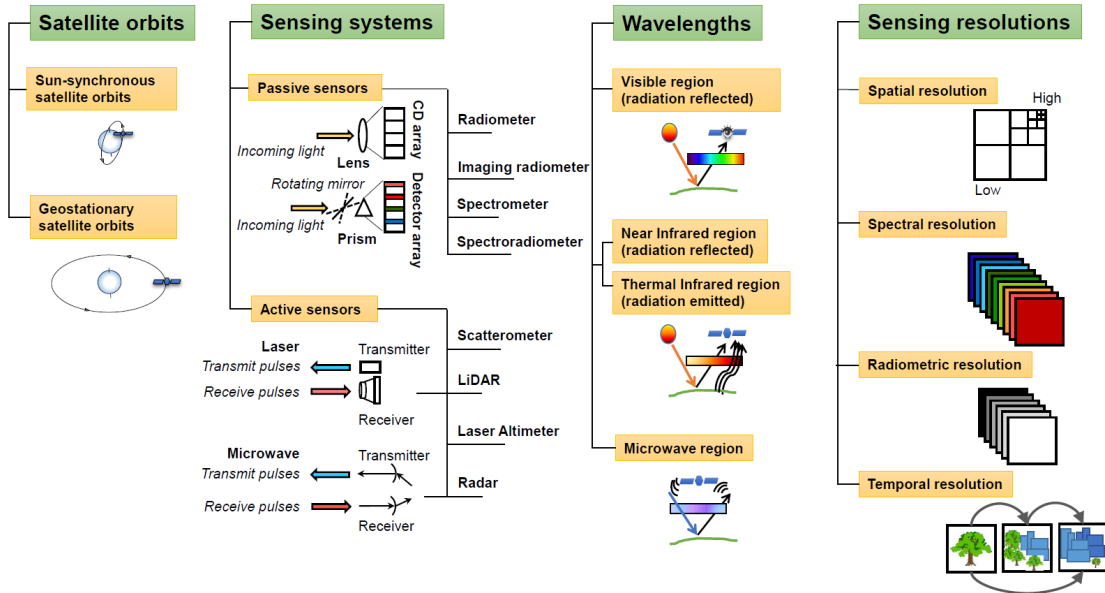
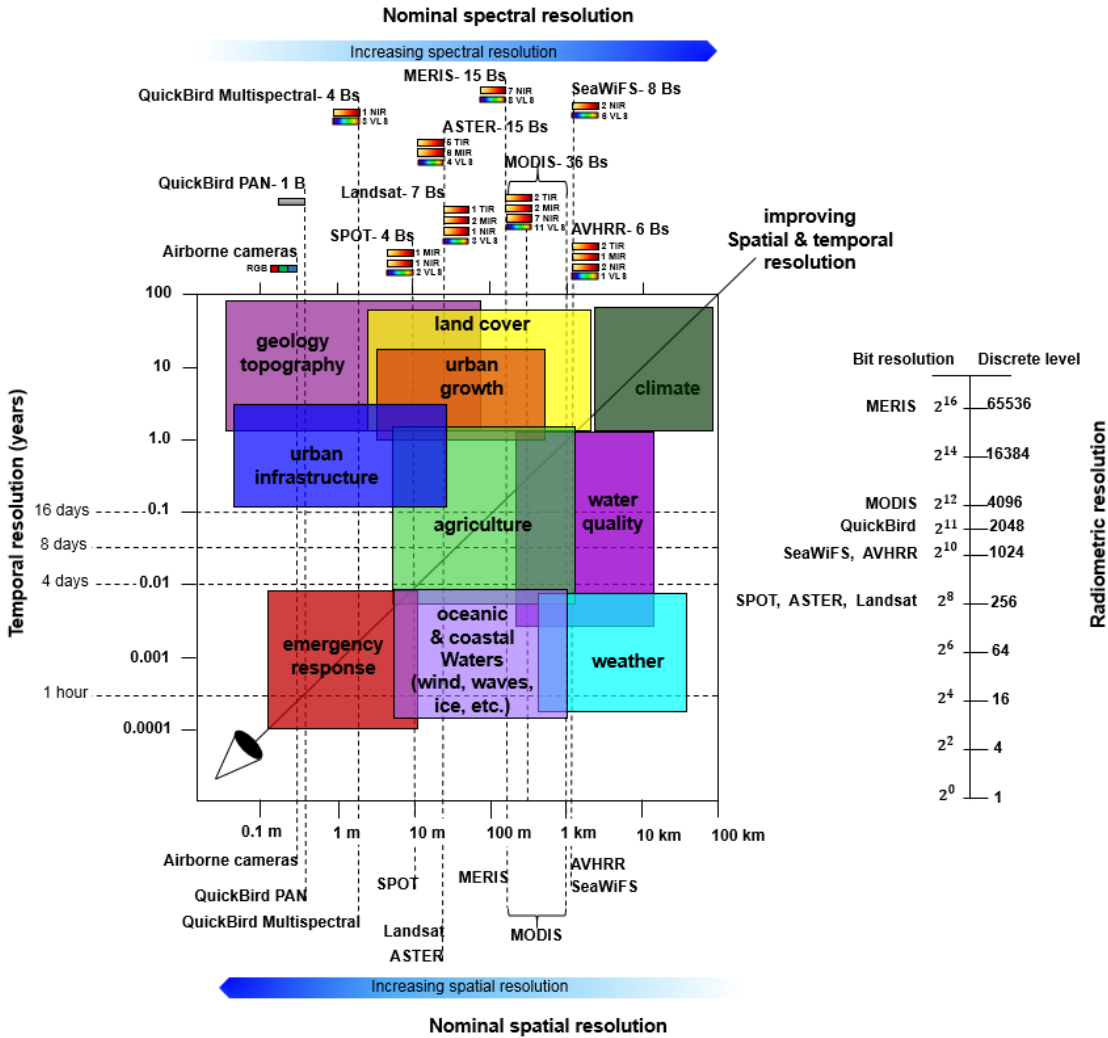


Figure 2.2: Classification of remote sensing sensors based on their characteristics

10 m [43]. Depending on the on-board sensors' spatial resolution, remote sensing systems can be classified into two groups: low/medium, and high/very high. Existing low/medium, and high/very high remote sensing systems and their potential applications are given in Appendix A, Tables 1 and 2, respectively. Most of the data are available at low cost, and are often free to download on the Internet. A summary of selected websites for obtaining data, such as satellite imagery, radar, LiDAR, hyperspectral, aerial orthoimagery and digital spectral library data are presented in Appendix A, Table 3.

**Resolution.** The trade-off between spatial and temporal resolution needs to be reconciled for the selection of satellite images for a particular application, as illustrated in Figure 2.3. For instance, a high temporal resolution is essential for emergency situations, such as landfall due to hurricanes, because emergency situations change rapidly and require frequent observations on the day. In contrast, urban infrastructure planning applications require spatial understanding over a longer period, for which annual observations are often sufficient. However, both cases sometimes require high spatial resolution images to observe their processes comprehensively. On the other hand, high temporal resolution is required for rapidly changing applications such as weather. Operational weather forecasts, therefore, require satellite observations with high temporal resolution, which often comes at the cost of spatial resolution. Each remote sensing application, thus, has its own unique resolution requirements which need to be appreciated.



**Figure 2.3:** An overview of the spectral, spatial, temporal, and radiometric resolution of different optical satellite systems. Spatial and temporal resolution requirements vary widely for monitoring terrestrial, oceanic, and atmospheric features and processes. Each application of remote sensing sensors has its own unique resolution requirements and, thus, there are trade-offs between spatial resolution and coverage, spectral bands and signal-to-noise ratios. Notes and symbols: Bs the number of spectral bands, which include the visible light spectrum (VLS), near-infrared (NIR), mid-infrared (MIR), and thermal infrared (TIR) portion of the electromagnetic spectrum; RGBa colour digital image; and, PANa panchromatic image. Adapted from Jensen [44] and Purkis & Klemas [43]

## 2.2.2 remote sensing applications in urban environments

**Urban growth, sprawl and change.** Urban growth refers to the transformation of the landscape from undeveloped to developed land [45]. More specifically, the growth away from central urban areas into homogeneous, low-density and typically car-dependent communities is often referred to as urban/suburban sprawl. In developing countries, urban sprawl can be unplanned

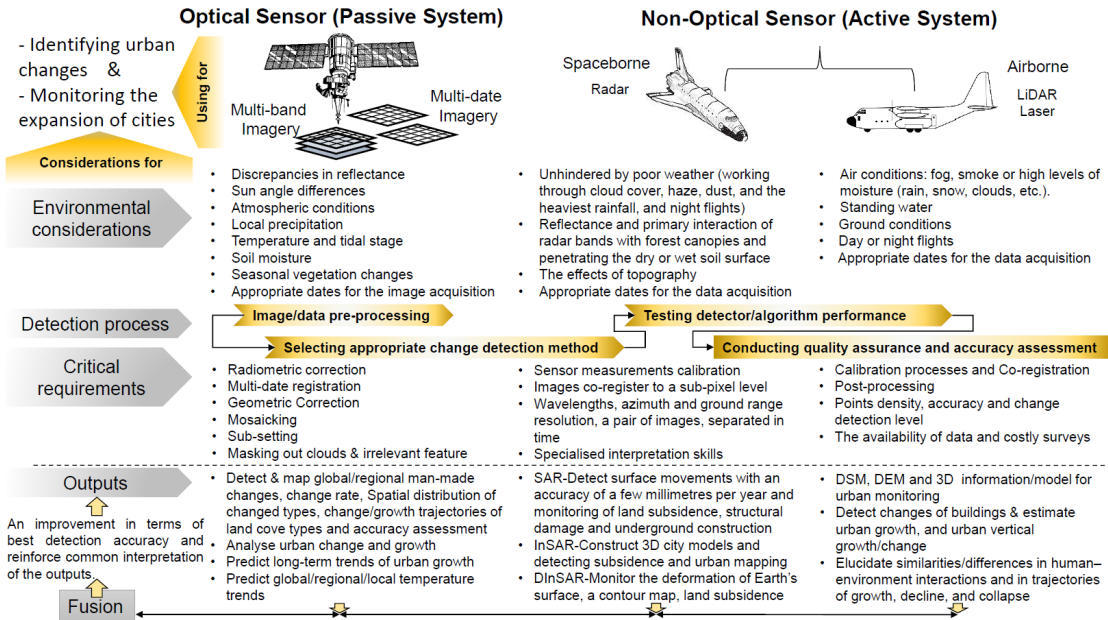


**Figure 2.4:** A comparison of environmental considerations and critical requirements between optical and non-optical sensors for urban change detection and the monitoring of city expansion

and uncontrolled [46]. Consequently, urban growth leads to the loss of farmland, rising economic and social issues, and increased water and energy consumption, with associated greenhouse gas emissions [47]. From the stakeholders' point of view, the expansion of cities is a crucial change in terms of landscape transformation processes and urban sustainability. Continuous spatial and temporal monitoring is required to evaluate and understand such changes. The capabilities of remote sensing satellites make them a robust and reliable source of data for monitoring the expansion of cities at different spatiotemporal scales [48].

In a recent study, Cockx et al. [49] reported that land-cover and land-use information from remote sensing data is a key component in the calibration of many urban growth models. Van de Voorde et al. [50] noted that there is a strong relationship between the change of form in land-cover and the functional change in land-use through the analysis of satellite imageries. Classification-based approaches are routinely used to detect the expansion of cities by investigating land-cover and land-use changes [51–58], and the analysis of urban sprawl [59–64]. Figure 2.4 provides a comparison of the environmental considerations and critical requirements between optical and non-optical sensors for urban change detection and the monitoring of city expansion.

Medium-resolution satellite Landsat imagery has been widely used for urban change detection. Yang and Liu [65] detected the presence of urban impervious surfaces to characterise

urban spatial growth. Ji et al. [66] characterised the long-term trends and patterns of urban sprawl using multi-stage Landsat Multi-Spectral Scanner (MSS), Thematic Mapper (TM) and Extended Thematic Mapper (ETM+) images, based on landscape metrics. Similarly, Du et al. [67] used a time-series of multi-temporal Landsat TM images to derive overall change trends through a normalised difference vegetation index-based (NDVI) classification. Taubenbck et al. [68] detected temporal and spatial urban sprawl, while Abd El-Kawy et al. [69] demonstrated that human activities were responsible for land degradation processes. Pham et al. [70] and Schneider [71] showed that remote sensing time-series data can be effectively used to determine long-term urban change trends. However, the mapping of some inner city areas for the observation of urban growth or detection of subtle change is challenging at this level of spatial resolution.

Satellite images at medium spatial resolution 10 m - 100 m cover a large area, often making the urban landscape appear homogeneous, as different attributes of land within one pixel are combined. Researchers have, therefore, attempted to fuse multi-source (remote sensing, socio-economic, vector) data with medium-resolution images to improve the overall resolution, increase model accuracy, and make change detection more perceptible. Jia et al. [72] proposed a method of improving land-cover classification by fusing Landsat 8 Operational Land Imager (OLI) NDVI at 30 m with MODIS NDVI at 250 m, resulting in a 4% improvement in the overall classification accuracy compared to a single temporal Landsat data. On the other hand, Singh et al. [57] showed that the fusion of LiDAR and Landsat data can lead to increased accuracy in distinguishing heterogeneous land-cover over large urban regions. In another study by Martinuzzi et al. [73], land-use change was inferred from Landsat ETM+ images integrated with aerial photos and population census data to reveal urban growth and sprawl. Change detection of urban land-use from low- and medium-resolution imagery is error-prone without any improvement from other high-resolution remote sensing data or integration with supplementary data, such as census data. This inaccuracy is attributed to mixed pixels that represent a spectral mixture of diverse built-up materials, eventually leading to greater uncertainties in land-cover/land-use classification.

The issue of mixed pixels can be resolved by obtaining more detailed information on urban morphology using high spatial resolution sensors. IKONOS pan-sharpened and SPOT images were combined with different vector maps by Noor and Rosni [74] to analyse the geospatial indicators based on spatial factors. Nassar et al. [75] identified the spatial evolution, urban

expansion and growth patterns based on a hybrid classification method and landscape metrics, using different datasets to derive suburban classes (e.g. residential, commercial and industrial). Further, Kuffer and Barroso [76] proposed an approach to monitor unplanned settlements in residential areas by identifying the morphology (size, density, and layout pattern) of urban areas. The mapping of urban land-cover and land-use from high spatial resolution images often faces the issue of spectral variability within one-class and the shadows of buildings and trees that reduce class separability and classification accuracy. Nevertheless, NASA [77] reports that the progression in remote sensing-based urban area mapping is contributing to the creation of more accurate and detailed maps of cities, enabling an unprecedented understanding of the dynamics of urban growth and sprawl.

**The environmental impacts of urban growth.** At a time when informal settlements are emerging as a result of population growth, the likelihood of increasing the occupation of spaces inside and outside cities will be higher, as is the risk of inappropriate urbanisation. The occupation of land as an uncoordinated form is motivated by several factors, namely: the limited income of urban dwellers, increased housing demand, the lack of sustainable long-term urban planning, and the lack of legal buildable land. These factors have led to the improper development of cities/urban areas, even in areas considered to be at high risk of natural disasters, such as landslide and flooding. The negative effects of the expansion of cities and urban growth are more motivational as a research agenda than the positive ones. One such application is the assessment of the quality of life and socio-economic conditions in urban slums, since for every three city dwellers worldwide, one lives in a slum [78]. Many authors have applied remote sensing techniques to identify slum locations and classify slums from other land-use types [79–84]. Graesser et al. [85] distinguished the boundaries between formal and informal settlements using an image classification approach. Weeks et al. [86] identified the location of slums and quantified their area using a vegetation-impervious-soil (VIS) model, image texturing, and census data, deduce land-use effects and to produce a slum index map. According to Hagenlocher et al. [87], there is a clear link between the increasing number of new, temporary population settlements and decreasing natural resources in the vicinity of these settlements. This was revealed using a time-series of VHR optical satellite imagery. In this context, the identification of a slum core and its impact on the environment using texture-based identification of urban slums was performed by Kit et al. [81], and slum area change patterns were identified by Kit and Lüdeke [83]. Exploiting textural differences between urban land-uses derived from

satellite imageries can be beneficial for improving urban mapping with regards to spectral heterogeneity within urban landscapes, as illustrated in Figure 2.5. It shows the degree of spatial autocorrelation in the slums (informal) compared to the residential areas (formal).

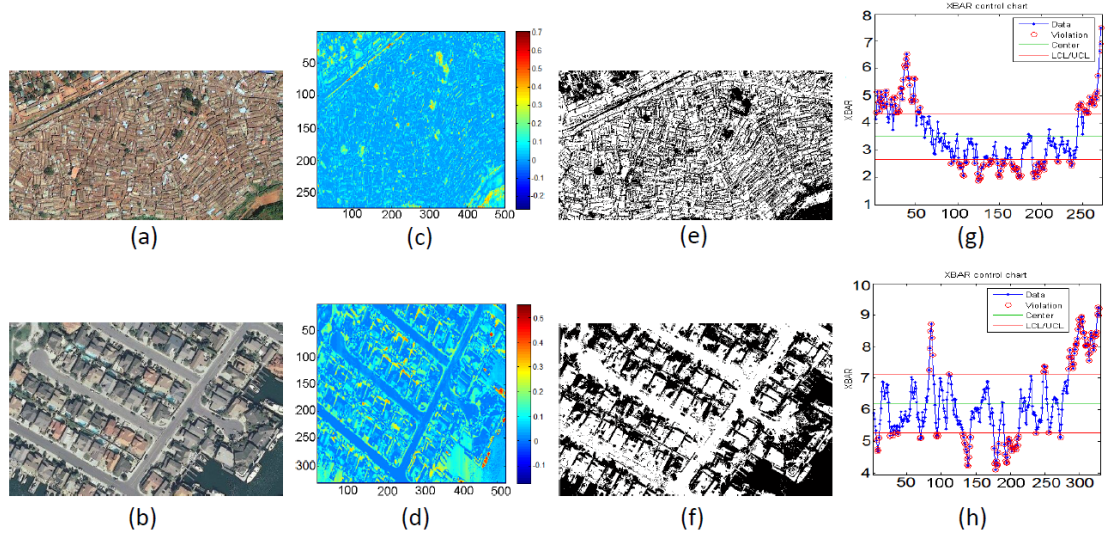


**Figure 2.5:** The texture-based identification of urban slums from remote sensing data. (a) A QuickBird scene of informal residential area (slums). (b) A GeoEye-1 scene of a formal residential area. (c) and (d) Moran's I measuring spatial autocorrelation based on simultaneous feature locations and values. (e) and (f) The difference in the texture in the binary form. (g) and (h) The XBAR control chart of (c) and (d) to analyse the greatest similarity between the pixel values in each subgroup and the greatest difference between the pixel values in different subgroups

Regarding other negative impacts, increased city size and dweller numbers causes a corresponding rise in urban air and surface temperatures, known as an Urban Heat Island (UHI) Figure 2.6. A positive correlation has been deduced between impervious surfaces and land surface temperature (LST) in the sprawled areas [32, 88], where impervious surface areas become warmer than the surrounding areas. Two main factors cause the UHI effect. First, heat is absorbed from sunlight and subsequently released as thermal infrared radiation by dark surfaces, such as pavements, roads and rooftops. The temperature of these surfaces can reach 28-39 °C higher than the surrounding air [89]. Second, there is a relative lack of vegetation cover in urban areas, especially trees, which work to cool air and balance the components of the environment.

Li and Yin [90] developed an approach to calculate the UHI effect ratio (UHIER), and this suggests that urban areas have a relatively higher temperature than the neighbourhoods surrounding the city. Senanayake et al. [91] identified UHIs and the distribution of LST by analysing

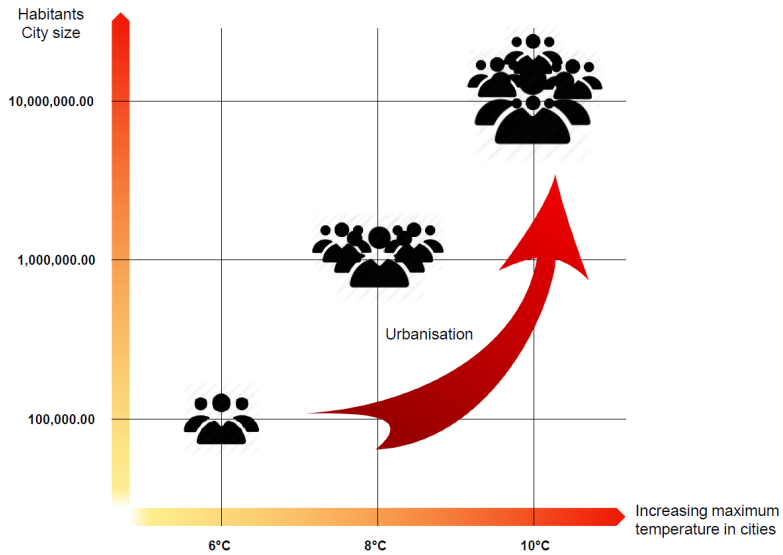


**Figure 2.6:** Increasing temperature due to increased city size and the number of city dwellers.  
Adapted from Bhatta [89]

vegetation cover using NDVI. Le-Xiang et al. [92] assessed the impact of land-use and land-cover on LST, suggesting a higher surface temperature of around  $4.56^{\circ}\text{C}$  in newly developed urban areas, due to decreased vegetation caused by urban expansion.

Several studies have illustrated the use of remote sensing data in analysing air pollution and its quality. Numerical simulations based on satellite data were performed by De Ridder et al. [93] to evaluate the effect of urban sprawl on air quality, surface temperature and their effects on people. In a recent study, Bechle et al. [94] evaluated the ability of the satellite data to resolve urban-scale gradients in ground-level nitrogen dioxide ( $\text{NO}_2$ ) within a large urban area. Wang et al. [34] derived high resolution aerosol optical thickness (AOT) from Terra-MODIS data, and created four models to analyse the relationship between AOT and  $\text{PM}_{2.5}$ . Data from the same satellite were used by Nichol et al. [95] to assess 3D air quality over an urban landscape. Sifakis et al. [96] developed an approach to quantify AOT over urban areas by fusing different spectral bands of satellite imageries based on image processing techniques.

With regards to the evaluation of water quality and quantity, Chawira et al. [97] proposed a semi-empirical band ratio model to derive and quantify water quality parameters in two polluted lakes. They also identified the causes of pollution as domestic waste and raw industrial sewage, poor garbage collection, agriculture, and certain mining activities, *inter alia*. Jay and Guillaume [98] used hyperspectral data to map depth and water quality. Trochta et al. [99] presented the identification of water types with different biogeochemical properties and drivers through an optical classification scheme based on remote sensing data. Hunink et al. [100] studied

the relationships between groundwater usage and crop type in irrigated areas. The realistic spatial distribution of air and water quality can help to define the urban landscape quality (ULQ). However, the use of census data alone to quantify ULQ can result in unreliable estimates as census data do not adequately capture environmental factors such as waterborne diseases and various types of pollution (air, water, and toxic chemicals). Satellite remote sensing data can fill this gap and improve our understanding of the relationships between environmental factors and the urban landscape. Table 2.1 summarises the potential and shortcomings of remote sensing data for investigating the impact of urban expansion.

**Table 2.1:** Consequences of expansion of cities against observation variables, impacts, potential and limitations of urban remote sensing applications

Consequences of the expansion of cities			
	Temperature	Air quality	Water quality
Observation variables or parameters	<ul style="list-style-type: none"> <li>Dark surfaces (low albedo)</li> <li>The lack of vegetation</li> </ul>	<ul style="list-style-type: none"> <li>Ozone</li> <li>Nitrogen dioxide</li> <li>Sulphur dioxide</li> <li>PM<sub>2.5</sub> and PM<sub>10</sub></li> <li>Carbon dioxide</li> <li>Dust aerosol</li> </ul>	<ul style="list-style-type: none"> <li>Turbidity</li> <li>Total suspended sediment</li> <li>Volatile suspended solids</li> <li>Polychlorinated biphenyls</li> <li>Chlorophyll</li> </ul>
Impacts	<ul style="list-style-type: none"> <li>Increased energy consumption &amp; cost</li> <li>Elevated emissions of air pollutants (<math>SO_2</math>, <math>CO</math> and <math>PM</math>) and greenhouse gases (<math>CO_2</math>) global warming</li> <li>Compromised human health and comfort</li> <li>Impaired water quality</li> </ul>	<ul style="list-style-type: none"> <li>Serious human health problems</li> <li>Inhibited plant growth</li> <li>Smog and acid rain</li> <li>Climate change</li> </ul>	<ul style="list-style-type: none"> <li>Change in colour</li> <li>More total runoff volume and flooded land, untreated or poorly treated sewage</li> <li>Surface water pollution</li> <li>Groundwater pollution</li> <li>Reduced storage capacity, flood control, light penetration in water-minimising fish yield</li> <li>Human health</li> </ul>

*continued on the next page*

**Table 2.1:** Consequences of expansion ...

(cont. from previous page)

Consequences of the expansion of cities			
	Temperature	Air quality	Water quality
Potential	<ul style="list-style-type: none"> <li>• Observe and map the surface urban heat island (SUHI)</li> <li>• Identify the spatial patterns of upwelling thermal radiance</li> <li>• Identify urban construction materials</li> <li>• Time synchronised dense grid of temperature over a large area</li> </ul>	<ul style="list-style-type: none"> <li>• Monitor and map the compositions of air over the globe with high spatial and temporal coverage</li> <li>• The combination of satellite observations with ground based in situ for monitoring, modeling, simulating and forecasting the air quality and climate change</li> <li>• Improve the qualification of the air compositions</li> </ul>	<ul style="list-style-type: none"> <li>• Assess surface water, subsurface water, soil moisture and groundwater with reasonable accuracy</li> <li>• Assess pollutants spectrally and suspended sediments using regression based optical models</li> <li>• Monitoring the vast spatial coverage and long term, remotely recognition concentrations of sediments chlorophyll and detecting the presence of water beneath vegetation using the microwave spectrum</li> </ul>
Limitations and/or considerations	<ul style="list-style-type: none"> <li>• Clouds (thermal imageries)</li> <li>• Surface radiative properties</li> <li>• Spectral wavelength</li> </ul>	<ul style="list-style-type: none"> <li>• Cloud (the accuracy of air quality models)</li> <li>• The lower levels of the atmosphere where exposure to pollution occurs</li> <li>• Chemical and physical measurements through the atmosphere</li> </ul>	<ul style="list-style-type: none"> <li>• Properties of scattering and absorption of suspended sediments and dissolved organic matter make it difficult to determine the intensity of reflected light</li> <li>• Demand repeated monitoring on short time-scale</li> <li>• Demand in situ measurements for calibration the estimation of water quality</li> <li>• Poor retrieval of water constituents due to shadows cast on water bodies</li> <li>• Correction for atmospheric influence on remote sensors is necessary to differentiate the patterns of water quality</li> </ul>

## 2.3 Sustainable urban environments

From the aforementioned challenges, sustainable urban development is a notable trend arising from the need to maintain sustainable urban and ecological environments. Sustainable urban development faces increased challenges on a daily basis due to deficiencies in the planning

approaches employed to address these challenges [101]. The next sections illustrate the importance of using remote sensing techniques as an effective tool in facilitating the establishment of sustainable development, through providing a wealth of environmental data on a range of spatial and temporal scales. A major role that remote sensing can play is in the provision of indicators of environmental conditions for sustainable development, and its associated decision-making [102].

### **2.3.1 Sustainable development**

In recent years, there is an emerging trend worldwide towards pursuing green technologies and low-carbon economies and lifestyles [25]. However, the sustainability issue is not new because it began with the 1992 United Nations Conference on Environment and Development (UNCED) in Rio. UNCED Principle Three characterised sustainable development as that “the right to development must be fulfilled so as to equitably meet the developmental and environmental needs of present and future generations.” Principle Four stated that “in order to achieve sustainable development, environmental protection shall constitute an integral part of the development process and cannot be isolated from it”, as mentioned by Weng [25]. In practical terms, sustainable development is a multifaceted concept, subject to many perspectives according to personal experience, viewpoint and discipline [103]. From the perspective of the ecosystem, and according to the three pillars of sustainable development ecological, economic, and social objectives the balance between these three values and sustainability should come from the interaction of all three components in any sphere. The inability to promote these components together in an efficient manner is likely to prevent the achievement of sustainable cities. Therefore, in order to study and model the objectives of what we try to sustain, and over which time scale and geospatial scope, the spatial and temporal scales must be considered as the key elements in assessing environmental and ecological sustainability [104]. Accordingly, *in situ* data collection with the aid of earth observation technology has greatly increased research and development in terms of observing, monitoring, measuring, and modelling many of the variables related to human and natural ecosystem cycles.

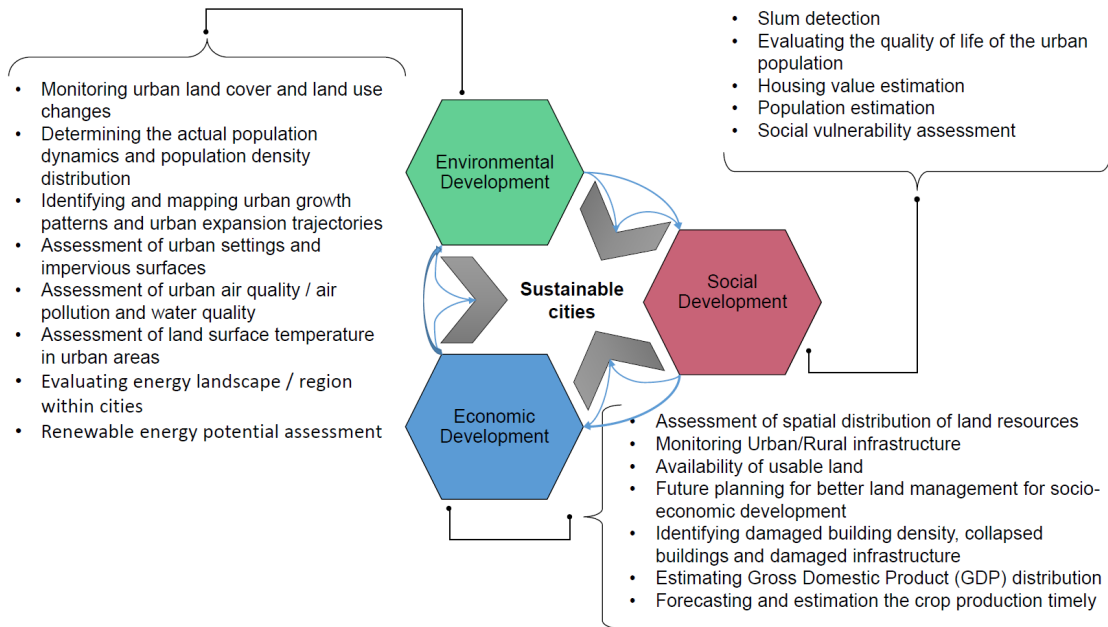


Figure 2.7: Key urban sustainability applications of remote sensing

### 2.3.2 Urban sustainability using remote sensing technology

Urban sustainability must be taken into account for planned urban change, such as urban growth, to minimise our reliance on natural resources and non-renewable energy. As our cities grow, the impact on climate change can be mitigated by minimising the ecological footprint, reducing pollution, increasing land-use efficiency, recycling waste, and increasing the use of sustainable materials, as well as by maximising renewable energy use. In essence, the aim of urban sustainability is therefore to manage resources and provide services through the effective design and implementation of policies; this requires access to detailed information on urban indicators. Remote sensing can offer cost-effective solutions for collecting vast amounts of data compared to resource-intensive conventional approaches, such as survey and field monitoring. In this context, Figure 2.7 provides an overview of the key urban sustainability applications of remote sensing when integrated with the available environmental, economic, and social data. Furthermore, because of the aforementioned advantages of remote sensing data in urban areas, satellite-based Earth observation provides promising applications to implement a sustainable energy supply. Examples of remote sensing-aided applications are detailed in the following sections.

### 2.3.3 Renewable energy

Renewable energy resources in urban areas are highly sensitive to their location, surroundings Mourshed et al. [105] and micro-climate [28], and are dependent on geographical constraints on development and regional economic policies [106]. Remote sensing is particularly suited to the geospatial assessment of the potential of Renewable Energy Technologies (RET), such as wind, solar, wave, biomass, and geothermal energy. Gooding et al. [107] estimated the physical and socio-economic potential for generating electricity from roof-mounted PV using digital surface models (DSMs) from LiDAR. LiDAR data was used by Jakubiec and Reinhart [108] to create a map of the PV potential of individual buildings.

Remote sensing can offer a cost-effective means of identifying those urban surfaces where solar PV can be installed. Kabir et al. [109] used QuickBird scenes to determine suitable bright rooftops in Dhaka for PV applications, by applying an object-based image analysis (OBIA) approach. Wang and Koch [110] investigated the optimal locations of PV and base electricity prices resulting from solar energy. Bergamasco and Asinari [23] computed the actual roof surface available for PV installations by classifying roof typologies. Baluyan et al. [111] discriminated rooftops from non-rooftops based on colour/grey level during image segmentation, support vector machine (SVM) classification, and the histogram method. Jiang et al. [112] analysed the spatiotemporal properties of the wind field using the QuikSCAT satellite data to produce a wind resource map. Walsh-Thomas et al. [113] extended the use of satellite remote sensing data to provide insights into the impact of large scale wind farms on land surface temperature (LST). An extensive review of the potential of remote sensing techniques in examining geothermal resources was published by Van Der Meer et al. [114]. Ahamed et al. [115] reviewed the biophysical characteristics of biomass for managing energy crops at given sites. Rusu and Onea [116] evaluated wind and wave energy resources along the Caspian Sea. Based on the fused data from multiple satellites, Kaiser and Ahmed [117] derived the spatial distribution of hot springs, lineaments, and geothermal localities for RET applications.

The use of remote sensing techniques has advantages over established approaches and datasets arising from the ability to use them for the detection, visualisation, and documentation of developments and trends. For instance, this includes the transformation of landscapes in the context of energy policy decisions, increasing energy consumption, and growing land use conflicts, in the wake of steadily progressing land use by settlements and transport infrastructure [118]. To succeed in the energy-related planning and management sector, the provision

of geoinformation by satellite-based remote sensing with regard to timeliness, coverage, comparability, spatial details, and update costs in the form of reliable services is central. This is especially so concerning the exploitation of synergies with existing datasets, such as spatial data produced by cadastral survey. Nevertheless, unclear responsibilities, requirements, and user needs currently complicate targeted developments. In this vein, the next section focuses on an urgent need for the coordination and pooling of research and development activities to sustain cities and their environmental systems utilising remote sensing technology.

## 2.4 Remote sensing challenges and opportunities and key trends in the existing literature

The studies discussed in the previous sections demonstrate the significant potential of remote sensing in the assessment, monitoring and planning of sustainable urban areas. Figure 2.8 summarises the reviewed literature on urban growth, sprawl, and land-cover and land-use changes, while Figure 2.9 summarises previous work on slums, air and water quality, temperature assessment, and renewable energy. In addition, Table 2.2 presents the state-of-the-art in taxonomy, detection, extraction and pattern recognition in urban applications, focusing on machine learning algorithms such as neural networks, decision trees, and random forests. The algorithmic aspects of data analysis for various urban applications are also summarised.

In the context of constrained resources, increasing urbanisation, rising vulnerability to climate change impacts, and ageing populations, cities need to be sustainable, adaptable, smart and resilient [119]. Decisions have to be based on the contextual evidence of the performance of the urban environment, which must be collected at a higher resolution in a cost-effective manner. Moreover, expanding urban areas affect the environment primarily by increased energy consumption from buildings, transport, and industry [43], and by reducing albedo through land-cover change from vegetation to built-up, and this results in increased LST [120]. In turn, these issues can further reinforce climate change drivers and act as a positive feedback loop, i.e. increased LST may result in more energy consumption, and therefore more warming, which in turn will result in further increases in LST. The potential for the use of remote sensing in tackling these urban challenges is summarised in Figure 2.10.

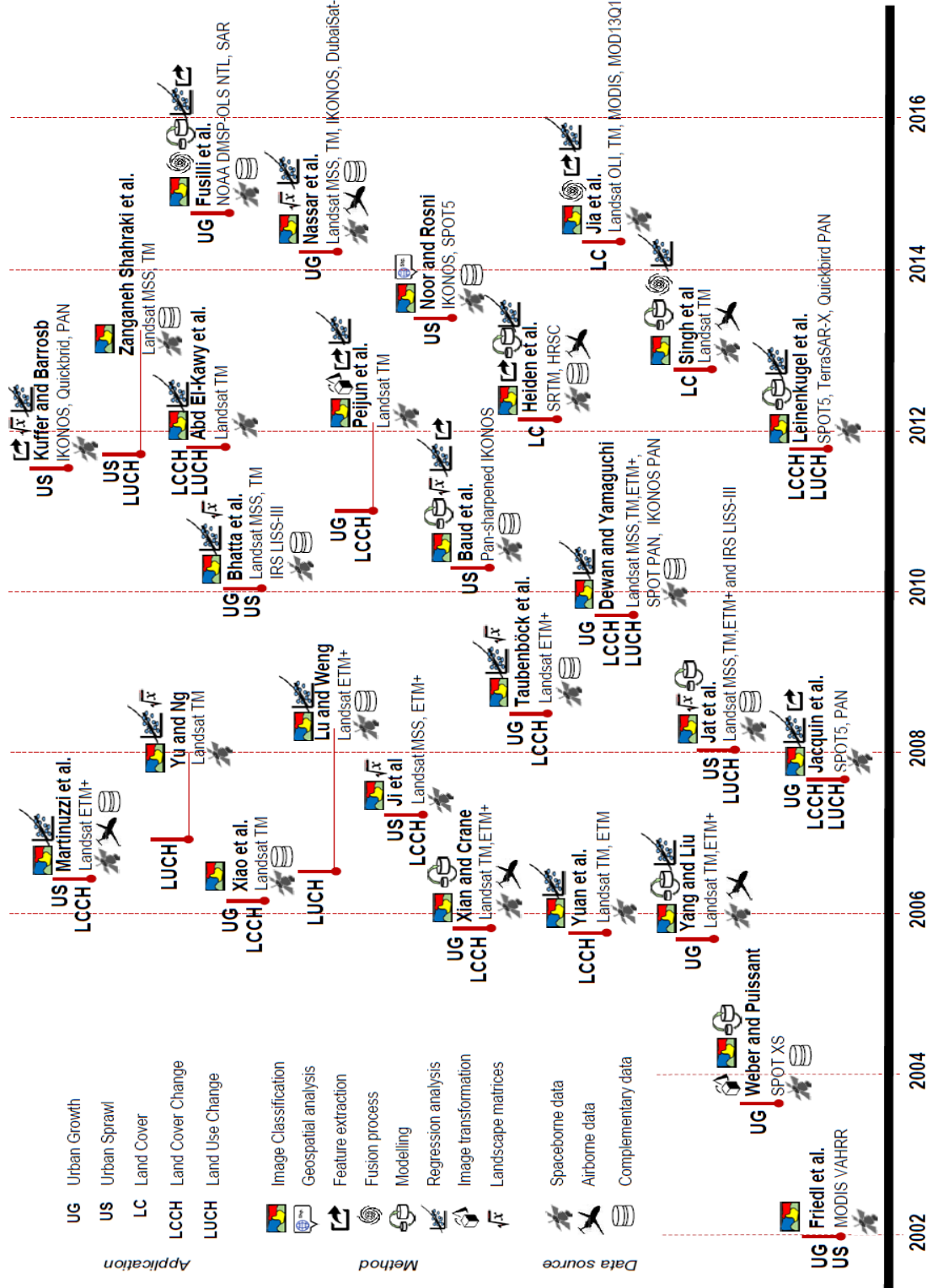
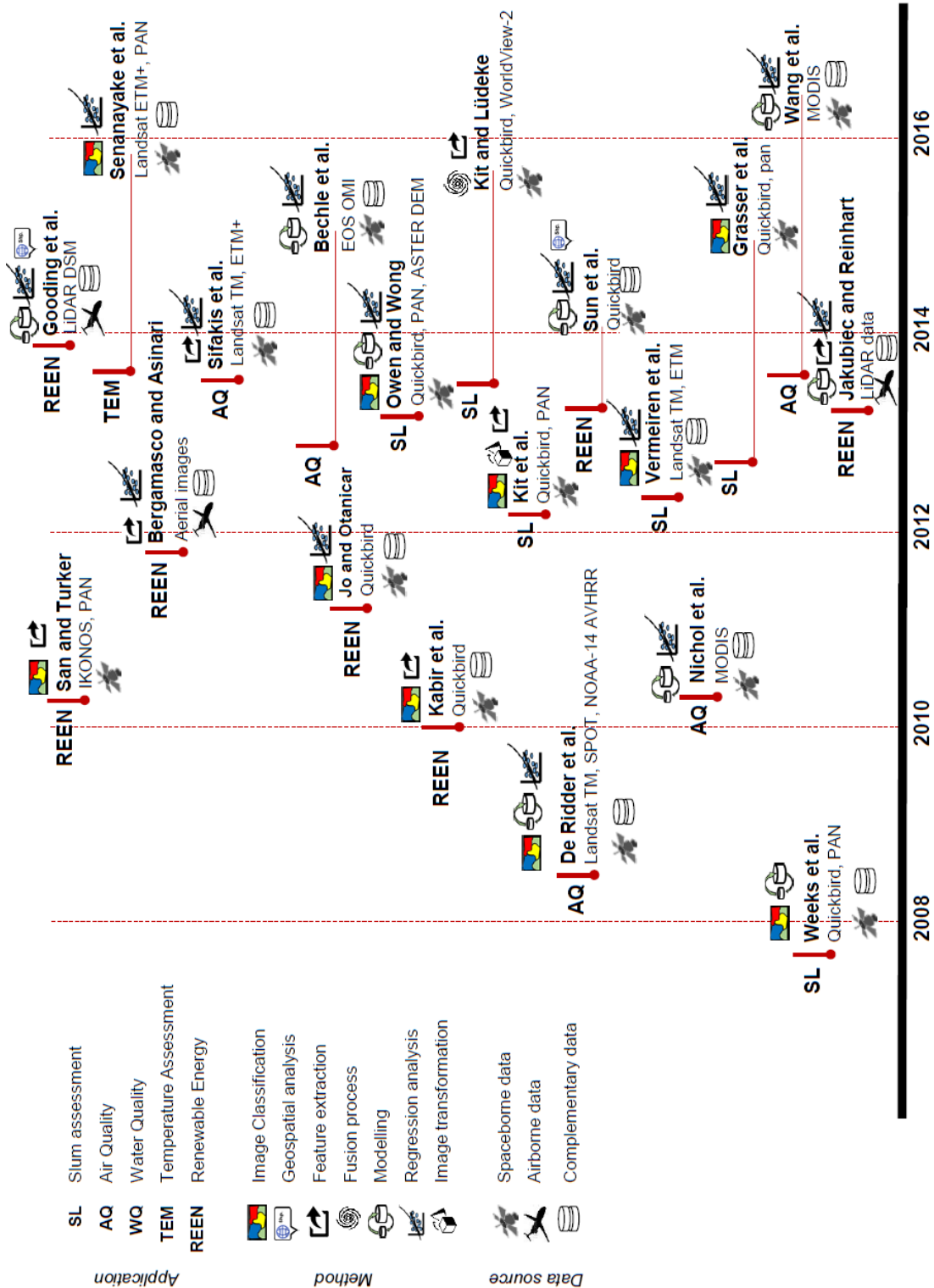


Figure 2.8: Previous work on urban growth and sprawl, and land-cover and land-use changes



**Figure 2.9:** Previous work on slums, air and water quality, temperature assessment, and renewable energy

**Table 2.2:** State-of-the-art studies in taxonomy, detection, extraction and pattern recognition in urban applications

<b>App.<sup>a</sup></b>	<b>Alg.<sup>b</sup></b>	<b>Merits</b>	<b>Limitations</b>
Seismic hazard. [121]	SVM & RF	<ul style="list-style-type: none"> <li>- Classify the combination of different remote sensing data</li> <li>- Derive sets of valuable features to characterise the urban environment</li> <li>- Model an effective earthquake loss and spatial distribution</li> <li>- SVM &amp; RF classifiers outperform other multi-class SVM classifiers</li> </ul>	<ul style="list-style-type: none"> <li>- Hierarchical supervised classification scheme has uncertainties in separating SBSTs</li> <li>- Performance depends on the ranked features</li> <li>- Accuracy is subject to the addition of further features and subset based categories</li> </ul>
Change detection. [122] <sup>1</sup> [123] <sup>2</sup>	(1) BOVW (2) ANN	<ul style="list-style-type: none"> <li>- Obtain semantic scene classes</li> <li>- Effectively analyse landuse changes</li> <li>- Satisfactory accuracy</li> <li>- Robustly highlight changes</li> <li>- Better representation of the relationships between feature- and pixel-pair</li> </ul>	<ul style="list-style-type: none"> <li>- Time-consuming</li> <li>- Very difficult to achieve the direct selection of the "from-to" samples from the dataset</li> <li>- Negatively affected by the redundancy of information</li> <li>- High computational cost</li> <li>- Complexity structures</li> </ul>
Landcover & landuse classification. [124]	SVM	<ul style="list-style-type: none"> <li>- Improve classification accuracy</li> <li>- Classify hyperspectral images adequately</li> <li>- Ease of interpretation of urban classes</li> </ul>	<ul style="list-style-type: none"> <li>- Confusion between road and bare soil classes</li> <li>- Instability and complexity in the structure and parameters of the binary tree SVM</li> </ul>
Monitoring changes. [125]	MRGU	<ul style="list-style-type: none"> <li>- Analysis of regression residuals and spatial distribution by (Getis Ord) with Moran's I</li> <li>- Quantify and identify the magnitude of impervious surface changes</li> </ul>	<ul style="list-style-type: none"> <li>- Not universally applicable</li> <li>- Difficult to use for quantifying changes in urban centres</li> <li>- Performance is subject to the structure of urban regions</li> </ul>
Water resources management. [126]	IDFM & ANN	<ul style="list-style-type: none"> <li>- A near real-time monitoring</li> <li>- Efficiency</li> <li>- Forecasting reliability</li> <li>- Potential for local adoption</li> </ul>	<ul style="list-style-type: none"> <li>- Uncertainties in the fused data</li> <li>- A large number of variables</li> <li>- Not applicable for regional meteorology parameters</li> </ul>
Population estimation. [127]	RF & LRM	<ul style="list-style-type: none"> <li>- Classify building types in the heterogeneous urban areas</li> <li>- Improved classification accuracy</li> <li>- Ease of adoption</li> </ul>	<ul style="list-style-type: none"> <li>- Subject to the selected morphology filter</li> <li>- Large numbers of metrics and variables</li> <li>- Uncertainty classification results</li> </ul>
Impervious surfaces estimation. [128]	SVM & RF	<ul style="list-style-type: none"> <li>- Improve classification accuracy</li> <li>- Not need for the combinations of features</li> <li>- Optimise parameters efficiently</li> <li>- Easy to use</li> </ul>	<ul style="list-style-type: none"> <li>- Using many texture matrices</li> <li>- Inability to handle the confusion in shaded areas and bare soil</li> <li>- Over-fitting</li> </ul>

<sup>a</sup>App.: Applications and <sup>b</sup>Alg.: Algorithms

SVM: support vector machine, RF: random forest, SBSTs: seismic building structural types, BOVW: scene classification with a bag-of-visual-words, ANN: artificial neural network, IDFM: Integrated data fusion and mining, LRM: linear regression modelling

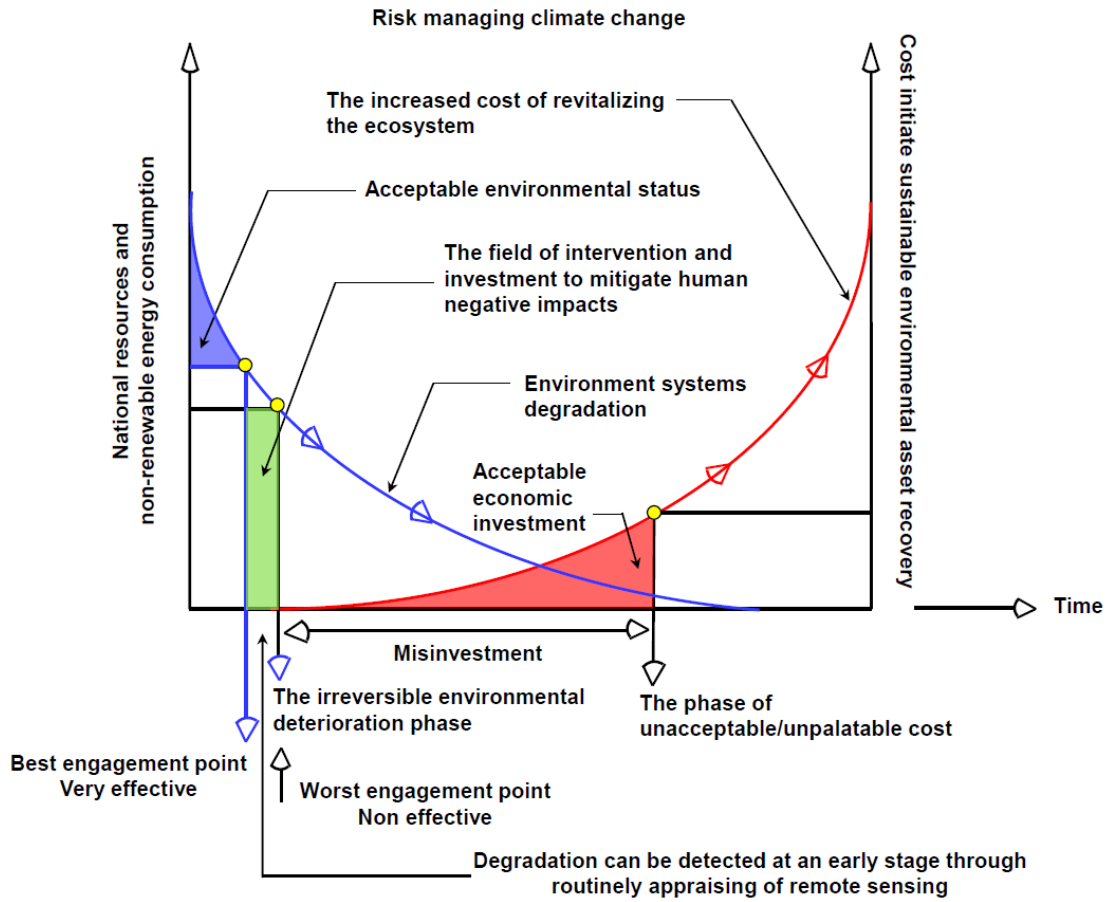


**Figure 2.10:** The hypothetical deterioration of environmental systems and the potential for the use of remote sensing in their restoration. Adapted from Purkis and Klemas [43].

Considering all of this evidence, it seems that there are still challenges and limitations in using remote sensing technology in urban studies. Challenges are related to the remote sensing data itself, as well as its methods of calibration, such as those for dealing with the complex and heterogeneous urban environments. Although the accuracy of the extracted information in remote sensing-based studies has improved, obtaining an accurate thematic map from remote sensing-based classifications remains a challenge, due to: (a) the complexity of the urban landscape; (b) limitations of selected computer vision and image processing techniques; and (c) the complexities and nuances in integrating or fusing multi-source data. Spectral uncertainty still exists between the separated classes of the urban land-cover and land-use, such as bare soil and/or dry mud with impervious surfaces. Furthermore, the concentration of diverse built-up materials in a small area results in pixel generalisation, eventually leading to classification errors, which can be particularly problematic when working with low-resolution images. The key advantage of remote sensing technology arises from the capability to integrate data from multiple sensors with similar or dissimilar spatial, spectral, or temporal resolutions to collate information on a common theme. However, there is a need for robust algorithms for fully

automating the registration of data captured with many sensors, such as optical and radar, hyperspectral imagery and LiDAR data, which operate at disparate resolutions and use diverse acquisition approaches. Although the derived information from such sensors are potentially very useful for urban sustainability assessment, fusing their data is a real challenge using the conventional approaches of data processing. Additionally, techniques for object recognition, classification, segmentation, and change detection from the outputs of data fusion are still in their infancy. Therefore, to take full advantage of the diversity of remote sensing data within the urban environment, there is a need to develop new strategies and further refine existing techniques and approaches.

In addition to the challenges in the assimilation and integration of data, the review of previous studies clearly indicates that there are some of the performance defects relating to the process of object detection; inference of contextual and semantic information using computer vision techniques; extraction of the geometric attributes of urban features such as 3D objects, and the enhancement of the degree of automation in accelerating the deduction of useful information from satellite images.

In Table 2.3, the challenges and/or opportunities are presented in three key research trends: (a) the integration of heterogeneous remote sensing data; (b) algorithms for extracting urban features; and (c) the accuracy of urban land-cover and land-use classifications. We highlighted the main benefits and limitations in each research trend for further investigation in the future.

**Table 2.3:** Directions for future research

	Integration of heterogeneous data	Algorithms to identify urban features	Improve accuracy for spectral classification algorithms
Objective	<ul style="list-style-type: none"> <li>• Improve the spatial and spectral resolution</li> <li>• Enhance the ability of features detection and display</li> <li>• Promote the geometric precision</li> <li>• Increase the capability of the change detection</li> <li>• Refine, replace or repair the defect of image data</li> <li>• Handle multi-source remote sensing data at the level of pixel, feature and decision fusion</li> </ul>	<ul style="list-style-type: none"> <li>• Accelerate future processing and improve classification accuracy</li> <li>• Automated processes for detecting, extracting, simulating, classifying and modelling urban features</li> <li>• Capability of handling and fusing the large number of datasets</li> <li>• Improve image objects segmentation</li> <li>• Increase the reliability and precision of the feature extraction</li> <li>• Mitigate the ambiguous and uncertainty</li> </ul>	<ul style="list-style-type: none"> <li>• Capability of separating urban land-cover and land-use classes in an adequate manner</li> <li>• Better visualisation and interpretation of urban landscape</li> <li>• Performing a change detection analysis and pattern recognition</li> <li>• Accurately characterise the model parameters for different urban remote sensing applications</li> </ul>
Problems requiring solutions	<ul style="list-style-type: none"> <li>• A rescaling of multisource data of diverse EO instruments</li> <li>• Assessing the distortion of the spatial and spectral resolution time-consuming and subjective</li> <li>• The complexity and/or availability of a large training datasets for the deep learning features</li> <li>• Manual or semi-automated the post-processing process</li> <li>• Computation efficiency and effectiveness</li> <li>• The quality of the distinguishing features</li> <li>• With the fusion schemes, the optimal combining strategy of the current fusion algorithms is a challenging task and requires further investigations in the near future</li> </ul>	<ul style="list-style-type: none"> <li>• Further developments for fusing LiDAR data with thermal, multispectral and hyperspectral imagery</li> <li>• Reliable determination of the boundaries of urban objects in an automated manner</li> <li>• Further improvements for addressing different characteristics of EO data</li> <li>• Ability to cope with unpredictable environmental and illumination factors of diverse datasets</li> <li>• Similarity in the characteristics of spectral, textural and geometrical-based features between the urban objects and their background</li> <li>• Computational time to perform a task</li> </ul>	<ul style="list-style-type: none"> <li>• Mixed pixels</li> <li>• Uncertainty in the urban land-cover and land-use classes</li> <li>• Mixed objects</li> <li>• Promote pixel-based and object-based classification using contextual information</li> <li>• Over-fitting can cause speckled results that are difficult to interpret</li> <li>• An automatic labelling strategy is required for actual label sets in several applications</li> <li>• Further refinements for the fusion of diverse data sources</li> <li>• Integrate the derived urban features (e.g., building shadows) and/or spatial matrices with various classifier schemes</li> <li>• Investigate the recent computer vision techniques for improving the accuracy</li> </ul>

## **2.5 Summary**

This chapter aimed to review URS technologies and present their scope for assessing sustainable development in urban areas, and to describe the techniques in which remote sensing can be used in this field. According to this, it is essential to monitor urban evolution on spatial and temporal scales to improve our understanding of city changes and the subsequent impact on natural resources and environmental systems. Various aspects of remote sensing are routinely used to detect and map features and changes on land and sea surfaces, and in the atmosphere, as they affect urban sustainability. This chapter therefore provides a critical and comprehensive review of the characteristics of remote sensing systems, and in particular the trade-offs between various system parameters, as well as their use in two key research areas: (a) issues resulting from the expansion of urban environments, and (b) sustainable urban development. The analysis identifies three key trends in the existing literature: (a) the integration of heterogeneous remote sensing data, primarily for investigating or modelling urban environments as a complex system, (b) the development of new algorithms for the effective extraction of urban features, and (c) the improvement in the accuracy of traditional spectral-based classification algorithms for addressing spectral heterogeneity within urban areas. Growing interest in renewable energy has also resulted in the increased use of remote sensing for the planning, operation, and maintenance of energy infrastructures, in particular the ones with spatial variability, such as solar, wind, and geothermal energy. The proliferation of sustainability thinking in all facets of urban development and management has also acted as a catalyst for the increased use of, and advances in, remote sensing for urban applications.

# **Chapter 3**

## **Current state of 3D object creation**

Automation approaches of detection, segmentation, extraction and 3D reconstruction are a fundamental research task within the scope of remote sensing, image processing and computer vision sciences alike. Although buildings are one of the most important parts of the urban landscape for automatic detection and extraction, they manifest a major challenge when their footprints need to be extracted in monocular images. Additionally, the creation process of the 3D models of urban buildings becomes further complicated when 2D scenes are only used, although they are real geospatial data, and are required to depict urban landscapes. Therefore, this chapter provides a literature review of the state-of-the-art algorithms in image processing and computer vision for automatically detecting and extracting objects, such as buildings, from images. The chapter also presents various studies in which remote sensing data (e.g. Very High Resolution VHR multispectral satellite images), approaches, and techniques are used in the creation of 3D city models.

### 3.1 Optical satellite images characteristics

According to Chapter 2, there is a need to increase our understanding of the solar energy potential of the surfaces and roofs of building envelopes, to formulate future adaptive energy policies for the sustainability of cities. Esch et al. and Bonafoni et al. [118, 129] reported that the use of remote sensing technology provides magnificent data for sustaining cities and promising applications to implement a sustainable energy supply. In this respect, optical satellite sensors can offer a variety of spectral wavebands, including visible bands that offer images similar to how the human eye sees the world, and wavebands that are beyond human vision. They can detect objects on the Earth related to the temperature in the different spectral wavelengths. Passive optical datasets captured by sensors on board the satellites are often in the digital image form presented in an array of numbers, as shown in Figure 3.1. As a definition, an image (raster data) can be a matrix of rows and columns, two-dimensional (2D), in which each data value (or picture element, abridged as pixel) is represented logically by its position in the array. A greyscale image is an array of numbers required to hold the pixel values, each of which can lie in a specified range, commonly (0 'black colour' - 255 'white colour'), with 8 binary digits (bits), which is the grey level value stored in each pixel needed in the graphics memory of the computer. A colour image (multispectral image) is a combination of a minimum of three bands, with 24 bits representing the range. All datasets are considered in the raw form as they are received from imaging satellite sensors, until preprocessing is implemented. This means the correction of deficiencies and the removal of flaws. The operations of preprocessing the satellite images are carried out before the image data is used for a particular application or purpose. Despite the fact that some corrections are made at the ground receiving station, there is often still a need for the user to perform further preprocessing [130]. Thus, researchers' attention Lavender [40] has been focused on the geometrical properties of the image data, and the effects of external factors, such as the magnitude of the variations in emitted or reflected energy detected by sensors. Additionally, certain aspects related to the image data, for instance, the level of preprocessing and weather conditions (e.g. atmospheric haze), require an appropriate technique to correct the defect and estimate the external effect. In regard to the evaluation of the availability of the rooftops and facades of the buildings for solar energy potential within cities, a good understanding of the image's data characteristics will improve the results of the object extractions (e.g. buildings) when obtained for solar PV assessment.

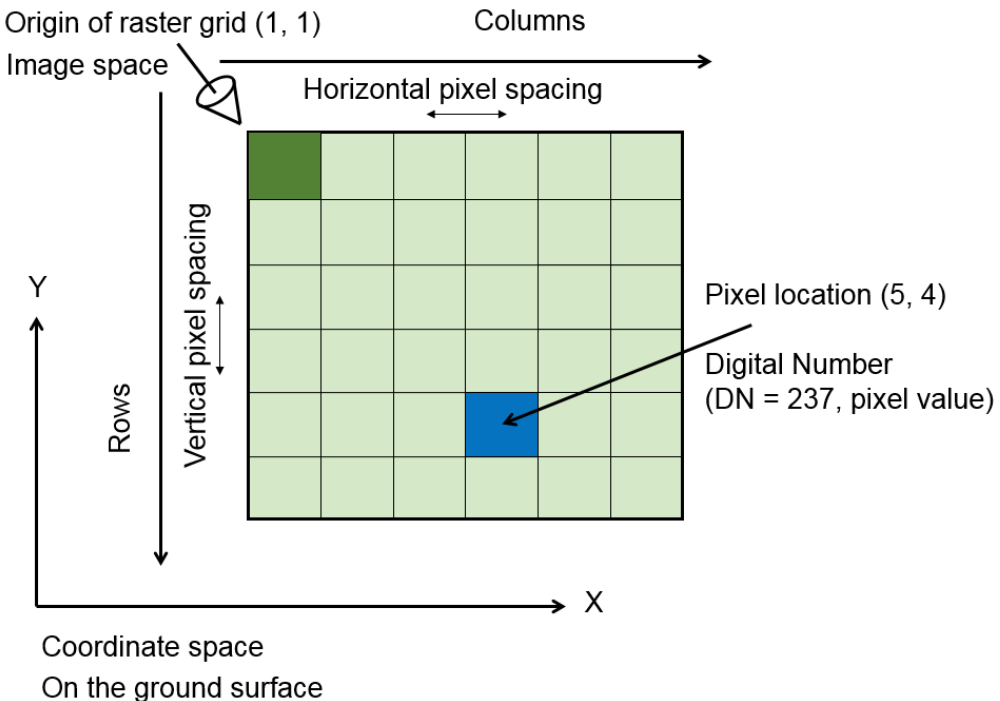


**Figure 3.1:** Raster data concept. The origin of the (row, column) coordinate system is the upper left corner of the grid, at a cell (row 1, column 1). The grid cell (pixel) size is usually expressed in units of ground distance, metres (m)

### 3.1.1 The importance of using satellite images

As an extension to what was presented in the previous Section 3.1, satellite images with different spatial resolution (ground covering with kilometres, metres and sub-metres) are one of the most important data input sources for detecting, extracting, modelling, analysing, and visualising urban objects and features. The satellites have the attributes of being highly manoeuvrable, low earth orbiting, high quality, versatile and accessible, and their captured imageries are used worldwide for a wide range of military and civilian applications. In this vein, imagery provides value in understanding the Earth and the impacts of man-made activities and natural processes. In particular, Very High Resolution (VHR) satellite imagery offers sub-metre resolution, which is considered one of the highest image qualities currently obtainable from remote sensing satellites. Sub-metre VHR satellites exhibit a smaller ground sampling distance (GSD) than other imaging satellites, making their images more suitable and reliable. These can be for natural and/or man-made site monitoring, object and landscape observation, object detection, and many urban purposes and tasks requiring precision data. Among its many advantages, VHR images enable the identification of urban structures in terms of their geometry and actual location on the ground in the real world. The high accuracy imagery has proven particularly useful for creating detailed 3D models of cities whenever it is available in the form of stereo or

multi-angle imagery. Hence, a great deal of previous research on urban studies has focused on employing VHR satellite images. Some examples of the extraction and analysis of urban objects and features based on satellite imageries include: roads [131] and [132], buildings [133] and [19], the shadows of urban structures [134] and [135], bridges [136] and [137], vegetation within urban areas [138] and [139], water within urban areas [140] and [141], and the geometry of urban structures [142] and [143].

Technical improvements to satellite sensor systems, and processing approaches for VHR satellite images, on other hand, should be developed and improved synchronously. Difficulty obtaining remote sensing data which can provide the third dimension of urban structures, such as LiDAR or VHR stereo-pair images, can also be taken into account when overcoming such restrictions. This can be achieved through developing algorithms able to derive such information. In addition, although VHR satellite images present a clear view of urban landscapes and their features, it is necessary to perform contrast manipulation on the VHR satellite images, as an image pre-processing technique, to eliminate any haze over the entire image before the extraction process of urban objects can begin. Satellite images used in this study have been processed from the haze effects by the provider of the satellite images.

### 3.1.2 Image enhancement

A good contrast between urban objects (e.g. buildings and their backgrounds and other surrounding objects) should first be obtained to facilitate the extraction process from VHR satellite images. According to Lavender S. and Lavender A. [40], images often do not use the entire range of brightness available to them. One well-known technique of image enhancement is to adjust and stretch the brightness histogram. The histogram stretching technique spreads the image pixels out along the  $x$ -axis and therefore the range of brightness levels used will be increased within the image [40], as shown in Figure 3.2. This process amplifies the intensity difference between pixels, thereby making them more visible to the eye. Enhancing the image contrast is a necessary process with the used images, so that particular features are enhanced to achieve the subsequent processes, such as detection, segmentation, fusion, and extraction. Numerous studies have attempted to enhance image contrast by applying the histogram adjustment technique before, for example, change detection [144], underground water detection [145], the evaluation of residential life quality [129], the calculation of a compact built-up areas [146], and satellite image fusion [147].

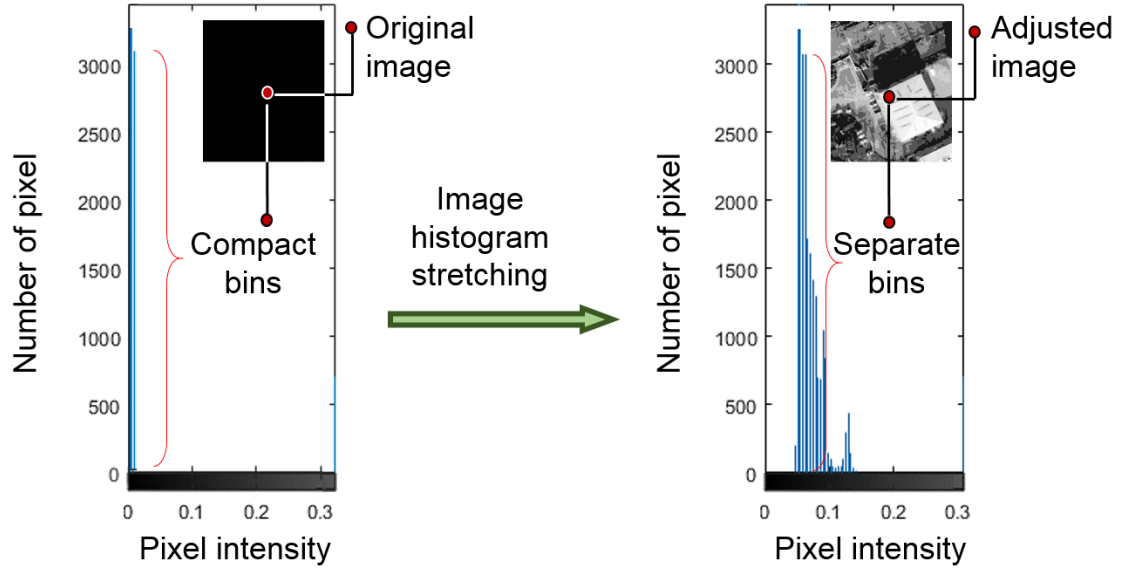


Figure 3.2: Image contrast stretch as applied to the image band

### 3.2 The extraction of information from satellite imagery

Very-High-Resolution (VHR) satellite imagery is a powerful source of data for detecting and extracting information about urban constructions. The growing availability of VHR images, for instance, QuickBird, GeoEye, WorldView and Pliades images, has caused an increase in the number of studies on urban structures extraction (e.g. buildings) from VHR images. This is particularly so in rapidly expanding complex urban environments, where the high level of detail present in VHR data facilitates object-based identification for building detection and reconstruction. Nevertheless, the most challenging task is to make a computer perform by analysing a scene, accurately reconstructing the 3D shape of an object, and recognising all of the constituent objects. Object identification is a very tough task because the real world is made of a jumble of objects, which occlude one another and appear in different poses [148]. In addition to the variability intrinsic within an object class, and due to complex non-rigid articulation and extreme variations in shape and appearance, it is unlikely that exhaustive matching against a database of exemplars can be simply performed [148]. Therefore, many researchers have tried to simplify this problem, especially when using VHR images, by knowing what objects they are looking for, so that the problem is one of *object detection*. The consequent process is a quick scan of an image to identify where a *match* may occur. A *labelling* process is then a necessary step in the recognition of objects, after determining their position within the image, based on a specific rigid object defined beforehand. Accordingly, and by searching for characteristic feature points and verifying that objects align in a geometrically plausible way, objects can thus

be extracted in the process of information *extraction* from VHR images. The state-of-the-art in object detection, extraction, and reconstruction continues to improve rapidly. The following sections focus on the information extraction of urban buildings and their shadow regions from VHR satellite images.

### 3.2.1 The importance of shadow detection in urban environments

Remote sensing with very high spatial resolution, such as Quickbird and WorldView-3, among others, can provide clearly detailed features of cities, for instance, roads, buildings, shadows, parks and trees. Shadow in the VHR satellite imageries provides vital information on urban construction forms, illumination direction, and the spatial distribution of the objects; all of these can help to further understand the built environment. However, the appearance of shadow increases with the spatial resolution, and whether or not the purpose of determining shadow regions is for removing these regions, or exploiting their information. Obviously, the main and first process in shadow analysis studies is to detect shadows.

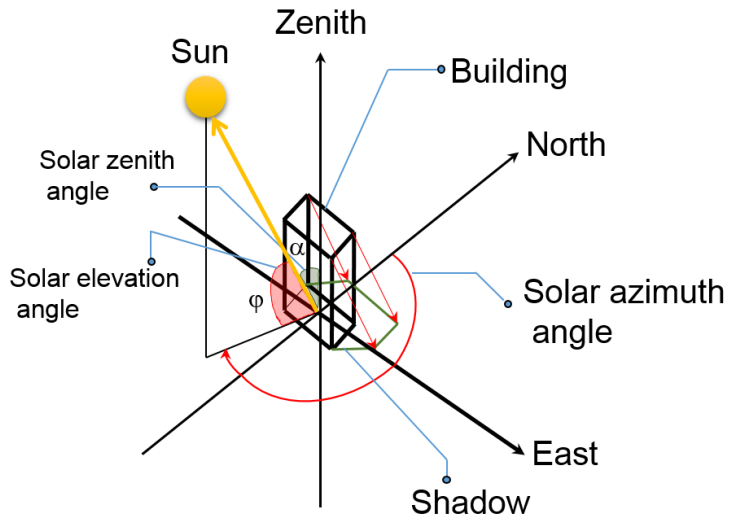
According to Řufenacht et al. [149], shadow is generated by standing an object in the path of a light source, as shown in Figure 3.3. On this basis, buildings have their own shadow regions cast on the ground, and when the sunlight hits those buildings they are in the opposite direction of the sun. The casting shadow area of the building is therefore considered the actual shadow area that can be captured by satellite images. Typically, the mean value of the digital number values of the image pixel within the area of the actual shadow is less than the other surrounding areas. This means the pixels representing shadows are darker in colour tone than the non-shadow pixels. Hence, it is possible to discriminate shadow regions from other urban features in space-born scenes.

The information derived from shadows can play an important role in urban studies. Many studies have therefore considered shadows in VHR satellite images as unwanted features and drawbacks that must be removed. However, studies on shadow detection and analysis have indicated the development of new improvements in image quality and enhanced algorithms of image segmentation and partitioning, as well as object extraction. Although the appearance of shadows can affect the performance accuracy of applications such as image classification and registration, shadows do provide information about the characteristics of surfaces and light sources, shapes and the location of objects. Additionally, because shadows cover a considerable portion of an image, they play a supporting role in automated analysis. In this context, the

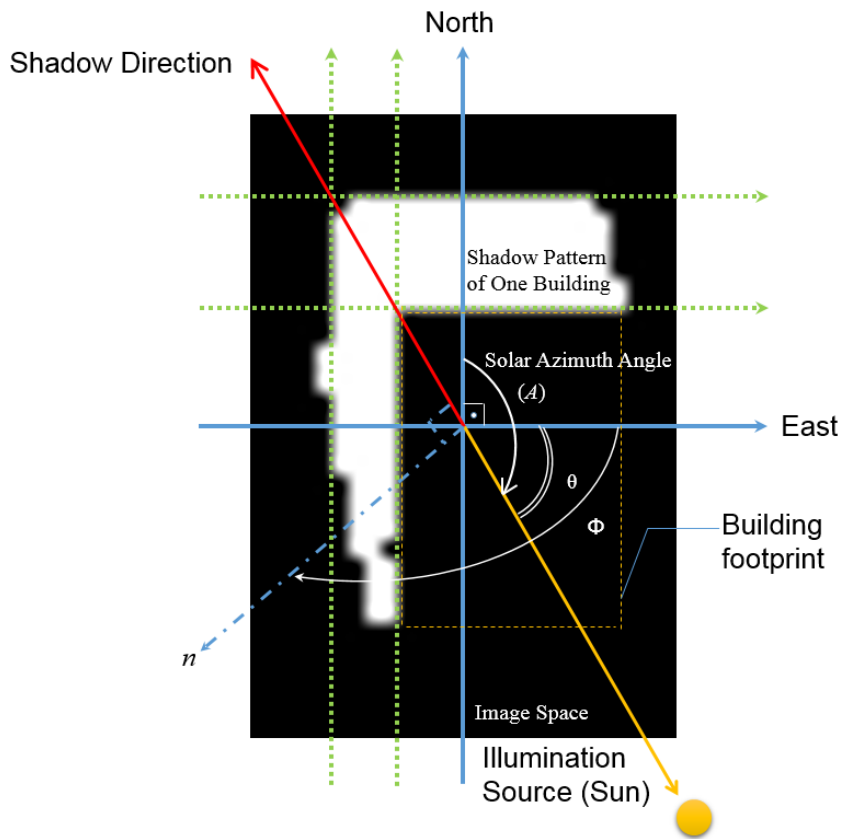
shadow presence in single VHR multispectral images has been exploited as strong evidence of the existence of a different building structure, such as buildings detection [19], arbitrarily shaped buildings in complex environments [150], the extraction of above ground circular structures [151], and the automated extraction of buildings and roads [152].

Shadows are, thus, an important cue for information about man-made structures and to support urban sustainability. The assessment of solar PV energy potential as a form of renewable energy within urban environments is an important application to secure future energy needs for cities. In this regard, shadow information within urban environments is a key element in the analysis of solar radiation across daylight. Using different datasets, Redweik et al. [153] developed a shadow algorithm to calculate shadow maps for the solar potential assessment of all surfaces (roofs and facades) of buildings within an urban landscape. Bergamasco and Asinari [23] proposed a method of computing the available roof surface for integrated solar PV installations through the analysis of shadow zones, space, brightness, and suitability for PV installation. Jo and Otanicar [154] analysed the patterns of shadow cast and their effects on the rooftop to estimate the available rooftop area for PV installation. Shadow impact is, thus, an important factor in the assessment of solar energy potential, and can play a role in potentiality and financial benefit.

A number of researchers have also published approaches to exploiting the derived shadow information from VHR images for different purposes of urban analysis. Izadi and Saeedi [17] introduced a method for the automatic detection and height estimation of buildings with polygonal roofs, using single satellite images based on shadows and acquisition geometry. In this study, a fuzzy logic-based approach was used to estimate building heights according to the strength of the shadows and the superposition between the identified shadows in the image and expected true shadows of the buildings, to generate a 3D polygonal building model. Raju et al. [155] proposed the extraction of the height of a building using shadow through two stages: rooftop and shadow extraction, followed by height estimation. This was achieved by example- and rule-based approaches based on the derived information and the relationship between rooftop, shadow and sun-satellite geometry. Using a volumetric shadow analysis (VSA) method, Lee and Kim [15] presented a scheme to extract building height automatically. This scheme was implemented by examining the location change of projected shadow lines with respect to the actual shadow regions with progressively increasing building heights. The approach has been applied to IKONOS, KOMPSAT-2, Quickbird and WorldView-1 images.



**(a)** 3D visualisation of solar angles: Sun Elevation, Azimuth and Zenith angle with the formation of a cast shadow of the urban structure



**(b)** a shadow pattern of the actual illumination direction and its opposite direction, which is composed of the cast direction of the shadow with the geometric angles of the relationships within the image space

**Figure 3.3:** The direction of illumination and the geometry of the shadow pattern

It seems likely that the derived information from shadow regions using VHR satellite images is not limited to the achievement of one goal or specific application within urban environments. Using advanced techniques in image processing and computer vision, and if appropriately exploited, shadow information can be used in different applications. Because shadows can support automated processes for deducing the structure of man-made objects, it is not necessary to build a distinct model to infer an object's structure. However, to make this information more useful and effective in every application, shadow regions should be precisely detected and extracted from images.

### 3.2.2 Shadow detection and extraction

As noted in Section 3.2.1, to exploit shadow information by detecting and extracting shadow regions from images, the automated detection of shadows from images must be accurate [20]. Many pioneering studies for the automated detection of shadows from VHR satellite images were devoted to improving the quality of an image after detecting and handling shadows, or to utilising shadows to detect man-made structures within the urban environment. Although the automated detection of shadow regions from VHR satellite imageries is a challenging task, automatic object detection and extraction is a very active scope of research. However, the literature presented here is focused on those studies which aimed to detect and extract the shadows of buildings from the VHR optical images automatically. A review paper on shadow analysis was produced by Dare [156]. The paper presents methods of detection and how to avoid problems with shadowing in high resolution satellite imagery. Four different techniques for separating shadow pixels from non-shadow pixels were described: thresholding, classification, region growing segmentation, and three dimensional modelling. The segmentation approach was proposed to detect shadow regions using four step processing: density slicing, thresholding, region encoding, and region filtering; all of these were applied to IKONOS and Quickbird panchromatic images. Thereafter, the radiometric enhancement technique was chosen to remove shadow areas from IKONOS and Quickbird images. It was concluded that although the quality of the image can be improved through techniques of detection and the removal of shadow areas, the results can be image-dependent. In one recent study, Wakchaure and Raut [157] reviewed a range of techniques for shadow detection and de-shadowing from VHR images. The study included the proposal of a processing chain based on binary classification. Canny edge detection algorithm was used to detect shadows and differentiate their areas from non-shadow areas in the image, with clear boundaries. Thereafter, the calculation of mean and

standard deviation values for both pixels in the shadow and non-shadow areas, together with the normalisation process, were suggested as potential improvements for the final results of removing shadow pixels and defining non-shadow pixel. This was achieved by increasing their brightness and shadow intensity values. However, the algorithm has not been applied to any VHR image in order to evaluate its performance and suitability in detecting shadows.

The segmentation approach is one of many different approaches used to detect shadow regions from single VHR multispectral images. Ma et al. [158] presented an approach in shadow segmentation and compensation implemented on an IKONOS image through a normalising Saturation-Value difference index (NSVDI). The approach was based on analysis of Hue-Saturation-Value (HSV) colour space to detect the shadow regions of buildings, and a histogram matching technique was exploited to retrieve the information under shadow. The results of segmentation illustrate that the shadow areas were effectively extracted from the IKONOS image. Nevertheless, the approach was not able to distinguish between dark objects, such as water and shadow regions, due to the similarity of the spectral values of pixels and the lack of validation of the final results. It was concluded that multiple images can compensate better for the information under the shadow regions because the retrieval information from a single image is insufficient. In the same context, a segmentation algorithm based on the contour model and isolation was proposed by Elbakary and Iftekharuddin [159] to detect man-made structures by their shadows. The approach was applied to a panchromatic image with a resolution of one pixel per meter in both directions. Thereafter, post-processing based on optimal thresholding and a geometric filter were implemented to determine the real shadows from other objects. Although the algorithm was used to detect and segment the shadow regions using the grey-level satellite image without depending on the colour information, and to handle the difficulty of shadow detection in satellite images, the problem of separating water bodies such as lakes from shadow regions remains unsolved. This is because they exhibit similar intensity characteristics.

In other recent studies, a classification-based approach has been used to detect shadows regions. Liu and Yamazaki [160] proposed shadow detection using an object-based classification that employs brightness values and their relationship with the neighbouring area; this was applied to Quickbird and WorldView-2 (PAN and multispectral images). A method for the correction of these detected shadow areas has also been proposed using a linear function to remove shadows from images. The idea is to classify images as vegetation, road, roof, or shadow, and to modify shadow pixels through three levels of darkness (dark, medium and light). These are

derived from twenty-six radiance measurements to demonstrate the natural variability of the radiance ratio. A linear-correlation function and NDVI were used to attain a smoothly restored image. The overall classification accuracy for sunlit areas was 74.94%, while for the corrected shadows areas it was 71.87%. The comparison between these results illustrates that the proposed shadow correction method is effective in correcting the radiance in shadow areas. Nevertheless, the detection step was entirely based on the results of the supervised classifier, which was the main reason for the moderate shadow regions. Moreover, a bright roof in light-shadow, small shadows cast by trees, and material with high reflectivity in shadow areas, were not extracted and properly observed by the object-based classification method. Later, the morphological filtering approach for shadow detection with a shadow reconstruction approach was suggested by Song et al. [161]. It sought to improve the classification performance applied to Quickbird and WorldView-2. Shadow detection comprises three steps: thresholding, morphological filtering, and edge compensation for the derived shadow mask as a first stage in this approach. In the second stage, a Markov random field (MRF) was used to sample shadow and non-shadow pixels manually, to produce a library for both types of pixels as a training stage. The final stage was to compensate and reconstruct the underlying land cover pixels using the Bayesian belief propagation algorithm to address the MRF. The supervised ISODATA classification method was applied before and after shadow construction to verify the performance of the proposed shadow removal approach. The results indicate that the constructed images can be classified more accurately than images before shadow reconstruction. However, the chain of image processing for shadow detection might affect the quality of the actual geometric shape and edge of shadows areas. Because of the morphological filtering in the shadow detection stage, some small shadow areas were not removed and remained in the classification map after shadow reconstruction.

A different recent work, a new index for detecting shadows regions, was introduced by Teke et al. [20]. In this approach, the use of near-infrared and visible information (especially green and red bands) of VHR satellite images was utilised to generate a false colour image. The processes of normalisation and transformation were implemented on this false colour image to compute the Hue-Saturation-Intensity (HSI) space and a ratio map. In their approach, Otsu's method was applied to the histogram of the ratio map in order to detect the shadow regions, because the thresholding scheme used is able to detect both shadow and vegetation regions at the same time. The final step in the approach is to derive a binary shadow mask through subtracting the regions of vegetation cover in an image. Although the results exhibited success

in detecting shadow regions, post-processing is required to improve the shape and boundaries of the derived shadow mask from VHR satellite image. This is so especially in cases where the shadow regions are used as evidence of the structure and location of the elevated objects within the urban area, such as buildings. The same approach was used by Ozgun [152] to detect shadow regions to identify the regions recognised as buildings and roads, implemented on a set of Quickbird and Geoeye-1 VHR images. A post-processing shadow mask, which included a constrained region growing process on detected shadow regions and probabilistic landscape approach Ozgun [19], was achieved using three different thresholds: pixel intensity, the ratio of the number of pixels involved, and non-building height, to obtain a regular shape identical to reality and eliminate the unwanted shadow areas.

Overall, image thresholding techniques are essential in the processes of object detection. In spite of the fact that thresholding techniques are a simple pattern of partitioning an image into isolated features, they are still effective. Nonetheless, the thresholding techniques applied on VHR satellite images (multispectral or PAN image) for shadow detection need to be more effective, taking into account the different characteristics of the used images. In addition, the fully automated algorithms of shadow detection often require further constraining assumptions about extracting shadow regions from VHR satellite images, to run them appropriately and obtain reliable precision of the shadow masks.

### 3.3 The creation of 3D models of urban buildings

VHR satellite imagery is such that data can provide reliable and efficient detail in the creation of 3D models of urban buildings within various urban landscapes. The automated creation of 3D objects from images is an open research area of image processing and computer vision, as well as remote sensing. However, the creation process of 3D building models is not an easy task using single satellite images without any complementary data. In addition, the automated extraction of 3D geometric structures from solely 2D scenes has had limited success when the urban landscape is complex. Nonetheless, the most distinct feature of utilising satellite images is their capability of providing additional information to facilitate the generation of 3D structures. A metadata file, which comes along with satellite images, contains solar information which can be significant inputs into a sequence of executive actions in the 3D creation of buildings.

A large and growing body of literature has investigated the extraction and reconstruction of the 3D building models from different types of remote sensing data. Various approaches have been presented in the context of 3D building extraction, including non-automated, semi-automated, and automated techniques. However, approaches in these categories have well-known limitations. For instance, both the non- and semi-automated methods for the acquisition of building geometry, run by an operator and related to users skills, require further time, cost and effort to accomplish. Such studies have considered how to implement these approaches automatically. Therefore, there is a considerable amount of literature on the importance of a 3D vision of buildings created in an automatic manner. Nevertheless, most former studies for automatically generating 3D building models based on the available geometric parameters of buildings is directly taken from field measurements, or from existing data, and integrated with the derived information from imagery. So far, however, there is little published research on extracting 3D building models from a single 2D satellite scene, without extra data, in complex urban landscapes.

At the fundamental level of data modelling, a model of the object must have, at least, the three dimensions of object geometry: the direction of axes ( $X$ ,  $Y$  and  $Z$ ), as shown in Figure 3.4. The size of the object's footprint (e.g. a building) is subject to the values of ( $X$ ,  $Y$ ), while ( $Z$ ) is the attribute of the object's height. Depending on the derived information from VHR satellite images, the *Level of Detail* (LOD) for the complexity of a 3D model's representation will be established. In computer graphics, the concept of LOD is the representation of a model in terms of geometric complexity, spatio-semantic coherence, and the resolution of the texture and attributes [162]. Accordingly, LOD involves increasing the complexity of a 3D model representation as it moves toward the viewer, or depending on other metrics, for instance, object importance, viewpoint-relative speed, or position [163]. The subsequent sections of this chapter will illustrate the approaches adopted by researchers to generate 3D city models based on remote sensing data, considering the LOD concept.

### 3.3.1 Geometry identification: Building detection and footprint extraction

Automated detection of building footprints from a VHR satellite image is an active research area of different scientific fields, such as remote sensing, computer vision and sustainable development [129]. However, due to the complexity of urban landscapes, the process of the automatic detection of buildings using monocular VHR multispectral images is not easy. In particular, the

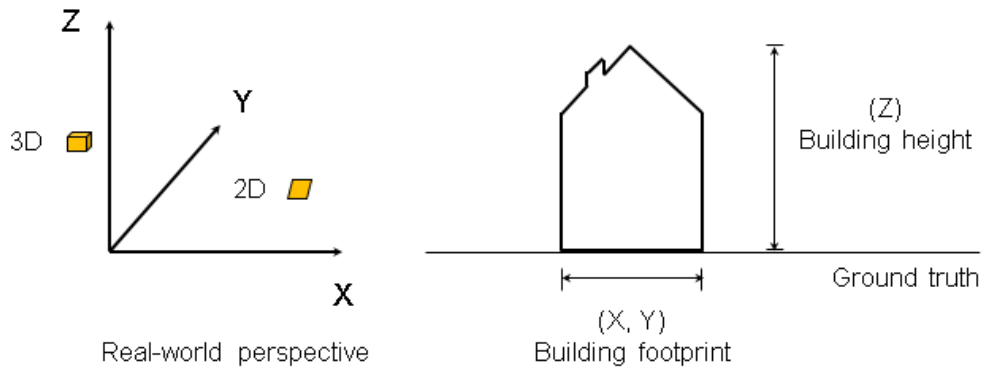


**Figure 3.4:** The fundamental concept of a building's geometry

automatic detection of urban structures from images will be more challenging when there is a lack of, or limited, geoinformation data. This includes: (1) the geometry, and the footprint area, shape complexity, and number of neighbouring objects; and (2) the building attributes, such as the number of storeys above ground, which can help the detection algorithms to derive the footprints of the buildings. Consequently, these automatic detection approaches do not rely on the cadastral database and statistical data using satellite images alone, and so they are very meaningful and valuable tools.

In this context, much of the current literature on using remote sensing data pays particular attention to detecting buildings. Because of the characteristics of VHR satellite images with multispectral information [129], such data have motivated researchers to develop new approaches for building detection. Sirmacek and Unsalan [164] proposed a scale invariant feature transform and graph theoretical tools for the detection of buildings based on panchromatic 1-m-resolution IKONOS imagery. Sirmacek and Unsalan [165] used local feature vectors and a probabilistic framework for the detection and classification of urban buildings. In another study using data fusion, Verbeeck et al. [166] studied four different segmentation and classification approaches using LiDAR and VHR multispectral Quickbird images to detect imperviousness and other land cover classes. In a rather recent study, Wang et al. [167] introduced an approach based on distinctive image primitives, such as lines and line intersections, using a graph search-based perceptual grouping approach to extract buildings from VHR optical satellite imagery.

A group of researchers focused on employing a monocular VHR satellite image for detecting urban structures. A different approach used to detect buildings from single VHR multispectral images (pan-sharpened GeoEye-1 images) was based on an original two-level graph theory using a GrabCut approach based on the partitioning technique [19]. Another study

with the same graph partitioning approach, Ozgun [152] presented an unsupervised framework to detect buildings and roads. In a recent study, Ghaffarian S. and Ghaffarian S. [168] developed a method for automatically detecting buildings from high resolution Google Earth imagery based on three steps: using the Moore Penrose pseudo-inverse matrix model for improving the FastICA algorithm; proposing simple rules and automated seeding of the PFICA algorithm; and, using the K-means clustering algorithm for masking out the final building detection results from PFICA outputs. Ozgun [151] proposed a new method to detect and extract the above ground circular structures within an urban area from VHR GeoEye-1 imagery based on a Hough transform approach and a set of constraints, followed by a circle fitting technique. In a different work, Li et al. [169] proposed a new framework for building extraction in visible band images based on the identification of rooftops through applying an initial unsupervised classification and conditional random field (CRF) formulation techniques. Manno-Kovcs [170] presented a flexible multilabel partitioning procedure based on a graph cuts technique for automatic building detection by fusing shadow and urban area information.

In fact, most of the aforementioned building detection approaches developed using single VHR multispectral images depended on employing evidence of shadow regions for verification of the generated hypotheses [16, 19]. Because a cast shadow strongly indicates an off-terrain object, the presence of shadow regions can be efficiently used to confirm the existence of a building structure [19]. In addition to the automatic extraction of the building footprints, many researchers have exploited the extracted shadow information from VHR images to derive the estimated heights of the buildings. The automatic estimation of the building heights is detailed in the following section.

### 3.3.2 Geometry identification: Building height estimation

Building height ( $H_B$ ) is one of the key geometric parameters used to transform the two-dimensional (2D) footprint area into a 3D model. Manually obtaining  $H_B$  of a large number of buildings for urban-scale 3D modelling and analysis is resource intensive. The difficulty and cost involved in  $H_B$  estimation also creates a barrier to the use and deployment of advanced modelling, analysis and the management of the built environment for most, if not all, cities and countries. Finding an efficient and cost-effective way to estimate  $H_B$  is, therefore, of paramount importance.

There are two main methods for deriving  $H_B$ : direct and indirect. Direct methods involve field measurements, often using land surveying equipment; however, these require time, effort and money, which is prohibitive for surveying large areas. Several studies have, therefore, attempted to overcome these challenges indirectly by applying mathematical inference on secondary data. Most indirect methods rely on elevation data (e.g. digital surface model (DSM) and point cloud) obtained through various aerial or satellite on-board sensors such as radar, LiDAR, and stereo imaging. Other indirect methods aim to infer building heights from 2D scenes without elevation features such as photogrammetry or satellite images. The estimation approaches for computing  $H_B$  from 2D images, however, are considered the most challenging.

In the context of obtaining  $H_B$  based on indirect extraction methods, many pioneering studies have used elevation data in various urban applications. Examples include the construction of building models for performing the solar potential estimation on roofs [132], the extraction of local heights to reshape the final urban candidate buildings [171], building type identification based on machine learning [172], the volume of a building using the object-based method with a multi-threshold framework [173], the reconstruction of 3D buildings [128], and the investigation of the height difference [174].

A common factor in  $H_B$  extraction approaches based on remotely sensed elevation data is that they require sophisticated data calibration and processing to obtain a reliable DSM. Although studies have shown the utility and usefulness of elevation data for extracting  $H_B$ , their implementation typically requires the use of additional data, and often multiple images from different angles to obtain a satisfactory view of building size and shape [175]. Another feature of elevation data based  $H_B$  extraction is the need for data pre-processing, because of point cloud sparsity and data misalignment [176]. As an alternative to costly data acquisition and processing, several studies have developed methods for obtaining  $H_B$  from one data source, such as satellite images utilising the shadows cast by buildings.

The first task in shadow-based estimation of  $H_B$  is the extraction of shadow regions from VHR satellite images. In this respect, a semi-automatic approach was proposed by Kim et al. [177] to estimate  $H_B$  from a single satellite image that manually adjusts the height of a simulated building and then matches the projected shadow with the actual in the image space. In contrast, a volumetric shadow analysis (VSA) method has been used to extract the heights of the buildings automatically [15]. However, the reported methods were designed primarily for buildings with full scenes of their bases and rooftops, including the side of the building. In

another study, Izadi and Saeedi [17] also matched shadow regions but building heights were estimated using simple triangulation. Estimation accuracy in this approach is dependent on the quality of the segmented rooftop polygons.

Shao et al. [178] proposed a classification approach to detect shadows and applied a simple trigonometric formula after characterising the relationship between buildings and their shadows to estimate the values of  $H_B$ . However the method overestimates the shadow lengths of buildings, resulting in large errors in calculated  $H_B$ . In Comber et al. [179], the number of storeys and the length and shape of a building were inferred based on the identification of shadow areas. However, the strategy proposed may only be practical for the presented case study and the imagery used, because of the empirical nature of the rule-based classification. In Raju et al. [155], the height of the building was estimated from the extracted shadow regions based on the sun-satellite geometry relationship. The method does not consider overlapping shadow regions caused by other buildings and vegetation, limiting its applicability in dense urban areas.

More recently, Qi et al. [16] estimated  $H_B$  from Google Earth<sup>1</sup> images by first calculating the ratio of  $H_B$  to the shadow length of known buildings, and thereafter utilising the identified shadow-length ratio to obtain the heights of other buildings with unknown heights. The approach sits somewhere between direct and indirect approaches in the sense that some field measurements are required. However, although the authors claim that their approach does not require any data, it is impossible to apply the proposed approach without measuring real  $H_B$  in the field, with the inevitability of the clear appearance of one vertical edge, three corners, and the shadow of the building in the image space. Liassis and Stavrou [180] developed a custom filter for enhancing shadows and reducing the spectral heterogeneity of the regions of interest (ROI) to form an optimized contour model for estimating  $H_B$  based on the shadow length and solar elevation angle. However, the presented approach was not tailored to detect the ROIs of the objects with spectral dissimilarity.

The results illustrate a large aggregate height variance due to the underestimation of building shadow lengths. Therefore, there is a need for the automated estimation of  $H_B$  from monocular VHR multispectral pan-sharpened satellite images based on shadow information. In particular, there is a need for: (a) the generation of artificial shadows,  $S_{Ar}$  from a simulation of the actual shadows,  $S_{Ac}$  of the buildings in the image space; (b) the consideration of the issue of overlapping shadows of the multiple buildings; and, (c) the development of an algorithm combining

---

<sup>1</sup>Google Earth. <https://earth.google.com>

(a) and (b) for the automated estimation of  $H_B$  by identifying the optimal height value for the given building.

### 3.3.3 The reconstruction of 3D building models

Automated creation of 3D models of objects based on the information derived from remote sensing data is a vibrant research area in remote sensing and computer vision alike. A considerable amount of research has been published on building detection, extraction, and 3D formation [18, 19]. In this study, the literature is briefly discussed in which the main aim was to extract 3D building models by non- and semi-automated approaches. In contrast, those previous studies which aimed to automatically extract 3D buildings from the monocular images of the optical satellite sensors will be discussed in greater depth.

Diverse approaches investigating the construction of the 3D version of buildings have been carried out on remote sensing data with user interface platforms and tools. Counsell et al. [181] developed web tools to create 3D urban models as an open source of digitisation from imagery. Another study based on digital elevation model (DEM) and space-borne imagery presented two applications of both a mobile- and web-user interface to generate 3D building models [182]. In a different approach, Yousefi et al. [183] used a semi-automatic method to create 3D building models using fuzzy-based segmentation from two single IKONOS images. The building heights were calculated manually by selecting the sides of building facades, while the rooftops were automatically segmented after applying the Fuzzy membership functions. In a different study conducted by Over et al. [184], a semi-automatic approach was presented to generate 3D visualisation of urban buildings and features by integrating free datasets from the Open-StreetMap (OSM) and DEM, based on producing a specific CityGML model. El-Garouani et al. [185] extracted 3D building models for 3D city planning utilities by overlapping a digital surface model (DSM) derived from aerial image stereo pairs and 2D building footprints using GIS. In a study conducted by Redweik et al. [153], it was shown that the direct measurements of urban objects (e.g. buildings), using a DSM derived from airborne LiDAR data, can provide elevation, slope, aspect, and shadow maps to generate 3D building models. In a similar manner, Catita et al. [186] proposed a semi-automatic approach for creating 3D building models using a DSM from LiDAR data integrated with other data using a GIS environment. However, to implement such an approach, a great deal of software must be installed to do the following: handle LiDAR data; create 3D models; enhance and codify the output of the 3D models; and

fuse building footprints, derived from aerial stereo photogrammetry and the 3D models, with other geo-spatial attributes, such as SketchUp, CityGML and ArcGIS.

Generally speaking, it is a fact that the aforementioned interactive or semi-automatic approaches require the intervention of a human operator, and basically depend on the user's skills and qualifications in constructing 3D building models. The most common shortcomings of all these studies is that the 3D building model outcomes depend on the availability of the elevation information derived from the measurements of the surface height, such as DEM and DSM, and/or other data availability, such as building footprints. The derived heights process from aerial photography or space-borne image pairs, in turn, requires a great deal of processing to capture the final height information. Further, non- and semi-automated approaches are always considered time consuming, in addition to requiring more effort and expense. Therefore, many attempts have been made to create 3D building models automatically. In this context, Vanegas et al. [187] presented an automatic approach based on computer vision techniques to reconstruct 3D building models based on calibrated oblique-angle aerial imagery using a Manhattan-world assumption. Colour segmentation, Generalized Rewriting Rule (GRR), and GRR optimisation were successfully employed to extrude the bounding box of the building footprint extracted from GIS data. Nonetheless, the proposed approach was confined for specific geometry shapes of buildings. Later, Woo and Park [188] presented an approach that employed the divergence-based centroid neural network algorithm to extract 3D line segments for rooftop detection using IKONOS images. The authors stated that the experimental results of the proposed method are efficient for rooftop detection and building reconstruction. Unfortunately, their approach only works on the availability of stereo images. In addition, the noise caused by other boundaries of trivial structures and objects gave an unvalidated irregular geometry of the building shapes. In a different approach, a graph- and fuzzy-based approach were proposed to infer polygonal building footprints and estimate building heights to visualise 3D building models as the final outputs derived from single QuickBird images [17]. However, the approach depends on the hypotheses definition and smoothness assumption to detect vertices from 2D rooftops and refine their shapes. Therefore, such hypotheses may only be valid for the selected building shapes. In a different context, Brédif et al. [189] presented a fully automatic framework based on an optimisation scheme to generate 3D buildings employing a DSM only from LiDAR data. Nevertheless, it should be noted that although the proposed framework is capable of merely addressing the DSM data, the final shape of the polygonal building footprint requires further subroutine schemes to refine and arrange building edges. In a similar context, Jakubiec and Reinhart

[108], created a 3D model of urban buildings using a combination of LiDAR and GIS data, but after uniformly sampling the LiDAR data with the geometric information to obtain the final 3D models. In the study performed by Lee and Kim [15], an automatic method for building roof extraction and height estimation was proposed to extract 3D building models with graph-based building hypothesis generation. The generated hypothesis for defining 2D rooftops is typically limited to representing the specific geometric properties of the buildings, and this means the proposed method may not be applicable with other building shapes. In another work, Partovi et al. [190] generated a DSM using two pairs of stereo data from the WorldView-2 satellite with 50 cm ground sampling distance (GSD), and a fully automated method of dense image matching based on convex optimisation, to extract the 3D building models. However, the authors stated that due to the low quality of the representation of building boundaries from DSM, K-means clustering and graph-based segmentation applied to the orthorectified panchromatic image were used to derive building roofs for further refinements to 3D models. This makes the proposed method limited to certain roof shapes. To the best of our knowledge, only two studies have exploited remote sensing data alone (i.e. monocular satellite imageries) without additional supplementary data to generate 3D building models in an automatic manner, as presented in [15, 17].

A common feature of most studies for producing 3D building models is that they employ either direct measurements (LiDAR or a laser scanner), or indirect measurements, such as stereo images, multiple images and multi-source data to acquire the geometric parameters of the buildings. The main problem of these approaches is that their implementation depends on the availability of the data used in terms of the location of the study areas (e.g. it would be more difficult if it is in a conflict area), cost (e.g. LiDAR and/or aerial images are more expensive than satellite imageries), and the time and effort of obtaining such data. Moreover, most research on the creation of 3D building models employing DSM and DEM derived from LiDAR or laser scanner or stereo images requires a high-degree of professional skill to handle their complicated parameters, and data from different sensors. Thus, the approaches are subject to low-resolution sampling or robustness or missing surfaces [16, 187].

Despite the aforementioned significant efforts, the findings of previous works indicate that the automated creation of 3D buildings from a single image is a very challenging task. Most of the previous studies, therefore, have implemented their approaches with a set of images or data sets from different sources, in order to extract building footprints and heights automatically. According to Ozgun [19] as well as Izadi and Saeedi [17], there has been some development

in new approaches with an advanced level of urban landscape. Further, Partovi et al. [190] pointed out that the complete automation and accurate extraction of realistic 3D building models remains open, especially when the only data used is satellite images.

### 3.4 The effect of building geometry on energy efficiency

The geometric identification of urban buildings plays an important role in a range of urban applications, including 3D representations of buildings, urban planning, and energy consumption analysis. In the solar energy potential assessment aspect particularly, the geometric identification of buildings as 3D models can provide a comprehensive vision of the assessment and simulation of solar exposed surfaces, which includes rooftops and facades.

Providing sufficient energy to meet the needs of urban dwellers is undoubtedly a challenging task. Solar energy is one form of clean renewable energy that can provide sustainable electricity without toxic pollution or global warming emissions. Therefore, there is a growing demand worldwide for the use of solar photovoltaic (PV) technology because it has a much lower environmental impact than other conventional energy sources. However, to exploit this renewable energy within urban areas, a crucial process is the automated detection and evaluation of the surfaces available for integrated solar installations. In particular, the evaluation of roof/surface brightness from a genuine source that presents the real characteristics and functionalities of buildings remains unsolved. Further, although considerable research has been devoted to detecting the rooftops of buildings, rather less attention has been paid to creating and completing a 3D building model. For this reason, there is a need to increase our understanding of the solar energy potential of surfaces and roofs to formulate future adaptive energy policies for the sustainability of cities.

Satellite imageries can provide a magnificent test domain for any application with a variety of illumination and environmental conditions, and are available in the public-domain (e.g. Google Earth). Such data are useful for locating individual buildings, connected buildings, and buildings of different sizes, providing information about their geometry, and depicting the surrounding environment of buildings and the urban fabric nearby. Therefore, it should be focused on assessing the solar energy potential not only of the rooftops but also the facades, including different geometry types of urban buildings.

Many previous studies in this context have evaluated the amount of insolation within urban areas on diverse data types, such as pre-existing maps of building footprints, LiDAR data, and/or aerial images. However, such data have proven their effectiveness in solar energy assessments within urban landscapes, even though the availability of such data in a particular urban area is mostly difficult to obtain. This is due to, for instance, their high costs (e.g. LiDAR and aerial images) or not being frequently updated (e.g. the building footprint maps). The production of the building location maps requires continued survey campaigns, which also require more money, time, and effort. Such data and maps cannot even be collected if there is a conflict within a study area or access is difficult. However, such cases have quite commonly collected real geospatial data to assess the solar energy potential for feeding the existing buildings with sufficient electrical energy as one form of solar energy utilisation. VHR satellite imageries are a good alternative to overcome the difficulty of collecting data from a genuine data source at lower cost, with continuous updating, and a wide area of coverage. In addition to the availability of visible bands (R, G, and B) in a VHR satellite image, the near-infrared band (INR) is an important spectral band that can be used to extract the shadow regions of buildings, which are considered significant data in the shadow analysis process, as part of the assessment process of the solar PV of building envelopes.

The extracted 3D object which represents an urban structure (e.g. buildings) can be used to evaluate the availability of the surfaces for integrated solar installations, and exploiting such renewable energy is a crucial assessment process. Many pioneering studies for the assessment of rooftop PV potential have been devoted to exploiting the potential of solar energy by investigating the availability and suitability of the rooftops of buildings. Based on modified solar-architecture rules of thumb, Peng and Lu [191] estimated the PV-suitable rooftop area from method, and the gross roof area is computed based on using a gross roof area vs. ground floor area ratio. Thereafter, solar suitability and architectural factors are used to calculate the potential PV-suitable rooftop area of two kinds of buildings, hotel and commercial, which is estimated at  $54 \text{ km}^2$  and with 5981 GWh as the predicted annual potential energy output. Another approach to evaluating the supply of solar energy to building rooftops (residential buildings) is based on the use of LiDAR data, introduced by Tooke et al. [192]. The approach contains Kernel window moving and thresholding methods to extract vegetation cover and buildings from a digital surface model (DSM). The calculation of the attributes in this approach, such as height and volume from DSM, was undertaken to investigate the solar radiation received by building rooftops. The total solar radiation received by residential buildings will be decreased

by around 38% because of urban structures, due to the influence of trees. Singh and Banerjee [193] presented a method for estimating the rooftop solar PV potential of a region based on various data (e.g. land use maps, Google Earth images, and climate data), and different tools (e.g. GIS and PVSyst simulation) with multiple strategies of analysis. The extraction of the total rooftop area available for PV installation is achieved by calculating the total Building Footprint Area (BFA) with the Photovoltaic-Available Roof Area (PVA) ratio applied to sample buildings through micro-level simulations using PVSyst. The estimated rooftop solar PV potential represents 2190 MW for the city, with median efficiency panels. The annual average capacity factor in this study was found to be 14.8%. A comparison between sample daily load profiles of the city and the typical expected photovoltaic generation profiles illustrates that the rooftop solar photovoltaic plan has the potential to provide 12.8-20% of the daily demand, during different months, with median efficiency panels. Using the highest (commercial) efficiency panels, this range goes up to 19.7-31.1%. The estimated rooftop solar PV potential shows its ability to bridge the energy shortage because the plan can meet 31% to 60% of the morning peak demand (9:00-12:00 hrs), and 47.7-94.1% of the morning peak demand with the highest (commercial) efficiency panels. Because the amount of sunlight is a crucial factor of solar PV efficiency, Ko et al. [26] evaluated the potential of solar PV power generation on rooftops. The approach was based on an analysis of building GIS layers (coordinates and stories) using a Hillshade module. A raster binarisation map was combined with hourly sun shadow greyscale values (including the solar azimuth and elevation angles of buildings), to distinguish bright and dark patches for computing roof shadow area. The results indicate about 12 428.5 MW as the rooftop solar PV installation capacity with a power generation capacity of 15 423.75 GWh. The installed power capacity for rooftop solar photovoltaic, when compared to the statistical data of the total electricity capacity for previous years, illustrates its capability to support the annual gross generation of the total electricity capacity of the selected city. The process of assessing the available solar radiation on the rooftops in the aforementioned studies was completely reliant on the existence of urban structure maps that may pose a problem in other study areas in which such maps are unavailable.

Many researchers have developed strategies that deal with the evaluation of urban structures by different applications, such as solar energy utilisation from VHR aerial/satellite images. Bergamasco and Asinari [23] proposed an approach to calculate the available roof surface for solar energy utilisations based on the systematic analysis and processing of aerial georeferenced

images. In a different work, Kabir et al. [109] attempted to recognise bright rooftops by classifying Quickbird images to estimate solar energy for PV application. Discrimination between rooftops and non-rooftops was achieved by Baluyan et al. [111], using image segmentation based on machine learning, namely: k-means clustering and support vector machines (SVM). The automated detection of different building structures through exploiting the shadow presence in VHR multispectral satellite images was proposed by Ozgun [19]. Because shadows in VHR satellite images can provide evidence of existing man-made structures, shadows are a key factor in the analysis of solar radiation across daylight [20]. In this regard, the estimation of the available rooftop area for PV installation was implemented by Jo and Otanicar [154], who analysed the patterns of shadow cast and its effects on the rooftops.

Interestingly, the calculation of the roofs and facades as a 3D solar building model has been taken into consideration by two recent studies. Redweik et al. [153] developed an approach to assess the solar energy potential of buildings based on the calculation, visualisation and integration of the potential of both building roofs and facades using LiDAR data (DSM) and a solar irradiation model based on climatic observations. The results of the solar 3D buildings analysis confirmed that the annual irradiation on vertical facades is lower than roofs. Spatiotemporal analysis was conducted for solar irradiation assessment on building roofs and vertical facades by Catita et al. [186], using three different datasets: a solar radiation model for roofs, ground and facades; a 3D building model; and, a DSM from LiDAR data fused in a GIS environment. The developed approach presents the assessment of multiple buildings with the details of the individual unit area at one end. However, the two approaches require the availability of DSM derived from airborne LiDAR data, which is a serious problem if we consider that the assessment of solar energy potential covers an entire city or large area of urban landscape.

The building envelope plays an important role in the protection of the interior environment from undesirable exterior conditions [194]. The amount of building area that is subject to solar gain is one of the most important determinants of energy efficiency, as shown in Figure 3.5. According to McKeen and Fung [194], the aspect ratio quantifies the building's footprint in a ratio of length and width ( $x:y$ ) and allows for the comparison of the surface area amongst different building designs. Figure 3.5 also shows that the geometrical relationship between surface area and the aspect ratio can determine the amount of surface area from which surfaces will be exposed from the light. Decreasing the amount of surface area minimises energy transfer [195]. Well-positioned buildings with well-designed envelopes in terms of the geometry, orientation, materials and construction methods affect energy consumption through heating and cooling. A

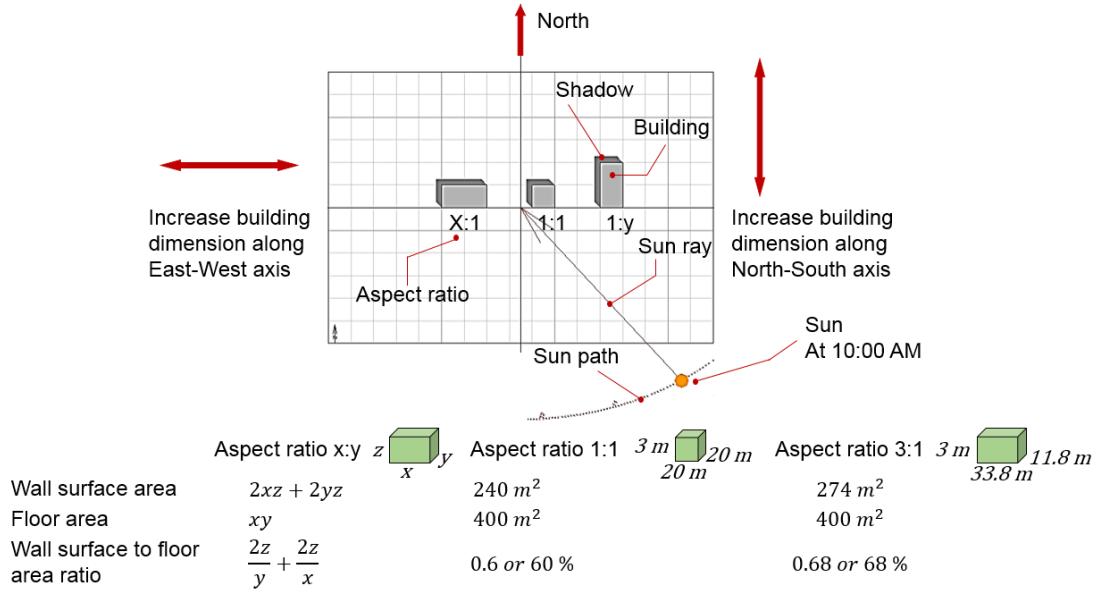


**Figure 3.5:** The effect of building geometry on energy efficiency. The increase of building dimensions ( $x, y$ ) in addition to the orientation and position of the buildings can change the amount of surface area which is exposed to sunlight. Reducing the amount of surface area decreases energy transfer. Modified after McKeen and Fung [194]

good building shape and orientation are two attributes considered the most critical elements of an integrated design, having a profound impact on energy consumption [194, 196]. However, to reveal the shape, position with respect to sun and other buildings, amount of the cast shadow, and orientation of the existing buildings from genuine and updated data covering a wide area of an urban landscape, VHR satellite images are therefore required. Furthermore, the creation of 3D building models is also required for a comprehensive view and actual evaluation of solar energy potential on the building envelopes.

### 3.5 Summary

The identification and creation of 3D building geometry from satellite images in an automatic manner is vital in both remote sensing and computer vision. All the derived information and details from VHR satellite images can offer important source data for understanding the complexity of urban landscapes or for addressing the ambiguity or problems in VHR satellite images within urban areas, using the development of computer vision and image processing techniques.

The chapter presents and describes the state-of-the-art methods and techniques that have been developed for deriving 3D building models from single VHR multispectral satellite images. The identification of the building's envelope geometry requires the extraction of the three dimensions of the building volume, represented by the building footprint and height. To create 3D building models from a single image (2D scene), very high performance algorithms that run automatically need to be developed to overcome issues with current approaches and techniques. For instance, shadow detection and extraction algorithms should cope with the uncertainty of discrimination between shadows and other dark objects spectrally (e.g. water), as well as the overlap between one shadow region and another (e.g. buildings, trees, cars). Regarding building footprint detection and extraction algorithms, the complexity of urban landscapes, weather and illumination conditions, different properties of the used images, the occlusion of the building's visibility, and similar characteristics between buildings and their background, must be taken into account to increase the efficiency of the developed algorithm. According to the aforementioned literature, although the theories and concepts of the reconstruction of 3D models has experienced a major development in their algorithms in recent times, the algorithm of the creation of 3D building models from a single 2D scene (e.g. an image) without additional complement data is still in its infancy.

## **Chapter 4**

### **Methodology**

The aim of this chapter is to describe and justify the methodology used by presenting the theoretical framework upon which this research is based. This chapter links to the literature chapters to explain the reasons for adopting and developing certain methods to achieve the obtained outcomes and to accomplish the thesis objectives on the academic basis of the choices of research design and data processing. The different stages of methodology are also explained in detail in this chapter, including the specific techniques used and algorithms developed, the controls used to ensure validity and the dimensions of the research strategy. A brief summary concludes this chapter. The findings of each stage of the research methodology are presented in the following chapter.

## 4.1 Research design

Buildings are the most prominent component and the core structure of urban environments. To assist in the decision-making process, which involves understanding, managing and planning the continuously changing environment and supporting sustainable city development, accurate and timely spatial information about buildings and their attributes in urban areas is needed [197]. To obtain geometric information related to urban buildings, remote sensing techniques, such as satellite imageries, can be used to monitor the earth's surface effectively due to the high temporal and spatial resolution. These techniques have the potential to automatically extract building information from urban areas [198]. Presenting the geometry of an urban environment using remote sensing data allows for the reconstruction of residential, commercial and industrial buildings in a 3D city model. Therefore, a completed database of 3D modelling, including information regarding geographic location, height, volume, compactness and other information (e.g. ownership for future use, occupancy status), for each building is important in the estimation of a building's solar potential. To this end, a new approach was developed to integrate the different components of the study in a coherent and logical manner so the methodology could be used to accomplish the study objectives. The methodology involved seven main stages that included validation techniques in the automatic creation of 3D building models. The chosen data for the developed approach included a set of pan-sharpened VHR multispectral satellite images. Optical VHR satellite images are considered one of the most important data input sources used in urban feature detection and extraction [150]. The developed approach for the 3D creation algorithm began with implementing a data enhancement to obtain a clear contrast between the objects in the urban landscape. Second, the shadow regions of urban buildings were detected, and their locations were distinguished from other non-building shadows and dark objects within the image space. Thereafter, the buildings' shadow evidence was effectively extracted after applying post-processing techniques to obtain a binary image that solely included the buildings' shadows. In the fourth stage, building footprints were detected based on shadow information and then extracted by applying a graph theory framework based on graph partitioning. During the fifth stage of the methodology, the geometric shapes of the extracted buildings were refined by improving the edges of the buildings' footprints. Sixth, the estimation of the buildings' heights is an important step in the creation of the 3D building models implemented with the aid of the solar information in the metadata file attached to the image data. After obtaining the footprints and heights of the buildings, in the seventh stage, 3D models of the existing buildings in the scenes were created. The methodology also included

a validation stage and a sensitivity analysis of the generated models, as shown in Table 4.1. Each stage of the methodology is explained in detail in the subsequent sections of this chapter to provide a complete overview of the developed approach.

#### 4.1.1 Rationale for the selected present methodology

The present methodology was set for two important reasons: (1) the method benefits from the NIR image band present in most VHR satellite images, and (2) the method is fully independent of user- and data-dependent threshold. Because the detection of the building footprint regions and the estimation of the building heights depend on the use of shadow information, the present method was created based on the extraction of the building shadow regions from single VHR multispectral satellite images in an automatic manner. Therefore, the key reason in creating this methodology in this form and/or design is to overcome other approach deficiencies in detecting and extracting shadow regions from satellite images, such as the similarity in the spectral characteristics of shadow regions with non-shadow man-made regions, the recognition of the shadow region edges with the ability to extract and separate them from other urban objects to reflect their true shapes, and the overlapping between shadow regions.

As stated in Chapter 3, shadow regions in the general exhibit lower radiance values over the entire spectrum, and sensor irradiance from shadow regions decreases from short to long wavelength due to scattering [199]. Therefore, it is easier to distinguish shadow regions from non-shadow regions with NIR image band. Moreover, the semi-automated approaches for extracting shadow regions or building regions or heights or even for creating 3D models were not applied in this study because they run by users and they require further time to achieve the image processing tasks.

#### 4.1.2 Data selection

The main data used in the methodology were the multispectral imageries at a VHR resolution, which were captured by state-of-the-art optical sensors onboard space platforms. Using satellite imageries extends the vision beyond what can normally be seen by the human eye. The scope of human vision is limited to the visible portion of the electromagnetic spectrum, which encompasses red, blue and green energy. Multispectral sensors can capture images beyond

these energy wavelengths, including near infrared (NIR), shortwave (SWIR) and thermal energy (TIR). These wavelengths are important because certain features of the earth's surface respond differently in these wavelengths. The exploitation of the advantages of multispectral imaging facilitates the process of the discrimination and detection of objects (e.g. buildings, vegetation, etc.) and features (e.g. the shadow regions are cast by urban structures and non-building man-made object like trees) within complex landscapes, such as urban areas. The radiance reflected from shadow regions and received by the satellite sensors decreases from short to long wavelengths over the electromagnetic spectrum, and thus shadow regions exhibit lower radiance values [199]. Therefore, the differentiation between shadow regions and non-shadow areas using the NIR channel (an image band) with RGB image bands becomes easier [19]. By combining the RGB bands with the NIR band, specific features are clearly contrasted with their backgrounds and surroundings, which facilitates the extraction of the objects (e.g. buildings). Band combinations are a quantitative approach used to visualise the information in the bands and to determine how a feature responds in different bands to become distinguished from the background and other features surrounding it [200].

Accordingly, the VHR multispectral satellite images have several environmental uses depending on the phenomenon or feature observed. VHR satellite imagery is considered one of the highest quality forms currently available from remote sensing satellites due to its ability to offer sub-metre resolution. This means that VHR satellite imageries are capable of providing a high level of detail, making them a reliable and vital source of information. They support a range of services, especially in urban areas, for city planning and monitoring, urban change detection, estimation of human activities/population and urban object/feature detection. The presented approach utilised these data merits to detect and extract the footprints of buildings and their shadow information more easily. The approach employs pan-sharpened multispectral imagery with combined bands (B, G, R and NIR), which are mostly provided by most VHR satellite imaging sensors, as shown in Figure 4.1. Further details are provided in Chapter 3. In the next section, the first part of the methodology is presented, which includes additional details about the shadow information in the satellite images.

**Table 4.1:** The methodology flowchart for a 3D building creation algorithm. The flowchart provides the summary of the key processes, formulae and parameters

Stage	Task	The subroutine process of Alg. <sup>a</sup>	The key formulae & parameters
1	Image enhancement	<ul style="list-style-type: none"> <li>- Normalise image bands values</li> <li>- Adjust image intensity values</li> </ul>	<ul style="list-style-type: none"> <li>- <math>\text{ImgR} = (\text{imgR} - \text{min\_img}) / (\text{max\_img} - \text{min\_img})</math>, (<math>R</math>= red image band)</li> <li>- Contrast stretching threshold</li> </ul>
2	Shadow detection	<ul style="list-style-type: none"> <li>- Normalise all images bands</li> <li>- Divide between RGB and NIR</li> <li>- Apply the non-liner mapping function to RGB and NIR, then Multiply their outcomes</li> <li>- Multiply the results from division and multiplication operations</li> <li>- Thresholding and Refining</li> <li>- Subtract vegetation cover</li> </ul>	<ul style="list-style-type: none"> <li>- <a href="#">4.1 – 4.7</a></li> <li>- The slope of the sigmoid function <math>\alpha</math>, the inflection point <math>\beta</math> and <math>\gamma</math> to stretch the histogram in the dark parts before applying the sigmoid function</li> </ul>
3	Post-processing of the shadow regions	<ul style="list-style-type: none"> <li>- Region growing function</li> <li>- Create morphological structuring element</li> <li>- Apply morphological opening</li> <li>- Apply Fuzzy landscape</li> </ul>	<ul style="list-style-type: none"> <li>- <a href="#">4.8, 4.9 and 4.10</a></li> <li>- Intensity (<math>T_I</math>), ratio (<math>T_R</math>), search region (<math>T_{\text{low}} - T_{\text{high}}</math>), and vegetation ratio (<math>T_{\text{veg}}</math>) thresholds.</li> </ul>
4	Building footprint identification	<ul style="list-style-type: none"> <li>- Apply Gaussian Mixture Models (GMM)</li> <li>- Define ROI and bounding box</li> <li>- Apply GrabCut Algorithm</li> <li>- Select only the buildings, inside the ROI, adjacent to the shadow region</li> <li>- Create the building mask (binary image)</li> </ul>	<ul style="list-style-type: none"> <li>- <a href="#">4.11, 4.12 and 4.13</a></li> <li>- Shrinking distance (<math>d</math>), ROI size, smoothing constant (<math>\gamma_1</math>), area threshold of the selected bounding box</li> </ul>
5	Shape refinement, and solar rooftop analysis	<ul style="list-style-type: none"> <li>- Apply Active Contour Algorithm</li> <li>- Apply shape fitting functions</li> <li>- Extract the refined building Mask</li> <li>- Calculate roof area and orientation</li> </ul>	<ul style="list-style-type: none"> <li>- <a href="#">4.14 – 4.18</a></li> <li>- Number of iterations, area and shape fitting thresholds</li> </ul>
6	Building height estimation	<ul style="list-style-type: none"> <li>- Generate artificial shadows</li> <li>- Simulate actual shadow regions</li> <li>- Compute Jaccard index</li> <li>- Extract the optimal estimated height value</li> </ul>	<ul style="list-style-type: none"> <li>- <a href="#">4.19 – 4.24</a></li> <li>- Minimum height (<math>h_{\text{max}}</math>), minimum height (<math>h_{\text{min}}</math>), height interval, Jaccard index, area (<math>\rho</math>) thresholds</li> </ul>
7	3D Models of Buildings and validation	<ul style="list-style-type: none"> <li>- Create a 3D volumetric image</li> <li>- Perform image convolution by a Gaussian filter</li> <li>- Apply Marching Cubes algorithm</li> <li>- Create 3D models in level of details and overlay their real location on a given image</li> </ul>	<ul style="list-style-type: none"> <li>- <a href="#">4.25, 4.26 and 4.27</a></li> <li>- Gaussian low pass filter of size, <i>Sigma</i> (<math>\sigma</math>) and isovalue parameters</li> </ul>

<sup>a</sup>Alg.: Algorithm

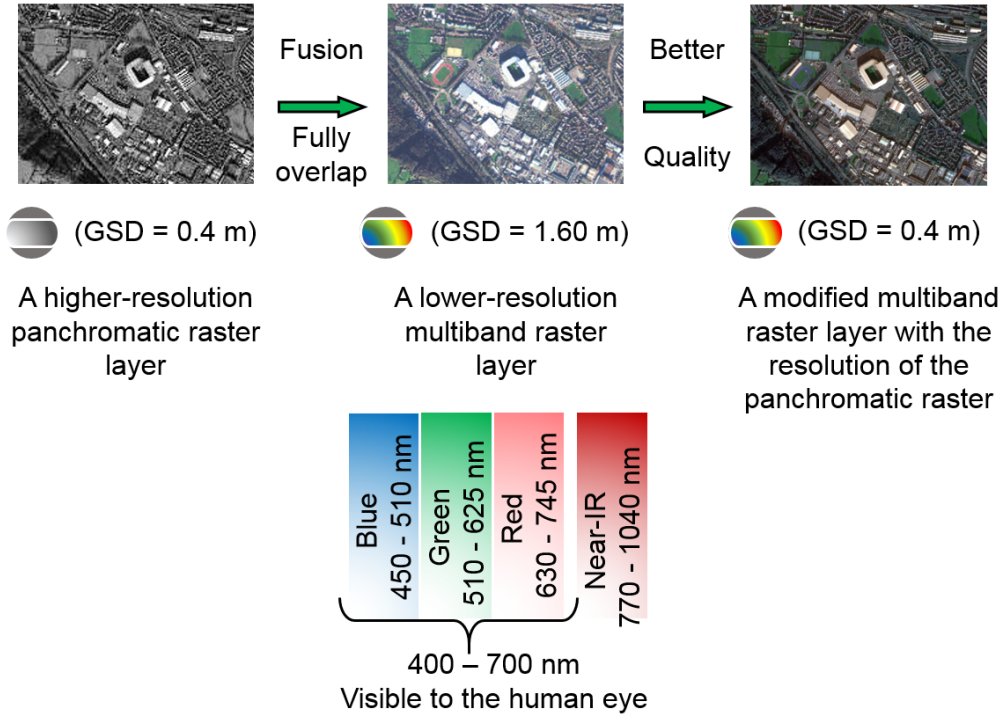


**Figure 4.1:** The employed data: pan-sharpened multispectral satellite imagery

#### 4.1.3 Shadow information and the theoretical concept

For above ground urban constructions such as buildings and bridges, shadows are the most common accompaniments, which can be seen in VHR images. When intercepted by an off-terrain object, incident light rays, usually sunlight, generate shadows that are cast on other urban surfaces/objects of image capture by optical satellites. Figure 4.2 presents the three conditions (a light source, an object to cast the shadow line and a surface to receive the shadow line and shadow) that must be met to produce a shadow. In this context, a shadow indicates the shape of the object casting it, and in many ways, it can indicate the texture of the surface receiving the shadow [201]. In contrast, shade can be defined as the side of an object opposite to the direction of illumination, which has less of a colour tone than full blackness (the value intensity of darkness) compared to the object's shadows, which have low values, mostly zero values, of brightness in VHR images (pure black colour).

The line that locates and separates the light and shade areas on the object determines the shadow line on a receiving surface. In turn, the shadow line determines the dark area cast onto the surface on which the object rests and that receives the shadow cast. Therefore, the shadow line and the dark area (shadow regions) in optical satellite imageries have become key topics that have attracted attention in the research field. The dark pixels that belong to

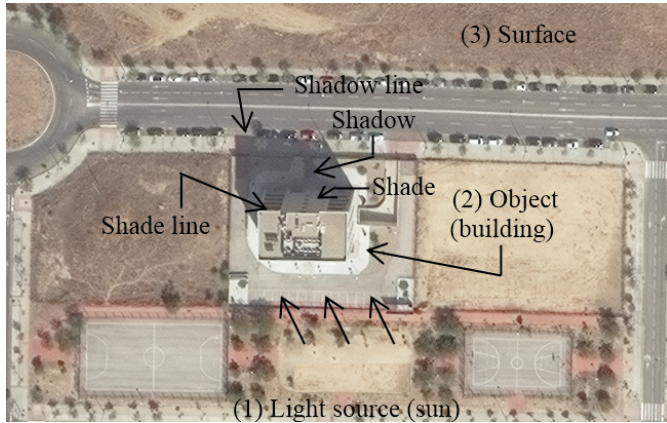


**Figure 4.2:** Shadow conditions from the VHR pan-sharpened multispectral satellite imagery

the shadow regions in an image were analysed based on two main aspects. These aspects depend on how the shadow regions in the VHR images have been treated by researchers; they are either viewed as a disadvantage that must be addressed or as an advantage to be exploited.

The shadow concept can therefore be understood as shadow progressions that begin from determining points and then move to lines (being composed of points), then to planes (being composed of lines) and lastly to solids (being composed of planes), as shown in Figure 4.3. In fact, the shadow of a line, a plane, or a solid is most efficiently determined by locating the shadows of the critical points of the line, plane or solid [201]. Moreover, if parallel lines (paralines) extending from an object to its shadow cast on a flat surface with a sufficient distance between them are drawn in the virtual world, the identical size, shape and orientation of the object will be obtained. This is because the greater the distance, the greater the shadow displayed; however, the situation is completely different with objects' shadows within urban areas in VHR satellite imageries in terms of urban fabric, as these often exhibit compact areas of buildings as one factor. This factor can affect the actual size and shape of urban objects presented by their shadows because the shadow line of the object will be shorter in the case of a rise in a horizontal receiving surface and longer where there is a drop in this surface for the other objects within urban areas. The second factor is the existence of trees and their shadows or even shadows from unconstructed areas, such as vehicles, which can distort the real boundaries of shadows (the geometric forms) and give an arbitrary shape to the constructed objects when they combine with the objects' shadows. Another factor to consider is that the shadow regions of objects in images are larger in the winter than in summer due to the sun's position in the sky vault and its angle and altitude. Spectrally, non-shadow regions, such as water, can present the same pixel intensity values or darkness with the shadow regions of the objects in images,

causing an error in detecting shadows. Therefore, shadow detection and its extraction from VHR satellite images is a complex task, and all image processing techniques used to detect shadows still depend on the estimation of shadow areas using various developed methods.

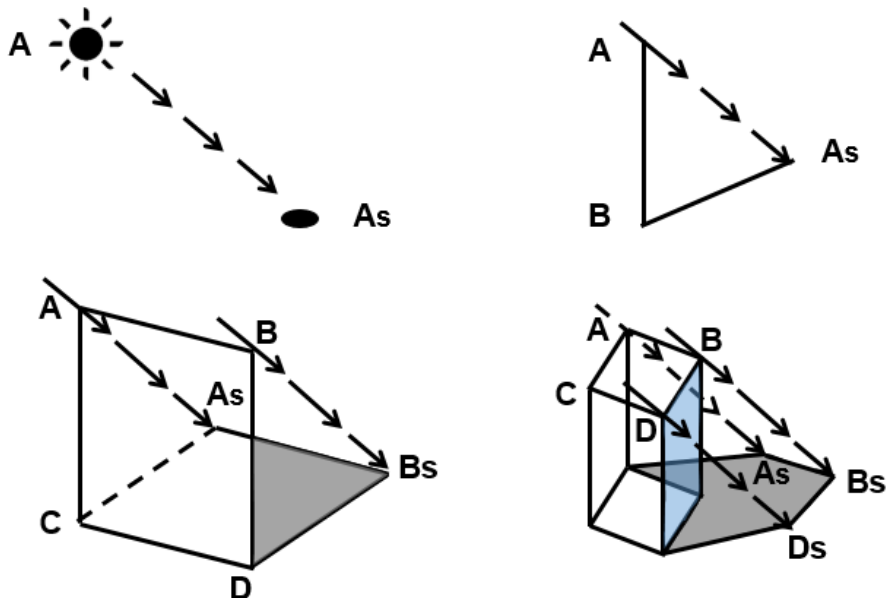


**Figure 4.3:** Shadow progressions: the shadows of a point (top left), a line (top right), a plane (bottom left) and a solid (bottom right)

## 4.2 Shadow detection and extraction

### 4.2.1 The detection of shadow regions using Near-Infrared information

Shadow regions are distinct in terms of tincture because they exhibit a dark colour compared with their surroundings in the image space; however, the automatic process of the detection of shadow regions from sensed data is a complex task [150]. This is because some non-shadow dark regions share the same characteristics with the cast shadow regions within urban landscapes captured by satellite sensors using visible images, such as colour, texture and shape. The utilisation of the advantages of the NIR image can help differentiate cast shadows from other dark objects because shadows tend to have a much lower sensor radiance than other urban objects over the entire reflective spectrum. According to Adeline et al. [199], sensor radiance received from shadowed regions decreases from short to long wavelengths due to scattering. Specifically, shadows mainly receive scattered light and reflected light. Scattering effects significantly decrease towards longer wavelengths from approximately 85% to 5%.

Because the NIR channel is longer than visible channels in the wavelength, it is easier to distinguish shadows from non-shadows using the NIR channel. Based on the principle and concept of the behaviour of shadows, shadow regions can be detected by the NIR band. To reliably detect the actual shadow regions of buildings,  $S_{Ac}$ , a state-of-the-art approach proposed by Rüfenacht et al. [149] was developed for building shadows specifically. The approach depends on detecting dark pixels in both visible (V) and near infrared (NIR) bands of images by computing a ratio between these bands on a pixel-by-pixel basis, which allows for disambiguation between shadows and dark objects. First, the values of the pixels  $P_{ij}^k$  were normalised for all image bands  $0 \leq P_{ij}^k \leq 1, k \in (R, G, B, NIR)$ , without any processing applied. Next, a brightness image  $L$  was created by calculating the average for each pixel  $l_{ij}$  in the visible image V (R, G, and, B) over its three colour bands (channels):

$$l_{ij} = \frac{P_{ij}^R + P_{ij}^G + P_{ij}^B}{3} \quad (4.1)$$

Then, the candidates of the shadow regions were obtained by applying a non-linear mapping function that compresses the shadows and highlights, which allows us to mark fewer but better controlled pixels as shadow candidates of the extracted dark pixels ( $D_V$  and  $D_{NIR}$ ) from the brightness image, as follows:

$$f(x) = \frac{1}{1 + e^{-\alpha(1-x^{\frac{1}{\gamma}}-\beta)}} \quad (4.2)$$

$$d_{ij}^V = f(l_{ij}); \quad d_{ij}^{NIR} = f(P_{ij}^{NIR}) \quad (4.3)$$

where,  $\alpha$ ,  $\beta$  and  $\gamma$  are parameters to control the sigmoid function. The slope of the sigmoid function is influenced by the value of the parameter  $\alpha$  with 14, which was obtained by optimisation over the datasets used; the inflection point is set by the parameter  $\beta$  with its value 0.5 to keep the inflection point centred; and the value of the parameter  $\gamma$  ( $>1.0$ ) allows the histogram to be stretched in the dark areas before applying the sigmoid function, and therefore the value for  $\gamma$  was 2.2 to imitate the non-linearity of common colour encodings. The same values for the three parameters were applied to all inputs.

The role of the non-linear mapping function  $f$  is to give greater strength or firmness to the output pixels of the detected shadow regions in addition to inverting the tonal values of the dark and bright areas in the test images to obtain an outcome in which the shadow regions have a high value. Because the dark pixels in both visible V and NIR images indicate the condition of the shadow region's presence, the pixels of the shadow regions are computed as the shadow image  $D$  using the following formula:

$$d_{ij} = d_{ij}^V d_{ij}^{NIR} \quad (4.4)$$

Thereafter, a ratio image  $T$  is calculated between V and NIR bands on a pixel-by-pixel basis because the output values of the ratios can have a significant impact on shadow detection. The division process of the image bands can refine the outcomes of the shadow image candidate. Because the difference in illumination far outweighs the difference in the reflectance of the shadow, and because sunlight actually emits approximatively as much energy in the NIR band as in the visible bands, the ratio image  $T$  outlines the shadows so that the image's tone is mapped for better visibility [149]. The pixel  $t_{ij}^k$  of the image ratio  $T$  can be calculated as follows:

$$t_{ij}^k = \frac{P_{ij}^k}{P_{ij}^{NIR}}; \quad t_{ij} = \frac{1}{\tau} \min(\max_k(t_{ij}^k), \tau) \quad (4.5)$$

where  $k = \{R, G, B\}$ , by applying an upper bound  $\tau$  to the value  $t_{ij}$  to avoid this value reaching infinity when  $P_{ij}^{NIR}$  approaches zero; however, depending on the outcomes of  $T$ , it may not be enough to detect the shadow regions due to the potential variability of the reflectance in the visible and NIR images. On the other hand, the max operator was used because image reflectance values can often have very low values in one or two of the colour bands, although rarely in all three. Therefore, the value of  $\tau$  was set at 10 to deduce the difference in illumination within image space, which also provided better discrimination results.

Finally, the produced shadow image  $D$  in Eq (4.4) includes not only every possible shadow pixel but also the pixels of the dark objects. Because both the V and NIR pixel values of a given object are dark, the multiplication of  $T$  by  $D$  will adequately discriminate between an actual shadow and a dark object. Therefore, the initial shadow image  $M_{S,I}$  in a binary image format can be obtained using the following formula because both  $T$  and  $D$  are in the range  $[0, 1]$ :

$$M_{S,I} = (1 - D)(1 - T) \quad (4.6)$$

Thus, the results are subject to the optimal threshold that can provide the best separation between the shadow and the non-shadow pixels. The thresholding process involves computing the histogram of the shadow image according to Sturges' rule, in which the threshold is set at the value of the first valley in the histogram. The first valley of the image histogram was defined as the smallest valued bin of the histogram where the two neighbouring bins to the left and the two to the right have larger, increasing values. Because the shadow detection method was applied to a wide variety of types of images, except for VHR optical satellite images, the final findings of the shadow detection method, which is a binary image  $M_{S,I}$ , were influenced by noise, and they contained other detected regions that did not belong to the shadow areas. Therefore, the shadow detection method was developed to detect shadows from satellite images by eliminating other small dark areas. To this end, a morphological filter was proposed to remove all small objects, i.e., the non-shadow pixels. Therefore, the process of elimination of small objects is controlled by removing the areas  $< 100$  pixels to keep only the building shadow areas. The entire developed shadow detection algorithm is presented in Figure 4.4. The following section focuses on extracting the shadow mask  $M_S$  only by removing vegetation within the urban landscape.

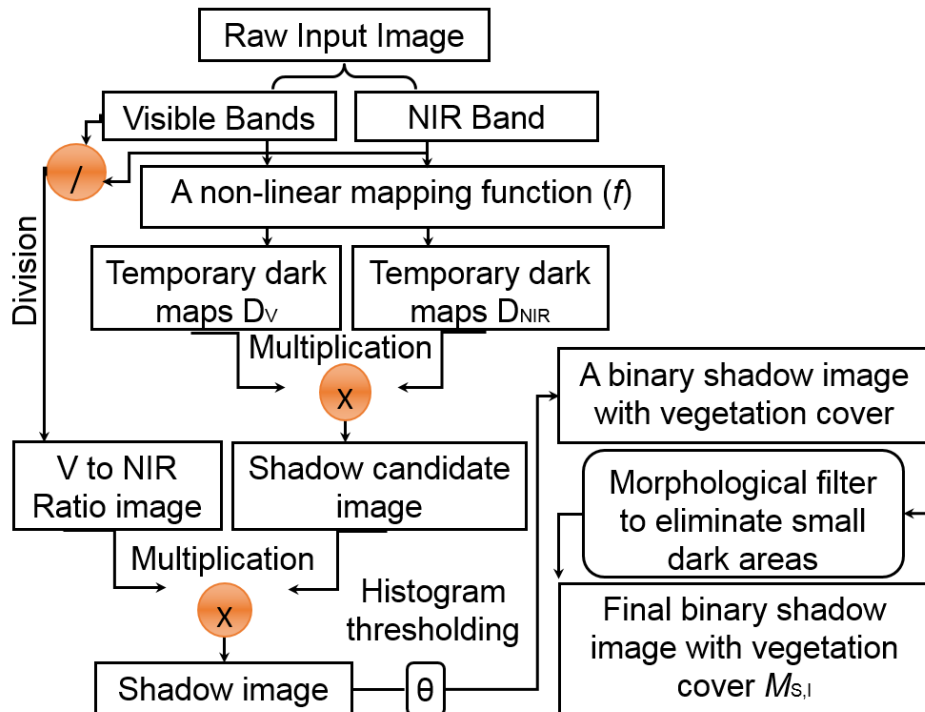


Figure 4.4: The developed shadow detection framework

### 4.2.2 Shadow region extraction

The removal of vegetation cover using Rufenacht's approach was not taken into account. Hence, the binary image (the initial shadow mask)  $M_{S,I}$  contained both shadow and vegetation regions. In addition to extracting the initial shadow mask  $M_{S,I}$ , the extraction of vegetation areas was achieved by applying the well-known Normalised Differential Vegetation Index (NDVI), as follows:

$$\text{NDVI} = \frac{\rho_{\text{nir}} - \rho_{\text{red}}}{\rho_{\text{nir}} + \rho_{\text{red}}} \quad (4.7)$$

where  $\rho_{\text{nir}}$  and  $\rho_{\text{red}}$  denote both image bands NIR and red, respectively. The use of the NDVI allows for the inference of healthy vegetation from the images. The presence of vegetation in the test images can be indicated by the larger values of the NDVI [150]. Next, a binary vegetation mask  $M_V$  was computed using automatic histogram thresholding [202]. The final shadow mask  $M_S$  was attained by subtracting the  $M_V$  from the  $M_{S,I}$ .

## 4.3 Building detection and extraction

### 4.3.1 Shadow post-processing

The effective performance of the building detection process depends on the accuracy of shadow region detection and the precision of the extraction. Therefore, two post-processing techniques were applied to the shadow mask  $M_S$ . The goals of the post-processing step were to: (a) improve the shape and boundaries of detected shadow regions; (b) eliminate all cast shadows that do not correspond to the main structure of the building; and (c) remove the landscapes that might result from the cast shadows of vegetation canopies. Therefore, a constrained region-growth process (Figure 5.5b) (Chapter 5), morphological operations with a thresholding scheme and pruning of the final shadow regions by modelling fuzzy landscapes were applied, as proposed in Ozgan et al. [150]. During the constrained region-growth process shown in Figure 4.5, the neighbouring pixels of each initial seed pixel, labelled as a shadow in the shadow mask, were examined to determine whether they were located within a region using an iterative region-based segmentation. The growth of the region depends on an 8-connected neighbourhood of the similarity of the adjacent pixels' intensities after normalising the false colour image

bands of the Hue-Saturation-Intensity (HSI) generated from the combination of bands (NIR, R, and G).

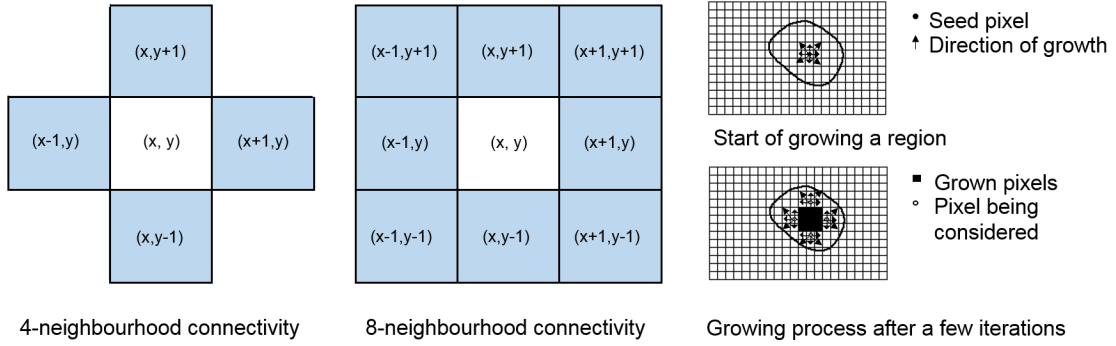


**Figure 4.5:** The concept of image pixel connectivity and region growth

With each iteration, the difference between the mean intensity of the region and the intensities of all the neighbourhood pixels were assessed, and pixels were allocated to the region with the smallest difference in the neighbourhood. The iteration stopped when this difference was larger than a threshold  $T_I$ . The growth process was also controlled using a ratio threshold  $T_R$  to remove the regions that were incorrectly labelled ‘shadow’ and that became large areas after the growth process. Thus, a comparison between the number of pixels in the shadow regions before and after the growth process was conducted. The cast shadows from other independent non-building, man-made objects (e.g. fences and cars) can become an issue when merged with the building shadows; however, a given elevation threshold for these objects can mask their shadow regions in the direction of the illumination. Nevertheless, the investigation of the length of shadow components in the illumination direction is insufficient if used alone to remove the cast shadows of these objects. Therefore, the morphological opening operation was applied to all shadow components by generating a flat structuring element ( $\nu_{L,\lambda+\pi}$ ). The creation of the specific flat structuring element is based on the captured solar information in the metadata file that allows for maintaining the directional information ( $\lambda = Az - \pi/2$ ) with the smallest length of connected single edge segment  $l$ . By setting a threshold value  $H_T^{\max}$  for non-building objects’ elevation, the length of the single edge segment  $l$ , is as follows:

$$l = \frac{H_T^{\max}}{\tan \phi R_{\text{img}}} \quad (4.8)$$

where  $\phi$  is the sun elevation angle, and  $R$  is the spatial resolution of the image required to determine a given illumination direction. After creating the structuring element, each shadow component was labelled and evaluated by applying the morphological process. This process

was applied to all 8-connected components of shadow that may exist in a single image, and then all improved outputs of shadow regions were gathered into the image.

To model the spatial configuration between buildings and their shadows, a morphological fuzzy relation approach was used for two purposes: investigating the vegetation presence within the illumination direction and eliminating the landscapes that might result from the cast shadows of vegetation canopies. Thus, the landscape  $\beta_\lambda$  around a given shadow object  $B$  is defined as a fuzzy set of membership values in an image space along the given direction  $\lambda$ :

$$\beta_\lambda(B) = (B^{per} \oplus \nu_{L,\lambda,\sigma,k}) \cap B^C \quad (4.9)$$

where  $B^{per}$  is the perimeter pixels of the shadow object  $B$ ,  $\nu_{L,\lambda,\sigma,k}$  represents a non-flat line-based structuring element, and  $B^C$  refers to the complement of the shadow object  $B$  calculated in the 8-neighbourhood connectivity. The operators  $\oplus$  and  $\cap$  are the morphological dilation and a fuzzy intersection, respectively. The non-flat line-based structuring element is calculated as follows:

$$\nu_{L,\lambda,\sigma,k} = \nu_{L,k,\lambda} * \nu_{\sigma,k} \quad (4.10)$$

where  $\nu_{L,k,\lambda}$  is the flat structuring element,  $L$  is the line segment,  $k$  is the kernel size to control the decrease rate of the membership values within the element and  $\lambda$  is the angle where the line is directed, while  $\nu_{\sigma,k}$  denotes a Gaussian non-flat structuring element with Kernel size  $k$ .

The existing vegetation within the directional neighbourhood of the shadow regions was investigated by generating a search region. The search region in the immediate vicinity of each shadow object was defined by setting the threshold values of  $T_{low}$  and  $T_{high}$  to the generated membership values of the fuzzy landscape. Once the region was defined, the existence of vegetation within the defined region was determined using a vegetation mask  $M_V$  and by applying a threshold  $T_{veg}$ . If there is substantial evidence of vegetation ( $\geq T_{veg}$ ) within the search region, then a fuzzy landscape region generated from a cast shadow was rejected. The investigation was conducted by calculating a ratio between the total number of pixels attributed as vegetation in the vegetation mask to the total number of pixels located in the search region. After the pruning process, the post-processing step was refined by adding another region

growing step of the shadow mask where the shadows were segmented with more precision (Figure 5.5e, Chapter 5).

### 4.3.2 Building footprint detection

A graph partitioning approach was used to accurately separate a given building region from its background, and the building detection task was considered a two-class partitioning problem. For full automatic detection and extraction of the building footprints from the image used, the GrabCut partitioning approach was utilised, which was proposed by Rother et al. [203] and implemented in a semi-automated manner, and a complete automated implementation that was proposed by Ozgun [19] was used. Based on the graph theory concept, the GrabCut approach treats the input image as a graph in which a given building region is accurately separated from its background. The issue involved in partitioning two classes of foreground/background image pixels was addressed through an iterative binary-label graph-cut optimisation, where a globally optimal segmentation solution can be found. To achieve the partitioning process for extracting building regions (footprints) automatically, therefore, Ozgun's first-level partitioning technique was adopted, as in [19]. The inputs consisted of the input image and labelling:  $\mathbf{z} = (z_1, z_2, \dots, z_N)$  is a given set of image pixels with an initial labelling from a tri-map  $T = \{T_B, T_F, T_U\}$  for assigning each pixel, which represents the background  $T_B$ , foreground  $T_F$  and unlabelled  $T_U$ , respectively. Each pixel was initially assigned to the value  $\underline{\alpha} = (\alpha_1, \alpha_2, \dots, \alpha_N)$  corresponding to background and foreground, where  $\alpha_n \in \{0,1\}$  and the underline operator indicates the parameters to be estimated/solved. First, the algorithm begins by applying the K-Gaussian Mixture Models (GMMs) with  $K$  components for foreground ( $K_F$ ) and background ( $K_B$ ) classes, constructed as the vector representing the mixture components for each pixel by defining  $\mathbf{K} = \{k_1, k_2, \dots, k_N\}$  with  $k_n \in \{1, \dots, k\}$ . Next, for the partitioning, the Gibbs energy function was applied, as follows:

$$E(\underline{\alpha}, \mathbf{K}, \underline{\theta}, \mathbf{z}) = U(\underline{\alpha}, \mathbf{K}, \underline{\theta}, \mathbf{z}) + V(\underline{\alpha}, \mathbf{z}) \quad (4.11)$$

where  $\underline{\theta}$  represents the probability density function as the output from mixture modelling for each pixel. The function has two steps: fitting models to data  $U(\underline{\alpha}, \mathbf{K}, \underline{\theta}, \mathbf{z})$  denotes the fit of the background/foreground mixture models to the data  $\mathbf{z}$ , taking into account  $\alpha$  values, which can be defined as:

$$U(\underline{\alpha}, \mathbf{k}, \underline{\theta}, \mathbf{z}) = - \sum_n D(\alpha_n, k_n, \underline{\theta}, z_n) \quad (4.12)$$

where  $D(\alpha_n, k_n, \underline{\theta}, z_n)$  denotes the optimal label preferences for each pixel  $z_n$  based on the observed pixel values. In the second part,  $\mathbf{V}(\underline{\alpha}, \mathbf{z})$  is the smoothness term for the class boundaries, which is written as:

$$\mathbf{V}(\underline{\alpha}, \mathbf{z}) = \gamma_1 \sum_{(m,n) \in C} [\alpha_n \neq \alpha_m] e^{-\beta \|z_m - z_n\|^2} \quad (4.13)$$

where  $\gamma_1$  and  $\beta$  are the constants that identify the degree of smoothness. The smoothness term  $\gamma_1$  is fixed to a constant value over a set of images. In contrast, the other smoothness  $\beta$  is computed automatically after evaluating all the pixels in an image. A binary indicator function is expressed by the term  $[\alpha_n \neq \alpha_m]$  that takes a value of 1 if  $\alpha_n \neq \alpha_m$ , and  $C$  refers to the set of the neighbouring pair of pixels computed in the 8-neighbourhood connectivity. To accomplish the partitioning by estimating the final labels of all pixels in the image, the minimum cut/max-flow algorithm was applied [203].

For a fully automatic reliable labelling of the building regions/foreground  $T_F$  and non-building regions/background  $T_B$ , the shadow regions and generated fuzzy landscapes are used to: (a) apply two thresholds  $(\eta_1, \eta_2)$  to the membership values resulting from the generated fuzzy landscapes; (b) define the  $T_F$  in the vicinity of each shadow object with its delineated boundaries; and (c) employ a single shrinking distance parameter (d) for acquiring a reliable  $T_F$  region.

The most probable locations for building footprints are extracted by dilating the shadow region for each shadow component, which is accomplished with a flat line structuring element, defined in the opposite direction of illumination. Therefore, for each shadow component, a bounding box is generated, whose extent is automatically determined after dilating the shadow region; the box is generated to select the  $T_B$  and to define the ROI region within the covering bounding box in which the GrabCut partitioning is performed. The extent of the ROI and the bounding box are subject to the single distance parameter and the ROI size values. Once the covering bounding box was determined, the automatic labelling of the background information pixels  $T_B$  was conducted based on considering all the pixels within the bounding box that belong to the shadow and vegetation regions. The regions outside the ROI region are  $T_B$  and inside the ROI

are  $T_F$ . The labelling process was repeated for all sets of building regions in the entire image domain.

#### 4.3.3 Geometry adjustment of the extracted building footprints

According to Ozgun [19], an incorrect assignment of the labels of buildings, vegetation and shadow pixels and others (a class for assigning pixels that do not belong to any of these classes) may occur after the GrabCut partitioning process. This can cause additional or diminishing areas at the edges of the detected building regions. Therefore, a geometric-adjustment approach was developed at two sequential levels to refine the extracted shapes of building footprints. The first step consists of applying for shape recovery, which is also one of the computer vision approaches proposed by Chan and Vese [204]. Active contours  $A_{AC}$  is an image segmentation algorithm, which is an energy-minimising, two-dimensional spline curve that evolves (moves) towards image features, such as strong edge [148], as shown in Figure 4.6. The output image is a binary image where the foreground is white (logical true) and the background is black (logical false). An input mask is a binary image that specifies the initial state of the active contour. The boundaries of the object region(s) (white) in the mask define the initial contour position used for contour evolution to segment the image. To obtain faster and more accurate segmentation results, an initial contour position is specified that is close to the desired object's boundaries. Therefore, the active contour approach is used to penalise a shape with high curvature, starting with the inputs of greyscale images of datasets and the binary images derived from the partitioning process (including building footprints) with the maximum number of iterations, as shown in Figure 5.7 (see Chapter 5). The implementation of the algorithm continues until the maximum number of iterations is reached to accurately obtain the required building boundaries. In order, the tasks that are achieved by the  $A_{AC}$  are: (1) creating a single distance map from the binary image; (2) obtaining the curve's narrow band; (3) calculating the mean inside and outside the curve; (4) computing the two forces to shrink and expand the contour; (5) calculating gradient descent to minimise energy; and (6) evolving the curve to attain the final enhanced building mask.

Although the output of the application of the active contour without edges approach improves the shape of the detected buildings, as shown in Figure 5.7f (see Chapter 5), and a given building region is without an increase or decrease in its area, the building edges are not in a regular geometric form (e.g. rectangle, circle). Due to the different initial conditions where the

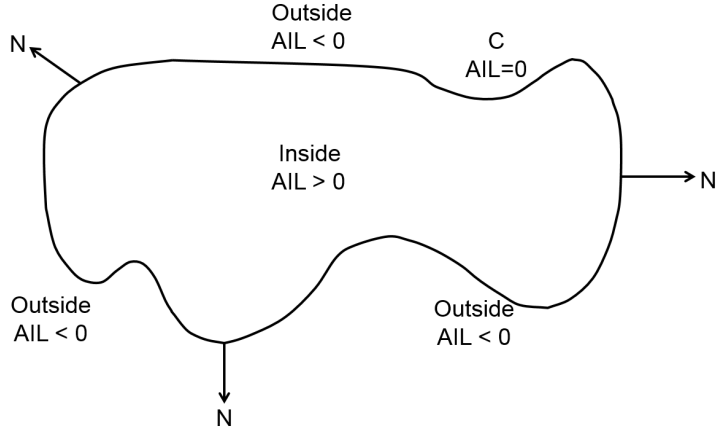


**Figure 4.6:** Curve propagating in normal direction. C: contour; AIL: the average intensity levels of image pixels inside and outside of the contour, Chan and Vese [204]

algorithm  $A_{AC}$  performance depends on a particular segmentation of the image (in case Figure 5.7b, see Chapter 5), the active contour might also acquire a different segmentation. This means the active contour approach does not precisely adapt to the object topology, particularly its real edges. To mitigate this problem, a second step is proposed that was implemented to adjust the building edges.

In the second step of building geometry modification, the edges of the building regions were refined with the shape fitting based on the automatic identification of the best parameters of the geometric shapes through the optimisation process. The optimisation process depends on finding the minimum constrained nonlinear multivariable function based on the interior-point algorithm  $A_{IP}$ , as in Byrd et al. [205] and Byrd et al. [206]. The  $A_{IP}$  achieves the optimisation process by analysing the strict interior of the feasible region defined by the problem rather than around its surface. The constrained nonlinear optimisation process attempts to find a constrained minimum of a scalar function of several variables beginning at an initial estimate of the solution ( $b_0$ ), where a minimiser of the function is subject to the optimisation options specified in *options*. A set of lower and upper bounds was defined to identify the optimal parameters of the building's footprint shapes within these bounds, so that the solution is always in the range  $lb \leq b \leq ub$ . The process outputs are the objective function for the best parameter values at the solution ( $b$ ), which are the final coordinates of the optimal shape. To achieve this, a new technique was developed to create the objective function that will be minimised and evaluated at ( $b$ ) to identify the optimal fitting edges of the buildings. The geometric parameters were investigated to set the two basic and most spread shapes (rectangle and ellipse) to adjust the alignment of the edges between the building corners and to take the convexity in some cases into account for edges with rounded forms. The fitting optimisation subroutine begins by

identifying the rectangle parameters that minimise the objective function. Thus, two functions were generated as the objective function in the optimisation process to implement the fitting geometry for the best parameters of the two selected shapes. To acquire the coordinate of the point  $(x, y)$  on the rectangle border, as in Figure 4.7a, the input parameters were therefore defined in the parametric equations of the rectangle, as follows:

$$x = p \max(-1, \min(4/\pi \arcsin(\sin(\pi t/2 + \pi/4)), 1)) \quad (4.14)$$

$$y = q \max(-1, \min(-4/\pi \arcsin(\sin(\pi t/2 + \pi/4)), 1)) \quad (4.15)$$

where  $t$  denotes a function of an angle, it is defined as  $-\pi < t < \pi$ ,  $p$  and  $q$  parameters, which are the side length of the rectangle. A rotation matrix was applied by identifying a rotation angle  $\phi$  with the translation process after defining the coordinates of the rectangle's centre  $(x_t, y_t)$ . For an ellipse, the parametric equations were formulated, as follows:

$$x = p \cos(t) \quad (4.16)$$

$$y = q \sin(t) \quad (4.17)$$

where  $(x, y)$  refers to the coordinate of the point on the curve border. Next, the developed technique contains the calculation of the pairwise distance between two sets of observations for each point on the border. The pairwise distance includes: (1) the original shape obtained after applying the active contour approach  $d$ , and (2) the fitted shape  $d_2$ , as in Figure 4.7b. The objective function for minimisation is the output values of the sum of distance. To enable the algorithm to recognise and choose automatically between rectangles and ellipses, a ratio was defined as a measure of elongation of the object (the ratio of the minimum and maximum object side). The ratio value is 1 when both sides of the object are similar, but if the ratio value is near zero, this illustrates that one side is much smaller than the other side of the object. If the output value of the objective function of the rectangle shape is less than the ellipse shape or the ratio is less than the threshold (0.6 tuned), then the rectangle shape is chosen to find the coordinates  $(x_{opt}, y_{opt})$  of the optimal rectangle shape of the object, as shown in Figure 5.8 (see Chapter 5). If not, the ellipse shape is chosen instead.

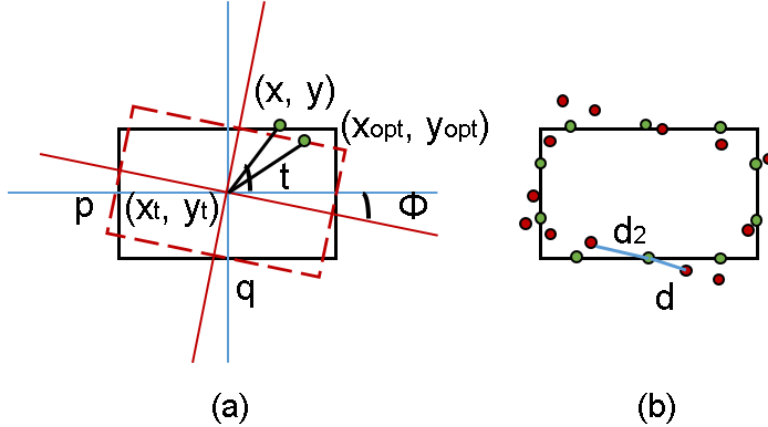


**Figure 4.7:** Building edges enhancement: (a) Parameters of shape fitting, (b)  $d$  is the minimum distance from each point of the original shape to the points of the fitted shape, and  $d_2$  is the minimum distance from each point of the fitted shape to the points of the original shape

To conduct the compatibility test between the amended shape extracted from the fitting-optimisation process with the original shape of the buildings extracted from the partitioning process, the Jaccard Index ( $JI$ ) used for measuring the similarity between two sets of building footprint regions, was utilised, as illustrated in Figure 4.7. First, the binary mask is created from the perimeter pixels of the refined shape  $M_{RS}$ . Then, the intersection and union between  $M_{RS}$  and the original mask  $M_B$  is computed to obtain the Jaccard Index ( $JI$ ). This is computed by:

$$JI(M_{RS}, M_B) = |M_{RS} \cap M_B| / |M_{RS} \cup M_B| \quad (4.18)$$

$JI(M_{RS}, M_B)$  computes the size of the intersection (the two building regions) divided by the size of the union of the two regions. Second, two thresholds were set to examine the performance of the adjustability process to ensure that inaccurate amendments to the building edges and shapes were avoided and restored from the original binary image. The first threshold ( $\Gamma_1$ ) was set to control the values of  $J_I$ , and if the value was less than ( $\Gamma_1 = 0.4$ ) the performance was rejected. Alternatively, the performance was also rejected if the area value of the intersection between the complement of the original binary mask ( $1 - M_B$ ) and the amended binary mask  $M_{RS}$  was greater than the second threshold ( $\Gamma_2 = 5000$ ). Both thresholds were tuned based on the test images. Otherwise, the algorithm extracts the optimal shape of the building and adds it to the other building shapes in the image.

## 4.4 Estimation of building heights

The extraction of building shadows not only allows for the inference of the shapes of urban buildings but can also be used to estimate building heights [180]. Accordingly, a new technique was developed that allows for the estimation of the height values using only image metadata information and the output of the shadow extraction and building detection without any additional data. In fact, under appropriate imaging conditions, each 3D building structure owns its cast shadow [207]. Thus, the cast shadows of the buildings were exploited to derive their height values based on a flat terrain assumption<sup>1</sup>. The shadow region was investigated in the shadow mask  $M_S$  to identify each shadow region that belonged to its building in the building mask  $M_B$ . The process includes the extraction and labelling of the largest areas of the connected components of the shadow regions in the binary image. Thereafter, the unique labels of a label matrix from the connected components structure of the shadows can be found in the shadow mask  $M_S$ , where the pixel values are larger than zero. For each unique label, 1 is set as the value of the pixels belonging to the shadow regions. After identifying a specific shadow region with the corresponding building in the shadow mask  $M_S$ , a flat linear structuring element ( $v_{L,\lambda+\pi}$ ) is specifically generated along the direction of the actual shadow region  $S_{Ac}$  and in the opposite direction of the solar illumination to simulate the shadow regions computed in 8-neighbourhood connectivity with a given height, as in Equation 4.8; however, the formula was re-written with a different threshold to identify the best length of edge segment  $L$  that can satisfy a sufficient distance for commencing the process of shadow simulation, as in Equation 4.19.

$$L = \frac{H_T^{\max}}{\tan \phi R_{\text{img}}} \quad (4.19)$$

where,  $H_T^{\max}$  is the maximum height threshold for the buildings that cast shadows, which allows for the determination of the best overlap between  $S_{Ac}$  and  $S_{Ar}$ .  $Az$  is azimuth,  $\phi$  is solar elevation angle  $El$ , and  $R_{\text{img}}$  is image resolution. After creating the line structuring element, first, the connected components of buildings in  $M_B$  were investigated, and then shadows were explored in  $M_S$  to label each component with an 8-connected neighbourhood. Thereafter, the connected components were extracted with a unique label to provide a mask of their perimeter pixels  $M_{Bp}$ , as in Equation 4.20.

---

<sup>1</sup>For the flat terrain assumption, the large cast shadow on the earth's surface can be obtained in case there are acute solar elevation angles ( $\phi < 30^\circ$ ) [19].

$$M_{Bp} = (M_{Bc} \otimes O_{3 \times 3}) \cap M_B \quad (4.20)$$

where,  $M_{Bc}$  is the complement of the building object ( $M_{Bc}$ , as per Equation 4.21),  $O_{3 \times 3}$  is a matrix of ones, and the operators  $\otimes$  and  $\cap$  denote the morphological dilation and a pixel value intersection, respectively. Once the  $M_{Bp}$  is identified, the algorithm,  $A_{SO}$  then simulates the  $S_{Ac}$  in the opposite direction of the solar illumination to generate new regions of building shadows  $S_{sim}^{max}$ , as in Equation 4.22.

$$M_{Bc} = 1 - M_B \quad (4.21)$$

$$S_{sim}^{max} = (M_{Bp} \otimes N_{se}) \cap M_{Bc} \quad (4.22)$$

where,  $N_{se}$  is the neighbourhood associated with the structuring element (se). The  $S_{Ar}$  for each building region was then identified using Equation 4.23.

$$S_{Ar} = S_{sim}^{max} \cap M_S \quad (4.23)$$

Next, the  $A_{SO}$  traces the trail of each  $S_{Ac}$  in the shadow mask  $M_S$  to fit each  $S_{Ar}$  with the corresponding  $S_{Ac}$  in the  $M_S$ .

To estimate the heights of the buildings,  $H_E$  from a single VHR satellite image, the shadow-fit function was developed  $f_{sf}$  based on using the Jaccard Index ( $JI$ ), which yields  $A_{SO}$  to compute the fitting connected components over the pixels between the  $S_{Ac}$  and  $S_{Ar}$  regions. The estimated values of the  $H_B$  were extracted depending on the investigation of the optimal height of a specific building using a set of  $H_B$ , solar angles  $Az$  and  $El$ , the number of buildings in the  $M_B$ ,  $R_{img}$ ,  $M_B$  and  $M_S$  into the  $f_{sf}$ . The fit and similarity of the two shadow regions were measured by the Jaccard similarity coefficient, as in Equation 4.24.

$$JI = |S_{Ac} \cap S_{Ar}| / |S_{Ac} \cup S_{Ar}| \quad (4.24)$$

$J_I$  calculates the size of the intersection ( $S_{Ac}$  and  $S_{Ar}$ ) divided by the size of the union of the two regions by simulating the actual shadow regions  $S_{Ac}$ . The computation of the overlap by  $J_I$  between  $S_{Ac}$  and  $S_{Ar}$  is iterated until  $A_{SO}$  finds the maximal index of fitting for the two shadow regions, which approaches 1. The algorithm then extracts the highest index which represents the value of the optimal height  $H_{opt}$  of a given building. The set of the building heights is determined by the  $h_{min}$  and  $h_{max}$ , which represent a possible range of the minimum and maximum heights of the buildings. Applying a set of the building heights in the process of the building height estimation controls the simulation of the artificial shadow regions  $S_{Ar}$  and identifies the fitting region. Hence, for each test height between  $h_{min}$  and  $h_{max}$  with the interval 50 cm,  $S_{Ar}$  is gradually increased and the size of the simulated shadow region will increase until it fits  $S_{Ac}$ , where the height value is estimated. The value of the interval used to implement the simulation process was chosen because it is appropriate and consistent with the spatial resolution of the test image.

The building height  $H_B$  was therefore chosen as the optimal height  $H_{opt}$ , which gives the highest fitting index between the two shadow regions. Once the optimal value of the building height  $H_B$  was obtained for all existing buildings in a given test image, a shadow region was re-generated using the value of  $H_{opt}$  for each building in the building mask  $M_B$  based on the morphological dilation operation. A new function  $f_{sf}$  was therefore created to represent the shadow region as an  $H_B$  map (image) with the following inputs: the derived value of the optimal height  $H_{opt}$ , sun elevation ( $El$ ) and azimuth ( $Az$ ) angles, image spatial resolution ( $res$ ) and the building mask  $M_B$ . The final shadow region was simulated within the image space to visualise and combine all outputs of the  $S_{Ar}$  regions, which represent the estimated values of  $H_B$  in a single image. Finally, an  $H_B$  map was produced by keeping only the building footprints with their estimated height values  $H_B$ , where the values of the pixels are the building height Figure 5.9, see Chapter 5. Simulating other objects was avoided when  $J_I$  was larger than a tuned threshold ( $J_I > 0.13$ ). The algorithm adds the simulated shadow region of the building to the image, which includes the simulated shadows of all buildings.

In addition, during this part of the algorithm's subroutine, the possibility that the simulated shadows may cast on another building was considered and investigated. The function  $f_{sf}$  allowed for overcoming the problem of the overlapping shadows of two buildings by measuring the area of the shadow cast on the other buildings. The algorithm tested whether the measured area was larger than a chosen threshold ( $\rho = 1600$  pixels, which was tuned to be appropriate with all test images). Then, the  $J_I$  was set to zero and the simulated shadow was not considered.

Moreover, the overlapping problem between the cast shadow regions by buildings and/or those by non-built man-made objects was also mitigated by the creation of the length of an edge segment of the flat linear structuring elements of a given height threshold. The height threshold was selected based on the test images and their characteristics, such as illumination conditions and spatial image resolution. The entire developed shadow-overlapping algorithm, *A<sub>SO</sub>*, algorithm is presented in Figure 4.8.

## 4.5 Automated creation of 3D models of urban buildings

The basic requirements and common prerequisites for creating 3D city models are footprints and elevation measurements; the latter is achieved through the use of LiDAR and Photogrammetry [208]. Although footprints are widely available as an open data source from governments and volunteer geoinformation [209, 210], some cities and urban areas still do not have such data. In particular, most cities in developing countries often lack master maps or updated databases for existing and new buildings. In addition, acquiring elevation datasets also poses a problem because they are costly, and the process is time-consuming, hindering the production and availability of 3D city models [208, 211]. Therefore, for the present study, the automatic creation of 3D objects was performed by employing outputs that were obtained from the building footprints extraction and the height estimation processes. On the other hand, according to [212], the elicitation of the level of detail (LOD) of 3D building models in computer graphics depends on the complexity of the geometry. The LOD concept of the Open Geospatial Consortium (OGC) standard CityGML 2.0 is intended to distinguish multi-scale representations of semantic 3D city models [213]. For OGC, there are five main LODs that describe the increase in the geometric and semantic complexity of 3D city models (Figure 4.9). LOD1 represents a coarse prismatic model usually created by extruding an LOD0 model [163]. Thus, the creation of a 3D building model depends on the former operations of the algorithm that are applied to the image; the LOD of a 3D building model is generated at level one of the complex details of the building geometry.

Therefore, the 3D models of the urban buildings are created in the form of the solid blocks. In the present study, the 3D building models were derived from the construction of the volumetric image  $V_{\text{img}}$ . To create the volumetric image  $V_{\text{img}}$ , a voxel in a regular grid in three-dimensional space is implemented. The voxel defines a point in three-dimensional space in terms of the

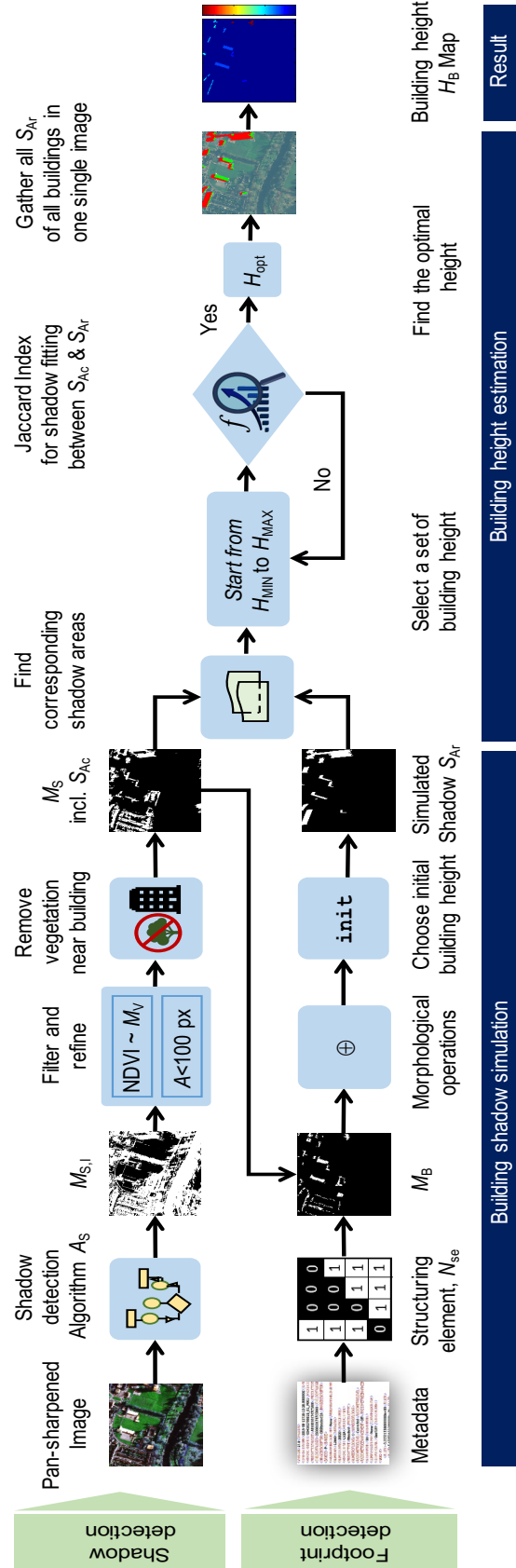


**Figure 4.8:** Framework of the shadow-overlapping algorithm  $A_{SO}$  for building height estimation



**Figure 4.9:** The five LODs of CityGML 2.0. The geometric detail and the semantic complexity increase, ending with the LOD4 containing indoor features [163]

values of coordinates ( $x$ ,  $y$  and  $z$ ) as a unit of graphic information like the pixel (picture element), which defines a point in a two dimensional space of its ( $x$ ,  $y$ ) coordinates, as shown in Figure 4.10. Based on graphic operations, the vectors  $\vec{x}$ ,  $\vec{y}$  and  $\vec{z}$  are created, respectively, with the Cartesian coordinates of volumetric images. The vector  $\vec{z}$  is created with the spatial resolution of the test images as an interval step between the lowest and highest value of the heights. Several elements of the vectors are calculated to transform the rectangular domain specified by vectors  $\vec{x}$ ,  $\vec{y}$  and  $\vec{z}$  into rectangular grid arrays  $X$ ,  $Y$  and  $Z$  to produce three-dimensional coordinate arrays. To represent 3D models, a uniform grid of 3D voxels is therefore required. The voxels of the  $V_{\text{img}}$  are derived by setting each voxel of the  $V_{\text{img}}$  to 1, which is located inside the building, and to zero for the voxels outside the building. To precisely extract the well-structured shape of the 3D solid blocks during their graphical computational geometry, a Gaussian low pass filter was applied to the building in the  $V_{\text{img}}$  as a spatial filter. For each slice of the volumetric building  $V_b$ , a convolution with a Gaussian filter was therefore performed to smooth the outputs of the 3D building models, as in Equations 4.25 and 4.26.

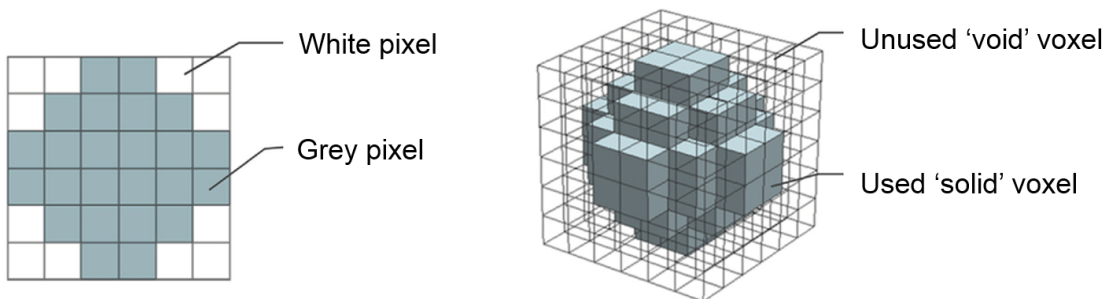


**Figure 4.10:** The conception of the voxel and pixel. On the left-hand side, an object in a 2D scene; on the right-hand side, the same object in a 3D scene. Modified after [214]

$$h_g(n_1, n_2) = e^{-(n_1^2 + n_2^2)/2\sigma^2} \quad (4.25)$$

$$h(n_1, n_2) = \frac{h_g(n_1, n_2)}{\sum_{n_1} \sum_{n_2} h_g} \quad (4.26)$$

where,  $h_g(n_1, n_2)$  is the pixel values within a filter-window. The parameter  $\sigma$  controls the overall shape of the curve. The Gaussian kernel is created with the values of the parameters, the filter size 15 and the standard deviation of the Gaussian 5, selected based on providing the best results. To extract a 3D surface  $F_v$ , all voxels in the  $V_{\text{img}}$  with a given co-localisation level were represented as an isosurface, which is defined by the implicit equation 4.27.

$$F(x, y, z) = f \quad (4.27)$$

where,  $F(x, y, z)$  refers to a continuous function whose domain is a 3D-space and  $f$  a constant that represents the density surface from a 3D array of data. An isosurface is a three-dimensional surface that represents points of a constant value (e.g. density) within a volume of space. The function computes the isosurface value from the volume data (e.g.  $V_{\text{img}}$ ). The isosurface connects points that have the specified value, much the way contour lines connect points of equal elevation. Therefore, the 3D surface  $F_v$  connects all voxels that have equal values in a 3D data distribution  $V_{\text{img}}$  to form and produce the 3D surface  $F_v$  in a meshgrid form (decomposed in triangles) for a given  $F$  by sampling over a regular grid, see Figure 4.11. The reconstruction process of the  $F_v$  of every building  $V_b$  from  $V_{\text{img}}$  is implemented using the well-known Marching Cube algorithm  $A_{MC}$  in Lorensen and Cline [215] and Nielson and Hamann [216], (see Figure 4.12). The  $A_{MC}$  is a 3D isosurface representation technique. The  $A_{MC}$  was used to create a triangle mesh from an implicit function ( $F(x, y, z) = 0$ ) by iterating (marching) over a uniform grid of cubes and over a region of the function. Accordingly, the 3D surface may intersect the cube with  $2^8=256$  possible configurations, but using the symmetries could reduce these 256 cases to 15 patterns (unique cases). By locating the surface in a cube of eight vertices, all eight vertices of the cube are positive (entirely above) or negative (entirely below) for the surface, and no triangles are emitted. Otherwise, the surface passes through the cube's eight vertices, and then some triangles and vertices are generated. The Marching Cube algorithm is therefore able to construct the structure  $F_v$  that contains the faces and vertices and estimates their intersections through the interpolation process along each edge. The algorithm then calculates the normals for each cube vertex and interpolates these normals at

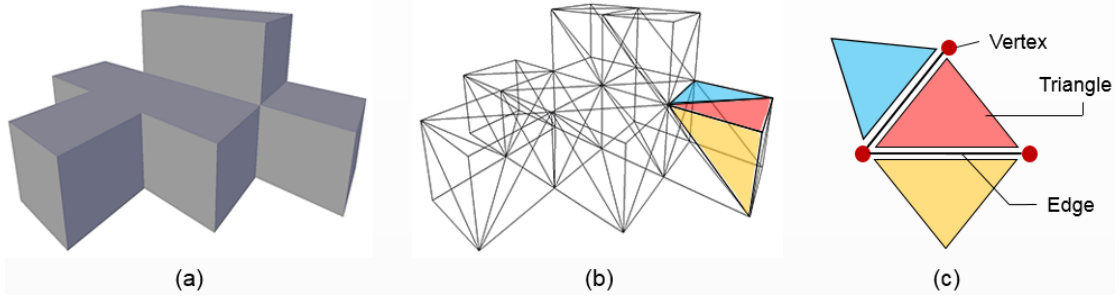


**Figure 4.11:** 3D model with triangles placed along the sides of voxel cubes: (a) voxel as a 3D solid model; (b) voxel as a 3D vector cube; (c) Decomposition approximating the 3D surface

vertices of the derived triangles. The final 3D buildings are rendered and presented visually using graphic functions, as shown in Figure 4.12.

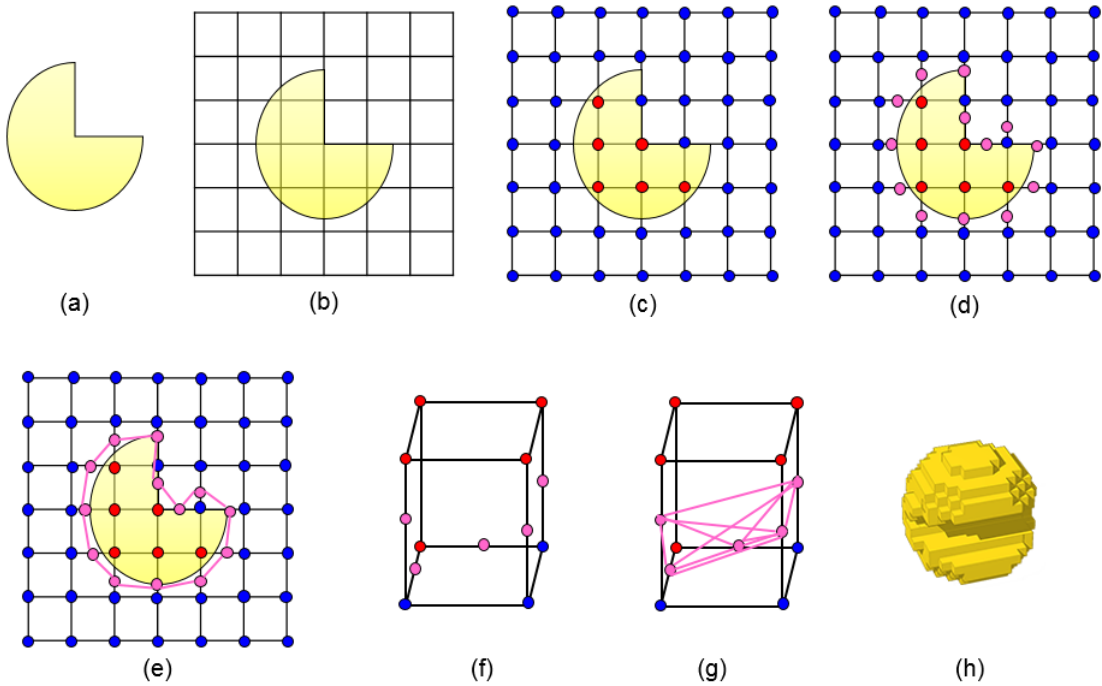


**Figure 4.12:** The conception of the marching cubes  $A_{MC}$ : (a) an object; (b) dividing it into squares; (c) labelling vertices, red for inside and blue for outside the object borders; (d) intersecting the edges of the original surface between inside and outside corners (purple dots); (e) connecting the purple dots to display an approximation of the original surface (the purple lines); (f) the surface intersects the cube along the edges in between corners of opposing labelled vertices; (g) triangulating the cube where filled triangles will represent the surface passing through the cube; (h) 3D model of the object

## 4.6 Assessment of solar energy potential

The effective determination of the availability of roof surface area on urban buildings can encourage the use of integrated systems rather than large scale solar farms, which may have a

negative impact on agricultural land; however, the automated extraction of the actual roof surface available for photovoltaic installations within complex urban landscapes is a difficult task. Although the roof surface areas can be accurately extracted from a given cartographical dataset, the computation process of the available roof surface for the entire city is a complex task in terms of time, effort and cost. Most importantly, a reliable assessment of the roof surface is limited due to the lack of a specifically developed tool for a solar-roof analysis.

Determining which side of the roof on which to mount panels to receive more sunlight throughout the day is essential in gaining the maximum possible energy production. To evaluate the available potential of solar PV generation, a solar potential analysis of rooftops related to the shadowing, brightness, orientation and the area of the roof is required. These factors affect the suitability of the integrated solar systems. The creation of 3D building models at LOD1 can be employed to assess the solar energy potential of the building facades. Therefore, the extracted building footprints (considered rooftops) from VHR multispectral satellite images were used to effectively compute the roof surface areas that are available and suitable for solar PV installations in urban areas. The areas of the buildings' roof surfaces that receive the most sunlight were calculated, and the orientation of these rooftops was determined with respect to the azimuth angle of the sun.

A PV array's outcome is proportional to the direct sunlight it receives. Although PV modules produce some energy in a shady location or without an ideal orientation, system costs are high, so the energy yield should be maximised [217]. PV installations are placed on the rooftops that directly face the sun, which results in capturing the most energy, especially when they are perpendicular to the sun's rays. The identification of the orientation of the building roofs is considered one of the most important factors that can impact the amount of received sunlight energy (solar energy) by PVs.

In the present work, the area and the orientation of the rooftops of the extracted building footprints were calculated in addition to obtaining a better understanding of the shadowing and brightness of the rooftops based on the analysis of the availability of the building surfaces. Thus, these factors were considered the properties for each connected component region (object) within an image. These properties were measured by a Matlab built-in function, which returns a struct array for each object (building footprints) in the binary image. Accordingly, the developed algorithm involving the aforementioned function computes the following set of the building region (rooftop/footprint) properties that provide shape measurements: (1) *Area*

introduces a scalar that specifies the actual number of pixels in the region. The area of the bright building roof surface was also computed in metres based on the image pixel size. (2) *Centroid* presents a 1-by- $Q$  vector that specifies the centre of mass of the region. The first element of the Centroid is the horizontal coordinate (or  $x$ -coordinate) of the centre of mass, and the second element is the vertical coordinate (or  $y$ -coordinate), as shown in Figure 4.13a. (3) The *length* of the major axis provides a scalar that specifies the length (in pixels) of the major axis of the ellipse that has the same normalised second central moments as the region. (4) *Orientation* returns a scalar that specifies the angle between the x-axis and the major axis of the ellipse that has the same second-moments as the region. The value is in degrees, ranging from -90 to 90 degrees, as shown in Figure 4.13b. For each existing building within the image space, the algorithm measures all the attributes of the available building roofs to assess and analyse the solar energy potential. The outcomes are tabulated and visually presented on the given image. The solar analysis was also conducted daily for the building facades in the 3D building models based on the sun's movement.

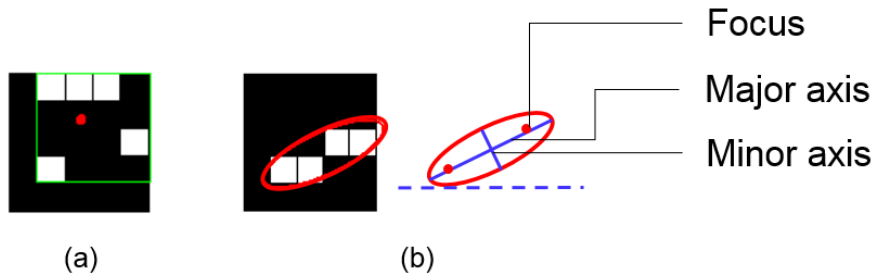


**Figure 4.13:** The measurement of the given object (e.g. building): (a) the centroid and bounding box for a given object region. The object region consists of the white pixels, the green box is the bounding box, and the red dot is the centroid; (b) the axes and orientation of the ellipse. The left side of the figure shows a given object region in the binary image and its corresponding ellipse. The right side shows the same ellipse with the solid blue lines representing the axes, the red dots are the foci, and the orientation is the angle between the horizontal dotted line and the major axis

## 4.7 Validation techniques

For verification and validation of the outcomes of the entire method and its developed algorithm, performance measures were conducted, and the accuracy was taken into account to assess the final findings of  $H_B$  and the 3D building models. The performance of the developed approach was therefore evaluated by comparing the results with reference data. The reference

data were taken from the Ordnance Survey<sup>2</sup> (OS) with highly accurate measurements. The actual height values of  $H_{Ac}$  in the reference data were used for the results comparison within the selected urban areas. The  $H_{Ac}$  were derived from a digital terrain model (DTM) and digital surface model (DSM) through a fully automatic algorithm based on a sophisticated mathematical computation process. The reference data contains the 3D models of urban buildings generated in the first level details of building envelopes (LOD1), which were used to evaluate the 3D building models produced; however, the reference data were generated as one geodatabase ( $\cdot gdb$ )<sup>3</sup> file format represented by the OS MasterMap Topography layer, which includes all buildings. Therefore, a new technique was developed to separate a specific to conduct the comparison. To evaluate the performance, three well-known measures (metrics) of a test accuracy (Precision, Recall,  $F_1$ ) were used to evaluate the pixel and object-based performance of the developed approach as applied in many studies, such as Aksoy et al. [218], Ozgun et al. [19] and Ozgun [150], as in Equations 4.28, 4.29, and 4.30.

$$Precision = \frac{| TP |}{| TP | + | FP |} \quad (4.28)$$

$$Recall = \frac{| TP |}{| TP | + | FN |} \quad (4.29)$$

$$F_1 = \frac{2 * precision * recall}{precision + recall} \quad (4.30)$$

where  $TP$  are the true positives,  $FP$  are false positives, and  $FN$  are false negatives. The operation  $| * |$  denotes the number of pixels assigned to each distinct category. The  $F_1$  considers both the *Precision* and the *Recall* of the test to compute the score, which can be interpreted as a weighted average of the *Precision* and *Recall*, where the  $F_1$  score reaches its best value at 1 and worst at zero.

For each test image, the ground true data (referenced data) in the binary map form were generated by vectorising the outlines of the building roofs using GIS software. Then, a function

---

<sup>2</sup>Britain's mapping agency: The UK government agency responsible for the official, definitive topographic survey and mapping of Great Britain. One of its products is the OS MasterMap Topography layer.

<sup>3</sup>The geodatabase is the native data structure for ArcGIS and is the primary data format used for editing and data management. While ArcGIS works with geographic information in numerous geographic information system (GIS) file formats, it is designed to work with and leverage the capabilities of the geodatabase. <http://desktop.arcgis.com/en/arcmap/10.3/manage-data/geodatabases/what-is-a-geodatabase.htm>

was created to convert the reference vector map into a binary image, where 1 referred to the buildings and zero labelled their background automatically; however, to this end, the true shape of the 3D models of the buildings in the reference data should be extracted, taking into account the actual coordinate systems by conveying the models from the geodatabase format to a readable extension using MATLAB commands. Hence, a tool was also developed to keep the original coordinates of the 3D models after extracting a given 3D model from the reference data by correcting the position of the model in the new binary image (ground truth). Next, the developed tool provides a new file format ( $\cdot STL$ ) of the outputs of the extracted 3D models from the reference data to enable the comparison. The STL (STereoLithography) approximated the surfaces of a solid model with triangles, which is appropriate for the 3D models created by the meshgrid pattern. Thereafter, the true and produced models in the  $\cdot STL$  format were compared to calculate the mean error between the two model geometrically. A new function was created within the developed technique to assess the produced 3D building models, which can extract the coordinates located on the perimeter of the 3D true models and the corresponding coordinates on the perimeter of the 3D produced models for their created shaped-border masks (2D). The comparison was implemented based on the calculation of the difference in the distance between the coordinates in both masks by computing the Euclidean distance, as in Equation 4.31.

$$d_{pt}^2 = (x_p - y_t)(x_p - y_t)' \quad (4.31)$$

where,  $d$  denotes a matrix of the various distances between the vector  $x_p$  and  $y_t$ , and  $p$  and  $t$  are the produced and true perimeter coordinates of the 3D models in their masks, respectively. Thereafter, the function computes the mean error of the 3D building models.

In addition, the mean absolute error (MAE) was computed between the prediction value of the building heights (Estimated building heights  $H_E$ ) and the true value of the building heights (Actual building heights  $H_A$ ). To quantify the difference between the two values, a comparison was made between the two sets of height values, as in Equation 4.32

$$MAE = \frac{\sum_{i=1}^n |y_i - x_i|}{n} \quad (4.32)$$

$$RMSE = \sqrt{\frac{1}{n} \sum_{i=1}^n (y_i - \hat{y}_i)^2} \quad (4.33)$$

where,  $y_i$  is the prediction, and  $x_i$  is the true value. The  $n$  denotes the number of observations.  $A_{SO}$  performance was evaluated using the RMSE measure, as in Equation (4.33), where  $y_i$  and  $\hat{y}_i$  are actual and predicted values, respectively. The results of the 3D building models assessment are shown in Chapter 5. Moreover, the estimated values of the building heights were compared with other outputs of the state-of-the-art building heights estimation approach for an additional sensitivity analysis of the performance of the developed algorithm.

## 4.8 Summary

In this chapter, the developed approach is presented and explained in terms of the input data, computer vision and image processing techniques; the reasons for using the state-of-the-art algorithms; the development of the method, functions and tools used for the methodology; the sensitivity analysis and validation of the performance of the approach; and the output of the processes. The methodology began with the detection of the building shadows from the VHR satellite images, and then the shadow regions were extracted as binary image outputs. Thereafter, based on the extracted shadow information and metadata information related to the image acquisition and solar angles, two important processes were conducted to deduce and identify the geometry of the buildings: the detection and extraction of the building footprints and the estimation and extraction of the height values of the buildings. Next, the developed algorithm created 3D building models from the outputs of the former computations at the first level of LoD and displayed the 3D models in their geospatial locations in the real world. The chapter provides an evaluation of the final 3D building models as well as the evaluation of the algorithms performance covering the parts of processing. All processes were implemented in an automatic manner. In the next chapter, the results of the developed approach are discussed, and the experiments are described.

# **Chapter 5**

## **Results**

As an extension of Chapter 4 which presented methodology, the developed algorithm's outputs will now be introduced. This chapter describes experiments utilising a new approach to automated modelling of 3D urban buildings from single very high-resolution (VHR) multispectral images. The 3D models of urban buildings were generated by investigating building footprints and heights. An image partitioning approach was applied to the chosen datasets and extracted building regions based on detection of buildings' shadows. The results of the automated building detection and height estimation processes are illustrated by explaining the subroutines and functions of the developed algorithm. After building footprints and heights are extracted, their 3D models are created automatically as solid block forms. This chapter also contains a description of the dataset type, study area, evaluation process, and a sensitivity analysis of the findings.

## 5.1 Results and study objectives

This study set out with six objectives related to achieving and exploring the importance of an advanced approach for the identification of buildings' geometry in complex urban landscapes for sustainable development purposes. The present thesis provides a critical and comprehensive review of the characteristics of cutting-edge remote sensing data and systems that can be exploited to accomplish the main aim of the current study, as well as other research and applications. Additionally, state-of-the-art computer vision and image processing algorithms and previous pioneering studies within the scope of the thesis were also reviewed to satisfy the first study objective, covered in two important chapters of the thesis. The second study objective was achieved by developing two recent algorithms, namely, shadow detection and building footprint detection approaches, to address the very challenging datasets used in this study and to overcome their limitations. Before fulfilling the 3D models of urban buildings objective, it was important to set the third study objective because the third dimension of the model (the model height) had to be obtained without using elevation data. One interesting study finding was successfully estimating heights of existing buildings within urban areas based on shadow information and the supplementary metadata file shipped with the WV3 image data, which provides information about the date, time, and solar angles information (azimuth and elevation). The study also illustrated the results of the fourth objective, which was automatic creation of 3D building models. In the fifth objective, spatial analysis of rooftops' solar energy potential was the target. The last objective was achieved using the  $F_1$  score evaluation method which combines Precision and Recall into a single number, in addition to verifying the developed algorithms outcomes compared to the reference data (ground truth data). According to the research objectives, the results were obtained at the level of computational intelligence, considering the complexity of different dataset characteristics, buildings, view perspectives, and unpredictable environmental and illumination factors. Consequently, reliable extraction of building geometry and attributes for automatically generating 3D city models satisfied the current study's aims. All the research objectives' findings are thus numerically and visually presented in this chapter.

## 5.2 Utilised satellite imagery and its preparation

According to Section 4.1.2 in Chapter 4, the developed approach involves utilising single pancharpened ortho-rectified multispectral images with a metadata file that is often provided with

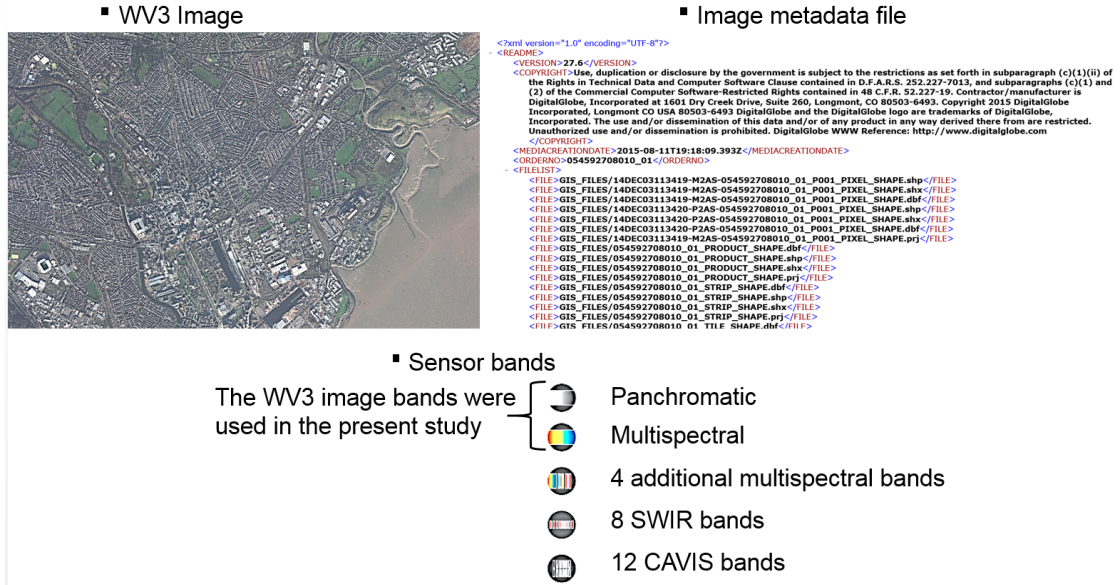


**Figure 5.1:** The pan-sharpened ortho-rectified multispectral images, its metadata file, and sensor bands

every image product, and includes the sun's angles at acquisition time, see Figure 4.1. The raster type, such as images, simplifies the processing of adding complex image data to a mosaic dataset. It is designed to understand the file format and specific information about a product such as metadata, georeferencing, acquisition date, and sensor type, processing, and wavelengths, along with a raster format, whereas a raster format only defines how pixels are stored, such as number of rows and columns, number of bands, actual pixel values, and other raster format-specific parameters. In this new research project, WorldView-3 (WV3) images with four bands (B, G, R, and NIR) are used, as shown in Figure 5.1, and the characteristics of the selected satellite and its sensor bands in Appendix A. The images have a radiometric resolution of 16 bits per band and a spatial resolution of 40 cm (GSD). The images are rectified to a datum and a map projection and were corrected for image distortions by conducting geometric correction and terrain displacement correction. However, the satellite image is very challenging due to the illumination conditions (Figure 5.2). To obtain a clear view of urban features, image contrast adjustment was therefore performed on each band by normalising the pixel values between 0 - 1 and stretching their histograms to improve image contrast. The process contains the image colourmap's conversion from the RGB system to Hue, Saturation, and Value (HSV) to adjust the image contrast automatically and obtain better contrast and object discrimination. Because histogram enhancement (Figure 5.2) of a colour image requires changing the intensity values of the image pixels, the conversion between an image's two colourmap systems is a necessary process. In computer vision, such a conversion process is often required to separate

colour components from intensity for various reasons, such as robustness to lighting changes. Thereafter, conversion from the HSV to RGB colourmap system was performed to display and deal with the true colour of urban objects within the enhanced image.

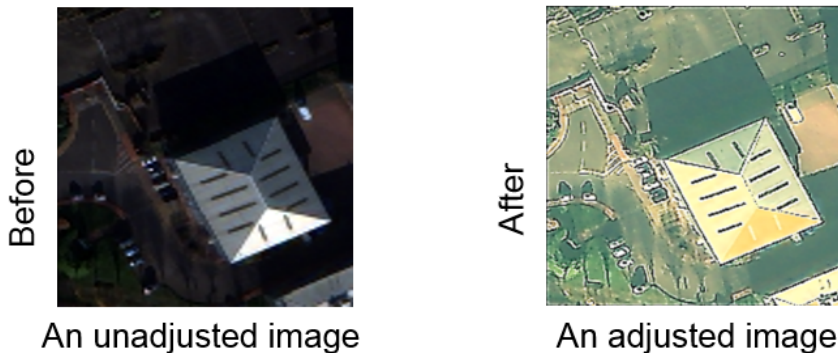


**Figure 5.2:** WorldView-3 pan-sharpened image, before and after the contrast adjustment

### 5.3 Study area

The goal of this research is to employ renewable energy within a city by assessing its potential, specifically solar energy potential, for sustaining an urban area. Cardiff is the capital and largest city in Wales and the eleventh-largest city in the United Kingdom. Because the research focuses on the building envelopes surface availability for assessing solar energy potential, Cardiff is a good example of an urban environment and its landscapes. One of the key imperatives for selecting this city was the availability of accurate datasets, including maps at different scales covering various formats (e.g. vector and raster), elevation datasets, topography data, and other categories such as locations and urban boundaries. These can be used as a reference source of ground truth (gt) (Figure 5.3). Such data were produced and updated by Ordnance Survey (OS)<sup>1</sup> in the United Kingdom. Datasets and maps can be downloaded in the UK from the Digimap platform which is delivered to UK tertiary education organizations by a collection of EDINA services [219]. Moreover, Cardiff is a sustainable city and an environmentally friendly urban area. One of the reasons for this advanced position is its government has been seeking to exploit renewable energy for sustainable development of urban environments.

Different image patches are chosen by cropping the whole image data as a specific aspect ratio for several reasons. The first, ease of uploading, processing, manipulation and retaining the small size of images via software, such as Matlab. Second, there is a reduction in the

---

<sup>1</sup>Ordnance Survey (OS) is a non-ministerial government department which acts as the national mapping agency for Great Britain and is one of the world's largest producers of maps.

required image processing time. The third reason is the ability to spot and correct errors in the visual presentation of each processing stage. Fourth, all test image patches are precisely chosen to comprise complex characteristics of buildings such as geometry, texture, roof colour, and orientation within complicated urban environments and challenging illumination conditions for a robust assessment of the new approach's performance.

## 5.4 The new approach's outputs

Elevation datasets, such aerial LiDAR and laser scanner data in the form of 3-D point clouds, are an essential but often unavailable element needed for constructing 3D city models [208]. Thus, the present work investigates the extent to which 3D building models can be generated solely from 2D data without elevation measurements or supplementary existing datasets such as cadastral maps and statistics. As previously stated in Chapter 1, this study aims to develop a new approach to modelling available surfaces for assessing and exploiting the solar energy potential within an urban environment in an integrated analytical framework. This section, as well as the following sections of the chapter, provide the new methodology's findings based on employing VHR satellite images presented in Chapter 4, in which building footprints are

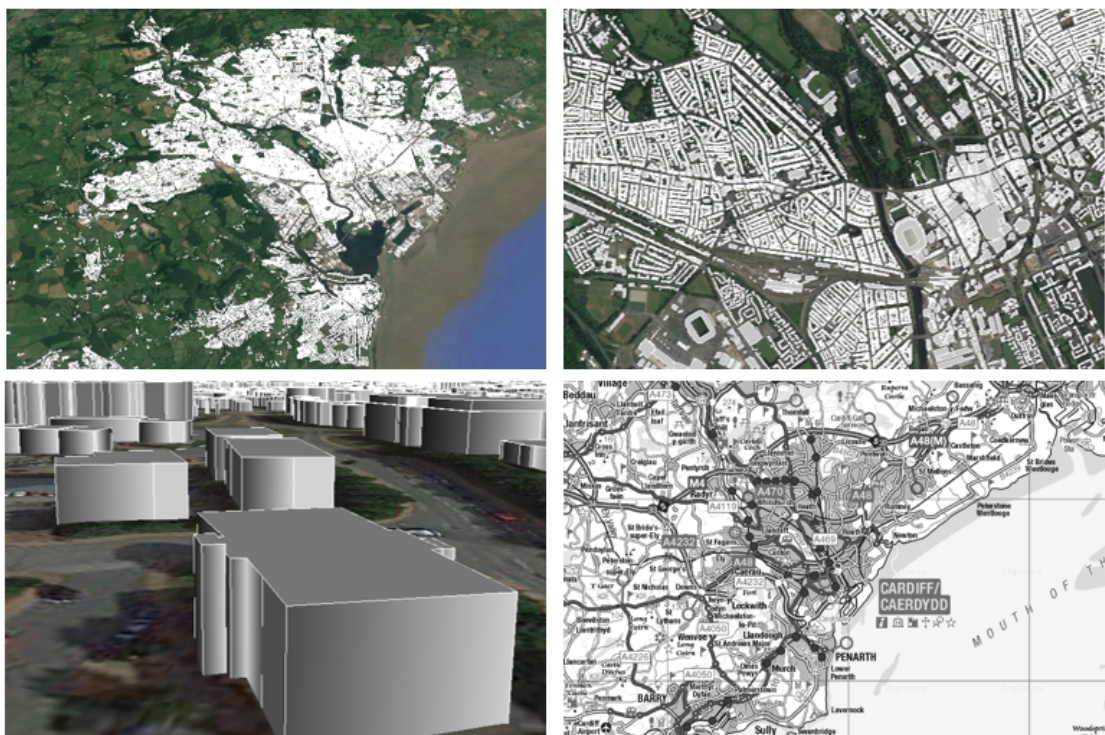


**Figure 5.3:** Reference data (ground truth): entire urban area of Cardiff city (top left), a part of the city (top right), city buildings (bottom left), and city map (bottom right)

extracted, building heights are estimated, and the 3D models of urban buildings are created for a multitude of applications.

### 5.4.1 Shadows

According to Section 4.2 in Chapter 4, the shadow detection process results are obtained as binary images (in the form of a shadow mask)  $M_S$ . Figure 5.4 presents an overview of shadow detection and extraction of  $M_{S,I}$ . The process comprises an enhanced image histogram, ratio map, NDVI, vegetation mask  $M_V$ , and identification of shadow regions  $M_{S,I}$ .

To extract the final shadow mask  $M_S$ , the shadow regions in the  $M_{S,I}$  are improved in terms of their shape and boundaries by conducting post-processing techniques. Figure 5.5 illustrates outputs of the shadow detection improvement method proposed by Ozgun [19]. In the first technique of shadow region improvement, a constrained region-growth was applied to the  $M_{S,I}$  to identify whether the shadow region's neighbouring pixels belong to it or not. Region growing approach is a region-based image segmentation based on the selection of initial seed pixels. Therefore, the approach starts by choosing an arbitrary seed pixel and comparing it with neighbouring pixels. The region is iteratively grown by comparing all unallocated neighbouring pixels to the region. The difference between a pixel's intensity value and the region's mean is used as a measure of similarity. The pixel with the smallest difference measured using this method is allocated to the respective region. This process stops when the intensity difference between region means and new pixels become larger than a certain threshold ( $T_I$ ).

The outputs from applying the region growing approach may contain a number of regions mistakenly detected as shadow regions, which might also grow after this process. Therefore, a ratio threshold ( $T_R$ ) is used to compare the number of pixels in the shadow regions before and after the region-growth process. Applying  $T_R$  allows us to determine and remove the regions which are exceedingly large after the growth process.

In Figure 5.5c, a cast shadow of non-building man-made objects and multiple separate objects (e.g. cars and fences) which are near the building object often merge with the cast shadow of a building. These mixed shadow pixels might result in a joint deterioration of the pruning process which is required to eliminate landscapes around the buildings. Hence, a given height threshold  $T_H$  is applied to the shadow regions to retain only the selected building's cast shadow and remove others. The  $T_H$  is calculated by creating a flat structuring element which maintains

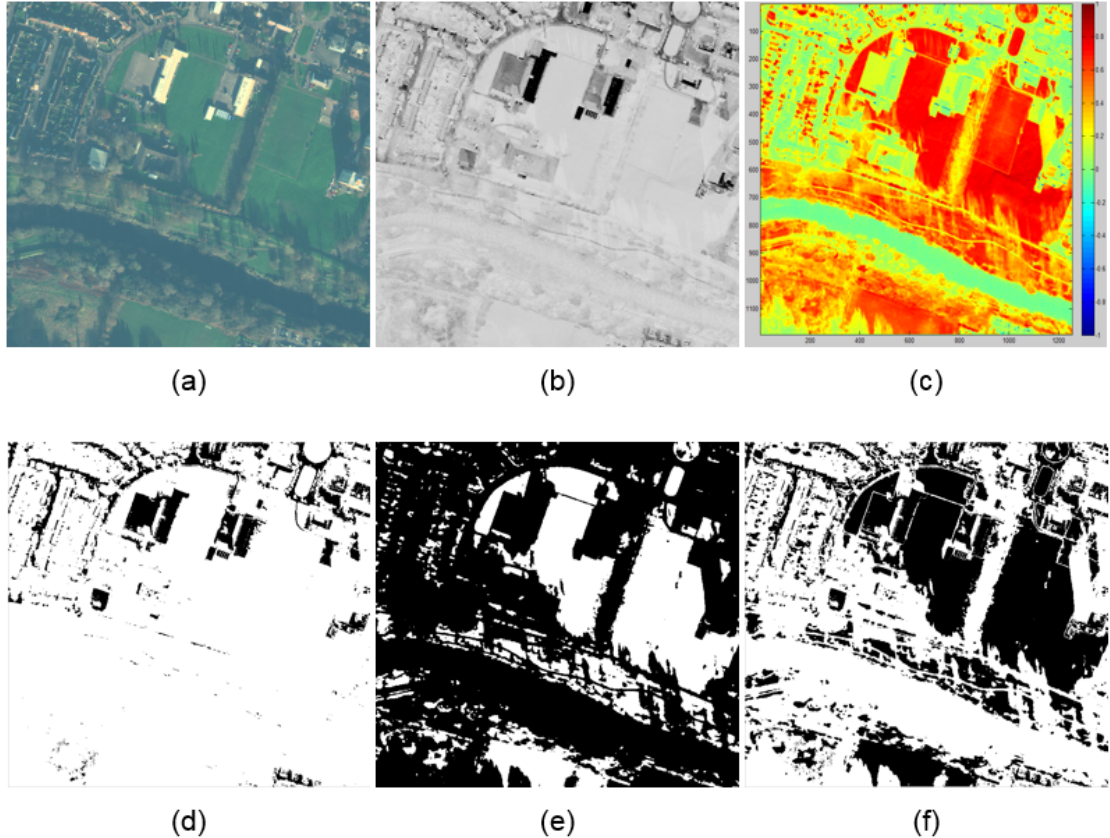


**Figure 5.4:** Shadow detection includes: (a) the enhanced WV3 image source; (b) the ratio map; (c) NDVI; (d) Shadow and vegetation mask; (e)  $M_V$  after thresholding the vegetation cover; and (f)  $M_{S,I}$

the connected single-edge segment's directional information. The flat structuring element is built with 8-neighbourhood connectivity for the connected components of shadow regions using solar information in the image metadata file.

A result from applying Fuzzy landscape pruning is shown in Figure 5.5d. The reason for utilising the generation and pruning of Fuzzy landscapes is eliminating the landscapes that might be generated by the cast shadows of vegetation canopies, as proposed by [19]. Therefore, the spatial arrangement was modelled between buildings and their shadows with the morphological Fuzzy relation approach in Equation (4.9). The generated landscapes' membership values are bounded in a search region defined by the object's extent and the direction defined by the angle ( $\lambda$ ). The values decrease when moving apart from the shadow area, and their decrease is controlled by the parameter ( $\sigma$ ). The region in the immediate vicinity of each shadow area was defined by applying two thresholds ( $T_{low}$  and  $T_{high}$ ) for searching the existing cast shadows for vegetation using  $M_V$ . The Fuzzy landscape region generated from a cast shadow will be rejected if there is substantial evidence of vegetation greater than a vegetation ratio threshold ( $\geq T_{veg}$ ) within the search region. The values of all parameters are presented in

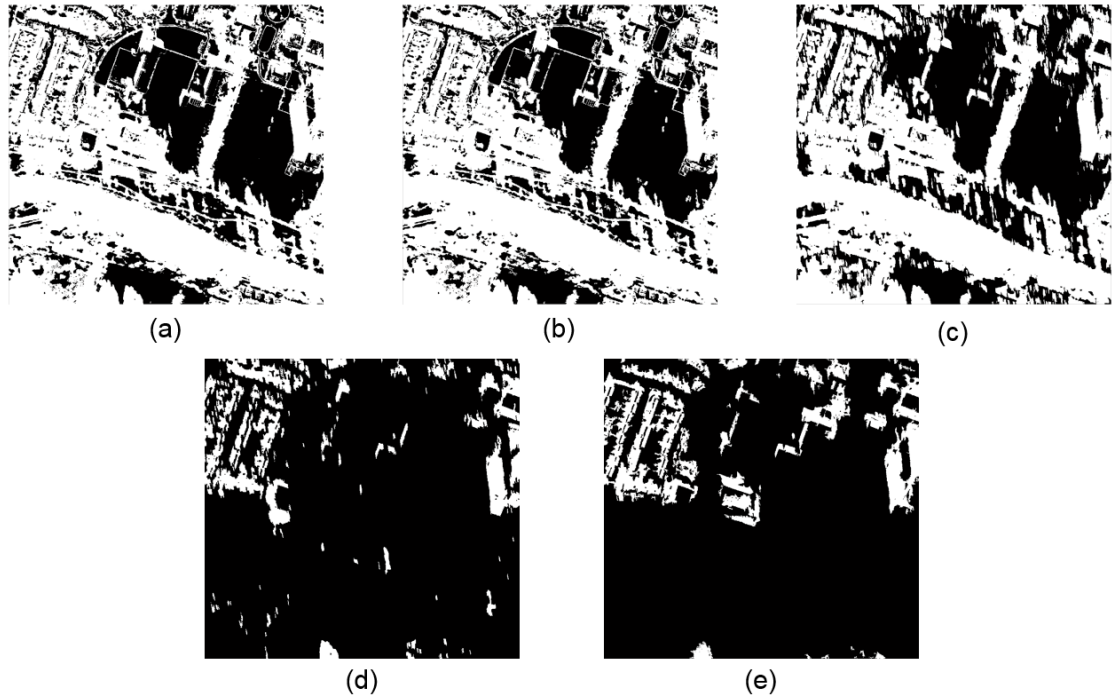


**Figure 5.5:** The extraction of the final shadow regions. (a)  $M_{S,I}$ ; (b) after applying a constrained region-growth; (c) the elimination of the height difference of the objects; (d) Shadow mask after applying Fuzzy landscape pruning; and (e) the final shadow regions of the buildings  $M_S$  after applying the region growing step

Table 5.1. However, another constrained region-growth was applied after the process of pruning due to erosion of some parts of the buildings' shadow regions as shown in Figure 5.5d. Therefore, the algorithm was developed to be appropriate for the data used by adding the step of region growing to obtain shadow region results segmented with more precision, as shown in Figure 5.5e. Table 5.2 shows the outcomes of the key subroutine process of the developed algorithm using alternative values of the process thresholds and parameters. Specific values of the process thresholds were chosen above and below the threshold value used in each stage of image processing to evaluate their effects on the performance results and provide a clear visualisation. The comparison between the threshold values used and the alternative values illustrates the differences in the outcomes which can impact on their performance and accuracy.

#### 5.4.2 Building footprints

Building footprints identification outputs are provided in Figure 5.6. According to the Section 4.3.2, the building footprints in the image space was detected and extracted based on their

**Table 5.1:** The main parameter settings of the present study

The task	Parameter	Value
Post-processing of the shadow mask	<ul style="list-style-type: none"> <li>– Intensity threshold (<math>T_I</math>)</li> <li>– Ratio threshold (<math>T_R</math>)</li> <li>– Height threshold (<math>H_T^{\max}</math>)</li> </ul>	<ul style="list-style-type: none"> <li>0.005</li> <li>0.8</li> <li>2 m</li> </ul>
The generation and pruning of fuzzy landscapes	<ul style="list-style-type: none"> <li>– Kernel size (<math>k</math>)</li> <li>– <i>Sigma</i> (<math>\sigma</math>)</li> <li>– Search region thresholds (<math>T_{\text{low}} - T_{\text{high}}</math>)</li> <li>– Vegetation ratio threshold (<math>T_{\text{veg}}</math>)</li> </ul>	<ul style="list-style-type: none"> <li>80 m</li> <li>40</li> <li>0.9 - 0.98</li> <li>0.9</li> </ul>
Building region partitioning	<ul style="list-style-type: none"> <li>– GMM components for each class: Foreground (<math>K_F</math>) and Background (<math>K_B</math>)</li> <li>– Smoothing constant (<math>\gamma_1</math>)</li> <li>– Foreground thresholds (<math>\eta_1 - \eta_2</math>)</li> <li>– Shrinking distance (<math>d</math>)</li> </ul>	<ul style="list-style-type: none"> <li>5</li> <li>5</li> <li>50</li> <li>0.9 - 0.4</li> <li>125</li> </ul>
Shape refinement	<ul style="list-style-type: none"> <li>– The maximum number of active contour iterations</li> <li>– Area lower bound</li> <li>– Area upper bound</li> <li>– Area threshold</li> <li>– Shape threshold</li> <li>– Geometric shape threshold (<math>\Gamma_1</math>)</li> <li>– Shape fitting thresholds: index of overlap and intersection region (<math>\Gamma_2</math>)</li> </ul>	<ul style="list-style-type: none"> <li>300</li> <li>1, 1, 0, 0, <math>-\pi/2</math></li> <li>1000, 1000, 1000, 1000, <math>\pi/2</math></li> <li>500</li> <li>0.6</li> <li>0.4</li> <li>5000</li> </ul>
Height estimation	<ul style="list-style-type: none"> <li>– Minimum height (<math>h_{\min}</math>)</li> <li>– Maximum height (<math>h_{\max}</math>)</li> <li>– Height interval</li> <li>– Jaccard index threshold</li> <li>– Area threshold (<math>\rho</math>)</li> </ul>	<ul style="list-style-type: none"> <li>3 m</li> <li>60 m</li> <li>50 cm</li> <li>0.13</li> <li>1600 pixels</li> </ul>
3D building models creation	<ul style="list-style-type: none"> <li>– Gaussian low pass filter of size</li> <li>– <i>Sigma</i> (<math>\sigma</math>)</li> <li>– <math>T_{\text{Iso}}</math></li> </ul>	<ul style="list-style-type: none"> <li>15</li> <li>5</li> <li>0.5</li> </ul>

In this study, the parameters of the shadow detection method used the same values applied in Rüfenacht et al. [149] as well as the active contour without edges approach in Chan and Vese [204]

shadow regions using a graph theory approach proposed by Ozgun [19]. The first level of partitioning is used only when building footprints are determined by iterative GraphCut performed in two-label partitioning as the background and foreground label information (Figure 5.6b).

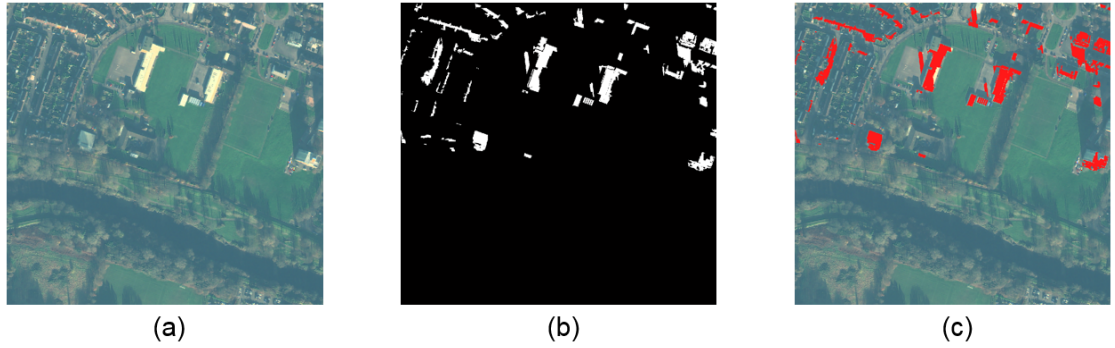


**Figure 5.6:** The extraction of the building footprints. (a) a pan-sharpened WV3 image (RGB); (b) building mask  $M_B$ ; and (c) the combination of WV3 (RGB) and  $M_B$

### 5.4.3 Edge adjustment of the building footprints

Referring to the Section 4.3.2, adjusting the extracted building footprint edges occurs in two main stages. In the first stage, the incorrect values of the assigned pixels, which are located on the building footprint's perimeter, are modified using the active contour without edges approach  $A_{AC}$ . Outcomes of applying  $A_{AC}$  to the grey image during the adjustment process are shown in Figure 5.7. Using the grey image rather than the colour image (RGB) is more appropriate for processing than an image with three colour components, and moreover, the grey image exhibits no noise (a clean image). With the colour image, the process will be subject to further calculations due to each colour component's mean value computation. This increases the complexity of conducting the computation of all components of forces<sup>2</sup> which eventually lead to using a different approach. As shown in images c, d, and e of Figure 5.7, iteration will continue until it reaches the maximum number of iterations in which the energy is not changing and the contour is not moving.

The second stage of the building footprints adjustment is aligning building edges in case of having orthogonal corners for a given rectangular geometry or regular curves for a given round geometry of the buildings. Figure 5.8 presents the fitting geometry process' outputs which were applied to the building footprint's refined mask using the active contour without edges approach shown in Figure 5.7f.

<sup>2</sup>The forces of the contour are two-fold: the force to shrink the contour, and the force to extend the contour. These two forces work as a balance when the contour searches for the boundary of a given object.

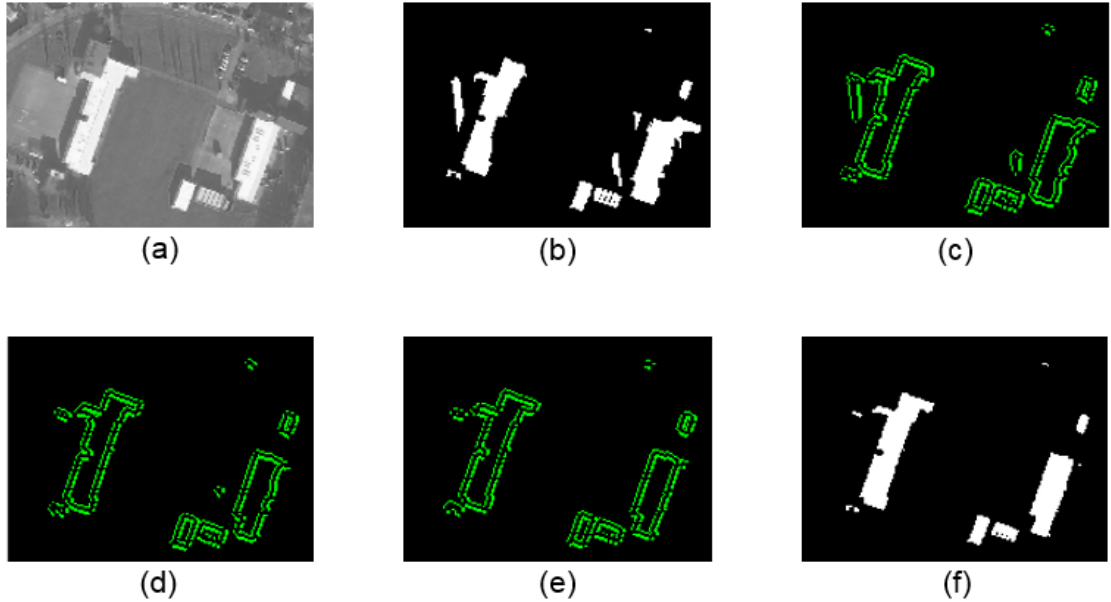


**Figure 5.7:** The first stage of the building footprint adjustment process: the automatic adjustment process of the edges of building footprints using active contour without edges approach. (a) gray image; (b) a mask of a building footprint; (c), (d), and (e) are the number of times of segment iterations at 40, 100, and 300 respectively; (f) the refined edge of the building footprints



**Figure 5.8:** The second stage of the building footprint adjustment process: the automatic adjustment process of building footprints' edges using the building shape fitting as a new approach. (a) the mask of the building footprints' refined edge; (b) WV3 pan-sharpened images and the building shape fitting, the red dots are the modified edges of shape of the building, while the blue dots denote the original shape of the extracted buildings; and (c) refined shapes and edges of the buildings with the fitting-adjustment in the binary image form

#### 5.4.4 Heights

The height values of the buildings  $H_B$  are estimated and derived based on the buildings' shadow regions. As stated in Section 4.4, the estimation process uses three main steps to obtain the 3D building model's third dimension value which represents the height of the building. First, the generation of artificial shadow  $S_{Ar}$  is based on the image's solar angles. The second step is measuring the similarity between the actual shadow regions  $S_{Ac}$ , which were extracted using the shadow detection process, and the artificial shadow  $S_{Ar}$  was extracted using the Jaccard index  $JJ$ . During the shadow regions' simulation process, the algorithm

searches the higher index. The large value of  $J\!I$  refers to the maximum value of fitting the two regions of shadows ( $S_{Ar}$  and  $S_{Ac}$ ), in which the optimal height  $H_{opt}$  of a given building is investigated and derived through applying a set of building heights. Third, the estimated height values are used to create a map of these building heights. The outcomes are shown in Figure 5.9

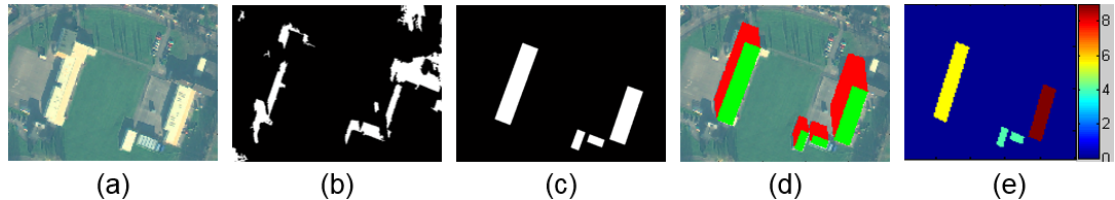


**Figure 5.9:** Estimation of the building heights. (a) pan-sharpened WV3 image; (b) shadow mask; (c) building mask; (d) simulated shadow with extracted building; and (e) building height map

#### 5.4.5 3D models

According to Section 4.5 in Chapter 4, outputs of the automatically created 3D building models, based on the marching cubes approach, are shown in Figure 5.10. The figure illustrates the reconstruction of 3D building models in the meshgrid surface. The meshgrid function generates  $X$ ,  $Y$ , and  $Z$  matrices for three-dimensional plots. The 3D grid coordinates are defined by the vectors  $x$ ,  $y$ , and  $z$ . The grid represented by  $X$ ,  $Y$ , and  $Z$  has size  $\text{length}(y)\text{-by-}\text{length}(x)\text{-by-}\text{length}(z)$ . The true spatial locations of the buildings in the image were overlaid by their created 3D models, as in Figure 5.11.

### 5.5 3D models' assessment and the validation of results

To evaluate the created 3D models of the buildings, two main geometric attributes of the 3D models should be considered to accomplish this purpose. According to Wu et al., and Izadi and Saeedi, Brèdi et al., and Biljecki et al. [17, 18, 189, 208], evaluation of the 3D models comprises the assessment for both the estimation of building heights as a  $z$ -dimension and the detection and extraction of the building footprints as  $x$  and  $y$ -dimensions of the 3D building model. Therefore, in this present study, all findings obtained from estimating building heights and from extracting building footprints are assessed by calculating the  $F_1$ -score and MAE as well as by conducting a comparison with other studies as shown in the state-of-the-art approaches in this scope of research.

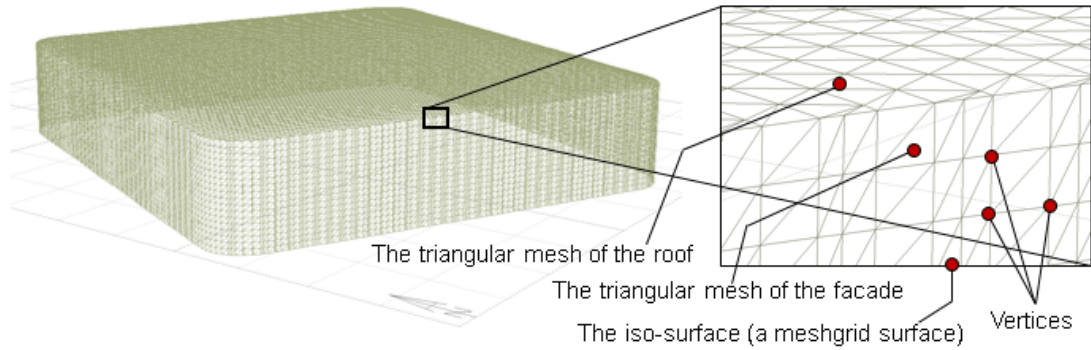


**Figure 5.10:** The creation of the 3D building with the meshgrid surface

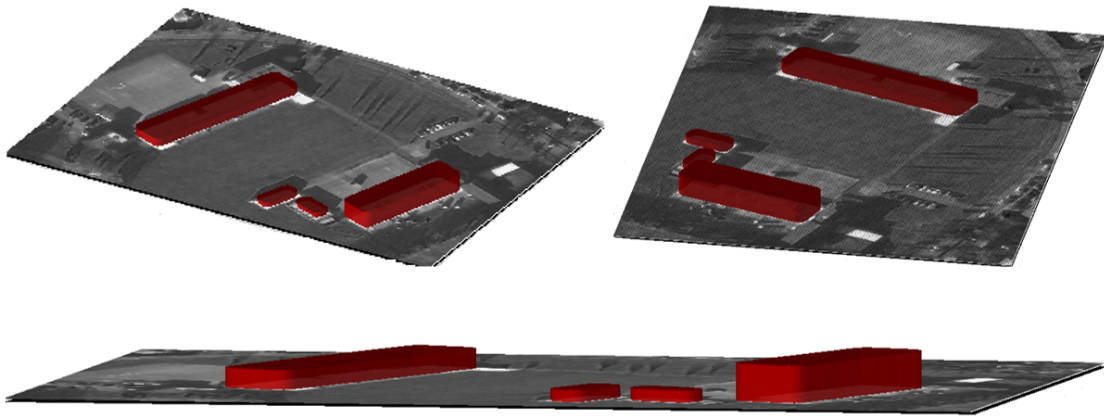


**Figure 5.11:** 3D models of the buildings at different viewing angles

However, quantitative assessment of the 3D models' production results is not simple. Biljecki et al. [220] noted that the reconstruction of an LOD1 model with any value of height is technically deemed valid, as there is no commonly agreed idea regarding accuracy that would determine a LOD1 model's acceptability. However, CityGML [213] references an accuracy benchmark concerning LOD1 where the position and height accuracy of points should be 5 m or less. In Chapter 6, quality of the generated 3D building models will be argued further, and recommendations and indications concerning the quality of the results will be given.

**Table 5.2:** Effects of different threshold values on the performance results of the present study

No.	The main process	The outcomes with the selected threshold value	The outcomes with an alternative threshold value	
1	Image enhancement	$T_{\text{Cont}}=0.05$ 	$T_{\text{Cont}}=0.10$ 	$T_{\text{Cont}}=0.01$ 
2	Shadow detection	$T_{\text{Rb}}=0.075$ 	$T_{\text{Rb}}=0.3$ 	$T_{\text{Rb}}=0.03$ 
3	Post-processing of the shadow regions	$T_{\text{I}}=0.005$ 	$T_{\text{I}}=0.02$ 	$T_{\text{I}}=0.001$ 
4	Building footprint identification	$d=125$ 	$d=62.5$ 	$d=190$ 
5	Shape refinement	$T_{\text{Sf}}=0.4$ 	$T_{\text{Sf}}=0.9$ 	$T_{\text{Sf}}=0.1$ 
6	Building height estimation	$T_{\text{JI}}=0.13$ 	$T_{\text{JI}}=0.5$ 	$T_{\text{JI}}=0.29$ 
7	3D Models of Buildings and validation	$T_{\text{Iso}}=0.5$ 	$T_{\text{Iso}}=0.9$ 	$T_{\text{Iso}}=0.1$ 

The key thresholds.

$T_{\text{Cont}}$ : Contrast stretching,  $T_{\text{Rb}}$ : Ratio band,  $T_{\text{I}}$ : Intensity,  $d$ : Shrinking distance,  $T_{\text{Sf}}$ : Shape fitting,  $T_{\text{JI}}$ : Jaccard index,  $T_{\text{Iso}}$ : Isovalue

## 5.6 The findings of the selected image patches

The developed algorithm was applied to the pan-sharpened WV3 image patches covering various spatial locations of the buildings. Automated creation of 3D building models is implemented based on selecting different scenarios of buildings' geometry, orientation, and position in relation to other urban features. This is important not only because the entirety of a building's characteristics and background is not always considered in computational intelligence, but also because testing the developed algorithm's performance in each scenario with a different urban landscape is important. Section 5.6.1 describes findings of the 3D building models' automated creation.

### 5.6.1 Experimental results

Results of building height estimation using the present approach are introduced in Figure 5.12. This part of the approach is evaluated using precision, recall, and  $F_1$  score as presented in Figure 5.13. Numerical validation outputs are presented in Table 5.3, for all test images, in addition to visual illustration of these results. We also list the overall accuracy of the other previous published works on image based building height estimation in Table 5.4 for a quantitative comparison.

As can be seen from Figure 5.12, results of the building height extraction process accuracy are quite promising and convincingly indicate the developed approach is highly robust for estimating building heights. Most estimated values of the detected building heights in the images are extracted successfully based on their detected shadows. Further, the algorithm's performance shows remarkably high efficiency overall when applied to test images despite buildings' complex characteristics such as geometry, texture, roof colour, and orientation within complicated urban environments and challenging illumination conditions. Evaluation results in Table 5.3 also support these findings. Besides applying a thresholding scheme, the developed algorithm can mitigate the issue of two buildings' overlapping shadow by investigating whether the specified building's simulated shadow hits other buildings. If so, the  $JJ$  is set to zero and the building shadow region is not simulated accurately, and the estimated  $H_B$  value has a lower level of precision. According to the numerical results in Table 5.3, test image #4 illustrates the highest difference between the  $H_A$  and  $H_E$  values because of their adjacency.

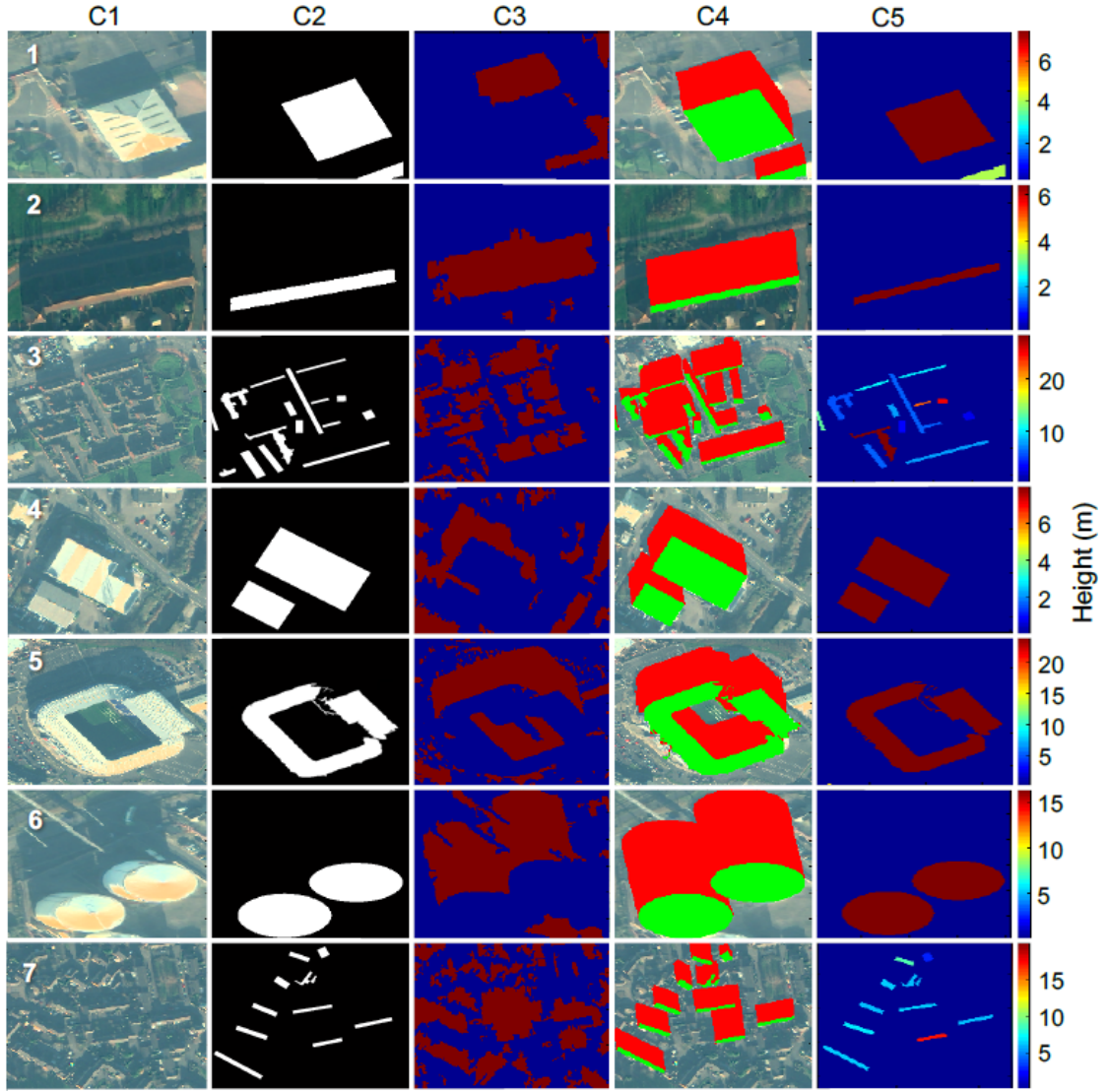


**Figure 5.12:** The estimated values of building heights. C1: Test images (#1–7). C2: Detected building footprints for test images. C3: Extracted shadow regions for detected buildings. C4: Artificial shadow regions for detected buildings. C5: Colour maps of estimated building heights

Despite the buildings' well-detected footprints,  $A_{SO}$  performance indicates the variation of  $H_B$  values in both test images #3 and #7, (Figure 5.12). This is due to the density of built-up areas. One possible reason for this variation is the spectral reflectance of some non-shadow dark objects, such as roads and building roofs, which are identical to each other or to their background. Therefore, other dark objects are considered shadow regions. Additionally, some adjacent buildings occlude shadows cast by other buildings. As a result, the shadow region length appears longer than their actual lengths of shadow regions if the shadow regions are combined with other objects or buildings' shadow regions, or they look shorter because some parts of the shadow regions are obstructed due to adjacent buildings. Nevertheless, this issue is considered in the simulation process to generate artificial shadow and it is mitigated by

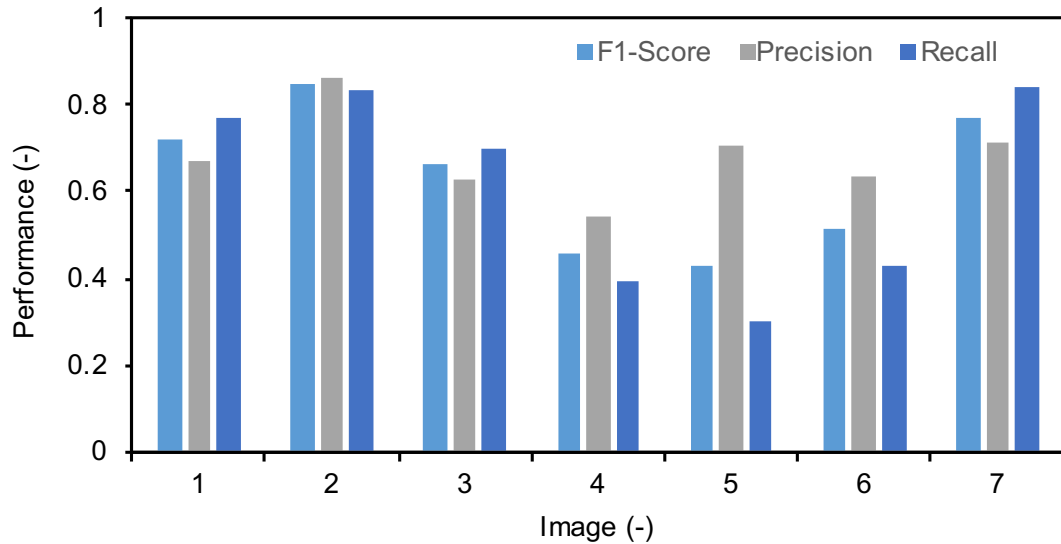


**Figure 5.13:** Sensitivity analysis for building heights estimation

implementing morphological post-processing and thresholding.

Considering the geometric relationship between the building and its shadow, correcting the shadow region lengths is required when the azimuth and elevation angles of both sun and satellite differ in the location. However, satellite azimuth and elevation angles determine the viewing direction of the captured image and this only affects whether a building's shadow is visible in the image space. Therefore, depending on the satellite viewing direction (the satellite azimuth angle), a shadow region might be occluded by the building itself. In this study, the shadow regions are not obscured by their buildings over the test images. Additionally, the corrected shadow length is generally not possible to compute because the measured height of buildings is needed beforehand to estimate the real shadow length on the Earth's surface.

Although differences exist in  $H_B$  values between the test images involved, results reveal that the present approach is generic for estimating the heights of buildings with different shapes, sizes, colours and orientations. Furthermore, the comparison between the overall accuracy of the new approach and previously published works in Table 5.4 proves that the building height estimation approach is superior for deriving the building height values based on shadow information in an automatic manner.

After extracting the buildings' footprints and heights, the developed algorithm continues processing the acquired outputs to create 3D building models without any further user input. As previously stated, various building candidates were chosen in different scenarios, such as illumination condition, orientation, and spatial position (adjacent buildings) to generate their 3D

building models. The building footprints' ground-truth was produced manually by a qualified human operator to compare the border perimeter coordinates of the buildings in the test images and models, as shown in Table 5.5. A technique to make comparisons between the two datasets was developed to run as a fully automatic process.

The results creating the buildings' 3D models are shown in Figure 5.14. Referring to the results presented in Figure 5.14, the developed algorithm is effectively able to generate reliable 3D models of the geometric buildings at LOD1. The 3D building segments are also recognised in most cases when the segments are not occluded. The numerical findings in Table 5.5 and the comparison results of the 3D city models in Figure 5.15 confirm these statements. It is also evident that the approach distinctively extracts height values from one single multispectral image without additional complementary data.

To assess the derived 3D models' accuracy, they are compared to the corresponding OS data (MasterMap Topography layer), which contains 3D models of the selected buildings generated at the LOD1. The comparison allows us to evaluate the extracted 3D building models. The

**Table 5.3:** Estimated building heights using the proposed algorithm

No.	Size: W × H (m)	$T_E^*$ (s)	Building			$H_A$ (m)	$H_E$ (m)	Error (m)
			Type*	Characteristics	Nos.			
1	85.6 × 99.6	6.76	C	Detached	1	7.5	7.5	0
2	72.4 × 113.6	3.36	R	Connected	1	6.1	6.5	0.4
3	201.2 × 208.8	132.36	R	Mixed size	6	7.75	7.5	-0.25
						6.05	5.0	-1.05
						9.5	10.5	1.0
						10.3	10.0	-0.3
						7.3	7.5	0.2
						6.7	6.0	-0.7
4	162.4 × 132.4	18.44	I	Mixed size	2	8.1	8.0	-0.1
						5.45	8.0	2.55
5	283.2 × 365.6	112.53	S	Mixed geometry	1	24.1	24.5	0.4
6	81.2 × 117.2	6.29	I	Mixed geometry	2	17.5	17.0	-0.5
						17.4	16.0	-1.4
7	192.4 × 172.4	89.99	R	Mixed size	5	6.8	6.5	-0.3
						6.7	6.5	-0.2
						6.8	5.5	-1.3
						6.8	6.0	-0.8
						6.7	6.5	-0.2
							MAE	0.65

\* $T_E$ : Execution time.; \*Type. C: Commercial, I: Industrial, S: Sports, R: Residential.

**Table 5.4:** Algorithm performance against previous works

Ref.	Year	VHR satellite imagery source	RMSE	Mean error (m)
[177]	2007	Panchromatic IKONOS	1.86	1.34
[178]	2011	Panchromatic IKONOS	12.99	—
[17]	2012	QuickBird	1.38	1.14
[15]	2013	Panchromatic IKONOS	1.34	—
		QuickBird	1.71	—
		KOMPSAT2	1.67	—
		WorldView1 (WV1)	1.88	—
[16]	2016	Google Earth	0.98	0.82
[180]	2016	Google Earth	22.66	—
This study	—	WorldView3 (WV3)	1.22	0.65

evaluation of 3D building models is therefore conducted based on creating 2D masks from both the true models (reference models from the OS data) and the output models. The border perimeter of each building in both masks from the reference and output models was extracted using morphological operations. Once the buildings' borders are attained, Cartesian coordinates ( $x, y$ ) are determined for buildings in the reference models ( $x_{ref}, y_{ref}$ ) and in the output models ( $x_{out}, y_{out}$ ) simultaneously. A technique for implementing automatic registration of the two coordinate systems (the image coordinate system and the layer map coordinate system) was developed to achieve this goal. Thereafter, for each pixel on the true model's perimeter, the algorithm finds the nearest point-coordinates (the smallest distance between two pixels, including the given points) on the perimeter of the output models. The calculated distance is the Euclidean distance between pair-coordinate points in the true and output 2D shapes of models.

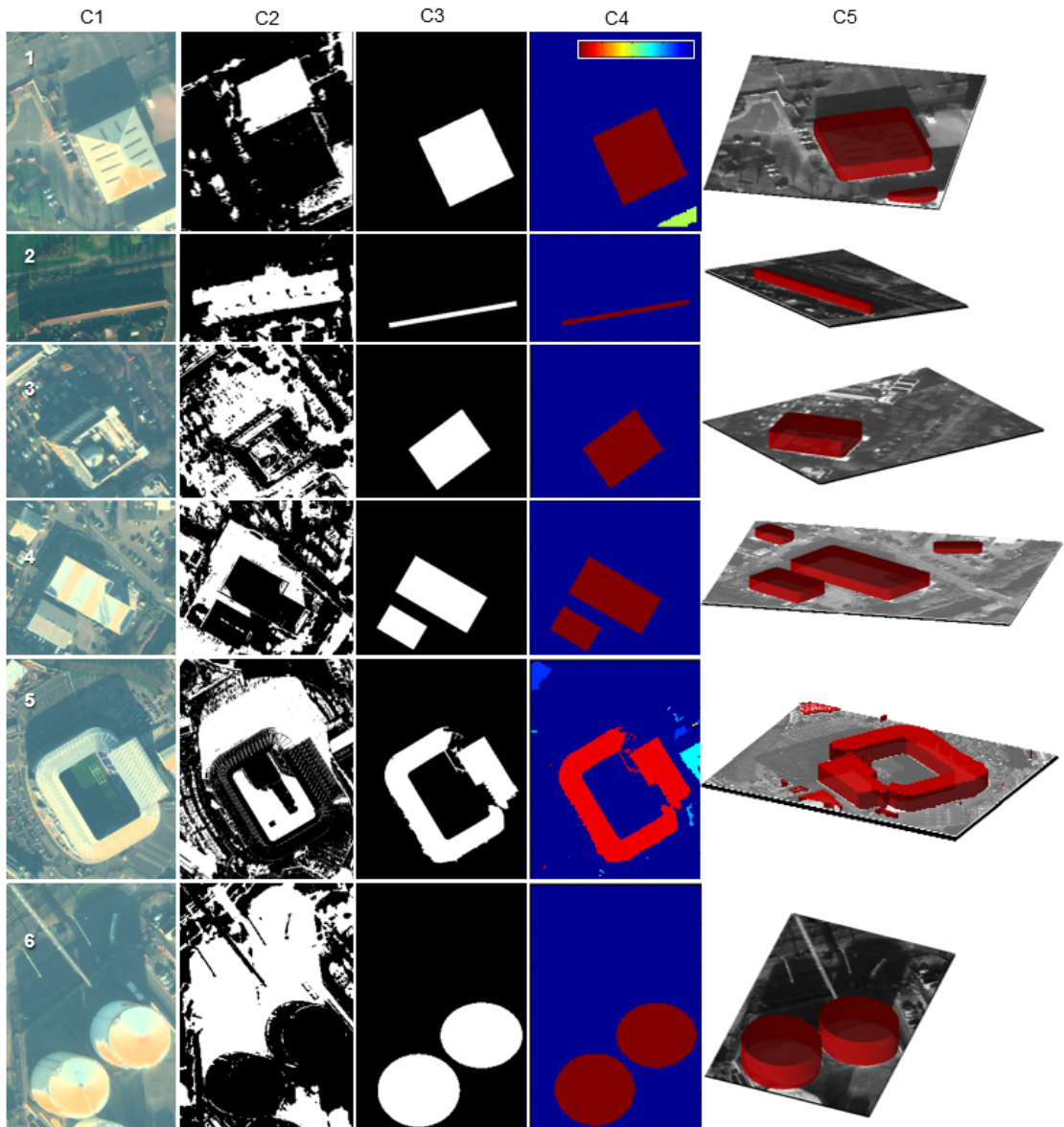


**Figure 5.14:** Automated creation of 3D building models: (first column) test patches (#1-6 RGB, pan-sharpened WV3 images); (second column) shadow detection of the buildings; (third column) the extraction of the building footprints; (fourth column) the maps of the building heights with colour bar referring to the height values; and (fifth column) the 3D building models at the LOD1

**Table 5.5:** Numerical results of the creation of 3D building models. The values between ground truth data and the results of the present study are compared to assess the algorithm performance

No.	The evaluation of 3D models			Error (m)
	True model	Created model	Execution time (sec)	
1			4.89	1.29
2			5.88	3.04
3			4.54	4.55
4			23.44	4.87
5			447.19	2.33
6			8.45	2.55

The 3D building model in test image #1 illustrates the smallest difference between two geometric models due to the simple shape of the building. However, the differences were larger in #2, #3<sup>3</sup>, and #4 images because of the building's geometric complexity. Moreover, due to the test images having very challenging illumination conditions and orientation within a complex urban landscape, the buildings' edges were occluded by other urban features or because of their shape complexity, so some of their edges obscure each other, making them very difficult

<sup>3</sup>Note: the size of the test image #3 is 280 × 361 (m).

to detect. Test image #5 shows some distortion in the 3D output model's shape because in some cases the buildings' sides can be seen as corresponding to the given perspective and the captured image's orientation angle. Nonetheless, the results demonstrate a novel method for creating 3D models of different building shapes within the complex urban environment. The creation of a 3D building model approach also proves the ability to derive 3D models from 2D information only.

Additionally, the models' differences, located within the error percentage of the OS data, indicate that the algorithm generates 3D models of urban buildings from one single image with acceptable accuracy. Moreover, and unsurprisingly, the approach achieves the best results when buildings' shadow regions are distinctly visible and not occluded or overlapped by any other object. Thus, despite the test images being very challenging, the results are encouraging and prove the proposed method's viability.

### 5.6.2 Solar rooftops analysis

Evaluating rooftops' solar energy potential is one reason for applying solar PV technology in cities' sustainable development. Using the developed method, rooftops and walls' solar yield can be determined, taking into consideration shadowing and shading obstructions, as well as surfaces exposed to solar radiation. Figure 5.16 illustrates measurements of the rooftop area and orientation for the building's modified geometry in the binary images. These case studies reveal the building rooftops' regular shape can be beneficial for determining the rooftops' total area, and it can allow estimation of the whole roof area's solar energy potential. However, Figure 5.17 shows another scenario and a different case study where the building rooftop's geometry is irregularly shaped. Therefore, the second case study presents the roof orientation's impact regarding which parts of the rooftops are dark (a shaded part) and which are bright (available for solar PV applications).

The calculation of building roof areas and orientation can result in significant heating and cooling savings. The results in Figure 5.16 and 5.17 provide two major advantages which can allow researchers and investors to know and determine the optimal position PV on the building roofs. First, the optimal building geometry will form a balance between heating and cooling energy demands. Because of the cost constraint, the reduction of the amount of heat transfer by the use of sufficient insulation is required to decrease conductivity.

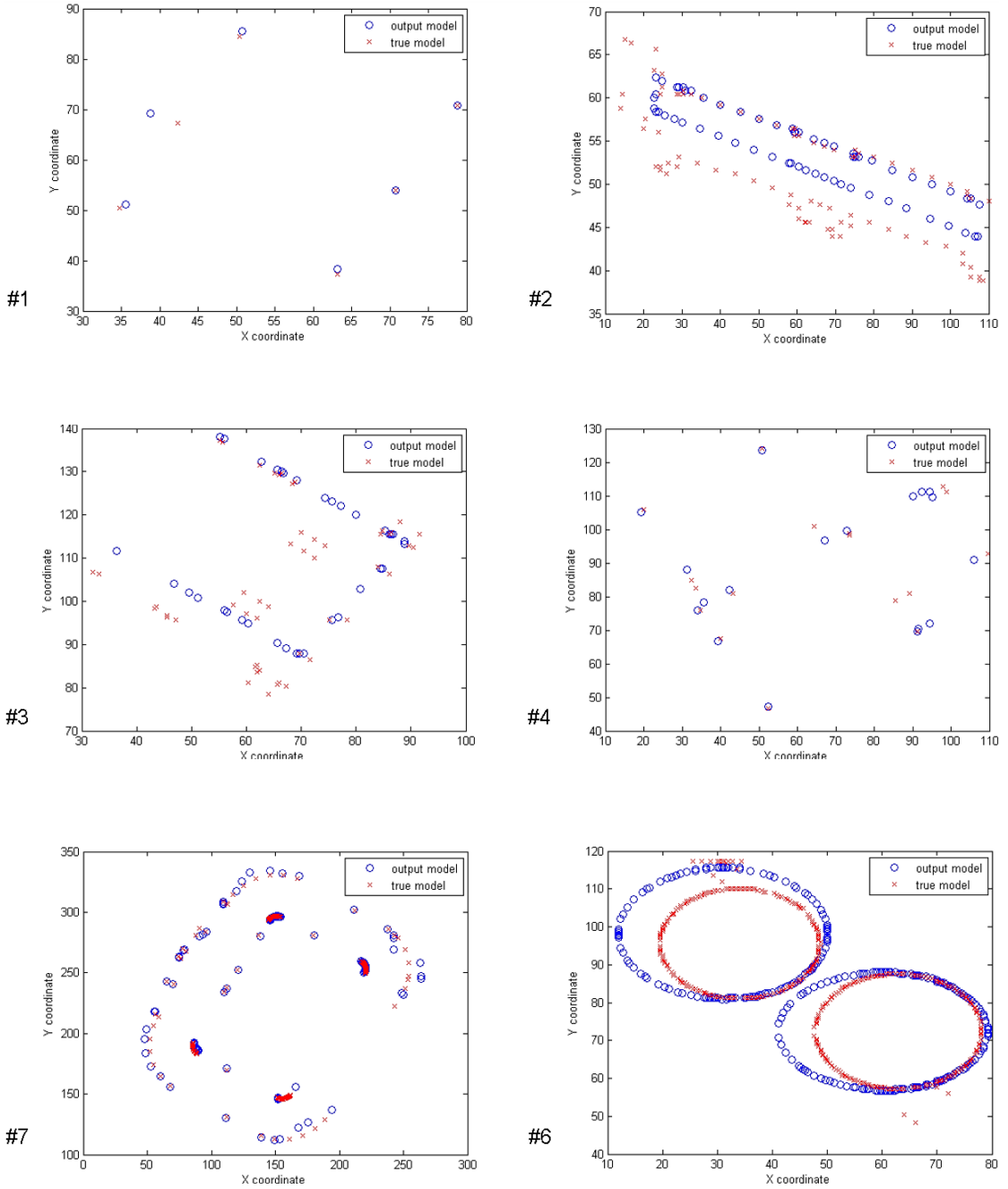


**Figure 5.15:** The validation of the perimeters of the 3D city models

A related point to consider is that the total quantity of heat transferred by conduction is largely dependent on area [194]. Second, regarding solar radiation, the results of the computation of the rooftop position concerning the azimuth angle of the sun show the ability to identify the roof orientation of the buildings. The latter can be very useful regarding the better estimation of the received energy for electricity, heating and cooling purposes. In this context, according to Hachem et al. [221] the south facade could receive more than twice the heat gain of east and west facades in the winter. However, the east and west facades have significant impacts on

overall heat gain in the summer months, and thus solar radiation can be harnessed to reduce the consumption of heating by the optimal position of the building.

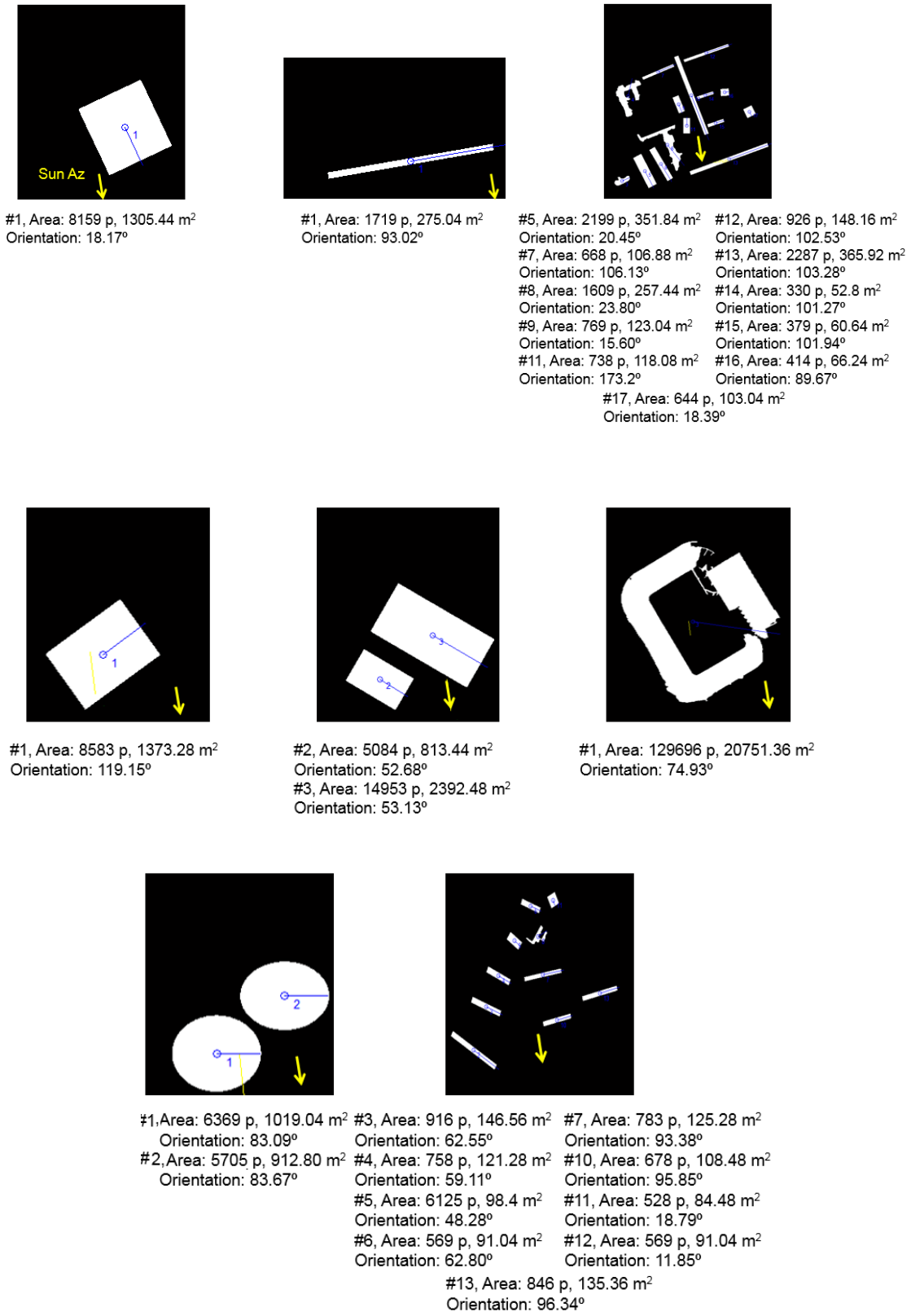
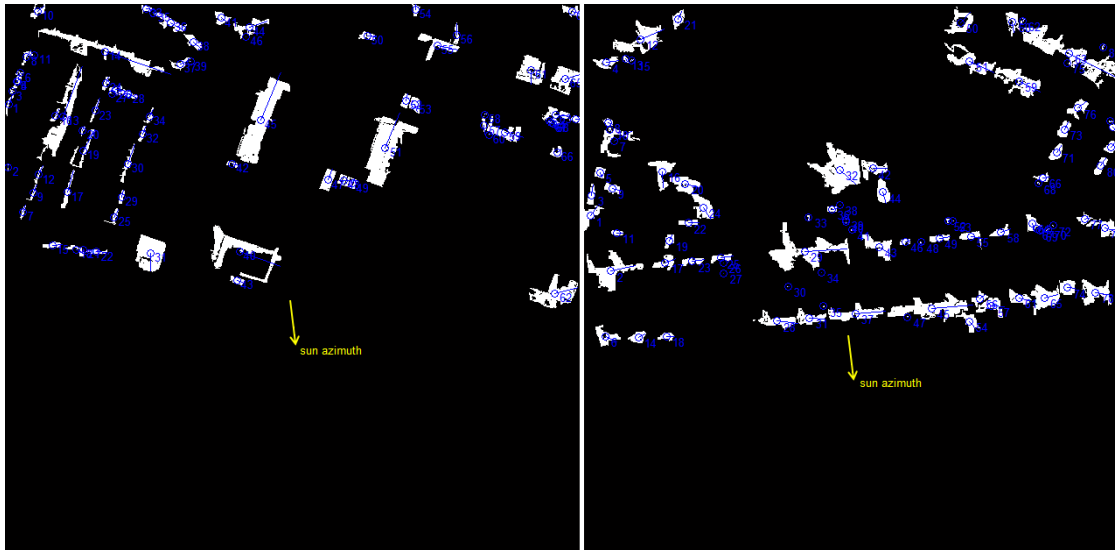


Figure 5.16: Solar building roof analysis

Understanding the degree to which the building geometry affects the building performance is useful in building design. Determining the optimal area and location of the building roof and walls for using PV systems allows the assessment of the solar potential to be more accurate. In particular, buildings that receive more solar gain in winter and shading in summer can help to decrease the demand for heating and cooling and have a considerable effect on the energy consumption of buildings.



**Figure 5.17:** Solar building roof analysis for two different urban areas

### 5.6.3 Computational time

All experiments were performed on a PC computer with an Intel 3.40 GHz i7-3770 quad core processor, 16 GB RAM and a 64-bit operation system. The approach's framework was developed in a MATLAB environment, and the sections related to GrabCut [19] and multi-label graph optimisation [222–224] were implemented in C++ code. The number of pixels in each test image is between 263,04 ( $137 \times 192$ ) and 1,494,829 ( $1193 \times 1253$ ). The process of creating the 3D building models for one test image's patches ranges approximately 31 (sec) and approximately 5 (min) total for all test image patches. This corresponds to the number of buildings existing in the image space. The estimated time that each portion of the developed algorithm takes to run includes the following: shadow extraction 1.34 (sec); the image partitioning 3.61 (sec); building shape refinement by active contour approach 4.73 (sec); building shape fitting 9.50 (sec); building height estimation 6.95 (sec); and 3D building models creation 5.71 (sec). The speed of implementing different portions of the developed algorithm is for one test image that includes a detached building, for instance, the 3D building model in Figure 5.14,

test image #1. In the other scenario with more than one building in the test image, the time estimation for each portion of developed algorithm is approximately as follows: shadow extraction 18.00 (sec); image partitioning 39.98 (sec); building shape refinement by active contour approach 16.00 (sec); building shape fitting 55.00 (sec); building height estimation 2.17 (min); and 3D building models creation 1.33 (min). An interesting point should be highlighted, which is that reaching a significant speed for each section of algorithm can be achieved in the present study.

## 5.7 Summary

The chapter has focused on the developed method's results from identifying the buildings' geometry and then creating 3D models of the buildings from monocular multispectral VHR pan-sharpened satellite WorldView-3 images (WV3). Various sections of the approach's implementation are highlighted in this chapter, illustrating how portions of the developed algorithm are applied to the selected images. The buildings' 3D models at the LOD1 are very well defined despite complex characteristics of buildings in the test images, for instance, shape, size, texture, roof type and colour, and building orientation. The 3D building segments were also recognised in most cases when the segments were not occluded.

Test patches derived from the VHR WV3 image were chosen to create different scenarios covering different types of buildings: detached, connected, adjacent (dense), small, and (large) multi-story buildings. In this chapter, outcomes from each part of the developed algorithm's process were introduced as figures and tables so the code implementation procedures can be readily understood and easy to replicate. The chapter exhibits the approaches and techniques that were developed, performed, and compared with state-of-the-art approaches, including shadow extraction, building detection, height estimation, and 3D building models creation approaches. An assessment of the present study's quantitative accuracy using the mean absolute error (MAE) and a comparison of the results are presented. The findings and their evaluation shows the strong impression that the introduced study is highly robust and that the 3D building models are quite convincing and representative. The results of 3D city models also reveal that it is possible to create feasible 3D models of the buildings without elevation data or other additional data, which satisfy the accuracy recommendations of CityGML for LOD1 models and the needs of several application analyses, such as GIS.

# **Chapter 6**

## **Discussion**

In this chapter, interpretation and substantial discussion of the results is introduced. Specifically, the developed method's findings are interpreted and discussed regarding the research questions and existing knowledge. This chapter sets out to present a coherent, well-structured explanation that accounts for the study's findings. A comprehensive discussion is provided in this chapter to clarify themes presented in the introduction and literature review chapters. This will demonstrate the current study's value and thoroughly interpret the results, with a clear understanding of their implications. The following sections are therefore organised to deliver the previously mentioned points.

## 6.1 Interpretation and discussion of the findings

A fully automatic method for creating 3D building models has been presented in this study. The automated extraction of objects in 3D form from remotely sensed data is an important research topic in the fields of computer vision, photogrammetry, remote sensing, and geoinformation. The generated 3D building model represents real-world urban environments and enables many applications such as visualisation, planning, analysis, and simulation. To assimilate a comprehensive suite of the developed method's results, this chapter focuses on the principal findings and their significance for the field of urban sustainability and renewable energy, based on remote sensing data. The current section is organised into three main subsections to deliver a clear view of the research.

### 6.1.1 A reminder of the purpose of the study

The aim of this study was to develop an approach for creating 3D models of urban buildings to assess solar energy potential from remote sensing data in an automatic manner. The new approach was established to investigate the possibility of deriving 3D models of the building envelopes at the LOD1 with minimum data availability. To this end, the developed method contains four main steps of research investigation, based on using a single VHR multispectral satellite image. First, there is extraction of the building footprints from very sophisticated urban landscapes. Second, there is the estimation of the building heights without additional information. With respect to the first research question, this study sought to determine the type of remote sensing data which could serve the aim of the present study and be used to extract significant information and accomplish the research purpose. Shadow information derived from VHR multispectral satellite images was the base for implementing the extraction and estimation processes' two steps. The third main step was to automatically generate 3D building models using derived information from two processes: building footprints extraction and height estimation. By achieving this step, the second research question was answered by verifying the developed method's findings. Fourth, the reason for reconstructing 3D building models is to provide elementary analysis and assessment concerning the solar energy potential of the building surfaces including roofs and facades. The calculation of the essential factors in the evaluation of the availability and suitability of the building roofs was fulfilled, whereas the assessment of solar energy potential was conducted using one of the building models by

creating a new tool to meet this purpose, which is mentioned and proposed as a future work in Chapter 7.

### 6.1.2 The study's major findings

Findings of the present study confirm that the 3D city models at LOD1 are generated by exploiting 2D data where there are no elevation data, particularly the creation of 3D building models from VHR satellite images. Our findings also suggest there is a potent ability to facilitate rapid updating and maintenance of data by supplementing existing datasets with 3D models of newly constructed buildings. In the present study, the buildings' shadow regions were found to provide very remarkable evidence of urban structures and features when they are accurately extracted from VHR satellite images. Utilising shadow information in the automatic detection process of urban buildings promotes the segmentation process of the buildings within their surroundings in single image space [19, 20], which indicates such information could be highly useful for automated detection of buildings with arbitrary shapes. A precise and reliable accuracy was obtained by examining the developed algorithm regarding the building footprints extraction, height estimation, and creating 3D models of buildings. This indicates the developed algorithm is remarkable and sufficient enough to construct 3D building models from monocular satellite images by mitigating and coping with a number of difficult aspects at the level of computational intelligence, such as complex urban landscapes, characteristics of the images used, the similarity between building regions and their backgrounds, occlusion in viewing angle, and environmental and illumination conditions at imaging time.

### 6.1.3 An indication of the importance of the findings

The study's results are consistent with research expectations, the literature, and existing knowledge about the creation of 3D building models. The developed method's results indicate several important points which can provide a full understanding of the research potential and implications as well as the limitations compared to previous studies. Referring to the literature, the results further support the idea of employing satellite imagery of remote sensing technology within the scope of urban planning and cities' sustainable development. Benefits of such data not only provide higher accuracy and greater precision in the object's measurements but also the types and levels of information that are either unavailable or of an inferior quality in

other data sources. This is because orthorectified VHR satellite images (geometrically corrected) are uniform in scale and allow the measurement of the detected objects true distances for creating their respective 3D building models. In addition, data can accurately present the Earth's surface because it has been adjusted for topographic relief, lens distortion, and camera tilt. Therefore, the detected objects precise position can be determined within complex urban landscapes as well as distances between it and other surrounding urban features. This feature has helped locate created models in their actual position on the image surface. Furthermore, very high spatial resolution facilitates identifying the shape of a building footprint, which in turn plays a significant role in reconstructing 3D models of urban structures.

Development of this robust technique to detect and extract buildings' shadow regions has many beneficial applications. According to Teke et al. [20], the extracted shadow regions provide important geometric and semantic information. For example, the building shadows findings provide evidence of the shape and position of objects (e.g. buildings, trees, fences, and cars), as well as the characteristics of surfaces and light sources. Shadow information is the main cue for man-made structures' detection in panchromatic high-resolution satellite images. The detection results of shadow regions can play an important role in automated analysis because shadow regions cover a significant portion of an image. In addition, the results of building shadow regions' detection and extraction could be used to assess the solar energy potential of roofs and facades of building envelopes, shadow analysis for urban planning, and new construction, because the shadow effect caused by building structures can substantially influence the amount of installed power capacity.

The most remarkable advantage of the findings indicates the ability to identify a building's geometry and create a 3D building model from 2D data with no additional data. With a developed fully-automatic algorithm for creating 3D models of buildings from VHR satellite images, running processes of the sophisticated and tedious operations for calibrating elevation data obtained by other sensors, such as LiDAR, radar, and laser, as well as processing time, effort, and cost are reduced or avoided. The creation process of 3D building models also comprises the image processing for deriving substantial information concerning buildings' shadow regions, footprints, and heights. The results were obtained from each of the algorithm's subroutines and can be useful for different purposes such as urban planning, sustainable cities, change detection, and risk assessment.

However, findings also illustrate the use of remote sensing data in locating available and suitable building surfaces for exploiting renewable energy such as solar. The findings have shown the capability of using detected rooftops (building footprints) in assessing solar energy potential for PV installation. Peng and Lu [191] reported an assessment of rooftop PV potential usually starts with determining the available rooftop area upon which to install a PV system. Moreover, the created 3D building models could be used to compute the ratio of gross wall to gross floor area which can help determine buildings' energy efficiency. In particular, utilising the optimal aspect ratio (a well-designed building envelope) yields how buildings receive more solar gain in winter and shading in summer, decreasing the demand for heating and cooling. Hence, the identification of a building's geometry, including its footprint and wall dimensions, is important because it has an impact on energy consumption. The following section illustrates in detail the results of the study, with a comprehensive interpretation of their indications.

## 6.2 Discussion and explanation of the results

The developed method's findings for identifying buildings' geometry and the creation of 3D building models are illustrated in Chapter 5. Many selected WV3 test images are also used during the evaluation process and presented in Figure 5.12 and Figure 5.14. All the results of the test image processing stages, as well as the developed approach's performance results are displayed in Figures 5.4 to 5.11. In addition to visual illustration, the present study's numerical results are listed in Tables 5.3 to 5.5. For a numerical assessment of all the test images and models, the results of previous methods are also presented, providing an opportunity to implement a fair quantitative comparison.

According to Section 5.2, and Sections 5.4.1 to 5.4.4, the developed algorithm's outcomes and new techniques have addressed the first research question with the particular content-related questions stated in Chapter 1. As previously discussed, one important reason for employing remote sensing data and, more precisely, the use of single VHR multispectral satellite images, is because elevation datasets remain expensive and time-consuming, impeding the production and availability of 3D city models [17, 211]. Because the new methodology in the present study suggests no additional data is used or needed to support the utilization of 2D data (satellite images) to facilitate object (urban structures) recognition, detection, segmentation, and extraction processes, there had to be an alternative way to develop the previously mentioned processes to generate 3D city models. The sub-question of the first research question asks: *What types*

*of information need to be extracted and inferred from optical satellite data to help characterise and detect the building regions in urban areas?* The answer is essentially, notably strong evidence of an off-terrain object must be found within the image space, which can be efficiently used to verify the existence of a building structure (footprint) and can also be beneficial for estimating the building's elevation (height). Therefore, shadow information was investigated and building shadow regions were extracted, as shown in Figure 5.4 and Figure 5.5. However, because the whole study depends on using shadow information for the 3D building models' automated creation process, the detection and extraction processes of the buildings' shadow regions from VHR satellite images should therefore be highly accurate and precise, as reported by Ozgun as well as Liassis and Stavrou [19, 180]. In this regard, a VHR multispectral satellite image was chosen to accomplish this purpose and address the first question of the main first research question of the study. One vigorous advantage of utilising such remote sensing data is that the multispectral satellite image, as stated previously, contains the NIR band in which shadow regions exhibit lower radiance values over the entire spectrum, and sensor irradiance from shadow regions decreases from short to long wavelengths due to scattering [19, 199]. This fact is considered when discriminating between shadow and non-shadow regions easier with NIR images. Accordingly, the shadow detection approach proposed by Rüfenacht et al. [149] was adopted and developed in Section 4.2, to detect and extract building shadow regions for two reasons: (1) the approach benefits from the NIR band which is presented in most VHR satellite images; and (2) the approach has fully independent user- and data-dependent thresholds.

The third and fourth questions of the main first research question of the present study were addressed when the extracted shadow regions were used to detect building footprints, and then to extract their shapes as well as estimate their height values. Figure 5.6 shows the detection of building footprints using Ozgun's method, first-level partitioning as described in [19], was refined to be more appropriate with the datasets used in the present study. The detection method proposed by Ozgun [19] was chosen to detect buildings in this study for three main reasons: (1) the approach takes advantage of using shadow information; (2) the approach is a full automatic technique and does not require any interference from users; and (3) the approach's results have been considered a benchmark for verifying the results of other approaches because they were obtained from using different datasets, were intensively tested regarding their parameters, and cover various environmental urban conditions. Figure 5.7 and Figure 5.8 show the developed part applied to the building detection approach proposed by

Ozgun [19] to obtain the regular geometry of building footprints. The active contour approach and the new technique were applied to the outputs derived from the first-level partitioning, as shown in Figure 5.7b, to attain straightness at the edges of the buildings. This part of the algorithm of building detection was developed because misclassification and mislabelling occurs between the pixels of buildings, vegetation, shadow, and other objects and regions after applying the first-level partitioning process. Hence, the building detection approach was required to be developed to determine and revise the erroneously assigned labels between these categories within the image space.

All parameters required to initialise the present method of the study are listed in Table 5.1. Many tests on alternative parameters and thresholding values were performed to select the best parameter values. In Table 5.2, the same example of the test image was used but it has been clipped to a small patch image to present few buildings to illustrate and focus on the differences which can be obtained when using and evaluating alternative parameter values of the chosen values. Thus, Table 5.2 presents the investigation of the effects of the key parameters of seven main tasks on the performance outcomes of the creation of 3D building models. Adjusting the contrast of the images is a critical process in the performance results because the best contrast can be obtained between urban features and the best detection of building shadow regions and building footprints can be accomplished. The effects of different contrast thresholds  $T_{\text{Cont}}$  indicate the reduction of the contrast between objects when increasing or decreasing the image intensity values of the selected value. The same deduction can be attained if the threshold values are increased or decreased in both shadow detection  $T_{\text{Rb}}$  and post-processing of the shadow regions  $T_{\text{I}}$  tasks. In the building footprint detection task, the shrinking distance  $d$  is fixed to 125 m, to ensure that incorrect pixels around the border of the shadow regions are rejected. If large numbers of pixels are collected as a building region from the directional neighbourhood of the shadow regions, performance improvements are observed with the fixed value of the shrinking distance  $d$ , whereas performance decreases are apparent for the pixel-based precision ratios when applying different values. It is concluded that the number of pixels assigned as foreground information affects the performance of the method. Significant improvement can be observed in each task of shape refinement  $T_{\text{Sf}}$  and building height estimation  $T_{\text{JI}}$  with their chosen threshold values compared to the alternative values. For the parameter  $T_{\text{Iso}}$ , it was found that the performances evaluated of the size dimensions of the created models are also significantly affected at lower and higher end of the

selected value of the isovalue threshold. In Table 5.2, all alternative values were chosen depending on visualising the clear difference and effect on the findings compared to the selected values. However, other values of the key parameters of the main processes between high and low threshold values also have effects on the performance outcomes, but they visually present less noticeable differences.

Shadow information was also used to estimate the buildings' height values, as shown in Figure 5.9 in which the 3D building models are generated and is also shown in Figure 5.10 and Figure 5.11. The results of the new approach developed for estimating building heights were illustrated in Figure 5.12 and its validation outputs in Table 5.3. Algorithmic accuracy was measured using precision, recall, and  $F_1$ -score, which are presented in Figure 5.13. The present approach's overall accuracy is compared against previous works on image-based building height estimation in Table 5.4.

The results in Figure 5.12 are promising, considering the test images' complex buildings, i.e. the variations in geometry, roof colour, orientation, and challenging illumination conditions. As expected, the algorithm performs very well for standalone buildings of regular shape. Zero error was found for test image #1, which is a detached commercial building. The algorithm underestimated the heights for mixed-geometry and mixed-size buildings in test image #6 and #7 respectively, by a small margin. The mean absolute error for all images was 0.65 m, demonstrating the algorithm's robustness.

One reason for the approach's success in challenging urban conditions is in addition to applying a thresholding scheme to filter out the building from the background, the developed algorithm is also able to mitigate the issue of two or more buildings with overlapping shadows. When a building's simulated shadow overlaps the shadow of another,  $J_I$  is set to zero to avoid erroneous estimation of the building's height. However, the performance appears to be affected by the presence of vegetation within the shadow region, as can be seen in image #4. Two buildings are separated by a narrow gap, and the smaller building's shadow gets blocked by the larger building to the north. According to the illustrated results in Table 5.3, the larger building's estimation error was 0.1 m ( $\approx 1\%$ ) while the smaller building's error was 2.55 m ( $\approx 47\%$ ). The situation was exacerbated by the presence of tall vegetation on the north-eastern side of the smaller building, preventing accurate filtering of the shadow.

The GraphCut segmentation method [19] used for detecting building footprint worked well except for image #6, in which the side of the oil storage silo and the roof were the same colour. The building footprint's shape, therefore, was larger than the actual measurements (Figure 5.12, C2). However, the shadows were unaffected and the overestimated footprint did not have a noticeable effect on estimating the building's height. However, in cases where there are many shallow buildings, such as images #3 and #7, the presence of darker pavements and roads can affect the algorithm's performance. One possible reason is the spectral reflectance of some non-shadow dark objects, such as roads and building roofs, is nearly identical to each other or to their background, resulting in dark objects being identified as shadow regions. Additionally, some adjacent buildings occlude the shadows cast by other buildings. As a result, the shadow region length appears longer than its actual length if the shadow regions are combined with other shadow regions cast by other objects or buildings. Conversely, they will appear shorter if some parts of the shadow region are obstructed by adjacent buildings. Our approach mitigated this issue with the help of morphological post-processing and thresholding in the simulation process. In this vein, the algorithm was tested on different urban scenarios with varying building and neighbourhood attributes. The findings were encouraging and outperform past approaches, with a 21% reduction in mean error and an overall accuracy of  $\approx 80\%$ . The increased accuracy is attributed to the ability of the algorithm to consider overlapped shadow regions, and the removal of landscape features such as shadows of vegetation canopies.

Closer inspection of Figure 5.13 shows the results of the pixel-based assessment and evaluation by  $F_1$ -score using simulated shadow regions compared to actual shadow regions. The computed pixel-based  $F_1$ -score for all test images is approximately 63%, a result that is quite acceptable for such a diverse and challenging set of test data. It is important to emphasise the dataset used in the present study involved two highly challenging images #4 and #5 in Figure 5.12, whose results also contribute to the overall pixel-based performance. The lower performance of test image #4 is due to the adjacent buildings and test image #5 is due to building geometry with very high elevation. Regarding the previously mentioned interpretation and explanation of the test images results, the length of the actual shadow regions of both case studies are affected by the phenomenon of lengthening or shortening. Accordingly, a better overall pixel-based performance of the developed approach was expected if these two test images' results had different scenarios of urban landscapes or were excluded from the evaluation.

Although satellite test images present diverse building attributes from different areas, results

reveal the new approach is efficient for estimating building heights. Furthermore, comparisons between the new approach's overall accuracy and previously published works in Table 5.4 proves that the proposed approach is superior for estimating the building height based on shadow information in an automatic manner. The average processing times for one building, one scene, and all seven test images were 0.10 sec, 1.50 min and 4 min, respectively. Execution time depends on the size of the image and the complexity of the scene, as shown in Table 5.3. Smaller images (e.g. #1 and #6) with one or two rectilinear buildings require less processing time and has the lowest estimation error.

The second set of research questions aimed to investigate the capability of using the derived information from optical satellite imageries in 2D form (footprints and heights) to automatically reconstruct building envelopes in 3D form. The results of the 3D models generated from the extracted building footprints and their estimated heights are shown in Figure 5.14. The sensitivity analysis, including the results' numeric evaluation and accuracy assessment of the created models, is introduced in Table 5.5. From Figure 5.14, the developed algorithm's ability to create 3D models at LOD1 works well and shows a robust cue for automatic 3D building extraction from a single image. All 3D building models are precisely located over their spatial positions in the test images. This is one remarkable outcome of the present study in the scope of remote sensing technology, computer vision, and image processing techniques. These findings raise intriguing questions regarding the nature and extent of remote sensing applications in urban studies and a powerful utilisation of the advanced and developed algorithms in extracting urban structures and features, by dispensing with the use of other datasets, such as the building attributes (e.g. polygons and heights) derived by sophisticated and overworked operations of cartography and photogrammetry technologies. It is also evidence that the present approach distinctively constructs 3D buildings from the test images with challenging environmental and illumination conditions. The numerical evaluation results in Table 5.5 reinforce these findings. The table shows the difference in the shortest distance between the created model and the original model of the buildings by calculating the errors of the perimeter of two models. Interestingly, the MAE of the total differences between two models was very encouraging in terms of the reliability in the representation and visualisation of the created 3D models for the existing buildings. In Table 5.5, the differences between the created and referenced model for the selected case scenarios in the present study range between 1.29 m to 4.55 m. This means the overall result of an evaluation and comparison of the two models reveals that the error value does not exceed 5 m.

The results obtained from the preliminary analysis of solar building roofs are presented in Figure 5.16 and Figure 5.17. Automated detection of the building roofs (footprints) in the binary image (monochrome), which has only two possible values for each pixel (0 and 1), allows the assessment of the rooftops for PV and solar thermal options to be achieved; this includes the identification of the bright part of rooftops, area, and orientation, where, 0 refers to black colour and 1 refers to white colour. As can be seen from the two figures, the results demonstrate the analysis of a solar building roof can achieve centimetre-level accuracy due to high spatial resolution in the VHR images. It can be seen also from the results in Figure 5.17, that the captured date and time of the satellite image with a given azimuth angle of the sun plays a significant role in facilitating the identification roof sections available and suitable for PV installations. Specifically, the rooftops have a variety of shape topology and geometry, or the rooftops have many structural details such as chimneys and roof windows. Results illustrate that the developed algorithm can recognise and distinguish building roofs' shape and detail, identify the orientation of the roofs with respect to the azimuth angle of the sun, and compute the rooftops' bright available areas. This bright available part of the rooftop is determined with pixel value 1 which is a white patch of the building roof. In contrast, the unsuitable part of the rooftop is the dark (black colour) with pixel value 0 at a specific angle of the satellite sensor's view when the image was taken. However, the dark part of the roof can also be illuminated in daylight. It is important to remember the exposure of the part (patch) of the building roof to sunlight, at a time other than the time of capturing the satellite image, can be less if it was in the opposite direction of the sun illumination and vice versa. Nevertheless, other factors, for instance, the degree of the inclination angle of the roof patch and the number of insolation hours also have an impact on the amount of solar energy received by that roof part. Similarly, this concept can be considered when the created 3D building model is used to assess solar energy potential on the building envelope's facades. The next section introduces implications of the present study and generalisations that can be made from the results.

### 6.3 Implications and practical applications of the study

With worldwide use of optical VHR satellite images, the results of the present research provide further support for the hypothesis that remote sensing is a magnificent data source which can greatly facilitate extraction of urban-area-related objects such as buildings, vegetation, and

roads. The findings also seem to be consistent with other research which found the utilisation of single VHR multispectral satellite images provides vital data for detecting and extracting shadow regions (e.g. [20, 149]), building footprints (e.g. [19, 150, 151, 225]), building heights (e.g. [16, 180]), 3D modelling (e.g. [17]), and renewable energy assessment (e.g. [23]). Moreover, the outcomes of the developed algorithm further support the idea of reliable extraction of 3D building models from VHR satellite images in an automated manner comprising new approaches and techniques in computer vision and image processing (evaluated by ground truth measurements), as claimed by many researchers, such as Ozgun as well as Izadi and Saeedi [17, 19]. This outcome is contrary to that of Michelin et al. [226], who found no generic method had been developed for generating 3D building city models with satisfactory results.

It is interesting to note that, in all cases of this study, the appearance of a building in VHR WV3 images is governed to a large extent by its roof structure. This means the various roof geometries lead to specific shapes in the reflected ray received by the optical WV3 sensor. For instance, L-shaped shadows are formed by flat-roofed buildings, a trapezoidal shadow shape may be seen when a building has a sloped rooftop, and a gabled rooftop casts a shadow with multiple lines close to a hexagonal-shaped shadow. Analysis of the character and geometry of building shadows in the WV3 images allows the detection and reconstruction of buildings, including extraction of 3D building models.

The selected different scenarios of building geometry allow the developed algorithm's performance to be examined. Considering the complexities in the test images involved, it is believed that the performance results achieved in creating 3D building models automatically by the present method are quite exceptional. Consequently, it is anticipated that the overall accuracy of the present study's findings increases when using the images captured from different seasons of the year. For example, this includes summer when the shadow regions are smaller than the present case studies, which were captured in winter at a sun elevation angle of less than (30°) [19]. The reason for this expectation is the large shadow region is most likely cast on and covers different urban features and objects near the building, where its true length may be affected. In contrast, a smaller shadow region at the sun elevation angle greater than (30°) can minimise the probability of its occurrence and lead, eventually, to reduced errors and more accurate results. This is based on considering the WV3 satellite operates in a sun-synchronous orbit<sup>1</sup> and passes over an observed area before noon, near 10: 30 am.

---

<sup>1</sup>A Sun-synchronous orbit (geocentric orbit) is a nearly polar orbit around Earth in which the satellite passes over any given point of the planet's surface at the same local solar time (the local time zone of the given area).

The evaluation results of the mean absolute error (MAE) from achieving the building heights' estimation values satisfy the accuracy recommendations of CityGML for LOD1 and the needs of several GIS analyses. Outcomes of the automated creation of the 3D building models for different types and utilities of the buildings such as small, large, connected, and detached buildings, prove that the present approach is generic, efficient, and robust enough to generate 3D blocks of urban structures in a dense city. However, the findings show the algorithms accuracy in creating 3D models of the detached buildings is higher than the adjacent or connected buildings which have arbitrary structural details and geometry. Nevertheless, all study cases demonstrate there is an ability to create 3D building models from VHR multispectral WV3 images, based on shadow information.

Each part of the current study and the developed algorithm can be used individually as an independent and powerful tool in urban studies and applications or as a whole process in producing 3D city models. Specifically, the detection and extraction of shadow regions can be exploited in urban planning and climate change to determine the impact of the cast shadow by other adjacent buildings (shading from nearby structures) on a newly built-up location (e.g. [227]). Shadow information can also be employed as an assessment parameters of buildings' roofs and facades' solar energy potential (e.g. [228]). In the scope of risk assessment, shadow analysis for the detection of earthquake-induced collapsed buildings was conducted by Tong et al. [229]. Another significant feature of the present study is use of the algorithm to detect objects (e.g. buildings) in any city or urban area that may or may not involve a complex urban fabric and landscape. In general, the developed algorithm has the capability of separating objects from their background and the surrounding features in the image space, as well as the detection and extraction other types of land cover such as vegetation (e.g. [19]). Furthermore, the results of the building height estimation proves the developed algorithm's strong performance in deriving building height values in a timely and cost-effective manner compared to traditional measurement methods. A clear benefit of this part of the present research can be exploited and used in a wide range of urban applications. For instance, it may determine and detect changes and expansion in the vertical direction of cities, specifically, urban structures (e.g. change detection for urban buildings) [174]; and the estimation of building storeys [230]. Considering the automated creation of 3D models, the current research introduces an effective, efficient, and alternative method to generate 3D city models where there is limited data availability for many areas around the world. Because there is an increasing interest in 3D city models for many different applications and users worldwide, the developed algorithm

can be a powerful automatic methods to construct 3D building models in LOD1 (the well-known block models without any roof structure, as defined by Kolbe [231]) in comparison to interactive or semi-automatic methods. Despite the simplicity of LOD1 models created, the models have multiple uses, such as shadows analysis during daytime (e.g. [232]), solar energy potential assessment (e.g. [233, 234]), flood simulation within urban areas (e.g. [235]), the different effects of sky view factor (SVF) on urban air temperature (e.g. [236]), the impact of urban air flow on building energy consumption (e.g. [237, 238]), examining the GPS satellite signal quality within urban areas (e.g. [239]), and noise pollution (e.g. [240]). In fact, some researchers prefer the use of LOD1 models over the more complex LOD2 models because of their simplicity and ease of acquisition, and the fairly good results they provide [220]. Accordingly, the resulting 3D models in the present study provides a complete spatial visualisation for many practical urban applications and better answers to the most interesting questions regarding sustainable cities. Additionally, a further advantage of the current method of the automated creation of 3D building models is that it has the potential to be applied in any chosen city without any spatial or temporal constraints.

## 6.4 Limitations of the study

Despite advantages and distinctive improvements, the present study's developed methodology has four major limitations. First, the algorithm is unable to create 3D models of buildings whose shadows are not visible. Note that the creation performance is not restricted by the extracted shadow mask, and the developed approach is able to distinguish full shadow regions during the first steps of the detection and extraction processes. Nevertheless, the developed approach's performance will break down when creating 3D building models for building regions where the cast shadows are completely (self-)occluded.

Second, the algorithm is unable to derive and accurately estimate building height values in high density residential areas, and creation of the 3D models will not provide a full regular block (model) of the building due to the narrow distance between one house and another. This close adjacency between the residential buildings (e.g. houses) causes the loss of their shadow areas. This means the cast shadow regions are obstructed by adjacent or near buildings. Nonetheless, the algorithm will perform robustly when all external edges of the cast shadow regions (the borders of shadow perimeter) are detected within the narrow distance between two houses or buildings. Particularly, this can occur when the satellite images are captured during

the summer season in each place where the sun's rays at the angle of incidence are shorter and proximately vertical on the Earth's surface. In fact, at the time of capturing the image, the area of cast shadows in the summer season will be smaller than winter. Therefore, even if the distance between two adjacent buildings is small and narrow but the building shadow is not cast on or blocked by the nearby another building, there is no limitation or problem with the algorithm's performance. This is related to the well-selected time and date of the VHR images used.

Third, the study's results might have been affected by the extreme topography and slope direction of the terrain, especially the estimated value of the building heights. However, the current research was conducted on small urban areas and the developed method focused on creating 3D building models for the specific scenarios of building types on a small scale (at a building level). Therefore, the problems that may arise when buildings are on a hill, for example, were not faced in these case studies. This is because the patches of the test VHR WV3 images covered different small areas of the city. In contrast, to study and make the required corrections to the 3D models considering their height values, the study area must be on a large scale and cover the most built-up areas in the city or display the whole city itself so the degree of slope and topography is very noticeable.

Fourth, the algorithm is not capable of determining differences in roof topology as well as the geometry of the building envelope. It is worth mentioning the algorithm performance was designed to generate 3D models of urban structures at LOD1, which is described as a block model with flat roof structures and simple envelope geometry [208, 231]. Because the building roofs are considered a major pillar of renewable energy strategies (e.g. solar PV applications) within urban areas [241], an initial solar analysis on the detected building roofs was conducted. The results illustrate the available parts of the rooftops in both roof types: flat and pitched roofs. The findings derived from the detection process of the developed algorithm for extracting building roofs display both types, and which part of the roof is bright (direct facing sunlight) and which part is shaded (the opposite direction) at the time of capturing image, as well as the orientation of those rooftops. Remarkably, in the case of the detached building, its flat roof orientation represents the actual building orientation itself and its created 3D model will acquire the same true orientation. Most importantly, the orientation of the building has an impact on the possible energy collecting area on the roof because the potential number of the solar panels strongly depends on the building's orientation [241]. Regarding the pitched roofs, the orientation, topology, and inclination of the solar collecting elements are determined by

the roof [241]. Consequently, pitched roofs' geometry is more complex than flat roofs when assessing solar energy potential. Another approach is required to construct 3D city models at LOD3, which considers the roof topology and geometry.

## 6.5 A summary of the results

The chapter has focused on explaining and discussing the research findings. It highlights the study's purpose, techniques, and datasets, and interprets the main results. The great potential of employing the VHR WV3 images in the urban studies as a powerful data source has been explained. The purpose of the research project is to develop an approach for creating 3D building models on LOD1 from VHR WV3 images automatically when no elevation data or supplementary datasets exist. The results of 3D models automatic creation demonstrate the developed method offers a reliable and low-cost process for generating 3D building models that can be applied to the analysis of solar energy applications and sustainable development of cities, in addition to urban planning and city understanding, where costly data and sophisticated processing practices are less accessible. The chapter displayed the possible implications of the study and method limitations. The performance of the new method will have high quality and accurate results if the buildings shadow regions are well detected and extracted within the image space. The chapter also indicates the 3D city models play an important role in identifying the surface availability of the building for assessing solar energy potential, not only on the roofs but also on the facades. This is an important issue for future research, as stated in the next Chapter [7](#).

## **Chapter 7**

### **Conclusions and future work**

This chapter introduces the conclusions of the main areas covered in the presented study, the significance of these findings, and recommendations, together with a final evaluation and suggestions for future work. This chapter also provides an explanation of where the results can lead and what next steps may be taken. The contents and contributions of the study are summarised to pave the way for other questions raised by the findings of the developed method in this work.

## 7.1 Significance of the study

Summarising Chapter 6, a robust algorithm was developed to create 3D city models, concentrating on urban structures (buildings), by detecting and extracting building footprints and estimating building height values. The automated algorithm developed in the present study for creating 3D building models will benefit society, since 3D modelling of urban buildings plays an important role in science and technology today. The great demand for the improved understanding of urban environments, with the possibility of applying renewable energy technologies in cities, justifies the need for more effective and sustainable development of city assessment approaches.

The present study provides a comprehensive view of urban structures as a 3D vision of the urban landscape. This method will help obtain a more accurate estimation of the availability of building surfaces for solar energy applications. The new algorithm for the automated creation of 3D building models using the LOD1 approach can be used in several application domains. For example, the algorithm can be used in the assessment of the impact that shadows of new buildings will have on their surroundings [220], the preliminary analysis of solar potential at a municipal or neighbourhood level [153], and the insolation of buildings in kWh per year [242]. The method can also detect and extract shadow regions and building footprints (roofs) and use this information to estimate building height values in an automatic, efficient and accurate manner. These elements can serve decision-makers, authorities, planners, and designers looking to employ automation in various sectors of work. In addition, the algorithm is easy to use, accurate, and with sufficient performance speed. The present study will help investors in the field of renewable energy to have a deeper understanding of the suitability of building surfaces as well as the effects of the shadows they cast. The algorithm provides an easier and more powerful tool that can enhance and improve the process of solar energy potential assessment industrial, commercial and residential levels. Furthermore, the current study provides a foundation for developments in 3D building model algorithms by developers and researchers by promoting 3D models from LOD1 to higher LODs using remote sensing data only and by improving the processes of building detection, extraction and height estimation.

### 7.1.1 Restatement of aims

The aim of this thesis was to develop an approach for the automatic creation of 3D city models, specifically buildings, based on remote sensing data. Single multispectral VHR satellite images were used, specifically WV3 images of remote sensing data. The process of the automated creation of 3D building models focused on extruding the footprints of 2D data (images) using the estimated height values. The key purpose of the automated 3D models is to provide a better understanding and a more accurate assessment of the solar energy potential of the surfaces of the building envelopes. The most distinctive feature of the presented work was the use of available data, such as satellite images, which were highly accessible in terms of cost and handling and did not require complementary data, such as elevation data, to generate 3D models in LOD1. The developed approach employs shadow presence to detect building footprints and estimate building heights, which are used to construct the 3D models of buildings.

The study had six objectives to achieve the main aim. The objectives were set to provide guidance to accomplish the main aim. The research objectives were to review and critique state-of-the-art approaches and algorithms for identifying building geometry and creating 3D models of buildings using satellite images. The second objective was to develop an approach for detecting and extracting building footprints based on their shadow regions while eliminating other urban features such as trees and fences. The third objective of this study was to investigate and develop a robust technique for estimating building height, which led to the fourth objective, the development of an approach for the creation of 3D building models based on the regions of the extracted building footprints and the estimated building heights. The fifth objective was to conduct solar analyses of rooftops. The sixth and final objective was to validate and verify the created models for all parts of the developed algorithm.

### 7.1.2 Summarising research findings

Chapter 5 briefly restates the major results of the study and summarises their significance for scientific knowledge and they complement finding in existing studies. What is striking about the datasets used is that monocular multispectral VHR satellite imagery is an intrinsic data source for extracting information about urban structures. The detection of urban features (e.g. residential, industrial and commercial buildings) from VHR satellite images is of great practical interest for different urban applications, such as change detection, urban monitoring, population

density estimations, 3D city modelling, and sustainable urban development. One important use of satellite imagery is to maximise the ability to detect spatial variation for using renewable energy collection systems to sustain urban environments. Satellite imagery can be used for the automated extraction of the reliable and suitable rooftops (footprints) of buildings as well as the automated creation of 3D building models at LOD1 without elevation data. The automation of information derivation processes from these images plays a vital role in the further analysis and assessment of the availability of the building facade surfaces and helps to exploit solar energy systems within urban areas.

The new methodology presented here can support sustainable development by allowing urban areas to be routinely appraised, thereby maximising the opportunity of avoiding degradation and deterioration of the natural environment and ecosystems. Inventorying existing buildings, identifying pattern and density, monitoring access to resources, and determining facilities and transport networks can play a role in mitigating the expansion risks of the built environment. Also, using renewable energy is an additional solution to reducing the dangers of the continuous and increasing use of fossil fuel. The results of this study contribute to sustaining urban areas in terms of the transformation of landscapes in the context of energy policy decisions. The algorithm developed in this study can also be used to assess the density of urban areas and increases in energy consumption by detecting existing buildings and identifying building geometry. According to McKeen and Fung as well as Asadi et al. [194, 243], the geometry of a building has an impact on heating, cooling, ventilation and lighting.

The approach developed in this thesis is also a potent tool to exploit geospatial technologies, such as satellites and computers for providing maps. These maps involve spatial data which represent the location, size and shape of an object on Earth, such as a building, lake, mountain or township. The research findings containing the maps of detected buildings, estimated heights, and 3D building models, provide more information about the entity of urban structures. The obtained spatial information and attributes of the buildings allow complex themes to be analysed and then communicated to wider audiences. The obtained precise location of the building footprints and their 3D models on the surface of the Earth can help in improving assessments and predictions of the different urban applications. Particularly, the research findings highlight the algorithm's capacity for finding the most suitable building surfaces available for solar PV applications.

This research extends our knowledge of employing remote sensing technology for various

urban studies and applications. The present study provides additional evidence with respect to using VHR satellite images, in particular WV3 images, which confirmed that optical VHR satellite images are the most useful data input source for urban feature detection (e.g. buildings). Furthermore, the findings of this thesis could be used to support information about urban features in complex landscapes. The key strength of this study is the automatic creation of 3D city models using only VHR WV3 images without requiring elevation data or additional and complementary datasets such as cadastral or statistic data. The experiments and the discussion illustrate that 3D building models could be advantageous in a number of spatial analyses. The study findings enhance our understanding of the capability of the creation of 3D models of buildings at LOD1 from 2D data based on shadow information. The study also improves our ability to more accurately assess the availability of building roofs suitable for solar PV installations.

## 7.2 The conclusion of the study

This thesis developed a novel approach for modelling and assessing available surfaces for the exploitation of solar energy potential within an urban environment in an integrated analytical framework. The developed approach displays the automated creation of 3D building models using single multispectral VHR satellite images without elevation data. Conclusions drawn from the data can be used for contemporary research and experiments. The key conclusions can be listed as follows:

- The algorithm developed in this thesis proves its ability to extract the attributes of the buildings from satellite images within complex urban environments. The method used was able to identify the geometric attributes of the buildings (footprints and heights) and generate the 3D models in LOD1 from 2D data in an automated, unique and comprehensive manner. Despite advancements in remote sensing technologies, elevation data required to create 3D city models is not available in many areas around the world. Many developing countries still lack national coverage of elevation suitable for producing 3D city models [208, 210], cadastral maps or masterplans for building footprints. This is true in Iraq. Depending on the need and purpose, the building footprints (rooftops) and 3D models obtained with the estimated heights can be a reasonable and significant provisional solution until such measurements become available. They can also be an advancement

on outdated methods. According to the evaluation research findings, the developed approach is highly robust and quite promising for diverse and challenging datasets.

- This thesis reviewed a number of current pioneering studies in the scope of shadow detection techniques using VHR satellite images and the performance of the advanced algorithms. The use of VHR images from advanced satellites such as WorldView-3 illustrates a promising method of object detection and extraction within urban areas. Shadow detection in an urban feature from such images provides vital information that can assist in better understanding the built environment. Shadow are evidence of elevated objects, confirming the existence of a building or structure. Therefore, the automated detection of shadows in VHR satellite images are important for applications that involve building detection, illumination direction analysis from the sun, and spatial distributions of objects casting shadows. Although the detection of shadow regions is challenging when derived from a VHR satellite images comprising a visible spectrum range (RGB true colour), the results using multispectral WorldView-3 images (RGB and NIR bands) were better and demonstrated a reasonable separation of shadow regions from other objects; this indicates significant performance of the ratio-band algorithm [149]. It is easier to distinguish shadow areas from non-shadow areas with NIR band because shadow regions generally exhibit lower radiance values over the entire spectrum, and sensor irradiance from shadow regions decreases from short to long wavelengths due to scattering [19, 199]. Moreover, the differences in the characteristics of the two satellite images in terms of spatial and spectral resolution can play an important role in the estimation and detection of the shadows of urban objects, such as buildings.
- The excellent performance of the algorithm in automatically detecting and extracting the building footprints illustrates a great opportunity to reduce the time, cost, and effort spent on producing cartographic and geospatial maps of any urban or rural area. After developing and enhancing the building detection approach at the first level of image partitioning proposed by Ok [19], the results demonstrate the highly precise representation of the true spatial location of the extracted building footprints as well as accurate, minute details of the detected rooftops. The developed algorithm is able to address the distortion of detected building edges by two levels of image processing. The active contour approach and the developed approach are shape-fitted for adjusting the parameters of the two most familiar building geometries, rectangle and ellipse, seen in urban landscapes. The adjusted geometry of the building footprints is quite accurate. However, there are

difficulties in detecting the footprints of the buildings using the GrabCut approach when the shadows cast by buildings are not completely visible and not well-detected after applying the shadow detection approach. The non-detected shadow regions can cause edge distortion of the building footprints, which eventually affects the final results of the automated 3D building model creation.

- A new shadow-overlapping algorithm  $A_{SO}$  was developed for estimating building heights from a single VHR multispectral image. The new approach is based on the automated identification of building shadow regions using the solar information in the image metadata, the morphological operations and the Jaccard Index ( $JI$ ). The algorithm was tested on different urban scenarios with a variety of building and neighbourhood attributes. Results are encouraging and the algorithm outperformed other approaches, with a 21% reduction in mean error and an overall accuracy of  $\approx 80\%$ . The increased accuracy is attributed to the ability of the algorithm to consider overlapping shadow regions and the removal of landscape features such as the shadows of vegetation canopies. The core benefit of the approach is the cost-effective extraction of building height and subsequent 3D construction of urban areas for modelling, simulation, and visualisation. Applications can range from 3D urban change monitoring to high-resolution assessments of potential locations and the forecasting of renewable energy, such as solar PV and wind. The speed and frequency of VHR acquisition compared to more expensive methods, such as LiDAR, opens up significant possibilities for emergency response immediately after a disaster, for example assessing infrastructure and building damage.
- A novel method was improved and developed to automatically create 3D city models solely from WV3 images (2D data) without the use of additional data, complementary information or elevation measurements. The present study discloses the considerable possibilities for modelling urban structures (e.g. buildings) based on extracting building footprints using estimated building heights and the Marching Cubes algorithm. Both the footprints and the heights of buildings were automatically derived from WV3 images. The creation of a 3D building model was achieved in LOD1, which indicates the generalised outer shell of buildings. Remarkably, the resultant 3D building models of the developed methodology satisfy the standard CityGML quality recommendations and those of several spatial analyses. Additionally, the results of the visual and numerical assessments reveal that the 3D building creation approach is promising in providing a 3D city model with fully automatic operation, indicating that the developed algorithm works fairly well

with challenging urban environments and illumination conditions. However, because the created 3D building models are in LOD1, the specific model reports the same height value for each point of the rooftop, representing a flat roof. Nonetheless, the improvement in the LOD of a 3D building model is negligible and does not improve shadow prediction accuracy without increasing cost of acquisition and requiring a larger storage footprint. Hence, the higher cost of acquiring 3D models in finer LODs is not always justified, as reported by Biljecki et al. [220], which can be seen in applications. However, with renewable energy applications, such as the assessment of the photovoltaic potential, the accuracy of the assessment may be considerably influenced in case having further structural details of the building surfaces. Nevertheless, the present study offers a robust approach to detect and extract shadow information during daylight hours and to provide an initial solar analysis of the extracted rooftops for PV applications.

- The analysis of the preliminary solar potential of building roofs shows the capability of the developed algorithm to derive significant information from satellite images that can be used for solar energy potential assessment within cities. It is concluded that the bright building roofs can be determined by the identification of the roof's location, area, and orientation. Those rooftops in an advantageous position in relation to the sun can provide a suitable area for PV application in the modern urban landscape. These findings can be exploited for the development of solar energy implementation policies and urban planning. Therefore, the initial solar analysis of the building roofs in this study can be an exploratory calculation of solar potential at the municipal level.

### 7.3 Implications for the field of urban modelling

The findings from this study make several contributions to the field of urban modelling. Firstly, the findings contribute toward the application of remote sensing technology. They can be used in photogrammetric satellite applications or aerial photography and cartographic mapping techniques. The results of the automated creation of 3D building models show that the developed method can be applied to identify the geometry of urban objects and features, such as buildings. The geospatial information derived from remotely sensed data (e.g. multispectral VHR satellite images) in this study can play an important role in providing a wide range of spatiotemporal information about the structure of cities and their growth and needs. The findings

can provide information for social, political, and economic decision-making for human development activities.

Second, the algorithm developed for this study is a robust multi-use, multi-purpose and multi-target tool which can be employed in various fields that use images as input data. The advanced, modern techniques used in this algorithm can also broaden knowledge regarding implementing essential operations for handling data, such as object detection, segmentation, extraction, data analysis, and morphological operations. In addition, the fully automated algorithm presented in the current study should be considered for numerous applications due to its cost-effective, timely, and safe design and its increased productivity. Its different uses and applications offer opportunities for developers and researchers to further development and innovations in the field of automation.

Third, the study improves the current understanding of the most suitable building surfaces for the optimal spatial distribution of renewable energy (e.g. solar PV installations) and makes accurate estimations for solar energy potential by exploiting the entire building envelope (roofs and facades). Spatial variation of solar energy is crucial for the estimation of area potential and the selection of construction locations (Sun, 2013). Overall, the study contributes towards an increased effort to reduce global  $CO_2$  emissions and boost power supplies for the sustainable development of natural resources, human society, and economic development in developing countries.

## 7.4 Recommendations for future research

The study could be extended in the two main directions of research. First, research could be conducted on work improvements and opportunities. Second, research could be conducted to develop a tool for solar energy potential assessments on the building envelopes using the created 3D building models. Future work can expand on the present methodology to enhance the accuracy of the outputs. To this end, the following research opportunities can be investigated:

- A future study investigating the shape of the building footprints would be very useful. More realistic in the representation of the envelope of the building can improve the findings of the assessment process. Tests could be planned to determine various shapes in addition to rectangles and ellipses. Shape parameters for defining the existing complex

shapes of the detected building footprints in the image space can be explored using the developed shape-fitting functions and new mathematical equations.

- Further research should focus on overcoming or at least to mitigating the limitations of the developed algorithm. These limitations include: (1) the visibility of shadow regions in the dense urban areas; (2) the estimation of different height levels in the topology of the buildings roofs; (3) the similar spectral characteristics between building surfaces and the surfaces of other urban objects (this issue also appears within a building when the building roof and one of its facades exhibit similar spectral reflectance, which in turn influences the overall performance of the building footprints detection); and (4) the sharp corners created in 3D building models.
- The impacts of the topography of the terrain on the actual length of building shadow regions would be a fruitful area for further work. Uneven terrain or slopes may cause an increase or decrease in the true length of the shadows cast by buildings. In this case, an investigation of the actual length of the shadow region is required. Integrating another remote sensing data source, such as digital surface models (DSM and/or DEM), may help with terrain difference recognition and assist in making necessary corrections.
- Future research could also be dedicated to investigating the impact of the 3D building model in the LOD1 on the outcomes of a given case study that uses estimated shadows as an input. For example, the evaluation of errors that can be occurred in the estimation of the loss of the solar potential in kWh/year due to shadows or in the forecasting of the duration a facade is shaded during the day.

The second direction future research could take is in the assessment of solar energy potential at the building scale. The assessment of local PV potential could be achieved based on the calculation of the annual cumulative solar radiation values for every surface (rooftops and walls) using climate data and 3D building models. Because the created 3D building models are in a mesh-grid form, the framework of future research should trace the rays from the sun to the building surfaces. This new framework could be implemented in the evaluation of solar building envelopes, leading the way to establishing and developing an assessment tool which enables users (e.g. planners, designers, researchers and decision-makers) to estimate the received amount of direct solar radiation on building surfaces suitable for PV installations. The assessment tool is already in the process of being built and will be coded using MATLAB for the calculation of solar irradiation value. The developed script will be recoded in Python to simulate

the sun's daily movements on its path and to visualise the whole computation process of the solar energy potential assessment. The assessment tool will automatically be implemented based on the created 3D building models and the inputs of latitude, longitude, day, and hour of a specific time of the year. A graphical user interface (GUI) will also be created to control the script inputs for assessing solar building surfaces on a given day of the year by the user. It is anticipated that the outputs of the assessment process will be the computed values of the Direct Normal Irradiance (DNI) on the building envelopes (mean values of irradiance in each triangle of the 3D building model). The developed work will also comprise the numerical and visual representation of the solar assessment tool results (Figure 7.1). Once the assessment tool is completed, it can help in ensuring the algorithm to be widely adopted.

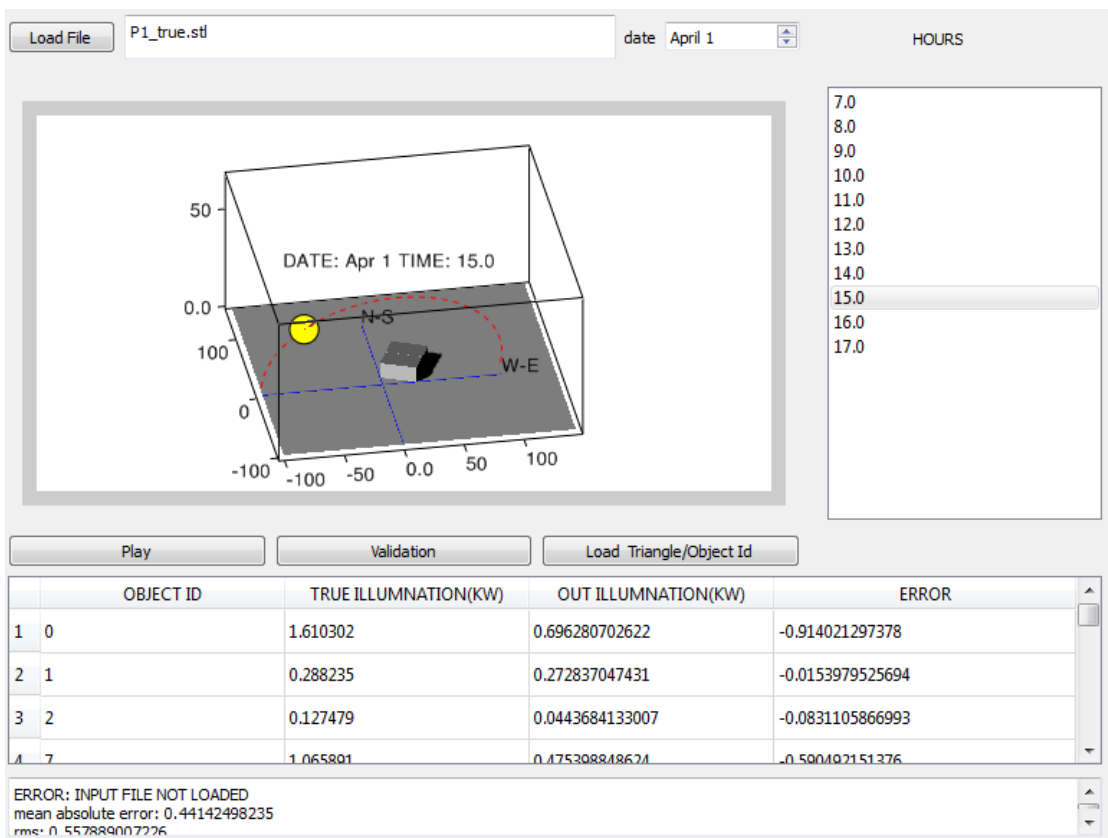


**Figure 7.1:** Proposed future work —a solar assessment tool

It is expected that this research, once complete, will evaluate the suitability of both the building roofs and facades for PV applications during daylight hours. In addition, this approach may provide insight into the value of isolating building surfaces (solar building envelope) and into the area and direction of the building shadow region, which is useful for urban spatial analysis. Facades in optimal positions relative to the sun can provide a suitable area for PV application in the modern urban landscape [153]. Furthermore, it is anticipated that the results of

solar energy potential assessments using the created 3D building models can offer a better understanding of which building types and locations receive more solar radiation in complex urban environments. The results can be exploited for the development of solar energy policies and urban planning. Therefore, the proposed future approach can be seen as an exploratory calculation of solar potential at the municipal level.

# References

- [1] Anish Turlapaty, Balakrishna Gokaraju, Qian Du, Nicolas H Younan, and James V Aanstoos. A hybrid approach for building extraction from spaceborne multi-angular optical imagery. *IEEE Journal of Selected Topics in Applied Earth Observations and Remote Sensing*, 5(1):89–100, 2012.
- [2] Mevlut Uyan. GIS-based solar farms site selection using analytic hierarchy process (AHP) in Karapınar region, Konya/Turkey. *Renewable and Sustainable Energy Reviews*, 28:11–17, 2013.
- [3] LK Wiginton, Ha T Nguyen, and Joshua M Pearce. Quantifying rooftop solar photovoltaic potential for regional renewable energy policy. *Computers, Environment and Urban Systems*, 34(4):345–357, 2010.
- [4] Lynne Eagle, Mark Hamann, and David R. Low. The role of social marketing, marine turtles and sustainable tourism in reducing plastic pollution. *Marine Pollution Bulletin*, 107(1):324–332, 2016. ISSN 0025-326X.
- [5] Mohamed Ibrahim Mohamed Ibrahim. Estimating the sustainability returns of recycling construction waste from building projects. *Sustainable Cities and Society*, 23:78–93, 2016. ISSN 2210-6707.
- [6] Zhaohua Wang, Lin Yang, Jianhua Yin, and Bin Zhang. Assessment and prediction of environmental sustainability in China based on a modified ecological footprint model. *Resources, Conservation and Recycling*, 2017. ISSN 0921-3449.
- [7] Chenchen He, Qi Han, Bauke de Vries, Xiaoming Wang, and Zhao Guochao. Evaluation of sustainable land management in urban area: A case study of Shanghai, China. *Ecological Indicators*, 80:106–113, 2017. ISSN 1470-160X.
- [8] Christoph Helbig, Christoph Kolotzek, Andrea Thorenz, Armin Reller, Axel Tuma, Mario Schafnitzel, and Stephan Krohns. Benefits of resource strategy for sustainable materials research and development. *Sustainable Materials and Technologies*, 12:1–8, 2017. ISSN 2214-9937.
- [9] Tobias Leichtle, Christian Geiß, Michael Wurm, Tobia Lakes, and Hannes Taubenböck. Unsupervised change detection in VHR remote sensing imagery—an object-based clustering approach in a dynamic urban environment. *International Journal of Applied Earth Observation and Geoinformation*, 54:15–27, 2017.
- [10] Marcel Lancelle and Dieter W Fellner. Current issues on 3D city models. *Proc. Image and Vision Computing*, pages 363–369, 2004.
- [11] Roland Billen, Anne-Françoise Cutting-Decelle, Ognen Marina, José-Paulo de Almeida, Matteo Caglioni, Gilles Falquet, Thomas Leduc, Claudine Métral, Guillaume Moreau, Julien Perret, et al. *3D City Models and urban information: Current issues and perspectives*. EDP sciences, 2014.

- [12] Jiaojiao Tian and Peter Reinartz. Fusion of multi-spectral bands and DSM from WorldView-2 stereo imagery for building extraction. In *Joint Urban Remote Sensing Event*, pages 135–138. IEEE, 2013.
- [13] Devrim Akca, Armin Gruen, Mark Freeman, and Isabel Sargent. Fast quality control of 3D city models. In *The International LIDAR Mapping Forum, New Orleans, Louisiana, US, January*, pages 26–28, 2009.
- [14] Cristian Rossi and Stefan Gernhardt. Urban dem generation, analysis and enhancements using tandem-x. *ISPRS journal of photogrammetry and remote sensing*, 85:120–131, 2013.
- [15] Taeyoon Lee and Taejung Kim. Automatic building height extraction by volumetric shadow analysis of monoscopic imagery. *International journal of remote sensing*, 34(16):5834–5850, 2013.
- [16] Feng Qi, John Z Zhai, and Gaihong Dang. Building height estimation using google earth. *Energy and Buildings*, 118:123–132, 2016.
- [17] Mohammad Izadi and Parvaneh Saeedi. Three-dimensional polygonal building model estimation from single satellite images. *IEEE Transactions on Geoscience and Remote Sensing*, 50(6):2254–2272, 2012.
- [18] Bin Wu, Xian Sun, Qichang Wu, Menglong Yan, Hongqi Wang, and Kun Fu. Building reconstruction from high-resolution multiview aerial imagery. *IEEE Geoscience and Remote Sensing Letters*, 12(4):855–859, 2015.
- [19] Ali Ozgun Ok. Automated detection of buildings from single VHR multispectral images using shadow information and graph cuts. *ISPRS journal of photogrammetry and remote sensing*, 86:21–40, 2013.
- [20] Mustafa Teke, Emre Bāseski, Ali Özgün Ok, Barış Yüksel, and Çāğlar Şenaras. Multi-spectral false color shadow detection. In *Photogrammetric Image Analysis*, pages 109–119. Springer, 2011.
- [21] Abdelkader ElGarouani, Abdalla Alobeid, and Said El Garouani. Digital surface model based on aerial image stereo pairs for 3D building. *International Journal of Sustainable Built Environment*, 3(1):119–126, 2014. ISSN 2212-6090.
- [22] Yan-wei Sun, Angela Hof, Run Wang, Jian Liu, Yan-jie Lin, and De-wei Yang. GIS-based approach for potential analysis of solar PV generation at the regional scale: A case study of fujian province. *Energy Policy*, 58:248–259, 2013.
- [23] Luca Bergamasco and Pietro Asinari. Scalable methodology for the photovoltaic solar energy potential assessment based on available roof surface area: further improvements by ortho-image analysis and application to Turin (Italy). *Solar Energy*, 85(11):2741–2756, 2011.
- [24] Ben Thompson. The Iraq power report 2011. Technical report, MEED, Middle East Economic Digest, 2011.
- [25] Qihao Weng. *Remote Sensing for Sustainability*. CRC Press, 2016.
- [26] Li Ko, Jen-Chun Wang, Chia-Yon Chen, and Hsing-Yeh Tsai. Evaluation of the development potential of rooftop solar photovoltaic in Taiwan. *Renewable Energy*, 76:582–595, 2015.

- [27] World Resources Institute WRI. CAIT climate data explorer, 2015. [Online; Accessed: 17-January-2017].
- [28] Monjur Mourshed. Climatic parameters for building energy applications: A temporal-geospatial assessment of temperature indicators. *Renewable Energy*, 94:55–71, 2016.
- [29] Basudeb Bhatta. *Analysis of urban growth and sprawl from remote sensing data*. Springer Science & Business Media, 2010.
- [30] United Nations. World urbanization prospects: the 2014 revision. Technical report, Pop. Division, Department of Economic and Social Affairs, UN, New York, 2014.
- [31] Richard A Easterlin, Laura Angelescu, and Jacqueline S Zweig. The impact of modern economic growth on urban–rural differences in subjective well-being. *World development*, 39(12):2187–2198, 2011.
- [32] Wei-wu Wang, Li-zhong Zhu, Ren-chao Wang, and Yong-jun Shi. Analysis on the spatial distribution variation characteristic of urban heat environmental quality and its mechanism. *Chinese Geographical Science*, 13(1):39–47, 2003.
- [33] Hendrik Merbitz, M Buttstädt, Sabrina Michael, Wolfgang Dott, and Christoph Schneider. GIS-based identification of spatial variables enhancing heat and poor air quality in urban areas. *Applied Geography*, 33:94–106, 2012.
- [34] Chao Wang, Qiming Liu, Na Ying, Xianhua Wang, and Jinji Ma. Air quality evaluation on an urban scale based on modis satellite images. *Atmospheric Research*, 132:22–34, 2013.
- [35] Laura E. Jackson. The relationship of urban design to human health and condition. *Landscape and Urban Planning*, 64(4):191–200, 2003. ISSN 0169-2046.
- [36] Jorge E. Patino and Juan C. Duque. A review of regional science applications of satellite remote sensing in urban settings. *Computers, Environment and Urban Systems*, 37: 1–17, 2013. ISSN 0198-9715.
- [37] Jeff Masek, FE Lindsay, and SN Goward. Dynamics of urban growth in the Washington DC metropolitan area, 1973–1996, from Landsat observations. *International Journal of Remote Sensing*, 21(18):3473–3486, 2000.
- [38] Paul A Longley. Geographical information systems: will developments in urban remote sensing and GIS lead to betterurban geography? *Progress in Human Geography*, 26(2): 231–239, 2002.
- [39] Raed Fawzi Mohammed Ameen, Monjur Mourshed, and Haijiang Li. A critical review of environmental assessment tools for sustainable urban design. *Environmental Impact Assessment Review*, 55:110–125, 2015. ISSN 0195-9255.
- [40] Samantha Lavender and Andrew Lavender. *Practical handbook of remote sensing*. CRC Press, 2015.
- [41] Sabins Jr. and Kamlesh Lulla. *Remote sensing: Principles and interpretation*. Taylor & Francis, 1987.
- [42] Paul J Curran et al. *Principles of remote sensing*. Longman Inc., 1985.

- [43] Sam J Purkis and Victor V Klemas. *Remote sensing and global environmental change*. John Wiley & Sons, 2011.
- [44] John R Jensen. *Remote sensing of the environment: An earth resource perspective 2/e*. Pearson Education India, 2009.
- [45] Basudeb Bhatta. *Analysis of urban growth and sprawl from remote sensing data*. Springer Science & Business Media, 2010.
- [46] Basudeb Bhatta, S. Saraswati, and D. Bandyopadhyay. Urban sprawl measurement from remote sensing data. *Applied Geography*, 30(4):731–740, 2010. ISSN 0143-6228. Climate Change and Applied Geography Place, Policy, and Practice.
- [47] Shima Hamidi and Reid Ewing. A longitudinal study of changes in urban sprawl between 2000 and 2010 in the united states. *Landscape and Urban Planning*, 128:72–82, 2014. ISSN 0169-2046.
- [48] Mark A Friedl, Douglas K McIver, John CF Hodges, XY Zhang, D Muchoney, Alan H Strahler, Curtis E Woodcock, Sucharita Gopal, Annemarie Schneider, Amanda Cooper, et al. Global land cover mapping from modis: algorithms and early results. *Remote Sensing of Environment*, 83(12):287–302, 2002. ISSN 0034-4257.
- [49] Kasper Cockx, Tim VandeVoorde, and Frank Canters. Quantifying uncertainty in remote sensing-based urban land-use mapping. *International Journal of Applied Earth Observation and Geoinformation*, 31:154 – 166, 2014. ISSN 0303-2434.
- [50] Tim VandeVoorde, Wolfgang Jacquet, and Frank Canters. Mapping form and function in urban areas: An approach based on urban metrics and continuous impervious surface data. *Landscape and Urban Planning*, 102(3):143 – 155, 2011. ISSN 0169-2046.
- [51] Christiane Weber and Anne Puissant. Urbanization pressure and modeling of urban growth: example of the Tunis metropolitan area. *Remote sensing of environment*, 86(3): 341–352, 2003.
- [52] George Xian and Mike Crane. Assessments of urban growth in the tampa bay watershed using remote sensing data. *Remote Sensing of Environment*, 97(2):203–215, 2005.
- [53] Fei Yuan, Kali E Sawaya, Brian C Loeffelholz, and Marvin E Bauer. Land cover classification and change analysis of the twin cities (Minnesota) metropolitan area by multitemporal landsat remote sensing. *Remote sensing of Environment*, 98(2):317–328, 2005.
- [54] Dengsheng Lu and Qihao Weng. Use of impervious surface in urban land-use classification. *Remote Sensing of Environment*, 102(1):146–160, 2006.
- [55] Jieying Xiao, Yanjun Shen, Jingfeng Ge, Ryutaro Tateishi, Changyuan Tang, Yan-qing Liang, and Zhiying Huang. Evaluating urban expansion and land use change in Shijiazhuang, China, by using GIS and remote sensing. *Landscape and urban planning*, 75(1):69–80, 2006.
- [56] Ashraf M Dewan and Yasushi Yamaguchi. Land use and land cover change in greater Dhaka, Bangladesh: Using remote sensing to promote sustainable urbanization. *Applied Geography*, 29(3):390–401, 2009.

- [57] Kunwar K Singh, John B Vogler, Douglas A Shoemaker, and Ross K Meentemeyer. Lidar-landsat data fusion for large-area assessment of urban land cover: Balancing spatial resolution, data volume and mapping accuracy. *ISPRS Journal of Photogrammetry and Remote Sensing*, 74:110–121, 2012.
- [58] Lorenzo Fusilli, Pablo Marzialetti, Giovanni Laneve, and Giancarlo Santilli. Urban growth assessment around winam gulf of Kenya based on satellite imagery. *Acta Astronautica*, 93:279–290, 2014.
- [59] Xi Jun Yu and Cho Nam Ng. Spatial and temporal dynamics of urban sprawl along two urban–rural transects: A case study of Guangzhou, China. *Landscape and Urban Planning*, 79(1):96–109, 2007.
- [60] Mahesh Kumar Jat, P K Garg, and Deepak Khare. Monitoring and modelling of urban sprawl using remote sensing and GIS techniques. *International Journal of Applied earth Observation and Geoinformation*, 10(1):26–43, 2008.
- [61] Anne Jacquin, Lucie Misakova, and Michel Gay. A hybrid object-based classification approach for mapping urban sprawl in periurban environment. *Landscape and urban planning*, 84(2):152–165, 2008.
- [62] Basudeb Bhatta, S Saraswati, and D Bandyopadhyay. Quantifying the degree-of-freedom, degree-of-sprawl, and degree-of-goodness of urban growth from remote sensing data. *Applied Geography*, 30(1):96–111, 2010.
- [63] Patrick Leinenkugel, Thomas Esch, and Claudia Kuenzer. Settlement detection and impervious surface estimation in the mekong delta using optical and sar remote sensing data. *Remote Sensing of Environment*, 115(12):3007–3019, 2011.
- [64] Uta Heiden, Wieke Heldens, Sigrid Roessner, Karl Segl, Thomas Esch, and Andreas Mueller. Urban structure type characterization using hyperspectral remote sensing and height information. *Landscape and urban Planning*, 105(4):361–375, 2012.
- [65] Xiaojun Yang and Zhi Liu. Use of satellite-derived landscape imperviousness index to characterize urban spatial growth. *Computers, Environment and Urban Systems*, 29(5):524–540, 2005.
- [66] Wei Ji, Jia Ma, Rima Wahab Twibell, and Karen Underhill. Characterizing urban sprawl using multi-stage remote sensing images and landscape metrics. *Computers, Environment and Urban Systems*, 30(6):861–879, 2006.
- [67] Du Peijun, Li Xingli, Cao Wen, Luo Yan, and Huapeng Zhang. Monitoring urban land cover and vegetation change by multi-temporal remote sensing information. *Mining Science and Technology (China)*, 20(6):922–932, 2010.
- [68] Hannes Taubenböck, Martin Wegmann, Achim Roth, Harald Mehl, and Stefan Dech. Urbanization in india–spatiotemporal analysis using remote sensing data. *Computers, Environment and Urban Systems*, 33(3):179–188, 2009.
- [69] OR Abd El-Kawy, JK Rød, HA Ismail, and AS Suliman. Land use and land cover change detection in the western Nile Delta of Egypt using remote sensing data. *Applied Geography*, 31(2):483–494, 2011.
- [70] Hai Minh Pham, Yasushi Yamaguchi, and Thanh Quang Bui. A case study on the relation between city planning and urban growth using remote sensing and spatial metrics. *Landscape and Urban Planning*, 100(3):223–230, 2011.

- [71] Annemarie Schneider. Monitoring land cover change in urban and peri-urban areas using dense time stacks of landsat satellite data and a data mining approach. *Remote Sensing of Environment*, 124:689–704, 2012.
- [72] Kun Jia, Shunlin Liang, Ning Zhang, Xiangqin Wei, Xingfa Gu, Xiang Zhao, Yunjun Yao, and Xianhong Xie. Land cover classification of finer resolution remote sensing data integrating temporal features from time series coarser resolution data. *ISPRS Journal of Photogrammetry and Remote Sensing*, 93:49–55, 2014.
- [73] Sebastian Martinuzzi, William A Gould, and Olga M Ramos Gonzalez. Land development, land use, and urban sprawl in Puerto Rico integrating remote sensing and population census data. *Landscape and Urban Planning*, 79(3):288–297, 2007.
- [74] Norzailawati Mohd Noor and Nur Aulia Rosni. Determination of spatial factors in measuring urban sprawl in Kuantan using remote sensing and GIS. *Procedia-Social and Behavioral Sciences*, 85:502–512, 2013.
- [75] Ahmed K Nassar, G Alan Blackburn, and J Duncan Whyatt. Developing the desert: The pace and process of urban growth in Dubai. *Computers, Environment and Urban Systems*, 45:50–62, 2014.
- [76] Monika Kuffer and Joana Barroso. Urban morphology of unplanned settlements: the use of spatial metrics in VHR remotely sensed images. *Procedia Environmental Sciences*, 7:152–157, 2011.
- [77] NASA. Satellite maps provide better urban sprawl insight. Technical report, National Aeronautics and Space Administration, USA, 2001.
- [78] Karen K Owen and David W Wong. An approach to differentiate informal settlements using spectral, texture, geomorphology and road accessibility metrics. *Applied Geography*, 38:107–118, 2013.
- [79] Hassan Rhinane, Atika Hilali, Aziza Berrada, Mustapha Hakdaoui, et al. Detecting slums from spot data in Casablanca Morocco using an object based approach. *Journal of Geographic Information System*, 3(03):217, 2011.
- [80] Karolien Vermeiren, Anton Van Rompaey, Maarten Loopmans, Eria Serwajja, and Paul Mukwaya. Urban growth of Kampala, Uganda: Pattern analysis and scenario development. *Landscape and Urban Planning*, 106(2):199–206, 2012.
- [81] Oleksandr Kit, Matthias Lüdeke, and Diana Reckien. Texture-based identification of urban slums in Hyderabad, India using remote sensing data. *Applied Geography*, 32 (2):660–667, 2012.
- [82] Divyani Kohli, Richard Sliuzas, Norman Kerle, and Alfred Stein. An ontology of slums for image-based classification. *Computers, Environment and Urban Systems*, 36(2):154–163, 2012.
- [83] Oleksandr Kit and Matthias Lüdeke. Automated detection of slum area change in Hyderabad, India using multitemporal satellite imagery. *ISPRS journal of photogrammetry and remote sensing*, 83:130–137, 2013.
- [84] Hannes Taubenböck and NJ Kraff. The physical face of slums: a structural comparison of slums in Mumbai, India, based on remotely sensed data. *Journal of Housing and the Built Environment*, 29(1):15–38, 2014.

- [85] Jordan Graesser, Anil Cheriyadat, Ranga Raju Vatsavai, Varun Chandola, Jordan Long, and Eddie Bright. Image based characterization of formal and informal neighborhoods in an urban landscape. *IEEE Journal of Selected Topics in Applied Earth Observations and Remote Sensing*, 5(4):1164–1176, 2012.
- [86] John R Weeks, Allan Hill, Douglas Stow, Arthur Getis, and Debbie Fugate. Can we spot a neighborhood from the air? Defining neighborhood structure in Accra, Ghana. *GeoJournal*, 69(1-2):9–22, 2007.
- [87] Michael Hagenlocher, Stefan Lang, and Dirk Tiede. Integrated assessment of the environmental impact of an idp camp in sudan based on very high resolution multi-temporal satellite imagery. *Remote Sensing of Environment*, 126:27–38, 2012.
- [88] Qihao Weng, Hua Liu, and Dengsheng Lu. Assessing the effects of land use and land cover patterns on thermal conditions using landscape metrics in city of Indianapolis, united states. *Urban ecosystems*, 10(2):203–219, 2007.
- [89] Bhatta Basudeb. Analysis of urban growth and sprawl from remote sensing data. *Advances in Geographic Information Science*, page 23, 2010.
- [90] Cheng-Fan Li and Jing-Yuan Yin. A study on urban thermal field of Shanghai using multi-source remote sensing data. *Journal of the Indian Society of Remote Sensing*, 41(4):1009–1019, 2013.
- [91] Indishe Prabath Senanayake, WDDP Welivitiya, and Parana Manage Nadeeka. Remote sensing based analysis of urban heat islands with vegetation cover in colombo city, Sri Lanka using landsat-7 etm+ data. *Urban Climate*, 5:19–35, 2013.
- [92] QIAN Le-Xiang, CUI Hai-Shan, and Jie Chang. Impacts of land use and cover change on land surface temperature in the Zhujiang delta11project supported by the science and technology project foundation of Guangzhou (no. 2005z3-d0551) and the science and technology project foundation of Guangzhou Education Bureau (no. 62026). *Pedosphere*, 16(6):681–689, 2006.
- [93] Koen De Ridder, Filip Lefebvre, Stefan Adriaensen, Ute Arnold, Wolfgang Beckroegge, Christine Bronner, Ole Damsgaard, Ivo Dostal, Jiri Dufek, Jacky Hirsch, et al. Simulating the impact of urban sprawl on air quality and population exposure in the German Ruhr area. part i: Reproducing the base state. *Atmospheric environment*, 42(30):7059–7069, 2008.
- [94] Matthew J Bechle, Dylan B Millet, and Julian D Marshall. Remote sensing of exposure to no 2: satellite versus ground-based measurement in a large urban area. *Atmospheric Environment*, 69:345–353, 2013.
- [95] Janet E Nichol, Man Sing Wong, and Jingzhi Wang. A 3D aerosol and visibility information system for urban areas using remote sensing and GIS. *Atmospheric Environment*, 44(21):2501–2506, 2010.
- [96] Nicolas I Sifakis, Christos Iossifidis, and Charis Kontoes. Christine code for high resolution satellite mapping of optical thickness and ångstrom exponent. part ii: First application to the urban area of Athens, Greece and comparison to results from previous contrast-reduction codes. *Computers & Geosciences*, 62:142–149, 2014.

- [97] Mary Chawira, Timothy Dube, and Webster Gumindoga. Remote sensing based water quality monitoring in Chivero and Manyame lakes of Zimbabwe. *Physics and Chemistry of the Earth, Parts A/B/C*, 66:38–44, 2013.
- [98] Sylvain Jay and Mireille Guillaume. A novel maximum likelihood based method for mapping depth and water quality from hyperspectral remote-sensing data. *Remote Sensing of Environment*, 147:121–132, 2014.
- [99] John T Trochta, Colleen B Mouw, and Timothy S Moore. Remote sensing of physical cycles in lake superior using a spatio-temporal analysis of optical water typologies. *Remote Sensing of Environment*, 171:149–161, 2015.
- [100] Johannes E Hunink, Sergio Contreras, Mariano Soto-García, Bernardo Martin-Gorriz, Victoriano Martinez-Álvarez, and Alain Baille. Estimating groundwater use patterns of perennial and seasonal crops in a mediterranean irrigation scheme, using remote sensing. *Agricultural Water Management*, 162:47–56, 2015.
- [101] Oluwole Soyinka, Kin Wai Michael Siu, Taibat Lawanson, and Olufemi Adeniji. Assessing smart infrastructure for sustainable urban development in the Lagos metropolis. *Journal of Urban Management*, 5(2):52–64, 2016. ISSN 2226-5856.
- [102] Giles M Foody. Remote sensing of tropical forest environments: towards the monitoring of environmental resources for sustainable development. *International journal of remote sensing*, 24(20):4035–4046, 2003.
- [103] Qihao Weng and Shihong Yang. An approach to evaluation of sustainability for guangzhou’s urban ecosystem. *The International Journal of Sustainable Development & World Ecology*, 10(1):69–81, 2003.
- [104] Qihao Weng. *Scale Issues in Remote Sensing*. John Wiley & Sons, 2014.
- [105] Monjur Mourshed, Sylvain Robert, Andrea Ranalli, Thomas Messervey, Diego Reforgiato, Régis Contreau, Adrien Becue, Kevin Quinn, Yacine Rezgui, and Zia Lennard. Smart grid futures: Perspectives on the integration of energy and ICT services. *Energy Procedia*, 75:1132–1137, 2015.
- [106] Kirby Calvert, Joshua M Pearce, and WE Mabee. Toward renewable energy geo-information infrastructures: Applications of GIScience and remote sensing that build institutional capacity. *Renewable and Sustainable Energy Reviews*, 18:416–429, 2013.
- [107] James Gooding, Holly Edwards, Jannik Gieseckam, and Rolf Crook. Solar city indicator: A methodology to predict city level PV installed capacity by combining physical capacity and socio-economic factors. *Solar Energy*, 95:325–335, 2013.
- [108] J Alstan Jakubiec and Christoph F Reinhart. A method for predicting city-wide electricity gains from photovoltaic panels based on lidar and GIS data combined with hourly daysim simulations. *Solar Energy*, 93:127–143, 2013.
- [109] Mohammed Humayun Kabir, Wilfried Endlicher, and Jonas Jägermeyr. Calculation of bright roof-tops for solar PV applications in Dhaka Megacity, Bangladesh. *Renewable Energy*, 35(8):1760–1764, 2010.
- [110] Shifeng Wang and Barbara Koch. Determining profits for solar energy with remote sensing data. *Energy*, 35(7):2934–2938, 2010.

- [111] Hayk Baluyan, Bikash Joshi, Amer Al Hinai, and Wei Lee Woon. Novel approach for rooftop detection using support vector machine. *ISRN Machine Vision*, 2013, 2013.
- [112] Dong Jiang, Dafang Zhuang, Yaohuan Huang, Jianhua Wang, and Jingying Fu. Evaluating the spatio-temporal variation of china's offshore wind resources based on remotely sensed wind field data. *Renewable and Sustainable Energy Reviews*, 24:142–148, 2013.
- [113] Jenell M Walsh-Thomas, Guido Cervone, Peggy Agouris, and Germana Manca. Further evidence of impacts of large-scale wind farms on land surface temperature. *Renewable and Sustainable Energy Reviews*, 16(8):6432–6437, 2012.
- [114] Freek van der Meer, Christoph Hecker, Frank van Ruitenbeek, Harald van der Werff, Charlotte de Wijkerslooth, and Carolina Wechsler. Geologic remote sensing for geo-thermal exploration: A review. *International Journal of Applied Earth Observation and Geoinformation*, 33:255–269, 2014.
- [115] Tofael Ahamed, L Tian, Y Zhang, and KC Ting. A review of remote sensing methods for biomass feedstock production. *Biomass and Bioenergy*, 35(7):2455–2469, 2011.
- [116] Eugen Rusu and Florin Onea. Evaluation of the wind and wave energy along the Caspian Sea. *Energy*, 50:1–14, 2013.
- [117] Mona F. Kaiser and Salah Ahmed. Optimal thermal water locations along the Gulf of Suez coastal zones, Egypt. *Renewable energy*, 55:374–379, 2013.
- [118] Thomas Esch, Markus Tum, and Annekatrin Metz. Earth observation and its potential to implement a sustainable energy supply—a German perspective, 2016.
- [119] Monjur Mourshed, Antonio Buccharone, and Fahmida Khandokar. Smart: A process-oriented methodology for resilient smart cities. In *Smart Cities Conference (ISC2), 2016 IEEE International*, pages 1–6. IEEE, 2016.
- [120] Brian Stone and John M Norman. Land use planning and surface heat island formation: A parcel-based radiation flux approach. *Atmospheric Environment*, 40(19):3561–3573, 2006.
- [121] Christian Geiß, Patrick Aravena Pelizari, Mattia Marconcini, Wayan Sengara, Mark Edwards, Tobia Lakes, and Hannes Taubenböck. Estimation of seismic building structural types using multi-sensor remote sensing and machine learning techniques. *ISPRS Journal of Photogrammetry and Remote Sensing*, 104:175–188, 2015.
- [122] Chen Wu, Lefei Zhang, and Liangpei Zhang. A scene change detection framework for multi-temporal very high resolution remote sensing images. *Signal Processing*, 124: 184–197, 2016.
- [123] Puzhao Zhang, Maoguo Gong, Linzhi Su, Jia Liu, and Zhizhou Li. Change detection based on deep feature representation and mapping transformation for multi-spatial-resolution remote sensing images. *ISPRS Journal of Photogrammetry and Remote Sensing*, 116:24–41, 2016.
- [124] Peijun Du, Kun Tan, and Xiaoshi Xing. A novel binary tree support vector machine for hyperspectral remote sensing image classification. *Optics Communications*, 285(13): 3054–3060, 2012.

- [125] Amir Reza Shahtahmassebi, Jie Song, Qing Zheng, George Alan Blackburn, Ke Wang, Ling Yan Huang, Yi Pan, Nathan Moore, Golnaz Shahtahmassebi, Reza Sadrabadi Haghghi, et al. Remote sensing of impervious surface growth: A framework for quantifying urban expansion and re-densification mechanisms. *International Journal of Applied Earth Observation and Geoinformation*, 46:94–112, 2016.
- [126] Sanaz Imen, Ni-Bin Chang, and Y Jeffrey Yang. Developing the remote sensing-based early warning system for monitoring TSS concentrations in Lake Mead. *Journal of environmental management*, 160:73–89, 2015.
- [127] Yanhua Xie, Anthea Weng, and Qihao Weng. Population estimation of urban residential communities using remotely sensed morphologic data. *IEEE Geoscience and Remote Sensing Letters*, 12(5):1111–1115, 2015.
- [128] Hongsheng Zhang and Hui Lin. Feature selection for urban impervious surfaces estimation using optical and sar images. In *Urban Remote Sensing Event (JURSE), 2015 Joint*, pages 1–4. IEEE, 2015.
- [129] Stefaniaand Bonafoni, Giorgio Baldinelli, and Paolo Verducci. Sustainable strategies for smart cities: Analysis of the town development effect on surface urban heat island through remote sensing methodologies. *Sustainable Cities and Society*, 29(Supplement C):211 – 218, 2017. ISSN 2210-6707.
- [130] Paul M Mather and Magaly Koch. *Computer processing of remotely-sensed images: an introduction*. John Wiley & Sons, 2011.
- [131] Anne Grote, Christian Heipke, and Franz Rottensteiner. Road network extraction in suburban areas. *The Photogrammetric Record*, 27(137):8–28, 2012.
- [132] Mengmeng Li, Alfred Stein, Wietske Bijker, and Qingming Zhan. Region-based urban road extraction from {VHR} satellite images using binary partition tree. *International Journal of Applied Earth Observation and Geoinformation*, 44:217–225, 2016. ISSN 0303-2434.
- [133] Örsan Aytekin and İlkay Ulusoy. Automatic segmentation of VHR images using type information of local structures acquired by mathematical morphology. *Pattern Recognition Letters*, 32(13):1618–1625, 2011.
- [134] Dan Assouline, Nahid Mohajeri, and Jean-Louis Scartezzini. Quantifying rooftop photovoltaic solar energy potential: A machine learning approach. *Solar Energy*, 141 (Supplement C):278 – 296, 2017. ISSN 0038-092X.
- [135] Alessia Movia, Alberto Beinat, and Fabio Crosilla. Shadow detection and removal in RGB VHR images for land use unsupervised classification. *ISPRS Journal of Photogrammetry and Remote Sensing*, 119:485–495, 2016. ISSN 0924-2716.
- [136] Jiebo Luo, D Ming, W Liu, Z Shen, M Wang, and H Sheng. Extraction of bridges over water from ikonos panchromatic data. *International Journal of Remote Sensing*, 28(16): 3633–3648, 2007.
- [137] Dipta Chaudhuri and Ashok Samal. An automatic bridge detection technique for multispectral images. *IEEE transactions on geoscience and remote sensing*, 46(9):2720–2727, 2008.

- [138] Juan P. Ardila, Wietske Bijker, Valentyn A. Tolpekin, and Alfred Stein. Context-sensitive extraction of tree crown objects in urban areas using VHR satellite images. *International Journal of Applied Earth Observation and Geoinformation*, 15:57–69, 2012. ISSN 0303-2434.
- [139] Simon Rougier, Anne Puissant, Andr Stumpf, and Nicolas Lachiche. Comparison of sampling strategies for object-based classification of urban vegetation from very high resolution satellite images. *International Journal of Applied Earth Observation and Geoinformation*, 51:60–73, 2016. ISSN 0303-2434.
- [140] Toby N Carlson. Analysis and prediction of surface runoff in an urbanizing watershed using satellite imagery. *JAWRA Journal of the American Water Resources Association*, 40(4):1087–1098, 2004.
- [141] Christine Jacqueminet, S. Kermadi, K. Michel, D. Bal, M. Gagnage, S. Branger, F. and Jankowsky, and I. Braud. Land cover mapping using aerial and VHR satellite images for distributed hydrological modelling of periurban catchments: Application to the Yzeron catchment (Lyon, France). *Journal of Hydrology*, 485:68–83, 2013. ISSN 0022-1694.
- [142] Sébastien Lefèvre and Jonathan Weber. Automatic building extraction in VHR images using advanced morphological operators. In *Urban Remote Sensing Joint Event, 2007*, pages 1–5. IEEE, 2007.
- [143] Sérgio Freire, Teresa Santos, Ana Navarro Navarro, Fernando Soares, J.D. Silva, N. Afonso, A. Fonseca, and J. Tenedrio. Introducing mapping standards in the quality assessment of buildings extracted from very high resolution satellite imagery. *ISPRS Journal of Photogrammetry and Remote Sensing*, 90:1–9, 2014. ISSN 0924-2716.
- [144] Kwong Sang Cheng, C. Wei, and S.C. Chang. Locating landslides using multi-temporal satellite images. *Advances in Space Research*, 33(3):296 – 301, 2004. ISSN 0273-1177.
- [145] Jyoti Singhai and Paresh Rawat. Image enhancement method for underwater, ground and satellite images using brightness preserving histogram equalization with maximum entropy. In *International Conference on Computational Intelligence and Multimedia Applications (ICCIMA 2007)*, volume 3, pages 507–512, Dec 2007.
- [146] Martino Pesaresi, Andrea Gerhardinger, and François Kayitakire. A robust built-up area presence index by anisotropic rotation-invariant textural measure. *IEEE Journal of Selected Topics in Applied Earth Observations and Remote Sensing*, 1(3):180–192, Sept 2008. ISSN 1939-1404.
- [147] Yun Zhang and Rakesh K. Mishra. A review and comparison of commercially available pan-sharpening techniques for high resolution satellite image fusion. In *2012 IEEE International Geoscience and Remote Sensing Symposium*, pages 182–185, July 2012.
- [148] Richard Szeliski. *Computer vision: algorithms and applications*. Springer Science & Business Media, 2010.
- [149] Dominic Rüfenacht, Clément Fredembach, and Sabine Süsstrunk. Automatic and accurate shadow detection using near-infrared information. *IEEE transactions on pattern analysis and machine intelligence*, 36(8):1672–1678, 2014.

- [150] Ali Ozgun Ok, Caglar Senaras, and Baris Yuksel. Automated detection of arbitrarily shaped buildings in complex environments from monocular VHR optical satellite imagery. *IEEE Transactions on Geoscience and Remote Sensing*, 51(3):1701–1717, 2013.
- [151] Ali Ozgun Ok. A new approach for the extraction of aboveground circular structures from near-nadir VHR satellite imagery. *IEEE Transactions on Geoscience and Remote Sensing*, 52(6):3125–3140, 2014.
- [152] Ali Ozgun Ok. Automated extraction of buildings and roads in a graph partitioning framework. *ISPRS Annals of Photogrammetry, Remote Sensing and Spatial Information Sciences*, 1(3):79–84, 2013.
- [153] Paula Redweik, Cristina Catita, and Miguel Brito. Solar energy potential on roofs and facades in an urban landscape. *Solar Energy*, 97:332–341, 2013.
- [154] JH Jo and TP Otanicar. A hierarchical methodology for the mesoscale assessment of building integrated roof solar energy systems. *Renewable Energy*, 36(11):2992–3000, 2011.
- [155] PLN Raju, Himani Chaudhary, and AK Jha. Shadow analysis technique for extraction of building height using high resolution satellite single image and accuracy assessment. *The International Archives of Photogrammetry, Remote Sensing and Spatial Information Sciences*, 40(8):1185, 2014.
- [156] Paul M Dare. Shadow analysis in high-resolution satellite imagery of urban areas. *Photogrammetric Engineering & Remote Sensing*, 71(2):169–177, 2005.
- [157] Shwetali Wakchaure and Poorva Raut. A review of shadow detection and reconstruction in VHR images. *The International Journal of Science and Technoledge*, 2(3):9, 2014.
- [158] Haijian Ma, Qiming Qin, and Xinyi Shen. Shadow segmentation and compensation in high resolution satellite images. In *Geoscience and Remote Sensing Symposium, 2008. IGARSS 2008. IEEE International*, volume 2, pages II–1036. IEEE, 2008.
- [159] Mohamed I Elbakary and Khan M Iftekharuddin. Shadow detection of man-made buildings in high-resolution panchromatic satellite images. *IEEE Transactions on Geoscience and Remote Sensing*, 52(9):5374–5386, 2014.
- [160] Wen Liu and Fumio Yamazaki. Object-based shadow extraction and correction of high-resolution optical satellite images. *IEEE Journal of Selected Topics in Applied Earth Observations and Remote Sensing*, 5(4):1296–1302, 2012.
- [161] Huihui Song, Bo Huang, and Kaihua Zhang. Shadow detection and reconstruction in high-resolution satellite images via morphological filtering and example-based learning. *IEEE Transactions on Geoscience and Remote Sensing*, 52(5):2545–2554, 2014.
- [162] Filip Biljecki, Hugo Ledoux, Jantien Stoter, and Junqiao Zhao. Formalisation of the level of detail in 3D city modelling. *Computers, Environment and Urban Systems*, 48:1–15, 2014.
- [163] Filip Biljecki, Hugo Ledoux, and Jantien Stoter. An improved LOD specification for 3D building models. *Computers, Environment and Urban Systems*, 59:25–37, 2016.
- [164] Beril Sirmacek and Cem Unsalan. Urban-area and building detection using sift keypoints and graph theory. *IEEE Transactions on Geoscience and Remote Sensing*, 47(4):1156–1167, 2009.

- [165] Beril Sirmacek and Cem Unsalan. A probabilistic framework to detect buildings in aerial and satellite images. *IEEE Transactions on Geoscience and Remote Sensing*, 49(1):211–221, 2011.
- [166] Klaartje Verbeeck, Martin Hermy, and Jos Van Orshoven. External geo-information in the segmentation of {VHR} imagery improves the detection of imperviousness in urban neighborhoods. *International Journal of Applied Earth Observation and Geoinformation*, 18:428–435, 2012. ISSN 0303-2434.
- [167] Jun Wang, Xiucheng Yang, Xuebin Qin, Xin Ye, and Qiming Qin. An efficient approach for automatic rectangular building extraction from very high resolution optical satellite imagery. *IEEE Geoscience and Remote Sensing Letters*, 12(3):487–491, March 2015. ISSN 1545-598X.
- [168] Saman Ghaffarian and Salar Ghaffarian. Automatic building detection based on purposive fastica (pfica) algorithm using monocular high resolution Google Earth images. *ISPRS Journal of Photogrammetry and Remote Sensing*, 97:152–159, 2014. ISSN 0924-2716.
- [169] Er Li, John Femiani, Shibiao Xu, Xiaopeng Zhang, and Peter Wonka. Robust rooftop extraction from visible band images using higher order CRF. *IEEE Transactions on Geoscience and Remote Sensing*, 53(8):4483–4495, Aug 2015. ISSN 0196-2892.
- [170] Andrea Manno-Kovcs and Ali Ozgun Ok. Building detection from monocular VHR images by integrated urban area knowledge. *IEEE Geoscience and Remote Sensing Letters*, 12(10):2140–2144, Oct 2015. ISSN 1545-598X.
- [171] Ivan Tomljenovic, Dirk Tiede, and Thomas Blaschke. A building extraction approach for airborne laser scanner data utilizing the object based image analysis paradigm. *International Journal of Applied Earth Observation and Geoinformation*, 52:137–148, 2016.
- [172] Zhenyu Lu, Jungho Im, Jinyoung Rhee, and Michael Hodgson. Building type classification using spatial and landscape attributes derived from lidar remote sensing data. *Landscape and Urban Planning*, 130:134–148, 2014. ISSN 0169-2046.
- [173] Bailang Yu, Hongxing Liu, Jianping Wu, Yingjie Hu, and Li Zhang. Automated derivation of urban building density information using airborne lidar data and object-based method. *Landscape and Urban Planning*, 98(34):210 – 219, 2010. ISSN 0169-2046. Climate Change and Spatial Planning.
- [174] Rongjun Qin. Change detection on lod 2 building models with very high resolution spaceborne stereo imagery. *ISPRS Journal of Photogrammetry and Remote Sensing*, 96:179–192, 2014.
- [175] Jinhui Hu, Suya You, and U. Neumann. Approaches to large-scale urban modeling. *IEEE Computer Graphics and Applications*, 23(6):62–69, 2003.
- [176] Syed Ali Naqi Gilani, Mohammad Awrangjeb, and Guojun Lu. An automatic building extraction and regularisation technique using lidar point cloud data and orthoimage. *Remote Sensing*, 8(3):258, 2016.
- [177] Taejung Kim, Ts Javzandulam, and Tae-Yoon Lee. Semiautomatic reconstruction of building height and footprints from single satellite images. In *2007 IEEE International Geoscience and Remote Sensing Symposium*, pages 4737–4740. IEEE, 2007.

- [178] Yang Shao, Gregory N Taff, and Stephen J Walsh. Shadow detection and building-height estimation using ikonos data. *International journal of remote sensing*, 32(22):6929–6944, 2011.
- [179] Alexis Comber, Masahiro Umezaki, Rena Zhou, Yongming Ding, Yang Li, Hua Fu, Hongwei Jiang, and Andrew Tewkesbury. Using shadows in high-resolution imagery to determine building height. *Remote sensing letters*, 3(7):551–556, 2012.
- [180] Gregoris Liasis and Stavros Stavrou. Satellite images analysis for shadow detection and building height estimation. *ISPRS Journal of Photogrammetry and Remote Sensing*, 119:437–450, 2016.
- [181] John Counsell, Steve Smith, and Andrew Richman. Overcoming some of the issues in maintaining large urban area 3D models via a web browser. In *Tenth International Conference on Information Visualisation (IV'06)*, pages 331–336. IEEE, 2006.
- [182] Kiwon Lee. 3D urban modeling and rendering with high resolution remote sensing imagery on mobile 3D and web 3D environments; system architecture and prototype implementation. In *2007 Urban Remote Sensing Joint Event*, pages 1–5. IEEE, 2007.
- [183] Bardia Yousefi, Seyed Mostafa Mirhassani, MM Hosseini, and MJ Rastegar Fatemi. A novel fuzzy based method for 3D buildings modelling in urban satellite imagery. In *Open Systems (ICOS), 2011 IEEE Conference on*, pages 190–195. IEEE, 2011.
- [184] Mover Over, Arne Schilling, S Neubauer, and Alexander Zipf. Generating web-based 3D city models from OpenStreetMap: The current situation in Germany. *Computers, Environment and Urban Systems*, 34(6):496–507, 2010.
- [185] Abdelkader El Garouani, Abdalla Alobeid, and Said El Garouani. Digital surface model based on aerial image stereo pairs for 3D building. *International Journal of Sustainable Built Environment*, 3(1):119–126, 2014.
- [186] Cristina Catita, Paula Redweik, J Pereira, and Miguel Centeno Brito. Extending solar potential analysis in buildings to vertical facades. *Computers & Geosciences*, 66:1–12, 2014.
- [187] Carlos A Vanegas, Daniel G Aliaga, and Bedřich Beneš. Building reconstruction using manhattan-world grammars. In *Computer Vision and Pattern Recognition (CVPR), 2010 IEEE Conference on*, pages 358–365. IEEE, 2010.
- [188] Dong-Min Woo and Dong-Chul Park. Stereoscopic modeling of building rooftop from IKONOS satellite image data. In *Information Science and Applications (ICISA), 2011 International Conference on*, pages 1–5. IEEE, 2011.
- [189] Mathieu Brédif, Olivier Tournaire, Bruno Vallet, and Nicolas Champion. Extracting polygonal building footprints from digital surface models: a fully-automatic global optimization framework. *ISPRS journal of photogrammetry and remote sensing*, 77:57–65, 2013.
- [190] Tahmineh Partovi, Thomas Krauß, Hossein Arefi, Mohammad Omidalizarandi, and Peter Reinartz. Model-driven 3D building reconstruction based on integeration of DSM and spectral information of satellite images. In *2014 IEEE Geoscience and Remote Sensing Symposium*, pages 3168–3171. IEEE, 2014.
- [191] Jinqing Peng and Lin Lu. Investigation on the development potential of rooftop PV system in Hong Kong and its environmental benefits. *Renewable and Sustainable Energy Reviews*, 27:149–162, 2013.

- [192] Thoreau Rory Tooke, Nicholas C Coops, James A Voogt, and Michael J Meitner. Tree structure influences on rooftop-received solar radiation. *Landscape and Urban Planning*, 102(2):73–81, 2011.
- [193] Rhythm Singh and Rangan Banerjee. Estimation of rooftop solar photovoltaic potential of a city. *Solar Energy*, 115:589–602, 2015.
- [194] Philip McKeen and Alan S Fung. The effect of building aspect ratio on energy efficiency: A case study for multi-unit residential buildings in canada. *Buildings*, 4(3):336–354, 2014.
- [195] Itai Danielski, Morgan Fröling, and Anna Joellsson. The impact of the shape factor on final energy demand in residential buildings in nordic climates. In *World Renewable Energy Forum*, pages 4260–4264, 2012.
- [196] Daniel D Chiras. *The solar house: passive heating and cooling*. Chelsea Green Publishing, 2002.
- [197] Qihao Weng et al. *Remote sensing and GIS integration: theories, methods, and applications*. McGraw-Hill New York, 2010.
- [198] Yuanfan Zheng and Qihao Weng. Assessing solar energy potential and building energy use in Indianapolis using geospatial techniques. In Q. Weng, editor, *Remote sensing for sustainability*, chapter 17, pages 317–350. CRC Press, Boca Raton, 2017.
- [199] KRM Adeline, M Chen, X Briottet, SK Pang, and N Paparoditis. Shadow detection in very high spatial resolution aerial images: A comparative study. *ISPRS Journal of Photogrammetry and Remote Sensing*, 80:21–38, 2013.
- [200] Gottfried Konecny. *Geoinformation: remote sensing, photogrammetry and geographic information systems*. cRc Press, 2014.
- [201] Rendow Yee. *Architectural Drawing: A Visual Compendium of Types and Methods*. John Wiley & Sons, 2012.
- [202] Nobuyuki Otsu. A threshold selection method from gray-level histograms. *Automatica*, 11(285-296):23–27, 1975.
- [203] Carsten Rother, Vladimir Kolmogorov, and Andrew Blake. Grabcut: Interactive foreground extraction using iterated graph cuts. In *ACM transactions on graphics (TOG)*, volume 23, pages 309–314. ACM, 2004.
- [204] Tony F Chan and Luminita A Vese. Active contours without edges. *IEEE Transactions on image processing*, 10(2):266–277, 2001.
- [205] Richard H Byrd, Mary E Hribar, and Jorge Nocedal. An interior point algorithm for large-scale nonlinear programming. *SIAM Journal on Optimization*, 9(4):877–900, 1999.
- [206] Richard H Byrd, Jean Charles Gilbert, and Jorge Nocedal. A trust region method based on interior point techniques for nonlinear programming. *Mathematical Programming*, 89(1):149–185, 2000.
- [207] Sanjay Noronha and Ramakant Nevatia. Detection and modeling of buildings from multiple aerial images. *IEEE Transactions on pattern analysis and machine intelligence*, 23(5):501–518, 2001.

- [208] Filip Biljecki, Hugo Ledoux, and Jantien Stoter. Generating 3D city models without elevation data. *Computers, Environment and Urban Systems*, 64:1 – 18, 2017. ISSN 0198-9715.
- [209] Robert Hecht, Gotthard Meinel, and Manfred Buchroithner. Automatic identification of building types based on topographic databases—a comparison of different data sources. *International Journal of Cartography*, 1(1):18–31, 2015.
- [210] André Hartmann, Gotthard Meinel, Robert Hecht, and Martin Behnisch. A workflow for automatic quantification of structure and dynamic of the German building stock using official spatial data. *ISPRS International Journal of Geo-Information*, 5(8):142, 2016.
- [211] Jochen Wendel, Syed Monjur Murshed, Akila Sriramulu, and Alexandru Nichersu. Development of a web-browser based interface for 3D dataa case study of a plug-in free approach for visualizing energy modelling results. In *Progress in Cartography*, pages 185–205. Springer, 2016.
- [212] Gonzalo Besuievsky and Gustavo Patow. Recent advances on lod for procedural urban models. In *Proceedings of the 2014 Workshop on Processing Large Geospatial Data, Cardiff, UK*, volume 8, 2014.
- [213] Gerhard Gröger and Lutz Plümer. CityGML—interoperable semantic 3D city models. *ISPRS Journal of Photogrammetry and Remote Sensing*, 71:12–33, 2012.
- [214] Adeyemi Oladapo Aremu, JPJ Brennan-Craddock, Ajit Panesar, IA Ashcroft, Richard JM Hague, Ricky D Wildman, and Christopher Tuck. A voxel-based method of constructing and skinning conformal and functionally graded lattice structures suitable for additive manufacturing. *Additive Manufacturing*, 13:1–13, 2017.
- [215] William E Lorensen and Harvey E Cline. Marching cubes: A high resolution 3D surface construction algorithm. In *ACM siggraph computer graphics*, volume 21, pages 163–169. ACM, 1987.
- [216] Gregory M Nielson and Bernd Hamann. The asymptotic decider: resolving the ambiguity in marching cubes. In *Proceedings of the 2nd conference on Visualization'91*, pages 83–91. IEEE Computer Society Press, 1991.
- [217] David Del Vecchio. Optimizing a PV array with orientation & tilt. Technical report, Home Power, 2009.
- [218] Selim Aksoy, Ismet Zeki Yalniz, and Kadim Tasdemir. Automatic detection and segmentation of orchards using very high resolution imagery. *IEEE Transactions on geoscience and remote sensing*, 50(8):3117–3131, 2012.
- [219] Digimap EDINA. Os mastermap building heights layer [dxf geospatial data] and [filegeodatabase geospatial data], scale 1:2500, tile(s): Cardiff, updated: Aug 2015, ordnance survey, using: Edina digimap ordnance survey service, downloaded: September 2015. August 2015.
- [220] Filip Biljecki, Hugo Ledoux, and Jantien Stoter. Does a finer level of detail of a 3D city model bring an improvement for estimating shadows? In *Advances in 3D geoinformation*, pages 31–47. Springer, 2017.
- [221] Caroline Hachem, Andreas Athienitis, and Paul Fazio. Parametric investigation of geometric form effects on solar potential of housing units. *Solar Energy*, 85(9):1864–1877, 2011.

- [222] Yuri Boykov, Olga Veksler, and Ramin Zabih. Fast approximate energy minimization via graph cuts. *IEEE Transactions on Pattern Analysis and Machine Intelligence*, 23(11):1222–1239, Nov 2001. ISSN 0162-8828.
- [223] Yuri Boykov and Vladimir Kolmogorov. An experimental comparison of min-cut/max-flow algorithms for energy minimization in vision. *IEEE Transactions on Pattern Analysis and Machine Intelligence*, 26(9):1124–1137, Sept 2004. ISSN 0162-8828.
- [224] Vladimir Kolmogorov and Ramin Zabin. What energy functions can be minimized via graph cuts? *IEEE Transactions on Pattern Analysis and Machine Intelligence*, 26(2):147–159, Feb 2004. ISSN 0162-8828.
- [225] Junwei Han, Dingwen Zhang, G. Cheng, L. Guo, and J. Ren. Object detection in optical remote sensing images based on weakly supervised learning and high-level feature learning. *IEEE Transactions on Geoscience and Remote Sensing*, 53(6):3325–3337, June 2015. ISSN 0196-2892.
- [226] Jean-Christophe Michelin, Julien Tierny, Florence Tupin, Clément Mallet, and Nicolas Paparoditis. Quality evaluation of 3D city building models with automatic error diagnosis. In *ISPRS Conference on SSG*, 2013.
- [227] Aviva Peeters. A GIS-based method for modeling urban-climate parameters using automated recognition of shadows cast by buildings. *Computers, Environment and Urban Systems*, 59:107 – 115, 2016. ISSN 0198-9715.
- [228] Hamid Moghadam and Saeed Moghadam Deymeh. Determination of optimum location and tilt angle of solar collector on the roof of buildings with regard to shadow of adjacent neighbors. *Sustainable Cities and Society*, 14:215–222, 2015.
- [229] Xiaohua Tong, Xiaofei Lin, Tiantian Feng, Huan Xie, Shijie Liu, Zhonghua Hong, and Peng Chen. Use of shadows for detection of earthquake-induced collapsed buildings in high-resolution satellite imagery. *ISPRS journal of photogrammetry and remote sensing*, 79:53–67, 2013.
- [230] Mohammed Alahmadi, Peter Atkinson, and David Martin. Estimating the spatial distribution of the population of riyadh, saudi arabia using remotely sensed built land cover and height data. *Computers, Environment and Urban Systems*, 41:167–176, 2013.
- [231] Thomas H Kolbe. Representing and exchanging 3D city models with citygml. *3D geoinformation sciences*, pages 15–31, 2009.
- [232] Aneta Strzalka, Nazmul Alam, Eric Duminil, Volker Coors, and Ursula Eicker. Large scale integration of photovoltaics in cities. *Applied Energy*, 93:413–421, 2012.
- [233] Felix Jaugsch and Marc-Oliver Löwner. Estimation of solar energy on vertical 3D building walls on city quarter scale. *International Archives of the Photogrammetry, Remote Sensing & Spatial Information Sciences*, 42, 2016.
- [234] Giuseppe Peronato, Stéphane Bonjour, Jérémie Stoeckli, Emmanuel Rey, and Marilyne Andersen. Sensitivity of calculated solar irradiation to the level of detail: insights from the simulation of four sample buildings in urban areas. In *Proceedings of PLEA 2016, 32th international Conference on Passive and Low Energy Architecture*, number EPFL-CONF-218046, 2016.

- [235] Vasco Varduhn, Ralf-Peter Mundani, and Ernst Rank. Multi-resolution models: Recent progress in coupling 3D geometry to environmental numerical simulation. In *3D Geoinformation Science*, pages 55–69. Springer, 2015.
- [236] Jaehyun Ha, Sugie Lee, and Cheolyeong Park. Temporal effects of environmental characteristics on urban air temperature: The influence of the sky view factor. *Sustainability*, 8(9):895, 2016.
- [237] Andrius Jurelionis and Demetri G Bouris. Impact of urban morphology on infiltration-induced building energy consumption. *Energies*, 9(3):177, 2016.
- [238] Florian Petrescu, M Aldea, O Luca, C Iacoboaia, F Gaman, and E Parlow. 3D geo-information in urban climate studies. *International Archives of the Photogrammetry, Remote Sensing & Spatial Information Sciences*, 42, 2016.
- [239] Claire Ellul, Mounir Adjrad, and Paul Groves. The impact of 3D data quality on improving gnss performance using city models initial simulations. *ISPRS Annals of Photogrammetry, Remote Sensing & Spatial Information Sciences*, 4(2), 2016.
- [240] Pichai Pamanikabud and Marupong Tansatcha. 3D analysis and investigation of traffic noise impact from a new motorway on building and surrounding area. *Applied Acoustics*, 71(12):1185–1193, 2010.
- [241] Miklós Horváth, Dominika Kassai-Szoó, and Tamás Csoknyai. Solar energy potential of roofs on urban level based on building typology. *Energy and Buildings*, 111:278–289, 2016.
- [242] Filip Biljecki, Gerard BM Heuvelink, Hugo Ledoux, and Jantien Stoter. Propagation of positional error in 3D GIS: estimation of the solar irradiation of building roofs. *International Journal of Geographical Information Science*, 29(12):2269–2294, 2015.
- [243] Somayeh Asadi, Shideh Shams Amiri, and Mohammad Mottahedi. On the development of multi-linear regression analysis to assess energy consumption in the early stages of building design. *Energy and Buildings*, 85:246–255, 2014.

# **Appendices**

# Appendix A

## ***WorldView-3***

Introducing WorldView-3<sup>1</sup>, the first multi-payload, super-spectral, high-resolution commercial satellite. Operating at an expected altitude of 617 km, WorldView-3 provides 31 cm panchromatic resolution, 1.24 m multispectral resolution, 3.7 m short-wave infrared resolution, and 30 m CAVIS resolution. WorldView-3 has an average revisit time of <1 day and is capable of collecting up to 680,000 km<sup>2</sup> per day, further enhancing the DigitalGlobe collection capacity for more rapid and reliable collection. Launching in 2014, the WorldView-3 system will allow DigitalGlobe to further expand its imagery product offerings. Figure A-1 shows the scenarios of the WV3 satellite data collection.

### **Features**

1. Very high-resolution
  - Panchromatic 31 cm
  - Visible & near-infrared 1.24 m
  - Short-wave infrared 3.7 m
  - CAVIS 30 m
2. The most spectral diversity commercially available
  - Panchromatic band
  - 4 standard VNIR colors: blue, green, red, near-IR1
  - 4 added VNIR colors: coastal, yellow, red edge, and near-IR2
  - 8 SWIR bands: Penetrates haze, fog, smog, dust, and smoke
  - 12 CAVIS bands: Maps clouds, ice and snow, corrects for aerosol and water vapor
3. Industry-leading geolocation accuracy
4. High capacity in various collection modes
5. Bi-directional scanning
6. Rapid retargeting using Control Moment Gyros (>2x faster than any competitor)
7. Direct Access tasking from and image transmission to customer sites

---

<sup>1</sup><http://www.digitalglobe.com/>

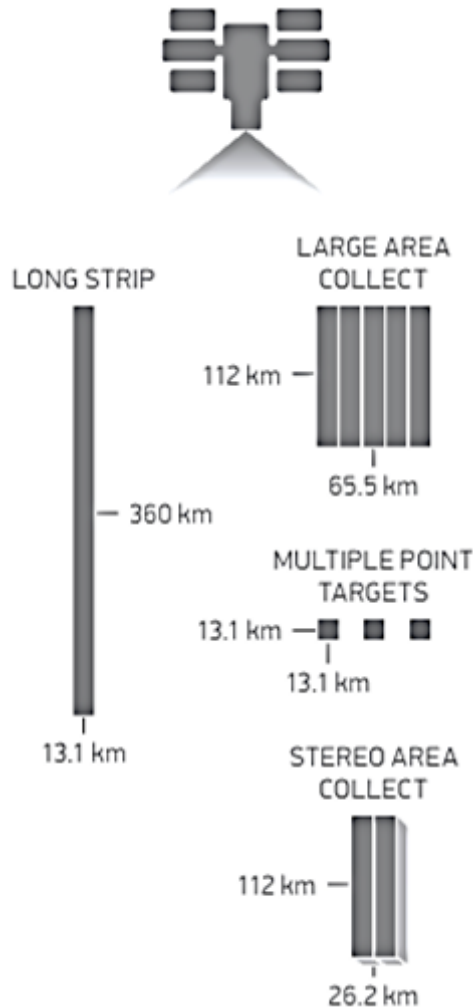


Figure A-1: Data collection scenarios

## 8. Daily revisits

### **Benefits**

1. Simultaneous, high resolution, super-spectral imagery
2. Large area mono and stereoscopic collection eliminates temporal variations
3. Precision geo-location possible without ground control points
4. Global capacity of  $680,000 \text{ km}^2$  per day
5. New and enhanced applications, including:
  - Mapping
  - Land Classifications
  - Disaster Preparedness/Response
  - Feature Extraction/Change Detection
  - Soil/Vegetative Analysis

- Geology: Oil & Gas, Mining
- Environmental Monitoring
- Bathymetry/Coastal Applications
- Identification of Man-made Materials

## 6. Superior Haze Penetration

### ***Design and specifications***

#### 1. Orbit

- Altitude: 617 km
- Type: SunSync, 10:30 am descending Node
- Period: 97 min.

#### 2. Life

- Spec Mission Life: 7.25 years
- Estimated Service Life: 10 to 12 years

#### 3. Spacecraft Size, Mass and Power

- Size: 5.7 m (18.7 ft) tall x 2.5 m (8 ft) across
- 7.1 m (23 ft) across deployed solar arrays
- Mass: 2800 kg (6200 lbs)
- Power: 3.1 kW solar array, 100 Ahr battery

#### 4. Sensor Bands

- Panchromatic: 450 – 800 nm
- 8 Multispectral:
  - Coastal: 400 – 450 nm
  - Blue: 450 – 510 nm
  - Green: 510 – 580 nm
  - Yellow: 585 – 625 nm
  - Red: 630 – 690 nm
  - Red Edge: 705 – 745 nm
  - Near-IR1: 770 – 895 nm
  - Near-IR2: 860 – 1040 nm
- 8 SWIR Bands:
  - SWIR-1: 1195 – 1225 nm
  - SWIR-2: 1550 – 1590 nm
  - SWIR-3: 1640 – 1680 nm
  - SWIR-4: 1710 – 1750 nm
  - SWIR-5: 2145 – 2185 nm
  - SWIR-6: 2185 – 2225 nm
  - SWIR-7: 2235 – 2285 nm
  - SWIR-8: 2295 – 2365 nm
- 12 CAVIS Bands:
  - Desert Clouds: 405 – 420 nm
  - Aerosol-1: 459 – 509 nm
  - Green: 525 – 585 nm
  - Aerosol-2: 635 – 685 nm
  - Water-1: 845 – 885 nm
  - Water-2: 897 – 927 nm
  - Water-3: 930 – 965 nm
  - NDVI-SWIR: 1220 – 1252 nm
  - Cirrus: 1365 – 1405 nm
  - Snow: 1620 – 1680 nm
  - Aerosol-1: 2105 – 2245 nm
  - Aerosol-2: 2105 – 2245 nm

5. Sensor Resolution (or GSD, Ground Sample Distance; off-nadir is geometric mean)

- Panchromatic Nadir:  $0.31\text{ m}$
- $20^\circ$  Off-Nadir:  $0.34\text{ m}$
- Multispectral Nadir:  $1.24\text{ m}$
- $20^\circ$  Off-Nadir:  $1.38\text{ m}$
- SWIR Nadir:  $3.70\text{ m}$
- $20^\circ$  Off-Nadir:  $4.10\text{ m}$
- CAVIS Nadir:  $30.00\text{ m}$

6. Dynamic Range

- 11-bits per pixel Pan and MS; 14-bits per pixel SWIR

7. Swath Width

- At nadir:  $13.1\text{ km}$

8. Attitude Determination and Control

- Type: 3-axis Stabilized
- Actuators: Control Moment Gyros (CMGs)
- Sensors: Star trackers, precision IRU, GPS

9. Pointing Accuracy and Knowledge

- Accuracy:  $<500\text{m}$  at image start/stop
- Knowledge: Supports geolocation accuracy below

10. Retargeting Agility

- Time to Slew  $200\text{ km}$ : 12 sec

11. Onboard Storage

- $2199\text{ Gb}$  solid state with EDAC

12. Communications

- Image & Ancillary Data: 800 and  $1200\text{ Mbps}$  X-band
- Housekeeping: 4, 16, 32, or  $64\text{ kbps}$  real time,  $524\text{ kbps}$  stored, X-band
- Command: 2 or  $64\text{ kbps}$  S-band

13. Max Contiguous Area Collected in a Single Pass ( $30^\circ$  off-nadir angle)

- Mono:  $66.5\text{ km} \times 112\text{ km}$  (5 strips)
- Stereo:  $26.6\text{ km} \times 112\text{ km}$  (2 pairs)

14. Revisit Frequency (at  $40^\circ$  N Latitude)

- $1\text{ m}$  GSD:  $<1.0$  day
- 4.5 days at  $20^\circ$  off-nadir or less

15. Geolocation Accuracy (CE90)

- Predicted  $<3.5\text{ m}$  CE90 without ground control

#### 16. Capacity

- $680,000\text{ km}^2$  per day

Table 1: Characteristics of high and very-high spatial resolution remote sensing systems and their applications

Year	Satellite	Sensor	SR <sup>a</sup> (nm)	Bands <sup>b</sup>	PS <sup>c</sup> (m)	C <sup>d</sup> (km)	RT <sup>e</sup> (days)	DR <sup>f</sup> (bit)	Scale <sup>f</sup>	Applications
1972	Landsat-1, Landsat-2, Landsat-3	MSS	500 - 1100	4 (MS) 5 <sup>h</sup>	80	185	18	6	A - G	Land-use planning; vegetation inventories; crop growth and health assessments; discriminating different types and amounts of vegetation; and cartography
1984	Landsat-5	TM	450 - 2,350 10,400 - 12,350	6 (MS) 1 (T)	30	185	16	8	G - H	Surface temperature; discriminating vegetation type; water penetration; plant and soil moisture measurements; and identification of hydrothermal alteration in certain rock types
1997	SeaStar	SeaWiFS	402 - 885	8 (MS)	1,100	2,800	Daily	10	G - H	The concentration of microscopic marine plants; phytoplankton based on the colour of the ocean
1998	NOAA-15	AVHRR/3	580 - 12,500	6 (MS)	1,090	2,940	Daily	10	G - H	Surface mapping (daytime); landwater boundaries; snow and ice detection; cloud mapping (daytime and night); sea surface temperature
1999	Terra & Aqua	MODIS	620 - 14,3385	2 (MS) 5 (MS) 29 (MS & T)	250 500 1000	2,330	Daily	12	G - H	Land, cloud, aerosols boundaries and properties; ocean colour, phytoplankton, biogeochemistry; atmospheric temperature; cirrus clouds and water vapour; ozone; surface and cloud temperature; cloud top altitude

<sup>a</sup> Spectral resolution

<sup>b</sup> MS: multi-spectral bands

<sup>c</sup> Spatial resolution

<sup>d</sup> Swath-width

<sup>e</sup> Temporal resolution

<sup>f</sup> Radiometric resolution

<sup>g</sup> Mapping scale

<sup>h</sup> Landsat-3 only

<sup>A</sup> A: scale 1:2500

<sup>B</sup> B: scale 1:7500

<sup>C</sup> C: scale 1:10 000

<sup>D</sup> D: scale 1:25 000

<sup>E</sup> E: scale 1:40 000

<sup>F</sup> F: scale 1:80 000

<sup>G</sup> G: scale 1:100 000

<sup>H</sup> H: scale 1:500 500

Continue on the next page

Table 1: Characteristics of low and medium spatial resolution remote sensing systems and their applications (cont.)

Year	Satellite	Sensor	SR <sup>a</sup> (nm)	Bands <sup>b</sup>	PS <sup>c</sup> (m)	C <sup>d</sup> (km)	RT <sup>e</sup> (days)	DR <sup>f</sup> (bit)	Mapping scale	Applications
1999	Terra	MISR	425 - 886	4 (MS)	275	360	9	14	G - H	Land use; ocean colour; air pollution; volcanic eruptions; desertification; deforestation; and soil erosion
1999	Landsat7	ETM+	450 - 2,350 10,400 - 12,500 500 - 900	6 (MS) 1 (T) 1 (PAN)	30 60 15	185	16	8	D - G	Agriculture; forestry; land use; water resources and natural resource exploration; human population census and monitoring the growth of global urbanisation; deletion of coastal wetlands; and generating DEM
1999	Terra	ASTER	520 - 860 1,600 - 2,430 8,125 - 11,650	3 (MS) 6 (MS) 5 (T)	15 30 90	60	16	8 8 12	A - E E - G G - H	Land surface climatology; vegetation and ecosystem dynamics; volcano monitoring; hydrology; geology and soils; land surface and land cover change
2002	SPOT5	2 HRGs	500 - 890 1,580 - 1,750 480 - 710	3 (MS) 1 (MS) 1 (PAN)	10 20 5	60	26	8	C - D C - D B - D	Urban and rural planning; land use and infrastructure planning; telecommunications; oil and gas exploration and mining; environmental assessment, natural disaster management; marine studies; agriculture; and 3D terrain modelling

<sup>a</sup> Spectral resolution

<sup>b</sup> MS: multi-spectral bands

<sup>c</sup> Spatial resolution

<sup>d</sup> Swath-width

<sup>e</sup> Temporal resolution

<sup>f</sup> Radiometric resolution

<sup>g</sup> Mapping scale

<sup>h</sup> Landsat-3 only

<sup>A</sup> A: scale 1:2500

<sup>B</sup> B: scale 1:7500

<sup>C</sup> C: scale 1:10 000

<sup>D</sup> D: scale 1:25 000

<sup>E</sup> E: scale 1:40 000

<sup>F</sup> F: scale 1:80 000

<sup>G</sup> G: scale 1:100 000

<sup>H</sup> H: scale 1:500 500

*Continue on the next page*

Table 1: Characteristics of low and medium spatial resolution remote sensing systems and their applications (cont.)

Year	Satellite	Sensor	SR <sup>a</sup> (nm)	Bands <sup>b</sup>	PS <sup>c</sup> (m)	C <sup>d</sup> (km)	RT <sup>e</sup> (days)	DR <sup>f</sup> (bit)	Mapping scale	Applications
2013	Landsat8	OLI & TIRS	435 - 1,551 10,600 - 12,510 503 - 676	8 (MS) 2 (T) 1 (PAN)	30 100 15	185	16	12	F - G F - G A - E	Mineral exploration; vegetation analysis; large regional coverage; extensive archive for change detection; availability of imagery over cloud affected areas (detecting cirrus clouds); and coastal zone

<sup>a</sup> Spectral resolution

<sup>b</sup> MS: multi-spectral bands

<sup>c</sup> Spatial resolution

<sup>d</sup> Swath-width

<sup>e</sup> Temporal resolution

<sup>f</sup> Radiometric resolution

<sup>g</sup> Mapping scale

<sup>h</sup> Landsat-3 only

<sup>A</sup> A: scale 1:2500

<sup>B</sup> B: scale 1:7500

<sup>C</sup> C: scale 1:10 000

<sup>D</sup> D: scale 1:25 000

<sup>E</sup> E: scale 1:40 000

<sup>F</sup> F: scale 1:80 000

<sup>G</sup> G: scale 1:100 000

<sup>H</sup> H: scale 1:500 500

Table 2: Characteristics of low and medium spatial resolution remote sensing systems and their applications

Year	Satellite	SR <sup>a</sup> (nm)	Bands <sup>b</sup>	PS <sup>c</sup> (m)	C <sup>d</sup> (km)	RT <sup>e</sup> (days)	DR <sup>f</sup> (bit)	Scale <sup>g</sup>	Stereo-view	Applications
1999	IKONOS	445 - 853	4 (MS)	4	11.3	2.3 - 3.4	11	C	Yes	Civil engineering works; land use and infrastructure planning; telecommunication; tourism; mapping and surveying; mining and exploration; oil and gas; environmental assessment; agriculture; and DEM generation
		445 - 900	1 (PAN)	1						
2001	QuickBird	450 - 900	4 (MS)	0.61	16.5	1 - 3.5	11	B	No	Environment studies; oil and gas exploration; engineering and construction; land use and planning; agricultural and forest climates; telecommunication; and tourism
		450 - 900	1 (PAN)	2.44						
2007	WorldView-1	400 - 900	1 (PAN)	0.5	17.6	1.7	11	A	Yes	Infrastructure planning; oil and gas exploration; mapping and surveying; telecommunications; and DEM generation
2008	GeoEye-1	450 - 920	4 (MS)	1.65	15.2	2.1 - 8.3	11	A	Yes	Land use and infrastructure planning; environmental assessment; civil engineering works; natural resources; oil and gas; mining and exploration; tourism; agriculture; 3D urban terrain model; and DEM generation
		450 - 800	1 (PAN)	0.41						
2008	RapidEye	440 - 850	5 (MS)	5	77	5.5	12	D	No	Industries; agriculture; forestry; oil and gas exploration; power and engineering and construction; cartography and mining

<sup>a</sup> Spectral resolution

<sup>b</sup> MS: multi-spectral bands

<sup>c</sup> Spatial resolution

<sup>d</sup> Swath-width

<sup>e</sup> Temporal resolution

<sup>f</sup> Radiometric resolution

<sup>g</sup> Mapping scale

<sup>h</sup> Landsat-3 only

<sup>A</sup> A: scale 1:1500

<sup>B</sup> B: scale 1:2000

<sup>C</sup> C: scale 1:2500

<sup>D</sup> D: scale 1:5000

*Continue on the next page*

Table 2: Characteristics of low and medium spatial resolution remote sensing systems and their applications (cont.)

Year	Satellite	SR <sup>a</sup> (nm)	Bands <sup>b</sup>	PS <sup>c</sup> (m)	C <sup>d</sup> (km)	RT <sup>e</sup> (days)	DR <sup>f</sup> (bit)	Mapping scale	Stereo-view	Applications
2009	WorldView-2	400 - 1,040	8 (MS) 1 (PAN)	2 0.5	16.4	1.1	11	D	Yes	Analysis of vegetation; coastal environments; agriculture; geology; tourism; civil engineering works; land use and infrastructure planning; and natural resources
2011	Pleiades-1A	430 - 940 470 - 830	4 (MS) 1 (PAN)	2 0.5	20	Daily	12	B	Yes	Land planning and management; urban density assessment; detection and identification of small features; agriculture; homeland security; forestry; maritime and littoral surveillance; civil engineering monitoring; 3D geometry creation for the applications of flight simulators; high precision mapping; and renewable energy
2012	SPOT6	450 - 890 450 - 745	4 (MS) 1 (PAN)	6 1.5	60	Daily	12	D	Yes	Defence; engineering; coastal surveillance; agriculture; deforestation; environmental monitoring; and oil, gas and mining industries
2014	WorldView-3	400 - 1,040 450 - 800 1,195 - 2,365 405 - 2,245	8 (MS) 1 (PAN) 8 (SWIR) 12 (CAVIS)	1.24 0.31 3.7 30	3.1 <1 (less than one day)	11 (PAN) & (MS) 14 (SWIR)	D - C	Yes		Defence and military applications; feature extraction and change detection; natural disaster and flooding, man-made materials and structures; oil and gas exploration; geology, mining, soil and vegetation; land classification; bathymetry and coastal

<sup>a</sup> Spectral resolution

<sup>b</sup> MS: multi-spectral bands

<sup>c</sup> Spatial resolution

<sup>d</sup> Swath-width

<sup>e</sup> Temporal resolution

<sup>f</sup> Radiometric resolution

<sup>g</sup> Mapping scale

<sup>h</sup> Landsat-3 only

<sup>A</sup> A: scale 1:1500

<sup>B</sup> B: scale 1:2000

<sup>C</sup> C: scale 1:2500

<sup>D</sup> D: scale 1:5000

Table 3: Remote sensing and geospatial data resources and providers

Provider	Source and type <sup>a</sup>			Comment
	Non-commercial		Commercial	
	RS	G	RS + G	
USGS Global Visualisation Viewer (GloVis) - <a href="http://glovis.usgs.gov/">http://glovis.usgs.gov/</a>	✓			Various satellite and land characteristics datasets including the free Landsat archive
USGS Earth Explorer - <a href="http://earthexplorer.usgs.gov/">http://earthexplorer.usgs.gov/</a>	✓			Aerial photography, DEM, and various satellite datasets including the free Landsat archive
Global Land-cover Facility (GLCF) - <a href="http://glcf.umd.edu/data/">http://glcf.umd.edu/data/</a>	✓			Various satellite and DEM datasets including the free Landsat archive
USGS LP DAAC Global Data Explorer - <a href="http://gdex.cr.usgs.gov">http://gdex.cr.usgs.gov</a>	✓	✓		ASTER Global DEM V2, SRTM, GTOPO30 and Blue Marble data
USGS Earth Resources Observation and Science (EROS) Centre - <a href="https://eros.usgs.gov/find-data">https://eros.usgs.gov/find-data</a>	✓	✓		A collection of data sources
Sentinel Data Hub - <a href="https://senthub.esa.int">https://senthub.esa.int</a>	✓			Data from the ESA GMES/Copernicus Sentinel satellites
NASA EOSDIS Reverb—ECHO - <a href="http://reverb.echo.nasa.gov/">http://reverb.echo.nasa.gov/</a>	✓	✓		A wide variety of satellite and DEM datasets including ASTER Global DEM (G-DEM)
ESA Landsat 8 Web Portal - <a href="https://landsat8portal.eo.esa.int">https://landsat8portal.eo.esa.int</a>	✓			Landsat 8 datasets hosted by the European Space Agency (ESA)
Canadian Geospatial Data Infrastructure (CGDI) GeoGratis - <a href="http://geogratis.gc.ca/">http://geogratis.gc.ca/</a>	✓	✓		Various RS, DEM and thematic data
Canadian Council on Geomatics (CCOG) GeoBase - <a href="http://www.geobase.ca/">http://www.geobase.ca/</a>	✓	✓		DEM, SPOT, Landsat and RADARSAT-1

Brazil National Institute for Space Research - <a href="http://www.dgi.inpe.br/CDSR/">http://www.dgi.inpe.br/CDSR/</a>	✓		CBERS-2 and CBERS-2B
CGIAR-CSI Geo- Portal SRTM - <a href="http://srtm.csi.cgiar.org/SELECTION/inputCoord.asp">http://srtm.csi.cgiar.org/SELECTION/inputCoord.asp</a>	✓		90 m DEM data
ERSDAC - <a href="http://www.jspacesystems.or.jp/ersdac/GDEM/E/index.html">http://www.jspacesystems.or.jp/ersdac/GDEM/E/index.html</a>	✓		ASTER Global DEM (G-DEM) with 30 m DEM data
USGS Global Multiresolu- tion Terrain Elevation Data 2010 (GMTED2010) - <a href="http://topotools.cr.usgs.gov/">http://topotools.cr.usgs.gov/</a>	✓		Global DEM
USGS National Map Viewer- <a href="http://viewer.nationalmap.gov/">http://viewer.nationalmap.gov/</a>	✓	✓	Orthoimagery, elevation, land-cover, US Topo, scanned historic topographic maps
USDA NRCS Geospa- tial Data Gateway - <a href="http://datagateway.ncrs.usda.gov/">http://datagateway.ncrs.usda.gov/</a>	✓	✓	Aerial orthoimagery and other geospatial data
Oregon State Uni- versity HICO - <a href="http://hico.coas.oregonstate.edu/">http://hico.coas.oregonstate.edu/</a>	✓	✓	Hyperspectral imager
USGS EROS Hazards Data Distribution System (HDDS) - <a href="http://hddsexplorer.usgs.gov/">http://hddsexplorer.usgs.gov/</a>	✓		Hazards related imagery
USGS Land-cover Institute (LCI) - <a href="http://landcover.usgs.gov/landcoverdata.php">http://landcover.usgs.gov/landcoverdata.php</a>	✓		Wide variety of land-cover datasets
Esri ArcGIS Online - <a href="http://www.esri.com/software/arcgis/arcgisonline/features">http://www.esri.com/software/arcgis/arcgisonline/features</a>	✓	✓	A wide variety of raster and vector geospatial datasets
Esri ArcGIS Online Image Services - <a href="http://www.arcgis.com/home/gallery.html">http://www.arcgis.com/home/gallery.html</a>	✓	✓	Providing multispectral, temporal, and event imagery, Basemaps
GIS Data Depot - <a href="http://data.geocomm.com/">http://data.geocomm.com/</a>	✓	✓	A wide variety of raster and vector geospatial datasets

Dundee Satellite Receiving Station - <a href="http://www.sat.dundee.ac.uk/">http://www.sat.dundee.ac.uk/</a>	✓	Images from NOAA, SeaStar, Terra and Aqua polar orbiting satellites
Landmap - <a href="http://www.landmap.ac.uk/">http://www.landmap.ac.uk/</a>	✓      ✓	Providing a combination of remotely sensed imagery and a high quality spatial data
ASTER Spectral Library - <a href="http://speclib.jpl.nasa.gov/">http://speclib.jpl.nasa.gov/</a>		Digital spectral libraries
ASU Thermal Emission Spectroscopy Laboratory Spectral Library - <a href="http://tes.asu.edu/spectral/library/">http://tes.asu.edu/spectral/library/</a>		Digital spectral libraries
USGS View - SPECPR - Software for Plotting Spectra - <a href="http://pubs.usgs.gov/of/2008/1183/">http://pubs.usgs.gov/of/2008/1183/</a>		Digital spectral libraries
Reflectance Experiment Laboratory (RELAB) at Brown University - <a href="http://www.planetary.brown.edu/">http://www.planetary.brown.edu/</a>		Digital spectral libraries
AVIRIS (Jet Propulsion Laboratory, Pasadena, CA) - <a href="http://aviris.jpl.nasa.gov/">http://aviris.jpl.nasa.gov/</a>	✓	Hyperspectral data
Airbus Defence and Space - <a href="http://www.astrium-geo.com/">http://www.astrium-geo.com/</a>	✓	A wide variety of remote sensing data products including SOPT-7 and providing sample imagery
Alaska Satellite Facility - <a href="https://www.asf.alaska.edu/">https://www.asf.alaska.edu/</a>	✓	A wide variety of datasets and SAR datasets
Apollo Mapping - <a href="https://apolломapping.com/">https://apolломapping.com/</a>	✓	A wide variety of remote sensing data products
DigitalGlobe - <a href="http://www.digitalglobe.com/">http://www.digitalglobe.com/</a>	✓	A wide variety of remote sensing data products and providing samples of imageries

LAND INFO Worldwide Mapping - <a href="http://www.landinfo.com/">http://www.landinfo.com/</a>	✓	A variety of imageries and geospatial data products and providing samples of imageries and prices
MapMart - <a href="http://www.mapmart.com">http://www.mapmart.com</a>	✓	A variety of imageries and geospatial data products and providing samples of imageries and prices
Satellite Imaging Corporation - <a href="http://www.satimagingcorp.com/">http://www.satimagingcorp.com/</a>	✓	A variety of imageries and geospatial data products
Spatial Energy - <a href="http://www.spatialenergy.com/">http://www.spatialenergy.com/</a>	✓	A variety of imageries and geospatial data and products
Penobscot Corporation - <a href="http://www.penobscotcorp.com/">http://www.penobscotcorp.com/</a>	✓	A variety of imageries and geospatial data products
MDA Geospatial Services - <a href="http://gs.mdacorporation.com/">http://gs.mdacorporation.com/</a>	✓	RS, RADARSAT-1 and RADARSAT-2
Infoterra - <a href="http://terrasar-x-archive.infoterra.de/">http://terrasar-x-archive.infoterra.de/</a>	✓	TerraSAR-X Archive
ImageSat International - <a href="http://www.imagesatintl.com/">http://www.imagesatintl.com/</a>	✓	EROS A data
i-cubed - <a href="http://www.i3.com/">http://www.i3.com/</a>	✓	Various geospatial data
German Aerospace Centre - <a href="http://www.dlr.de/hr/en/">http://www.dlr.de/hr/en/</a>	✓	E-SAR data
eMap International - <a href="http://www.emap-int.com/">http://www.emap-int.com/</a>	✓	Various geospatial data
Aero-Graphics - <a href="http://www.aero-graphics.com/">http://www.aero-graphics.com/</a>	✓	Aerial orthoimagery, hyperspectral, LiDAR & Radar
Aerial Services - <a href="http://www.aerialservicesinc.com/">http://www.aerialservicesinc.com/</a>	✓	Aerial Othoimagery, Hyperspectral, LiDAR & Radar with providing samples

<sup>a</sup>RS: remote sensing and G: geospatial.

# Appendix B

## ***List of publications***

### **Journal papers**

- Kadhim, N., Mourshed, M. “**A Shadow-Overlapping Algorithm for Estimating Building Heights From VHR Satellite Images.**” *IEEE Geoscience and Remote Sensing Letters*, 15(1):8–12, 2018. [doi:10.1109/LGRS.2017.2762424](https://doi.org/10.1109/LGRS.2017.2762424)
- Kadhim, N., Mourshed, M. and Bray, M. “**Advances in remote sensing applications for urban sustainability.**” *Euro-Mediterranean Journal for Environmental Integration*, 1(1):7, 2016. [doi.org/10.1007/s41207-016-0007-4](https://doi.org/10.1007/s41207-016-0007-4)

### **Conference papers**

- Kadhim, N., Mourshed, M. and Bray, M. “**Automatic extraction of urban structures based on shadow information from satellite imagery.**” Proceedings of BS2015: 14th Conference of International Building Performance Simulation Association. 2015.
- Kadhim, N., Mourshed, M. and Bray, M. “**Shadow Detection from Very High Resolution Satellite Image Using Grabcut Segmentation and Ratio-Band Algorithms.**” The International Archives of Photogrammetry, Remote Sensing and Spatial Information Sciences, 40.3, p: 95, 2015. [doi:10.5194/isprsarchives-XL-3-W2-95-2015](https://doi.org/10.5194/isprsarchives-XL-3-W2-95-2015)

### **Manuscript in preparation**

The Journal paper entitled “**The Automated Creation of Urban Building 3D Geometry Using WorldView-3 Satellite Images.**” is being prepared for submission to *IEEE Transactions on Geoscience and Remote Sensing* Journal.

The Journal paper entitled “**A new tool for estimating solar energy potential on 3D building models.**” is being prepared for submission to *Energy and Buildings* Journal.

# A Shadow-Overlapping Algorithm for Estimating Building Heights From VHR Satellite Images

Nada Kadhim<sup>✉</sup>, Member, IEEE, and Monjur Mourshed<sup>✉</sup>, Member, IEEE

**Abstract**—Building height is key geometric attribute for generating 3-D building models. We propose a novel four-stage approach for automated estimation of building heights from their shadows in very high resolution (VHR) multispectral images. First, a building's actual shadow regions are detected by applying ratio-band algorithm to the VHR image. Second, 2-D building footprint geometries are identified using graph theory and morphological fuzzy processing techniques. Third, artificial shadow regions are simulated using the identified building footprint and solar information in the image metadata at predefined height increments. Finally, the difference between the actual and simulated shadow regions at every height increment is computed using Jaccard similarity coefficient. The estimated building height corresponds to the height of the simulated shadow region that resulted in the maximum value for Jaccard index. The algorithm is tested on seven urban sites in Cardiff, U.K., with various levels of morphological complexity. Our method outperforms the past attempts, and the mean error is reduced by at least 21%.

**Index Terms**—Building detection, building height estimation, Jaccard index, morphological dilation, region fitting, shadow detection, very high resolution (VHR) satellite imagery.

## I. INTRODUCTION

**G**EOMETRY identification of buildings and subsequent (3-D) modeling play an important role in a range of urban applications—from urban energy and environmental analysis [1] and the estimation of renewable energy potential [2] to data-centric operation and management of smart and resilient cities [3]. Building height ( $H_B$ ) is one of the key geometric parameters that is used to transform the (2-D) footprint area into a 3-D model. Manually obtaining  $H_B$  from a large number of buildings for urban-scale 3-D modeling and analysis is resource intensive. The difficulty and cost involved in  $H_B$  estimation also create a barrier to the use and deployment of advanced modeling, analysis, and management of the built environment for most, if not all cities and countries. Finding an efficient and cost-effective way to estimate  $H_B$  is, therefore, of paramount importance.

Manuscript received June 13, 2017; revised August 18, 2017 and October 3, 2017; accepted October 9, 2017. Date of publication December 4, 2017; date of current version December 27, 2017. This work was in part by the Higher Committee for Education Development, Office of the Prime Minister, Baghdad, Iraq, and in part by the Cardiff University Open Access Support Team University Library Service, Cardiff University, U.K. (Corresponding author: Nada Kadhim.)

N. Kadhim is with the School of Engineering, Cardiff University, Cardiff CF24 3AA, U.K. (e-mail: mohammedsalihm@cardiff.ac.uk).

M. Mourshed is with the School of Engineering, Cardiff University, Cardiff CF24 3AA, U.K. (e-mail: mourshedm@cardiff.ac.uk).

Color versions of one or more of the figures in this letter are available online at <http://ieeexplore.ieee.org>.  
Digital Object Identifier 10.1109/LGRS.2017.2762424

A common factor in the extraction of  $H_B$  approaches based on remotely sensed elevation data is that they require sophisticated data calibration and processing to obtain a reliable digital surface model (DSM). Although studies have shown the utility and usefulness of elevation data for extracting  $H_B$ , their implementation typically requires the use of additional data and often multiple images from different angles to obtain a satisfactory view of building size and shape [4]. Another feature of elevation data-based  $H_B$  extraction is the need for data preprocessing because of point cloud sparsity and data misalignment [5]. As an alternative to costly data acquisition and processing, several studies have developed methods for obtaining  $H_B$  from one data source, such as satellite images utilizing the shadows cast by buildings.

This letter presents an original approach, termed the shadow-overlapping algorithm, *Aso*, for the automated estimation of  $H_B$  from monocular very high resolution (VHR) multispectral pan-sharpened satellite images. The contributions of this paper are threefold: 1) the generation of artificial shadows,  $S_{Af}$  from a simulation of the actual shadows,  $S_{Ac}$  of the buildings in the image space; 2) the solution to the issue of overlapping shadows of the multiple buildings; and 3) the development of an algorithm by combining 1) and 2) for the automated estimation of  $H_B$  by identifying the optimal height value for the given building.

The rest of this letter is structured as follows. Previous work on  $H_B$  estimation is reviewed in Section II. Our approach and the simulation process are described in Section III. Experimental results are discussed in Section IV, while Section V provides concluding remarks and directions of the future work.

## II. PREVIOUS WORK

The first task in shadow-based  $H_B$  estimation is the extraction of shadow regions from VHR satellite images. In this respect, [6] reported two widely used techniques: ratio-band and Graph-Cut partitioning via kernel mapping, with overall accuracies of 85% and 79%, based on two performance metrics,  $F_1$  score (harmonic mean of precision and recall) and probabilistic Rand index, respectively. A semiautomatic approach was proposed in [7] to estimate  $H_B$  from a single satellite image by manually adjusting the height of a simulated building and then matching the projected shadow with the actual. In contrast, [8] used volumetric shadow analysis to automatically extract  $H_B$ , which is primarily designed for buildings with full scenes of their bases and rooftops, including the sides of the building. Reference [9] also matched shadow regions but estimated  $H_B$  using simple triangulation. Estima-

### Advances in remote sensing applications for urban sustainability

Nada Kadhim<sup>1,2</sup>  · Monjur Moushedi<sup>1</sup>  · Michaela Bray<sup>1</sup>

Received: 5 July 2016 / Accepted: 23 September 2016  
© The Author(s) 2016. This article is published with open access at Springerlink.com

**Abstract** It is essential to monitor urban evolution at spatial and temporal scales to improve our understanding of the changes in cities and their impact on natural resources and environmental systems. Various aspects of remote sensing are routinely used to detect and map features and changes on land and sea surfaces, and in the atmosphere that affect urban sustainability. We provide a critical and comprehensive review of the characteristics of remote sensing systems, and in particular the trade-offs between various system parameters, as well as their use in two key research areas: (a) issues resulting from the expansion of urban environments, and (b) sustainable urban development. The analysis identifies three key trends in the existing literature: (a) the integration of heterogeneous remote sensing data, primarily for investigating or modelling urban environments as a complex system, (b) the development of new algorithms for effective extraction of urban features, and (c) the improvement in the accuracy of traditional spectral-based classification algorithms for addressing the spectral heterogeneity within urban areas. Growing interests in renewable energy have also resulted in the increased use of remote sensing—for planning,

operation, and maintenance of energy infrastructures, in particular the ones with spatial variability, such as solar, wind, and geothermal energy. The proliferation of sustainability thinking in all facets of urban development and management also acts as a catalyst for the increased use of, and advances in, remote sensing for urban applications.

**Keywords** Remote sensing systems · Remote sensing applications · Environmental sustainability · Urban environments · Sustainable cities

#### Introduction

Cities are engines of economic prosperity and social development that arise from the concentration of people and economic activities but often manifests in unsustainable urban environments [57]. Economic opportunities in cities act as a catalyst for rapid urbanisation across the globe. Urbanisation rates are uneven and are much faster in developing countries [7]. By 2030, the annual average rate of urban growth is expected to be 0.04 % in Europe, 1.5 % in the USA, 2.2 % in East Asia and the Pacific, 2.7 % in South Asia, 2.3 % in the Middle East and North Africa, and 3.6 % in Sub-Saharan Africa [80]. Increased urban migration has contributed to the unplanned or poorly planned and implemented growth and expansion of cities. The latter is a critical factor for urban stakeholders as unplanned urban growth can have a long-term negative impact on urban sustainability on a range of scales—local, regional, national, and potentially inter-governmental [75]. Impacts include *detrimental economic consequences* such as the reduction in the productivity of key economic sectors [18]; *environmental degradation* such as poor air quality, and increased urban temperatures and surface run-off

✉ Nada Kadhim  
MohammedSalihNM@cardiff.ac.uk;  
nada.m.kadhim@gmail.com  
Monjur Moushedi  
MoushediM@cardiff.ac.uk  
Michaela Bray  
BrayM1@cardiff.ac.uk

<sup>1</sup> Cardiff School of Engineering, Cardiff University,  
Cardiff CF24 3AA, UK

<sup>2</sup> Department of Civil Engineering, University of Diyala,  
Diyala, Iraq

## **Conference papers**

*Proceedings of BS2015:  
14th Conference of International Building Performance Simulation Association, Hyderabad, India, Dec. 7-9, 2015.*

### **AUTOMATIC EXTRACTION OF URBAN STRUCTURES BASED ON SHADOW INFORMATION FROM SATELLITE IMAGERY**

Nada M. Mohammed Kadhim<sup>1,2</sup>, Monjur Mourshed<sup>1</sup>, Michaela Bray<sup>1</sup>

<sup>1</sup>School of Engineering, Cardiff University, Cardiff, UK

<sup>2</sup>School of Engineering, University of Diyala, Diyala, Iraq

MohammedSalihNM, MourshedM, BrayM1 @ cardiff.ac.uk

#### **ABSTRACT**

The geometric visualisation of the buildings as the 3D solid structures can provide a comprehensive vision in terms of the assessment and simulation of solar exposed surfaces, which includes rooftops and facades. However, the main issue in the simulation process for accurately assessing buildings' surfaces is a genuine data source that presents the real characteristics of buildings. This research aims to extract the 3D model as the solid boxes of urban structures automatically from Quickbird satellite image with 0.6 m GSD for assessing the solar energy potential. The results illustrate that the 3D model of building presents spatial visualisation of solar radiation for the entire building surface in a different direction.

#### **INTRODUCTION**

Providing sufficient energy to meet the needs of urban dwellers is undoubtedly a challenging task. Solar energy is one form of clean renewable energy that can provide sustainable electricity without toxic pollution or global warming emissions. Therefore, there is a growing demand worldwide for the use of solar photovoltaic (PV) technology because it has a much lower environmental impact than other conventional energy sources. However, in order to exploit this renewable energy within urban areas, a crucial process is the automated detection and evaluation of the surfaces available for integrated solar installations. In particular, the simulation of roof/surface brightness from a genuine source that presents the real characteristics and functionalities of buildings still remains an open issue. Further, although considerable research has been devoted to detecting the rooftops of buildings, rather less attention has been paid to creating and completing a 3D model of urban buildings. For this reason, there is a need to increase our understanding of the solar energy potential of surfaces and roofs to formulate future adaptive energy policies for the sustainability of cities.

This paper is devoted to the automated extraction of 3D urban structures as solid blocks using Very High Resolution (VHR) satellite imagery. The motivation to use VHR satellite imagery is that such data can provide reliable and efficient detail in the creation of urban buildings within various urban landscapes.

Furthermore, satellite imageries can provide a magnificent test domain for any application with a variety of illumination and environmental conditions, and can be available in the public-domain (e.g. Google Earth). Satellite images are useful for locating individual buildings, connected buildings, and both small and large buildings, providing information about their geometry, and depicting the surrounding environment of buildings and the urban fabric nearby. Therefore, we focus on assessing the solar energy potential not only of the rooftops but also the buildings' surfaces in VHR satellite image acquired from urban area which solely contains the detached buildings through the automatic creation of a 3D vision of these buildings.

Many previous studies in this context have evaluated the amount of insolation within urban areas on diverse data types, such as pre-existing maps of building footprints, LiDAR data, and/or aerial images. However, such data has proven its effectiveness in solar energy assessments within urban landscapes, even though the availability of such data in a particular urban area is mostly difficult to obtain. This is due to, for instance, their high costs (e.g. LiDAR and aerial images) or not being frequently updated (e.g. the building footprint maps). The production of the building location maps requires continued survey campaigns, which also require more money, time and effort. Such data and maps cannot even be collected if there is a conflict within a study area or access is difficult. However, such cases have quite commonly collected real geospatial data to assess the solar energy potential for feeding the existing buildings with sufficient electrical energy as one form of solar energy utilisation. VHR satellite imageries are a good alternative to overcome the difficulty of collecting data from a genuine data source at lower cost, with continuous updating, and a wide area of coverage. In addition to the availability of visible bands (R, G, and B) in a VHR satellite image, the near-infrared band (INR) is an important spectral band that can be used to extract the shadow regions of buildings, which are considered strong evidence of the existence of urban constructions.

In this paper, we propose a new approach which will automatically create 3D models of isolated buildings from a VHR multispectral satellite image without any extra information. The proposed approach of the

## **Conference papers**

The International Archives of the Photogrammetry, Remote Sensing and Spatial Information Sciences, Volume XL-3/W2, 2015  
PIA15+HRIGI15 – Joint ISPRS conference 2015, 25–27 March 2015, Munich, Germany

### **SHADOW DETECTION FROM VERY HIGH RESOLUTION SATELLITE IMAGE USING GRABCUT SEGMENTATION AND RATIO-BAND ALGORITHMS**

N. M. Salih M. Kadhim<sup>a, b, \*</sup>, M. Mourshed<sup>a</sup>, M. T. Bray<sup>a</sup>

<sup>a</sup> Dept. of Architectural, Civil & Environmental Engineering, Cardiff School of Engineering,  
Cardiff University, Queen's Buildings, Newport Road, Cardiff, CF24 3AA UK – (MohammedSalihNM, MourshedM, BrayM1)  
@cardiff.ac.uk

<sup>b</sup> Dept. of Architectural, Sustainable Urban Planning & Civil Engineering, Diyala School of Engineering, University of Diyala,  
Diyala, Iraq – (nada.flower@gmail.com)

**Commission VI, WG VI/4**

**KEY WORDS:** VHR Satellite Imagery, Shadow Detection, Shadow Context, Image Segmentation, Grab Cut partitioning, Urban Area, WorldView-3

#### **ABSTRACT:**

Very-High-Resolution (VHR) satellite imagery is a powerful source of data for detecting and extracting information about urban constructions. Shadow in the VHR satellite imageries provides vital information on urban construction forms, illumination direction, and the spatial distribution of the objects that can help to further understanding of the built environment. However, to extract shadows, the automated detection of shadows from images must be accurate. This paper reviews current automatic approaches that have been used for shadow detection from VHR satellite images and comprises two main parts. In the first part, shadow concepts are presented in terms of shadow appearance in the VHR satellite imageries, current shadow detection methods, and the usefulness of shadow detection in urban environments. In the second part, we adopted two approaches which are considered current state-of-the-art shadow detection, and segmentation algorithms using WorldView-3 and Quickbird images. In the first approach, the ratios between the NIR and visible bands were computed on a pixel-by-pixel basis, which allows for disambiguation between shadows and dark objects. To obtain an accurate shadow candidate map, we further refine the shadow map after applying the ratio algorithm on the Quickbird image. The second selected approach is the GrabCut segmentation approach for examining its performance in detecting the shadow regions of urban objects using the true colour image from WorldView-3. Further refinement was applied to attain a segmented shadow map. Although the detection of shadow regions is a very difficult task when they are derived from a VHR satellite image that comprises a visible spectrum range (RGB true colour), the results demonstrate that the detection of shadow regions in the WorldView-3 image is a reasonable separation from other objects by applying the GrabCut algorithm. In addition, the derived shadow map from the Quickbird image indicates significant performance of the ratio algorithm. The differences in the characteristics of the two satellite imageries in terms of spatial and spectral resolution can play an important role in the estimation and detection of the shadow of urban objects.

#### **1. INTRODUCTION**

##### **1.1 Shadows in the VHR Satellite Imageries**

Very High Resolution (VHR) satellite imagery is considered one of the highest quality currently available from remote sensing satellites because of its ability to offer sub-meter resolution. That means the VHR satellite imageries are capable of providing a high level of detail, which make them a reliable and highly vital source of information. Therefore, the VHR satellite imageries support a range of services, especially in urban areas, for city planning and monitoring, urban change detection, estimation of human activities/population, and urban object/feature detection. However, due to urban constructions which are built above ground, such as buildings and bridges, *inter alia*, shadows are the most common component accompaniments for these constructions that can be seen in VHR images. In the fact that the incident light rays, typically

sunlight, when intercepted by an off-terrain object, shadows will be generated and cast on other urban surfaces/objects at the moment of image capture by optical satellites. Figure 1 presents three conditions (a light source, an object to cast the shadow line, and a surface to receive the shadow line and shadow) that must be met to produce a shadow. In this context, a shadow indicates the shape of the object casting it, and in many ways it can indicate the texture of the surface receiving the shadow (Yee, 2013). In contrast, shade can be defined as the side of an object which is opposite the direction of illumination, which has less colour tone of the full blackness (the value intensity of darkness) compared to the objects' shadows that have very low values of brightness in VHR images, or mostly have zero value (pure black), Figure 1.

The fact is that the line that locates and separates the light and shade areas on the object determines the shadow line on a receiving surface. The shadow line, in turn, determines the dark area cast onto the surface on which the object rests and which

\* Tel.: +447427618125.  
E-mail addresses: [MohammedSalihNM@cardiff.ac.uk](mailto:MohammedSalihNM@cardiff.ac.uk), [nada.flower@gmail.com](mailto:nada.flower@gmail.com)

## **Skills and achievements certificates**

1. The best poster award was obtained as the best poster presentation at the 7th GRE-GYNOG 2015 School of Engineering research conference, held on 29th June 1st July 2015. A part of our research was presented as a poster, won the best poster prize
2. A training certificate was awarded for Image Processing and computer vision with MATLAB-Training in Cambridge, United Kingdom MathWorks (the leading developer of mathematical computing software for engineers and scientists)
3. A training certificate was awarded for using the 3D scanner and processing the scan data to create 3D models of urban features
4. A letter of approval for a research stay of one month has been obtained from the department of Geodesy and Photogrammetry of the Nevsehir H.B.V. University, Nevsehir, Turkey, for visiting the aforementioned department in order to nominate for the PGR International Experience Fund in Cardiff School of Engineering
5. I was selected by the ESA EO Summer School Scientific Committee to take part on August 1-12th, 2016. According to the acceptance letter that I had received, the review process was quite challenging; as they stated, they received about 200+ applications for only 70 places, and I was one of them. The European Space Agency (ESA) is Europe's gateway to space. Its mission is to shape the development of Europe's space capability and ensure that investment in space continues to deliver benefits to the citizens of Europe and the world
6. The certificate of professional development (CPD): Leadership was awarded by PwC UK Careers & Cardiff University
7. The certificate of professional development (CPD): Communication was awarded by PwC UK Careers & Cardiff University
8. The certificate of professional development (CPD): Effectiveness was awarded by PwC UK Careers & Cardiff University
9. A member of SPIE Remote Sensing (an international society advancing an interdisciplinary approach to the science and application of light)
10. A member of IEEE Society (the world's largest technical professional organization dedicated to advancing technology for the benefit of humanity)
11. A certificate of completion was awarded by ESRI (an international supplier of geographic information system software, web GIS and geodatabase management applications, California, US), for the Going Places with Spatial Analysis, Online GIS course, on June 15, 2016
12. A certificate of completion was awarded by ESRI (an international supplier of geographic information system software, web GIS and geodatabase management applications, California, US), for the Earth Imagery at Work and ArcGIS Pro with a plenty of techniques that were applied to the variety of geospatial datasets, Online GIS course, on March 8, 2017



Training Dates: 1-2 Oct 2014

  
Director, Training Services



# Training Attendance Certificate

This is to certify that

Nada Mohammed Salih Mohammed Kadhim of Cardiff University

Has attended and completed the  
Faro Focus3D Operation & Data Processing Training  
Course – 2 Day Basic



## Modules Covered:

- Laser scanning basics
- Hardware programming & setup
- Target placement do's & don'ts.
- Local vs global registration
- Faro scene - creation of projects and import of data-sets.
- Manipulation & analysis of data
- Registration & QA of data registration
- Filtration & clean-up of data
- Data colourisation
- Webshare creation & use
- 'Project pointcloud' creation & use
- Data export for use within 3rd party software packages

1st Horizon Training Manager:

  
Date: 17-06-2016

[www.1sth.co.uk](http://www.1sth.co.uk)

Bridge Suite, The Old Corn Mill, Lee Lane, Millhouse Green, Sheffield S36 9NN  
Tel: +44 (0)1226 766 446 | email: office@1sth.co.uk

# *Certificate of Completion*

*This is to certify that NADA M. S. MOHAMMED  
KADHIM successfully completed the Earth  
Imagery at Work online course on March 8, 2017*

*Kevin Butler*

Kevin Butler, Instructor



Certificate no: UC-S2T6802W  
Certificate url: [udeemy.com/uc/UC-S2T6802W](https://www.udemy.com/uc/UC-S2T6802W)

# *Certificate of Completion*

*This is to certify that Nada Mohammed Salih  
Mohammed Kadhim successfully completed the  
Going Places with Spatial Analysis online course  
on June 15, 2016*

*Linda Beale David DiBiase*

Linda Beale, Instructor \_\_\_\_\_ David DiBiase, Instructor



**udemy**

Certificate no: UC-HC2DWYFC  
Certificate url: [udeemy/UC-HC2DWYFC](https://www.udemy.com/certificate/UC-HC2DWYFC)

**SPIE** Membership

CERTIFICATE OF  
MEMBERSHIP



**MISS NADA MOHAMMED SALIH  
MOHAMMED KADHIM**

Student SPIE Member

SPIE certifies the individual named above is a Member of the Society with all associated benefits, who supports the SPIE Mission, Bylaws, and commitment to advancing scientific research and engineering applications of optical, photonic, imaging, and optoelectronic technologies through its meetings, education programs, and publications.

A handwritten signature in black ink.

Robert Lieberman, SPIE 2016 President

A handwritten signature in black ink.

Gary Spiegel, SPIE 2016 Secretary/Treasurer

Date: September 27, 2016



**Skills Development Service  
Gwasanaeth Datblygu Sgiliau**

**Cardiff University Students' Union  
Undeb Myfyrwyr Prifysgol Caerdydd**

Mae

**Nada Mohammed Kadhim**

Has Completed the Skills Development Service  
Certificate of Professional Development  
Wedi cwblau Sgiliau Tystysgrif Gwasanaeth Datblygu  
Datblygiad Proffesiynol i Gynrychiolwyr y Myfyrwyr

**Leadership / Arweinyddiaeth**

1. Assertiveness / Blaengaredd
2. Coaching Skills / Sgiliau Hyfforddi
3. Leadership Styles / Dulliau Arwain
4. Tackling Poor Performance / Mynd i'r afael â Pherfformiad Gwael
5. Team Briefings (self study format) / Brifio Tîm (format hunanastudio)

IS-GANGHELLOR, PRIFYSGOL CAERDYDD  
VICE CHANCELLOR, CARDIFF UNIVERSITY

LLWYDD, UNDEB MYFWRWYR PRIFYSGOL CAERDYDD  
PRESIDENT, CARDIFF UNIVERSITY STUDENTS' UNION



22/10/15

Awarded by / Rhoddwyd gan

**Cardiff University Students' Union  
Undeb Myfyrwyr Prifysgol Caerdydd**





**Skills Development Service  
Gwasanaeth Datblygu Sgiliau**

**Cardiff University Students' Union  
Undeb Myfyrrwyr Prifysgol Caerdydd**

Mae

**Nada Mohammed Kadhim**

Has Completed the Skills Development Service  
Certificate of Professional Development  
**Wedi cwblau Sgiliau Tystysgrif Gwasanaeth Datblygu  
Datblygiad Proffesiynol i Gynrychiolwyr y Myfyrwyr**

**Communication / Cyfathrebu**

Speaking & Presenting - Siarad a Chyflwyno

Practical Presentations - Cyflwyniadau Ymarferol

Listening & Awareness - Gwrando ac Ymwybyddiaeth

Negotiation Skills - Sgiliau Cyd-drafod

The Confidence Factor - Pwysigrwydd Hyder

+

IS-GANGHELLOR, PRIFYSGOL CAERDYDD  
VICE CHANCELLOR, CARDIFF UNIVERSITY

LLWYDD, UNDEB MYFWRWYR PRIFYSGOL CAERDYDD  
PRESIDENT, CARDIFF UNIVERSITY STUDENTS' UNION

04/11/2015

Awarded by / Rhoddwyd gan

**Cardiff University Students' Union  
Undeb Myfyrrwyr Prifysgol Caerdydd**





**Skills Development Service  
Gwasanaeth Datblygu Sgiliau**

**Cardiff University Students' Union  
Undeb Myfyrwyr Prifysgol Caerdydd**

Mae

**Nada Mohammed Kadhim**

Has Completed the Skills Development Service  
Certificate of Professional Development  
Wedi cwblau Sgiliau Tystysgrif Gwasanaeth Datblygu  
Datblygiad Proffesiynol i Gynrychiolwyr y Myfyrwyr

**Personal Effectiveness / Effeithiolrwydd Personol**

Unit 1/Uned 1: Motivation - Ysgogiad

Unit 2/Uned 2: Problem Solving - Datrys Problemau

Unit 3/Uned 3: Successful Networking - Rhwydweithiau Llwyddiannus

Unit 4/Uned 4: Time Management - Rheoli Amser

Unit 5/Uned 5: Teamwork - Gweithio mewn Tim

  
**IS-GANGHELLOR, PRIFYSGOL CAERDYDD  
VICE CHANCELLOR, CARDIFF UNIVERSITY**

  
**LLWYDD, UNDEB MYFWRWYR PRIFYSGOL CAERDYDD  
PRESIDENT, CARDIFF UNIVERSITY STUDENTS' UNION**



**03/11/2015**

Awarded by / Rhoddwyd gan

**Cardiff University Students' Union  
Undeb Myfyrwyr Prifysgol Caerdydd**



# GREGYNOG 2015

SCHOOL OF ENGINEERING RESEARCH CONFERENCE

POSTER AWARD – 2<sup>ND</sup> PRIZE

Nada Kadhim

W.M.

PETER CLEALL  
DIRECTOR OF POSTGRADUATE RESEARCH

29<sup>TH</sup> JUNE – 1<sup>ST</sup> JULY 2015

# Appendix C

## ***The developed 3D city models algorithm structure overview***

The developed algorithm codes and scripts will be published with the paper - The Automated Creation of Urban Building 3D Geometry Using WorldView-3 Satellite Images. In [http : //ieeexplore.ieee.org/xpl/RecentIssue.jsp?punumber = 36](http://ieeexplore.ieee.org/xpl/RecentIssue.jsp?punumber=36).

<sup>1</sup>GMM: Gaussian Mixture Models

<sup>2</sup> $S_{Ac}$ : Actual shadow regions

<sup>3</sup> $S_{Ar}$ : Artificial shadow regions

